NASA Contractor Report 3259

Effect of a Zero g Environment on Flammability Limits as Determined Using a Standard Flammability Tube Apparatus

Roger A. Strehlow and David L. Reuss

GRANT NSG-3043
JUNE 1980

NASA Contractor Report 3259

Effect of a Zero g Environment on Flammability Limits as Determined Using a Standard Flammability Tube Apparatus

Roger A. Strehlow and David L. Reuss
University of Illinois at Urbana-Champaign
Urbana, Illinois

Prepared for
Lewis Research Center
under Grant NSG-3043

National Aeronautics
and Space Administration

Scientific and Technical
Information Office

1980

TABLE OF CONTENTS

EFFECT OF A ZERO G ENVIRONMENT ON FLAMMABILITY LIMITS AS DETERMINED USING A STANDARD FLAMMABILITY TUBE APPARATUS

Roger A. Strehlow and David L. Reuss

SUMMARY

This report contains a justification for and the results of a feasibility study of a program to study flammability limits at zero g in Space Lab. The conclusions of the report are that there is a very good justification for both studying flammability limits and the flow associated with lean limit flames under zero g conditions and for performing such studies in the Space Lab environment. The feasibility study shows that the only technique that one can use to determine the important flow parameters associated with lean limit flames is the Space Lab facility. It is the only feasible technique because of the delicate nature of the equipment which must be used to make such a determination and because observational times of more than 20 seconds are required in order to properly determine lean limit flammability. Additionally, the report makes some recommendations for the conceptual design of the Space Lab facility so that it can accommodate the lean limit flammability tube experiment.

I. INTRODUCTION

Historically, the determination of flammability limits has been important for both the determination of safe operating conditions in industrial environments and for the design of more effective burners for combustion processes. Recently, lean limit flammability has taken on added importance because of the emphasis on developing engines which produce low levels of pollutants in their exhausts. Lean limit combustion is very attractive for two reasons. On the lean side, carbon monoxide is not produced in any great quantity, and, because of the low flame temperatures, nitric oxide levels are also low. Thus, there has been a considerable resurgence of research relative to the mechanism of lean limit flammability.

It is well known that the actual lean limits as determined experimentally are very dependent not only on the apparatus that is used for the determination but also on the presence of the earth's gravitational field. It is true, in fact, that upward and downward propagation limits are markedly different for many fuels. Unfortunately, there is neither a good experimental explanation for why this is so, nor are there any realistic theoretical explanations for the observed experimental effects.

This report contains a justification for studying in detail the flows associated with a lean limit flame in a particular geometry and for doing this experiment in space. It also looks at the question of the feasibility of performing this particular experiment in space and makes some recommendations as to conceptual design of the Space Lab facility that will be required to house the preferred apparatus. A conceptual design for such a facility is contained in reference 1.

II. JUSTIFICATION

There are many techniques that one can use to determine a flammability limit. However, the technique that should be used for a study of this type has one primary requirement, that is, that the geometry of the apparatus and the flame system in the apparatus be such a type that is most tractable analytically. Additionally, we are looking for an experimental technique in which buoyancy has a well documented effect. Of the many geometries that are available for flammability studies, the standard flammability tube apparatus best meets the above requirements. An upward propagating flame in such an apparatus has a two-dimensional, steady configuration when one is traveling in a coordinate system at the flame's speed up the tube and therefore is by far the most tractable system available under limit conditions. Additionally, the zero g drops that were performed under this grant have shown that the flame retains a very similar shape and a constant propagation speed under zero g conditions (albeit, much less than that observed under 1-g conditions) and therefore that the zero g flame would also be tractable mathematically.

It is important to perform this experiment under zero g conditions because buoyancy forces markedly affect these very weak limit flames on earth. Since we have developed the techniques to measure the velocity field associated with these flames, the changes in such a velocity field that one would observe between normal and zero g conditions are very important to developing an analytic understanding of why these flames extinguish. Also, it is very important to determine how the lack of gravity affects the actual limit composition of the combustible mixture.

A more detailed description of the different types of apparatus used for measuring the flammability limits is given in the third chapter of the microfiche supplement, followed by a discussion of the reasons for choosing the standard flammability limit tube for this study. In the fourth chapter of the microfiche supplement a critique of the theories predicting the occurrence of the flammability limits is presented.

The experiments that we propose to do are necessary if one is to have any hope of preparing an analytic representation of these new limit flames. The experiments involve using an extremely delicate instrument, a laser Doppler anemometer (LDA), which could not be deployed safely in any of the other current experiments that produce short-term zero g. The instrument is extremely expensive and one time use would be prohibitive. Additionally, the experiments that were performed in the drop tower at NASA Lewis Laboratory have shown quite definitely that one will need at least 20 to 30 seconds to determine a lean limit for the methane-air system under zero g conditions. This much time is just not available in any of the other zero g facilities in which, from a practical point of view, this could be done.

III. FEASIBILITY

A. The Issues

The following issues have been identified as important to the question of the feasibility of placing a standard flammability tube apparatus in Space Lab for detailed studies under zero g conditions. These are:

1. Time required for a single zero g test.
2. Size of apparatus required.
3. Ignition system.
4. Particle seeding system.
5. Feasibility of using a LDA in a standard flammability limit tube.
6. Feasibility of using holographic interferometry for measuring the density distribution.

7. Gas requirements.
8. How flammability limits change in the zero g environment.
9. How flame shape and velocities change in the zero g environment.

B. Results

1. As applied to the feasibility issues.
    a. Time required for a single zero g test.

The actual test time will be somewhat less than 1/2 minute. However, the tube must be prepared between testing and this will take additional time. Before each test, the tube should be swabbed with an ethyl alcohol-soaked swab. Failure to swab the tube before each test will result in an increase in the flame propagation velocity (refer to Chapter 5 in the microfiche supplement). Swabbing is also necessary to prevent particle accumulation on the tube walls during LDA tests. After the tube has been swabbed, a flow of air or vacuum evacuation must be used to dry the tube. At this point the test mixture should be introduced and again approximately 10 tube volumes should be used to ensure the desired composition is attained. For this purpose both ends of the tube will be closed except for small ports. At one end the port will be connected to the gas supply system and at the other end the port will be connected to an exhausting system such that the excess combustible mixture or the ethyl alcohol-air mixtures do not contaminate the combustion facility or Space Lab environment.

It is felt that the combustion facility's volume is sufficiently large that four or five flammability tests can be run in the volume before the air in the volume should be displaced with fresh air. In this regard, the question as to whether the facility has to be opened between each run is still not finalized. More than one run could probably be made without opening the combustion facility to the Space Lab environment if all functions necessary for the test sequence could be implemented remotely. This would require a repetitive igniter, remote control of flow settings and apparatus positioning, and an automatic swabbing mechanism. In this case, a run would consist of the following sequence of events:

i. Both ends of the tube open - automatic clean ethyl alcohol swab pulled or pushed through the tube.

ii. Both ends of the tube open, one connected to supply system, one to exhaust system; ten changes of air through the tube to dry the tube, or evacuate.

iii. Ten changes of methane-air mixture of desired composition to refill the tube.

iv. Vent to outside closed; small quantity of methane injected near igniter cell; wait for 2 or 3 seconds for diffusion to occur (this can be calculated); igniter end opened to combustion facility and tube fired.

v. Observation of flame either with cameras, the eye, holographic or LDA techniques.

vi. Repeat the cycle.

Total elapsed time approximately 10 min/run. If the tube can not be swabbed remotely, it is estimated that an additional 10 min/run would be required.

b. Size of apparatus required.

The standard flammability limit tube is 51 mm internal diameter and 1.8 meters long. For this facility you would have to use a tube which would be only 1 meter long but of the same internal diameter as the standard flammability tube. The combustion experiment would fit nicely into the combustion facility chamber. The LDA and the cameras to photograph the events must be external to the system but there is space provided for them. This will be discussed in more detail later.

c. Ignition system.

An ignition system was developed which involved injecting methane near the location of the ignition wire and coating the ignition wire with a nitrocellulose film. If repetitive operations are desired, coated wires could not be used unless some mechanism was avilable to replace one wire with another by remote control. It is felt, however, that with methane injection near the igniter a properly designed uncoated wire would probably suffice as an ignition source. In this regard, a glow wire seems to be the most appropriate ignition source for this experiment.

d. Particle-seeding system.

The particle-seeding system that was developed during the experiment feasibility study is not a viable system under zero g conditions because it relies on gravity to develop a seeded gas flow. Figure 1 shows an illustration of the particle-feed system used in 1-g. For the low air flow rates used in the 1-g study, the impinging air jets were actually not needed. Therefore, only the "fluidized bed" and "settling tube" portions of the feed system will be needed in the Space Lab tests if similar flow rates are used while filling the SFLT. Figure 2 shows a proposed particle-feed system for zero g conditions. In this apparatus a tube is rotated at such a velocity that the fluidized bed at the terminus of the tube experiences essentially a 1-g force.

e. Feasibility of using a LDA in a standard flammability tube.

Figure 3 is a sketch of a forward scattering LDA system which could be intalled to surround the combustion chamber in the combustion facility rack. There is sufficient space to house such an LDA system in this facility. It appears that there is no question but that this LDA design will work under Space Lab conditions. The feasibility of using an LDA system in a SFLT has been shown in the ground-based experiments described in the microfiche supplement.

f. Feasibility of using holographic interferometry for measuring the density distribution in a standard flammability limit tube.

It appears that, at the present time, it is not feasible to place a holographic interferometer on the Space Lab for combustion studies. The reason for this is that the present combustion facility does not have the proper dimensions for interfacing with a holographic interferometer. However, a holographic interferometer suitable for studies in a standard flammbility limit tube could be constructed in the room available in a double rack. In addition, with the development of light-weight, compact and internally damped optical tables, the question of vibrational stability is not a problem. The nearly ideal low-g environment of Space Lab would make vibration even less of a problem since nonrigid table supports could be utilized. If the flammability tube is mounted directly to the optical table and the table is

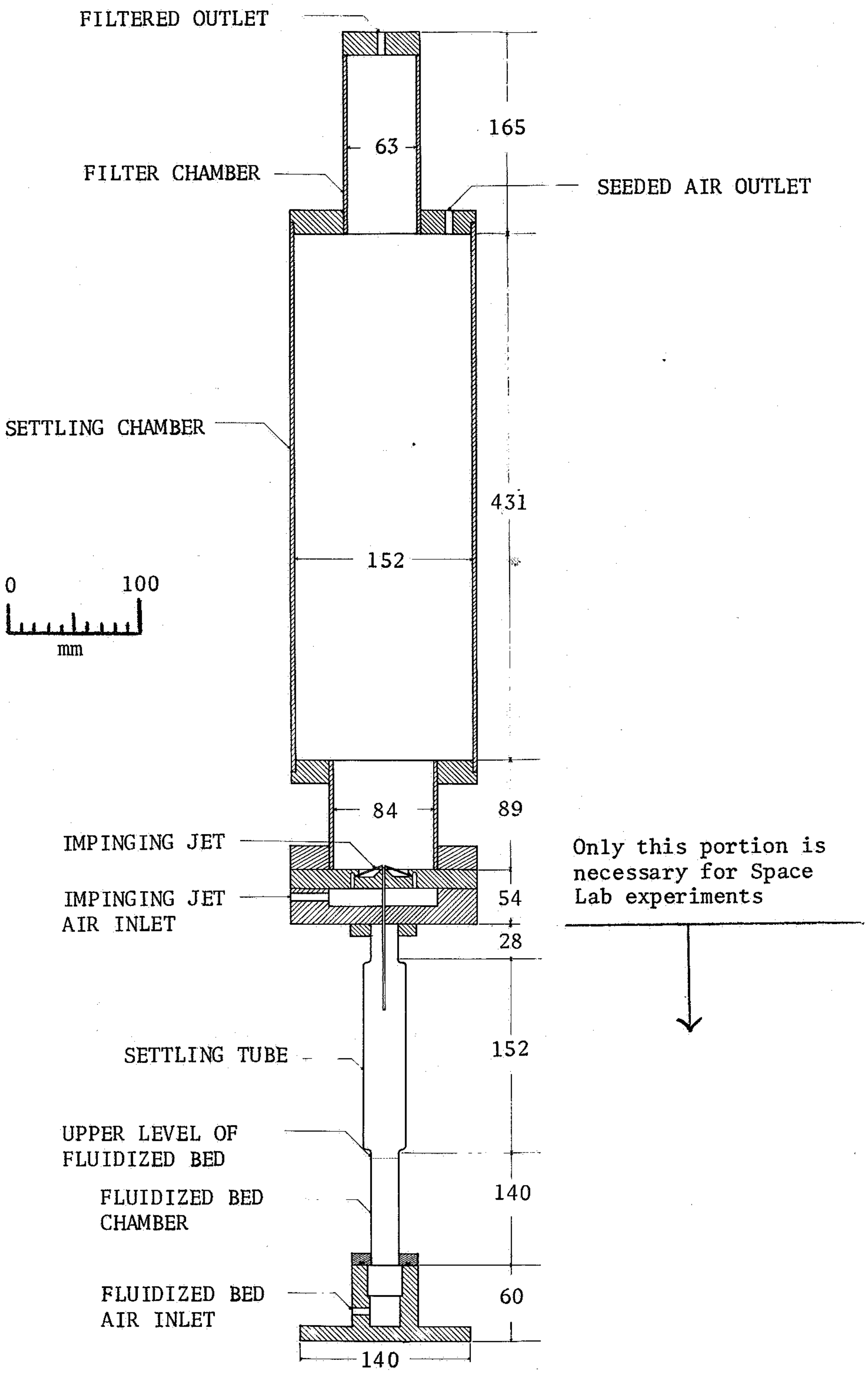

PARTICLE-FEED SYSTEM

Figure 1

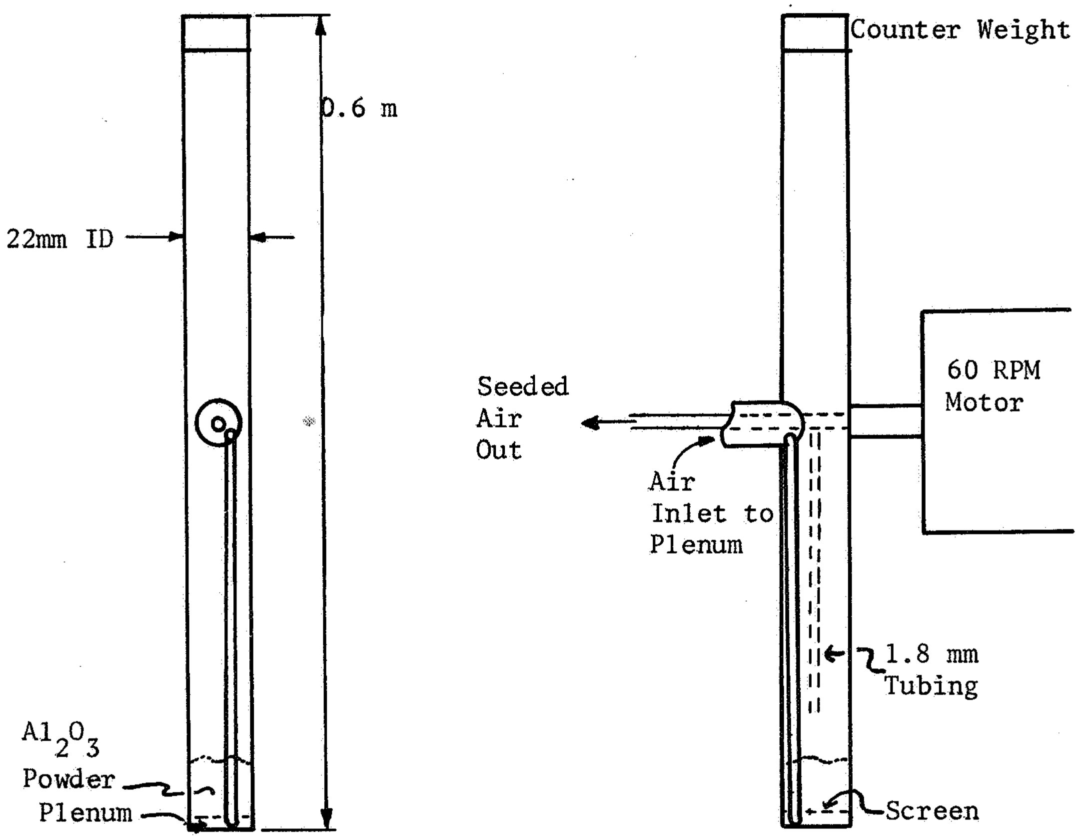

Fluidized Bed Particle Seeding System
for Use in 0-G Environment

Figure 2

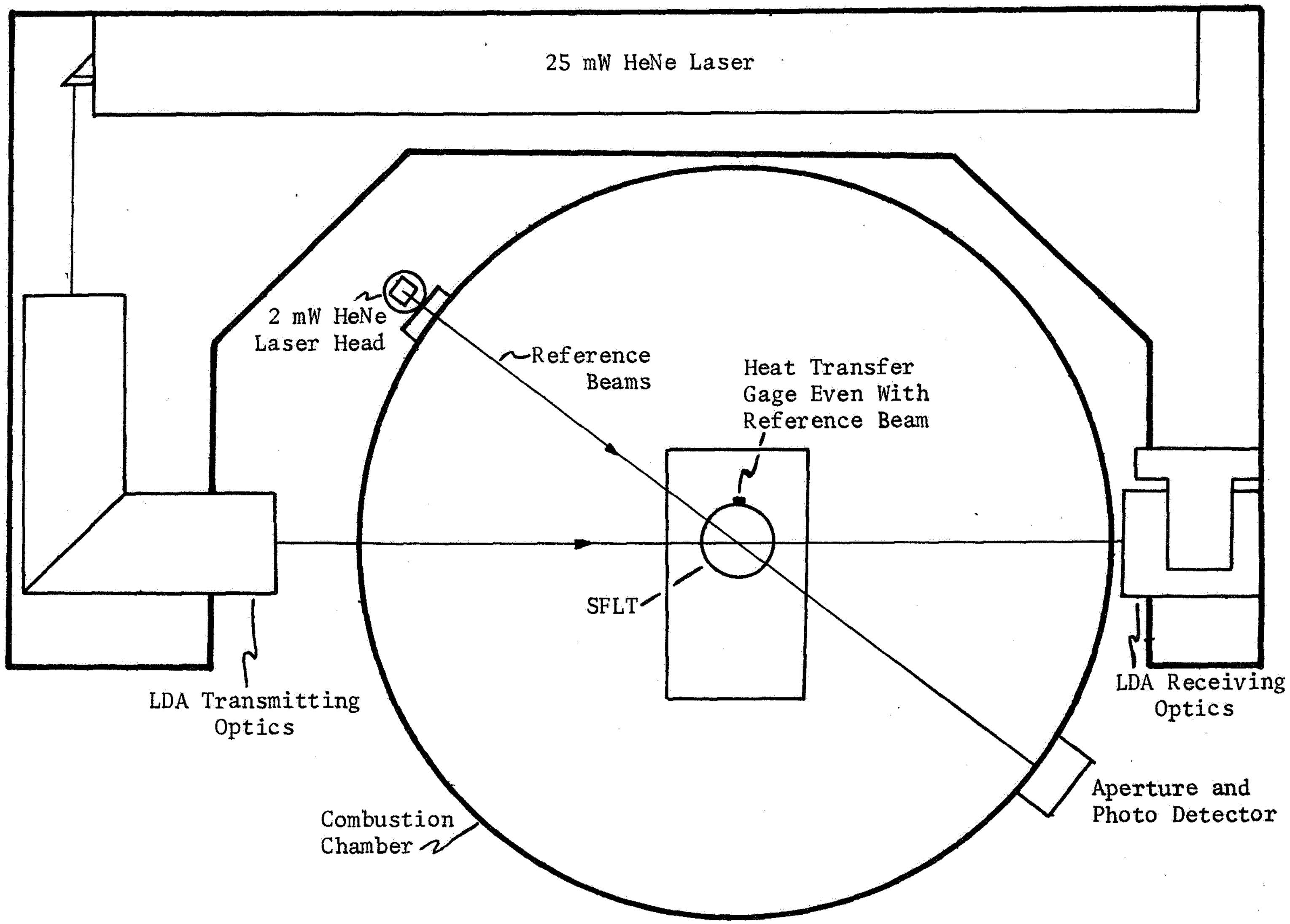

Illustration of Proposed Experimental Equipment
Top View

Figure 3

magnetically positioned, the only external force available to disturb the optical system would be through the flexible electrical and gas feed umbilicals. Since internal excitation of the optical system is the only problem, this external force would be negligible when compared to that in an on-earth laboratory. On board, photo processing of the hologram could be accomplished by a commercially available automatic processor while the plate is in place. Because the instrument is so useful for this and other studies (not only combustion studies), it would be highly desirable to investigate in greater depth the feasibility of constructing a holographic interferometer for use in space on some of the future Space Lab missions.

g. Gas requirements.

Assuming that the tube is cleaned by displacing with 10 volumes of clean air and filled by displacing with 10 volumes of the appropriate methane-air mixture, one would need approximately 40 liters of air at standard conditions and 2 liters of methane per test. After approximately 5 tests, one would have to purge and refill the combustion chamber itself in all probability. The air requirement that is given above is only to purge and fill the flammability tube itself.

h. How flammability limit changes in the zero g environment.

Figure 4 contains data that were obtained using the 2.3 second zero g drop tower facility at the Lewis Research Center. The major purpose of this work was to determine the leanest mixture composition that would allow flame propagation in a 0-g environment and the character of the flame near that limit. Due to the short amount of 0-g time available (2.3 s/test) the flame could not propagate the full length as leaner mixtures were used and the flame propagation velocities were below 10 cm/sec. However, homogeneous tests were made progressively leaner until the flame was observed to extinguish during the test. The results of these tests indicated that the flame in the 5.20% mixture attained a steady propagation velocity of approximately 4 cm/s. At a mixture of 5.1% methane, the flame did not obtain steady state in the available test time. However, with mixtures containing 4.98% methane, the flame always extinguished. It is tentatively concluded that the 0-g lean limit mixture composition is about 5.20%. However, longer 0-g times

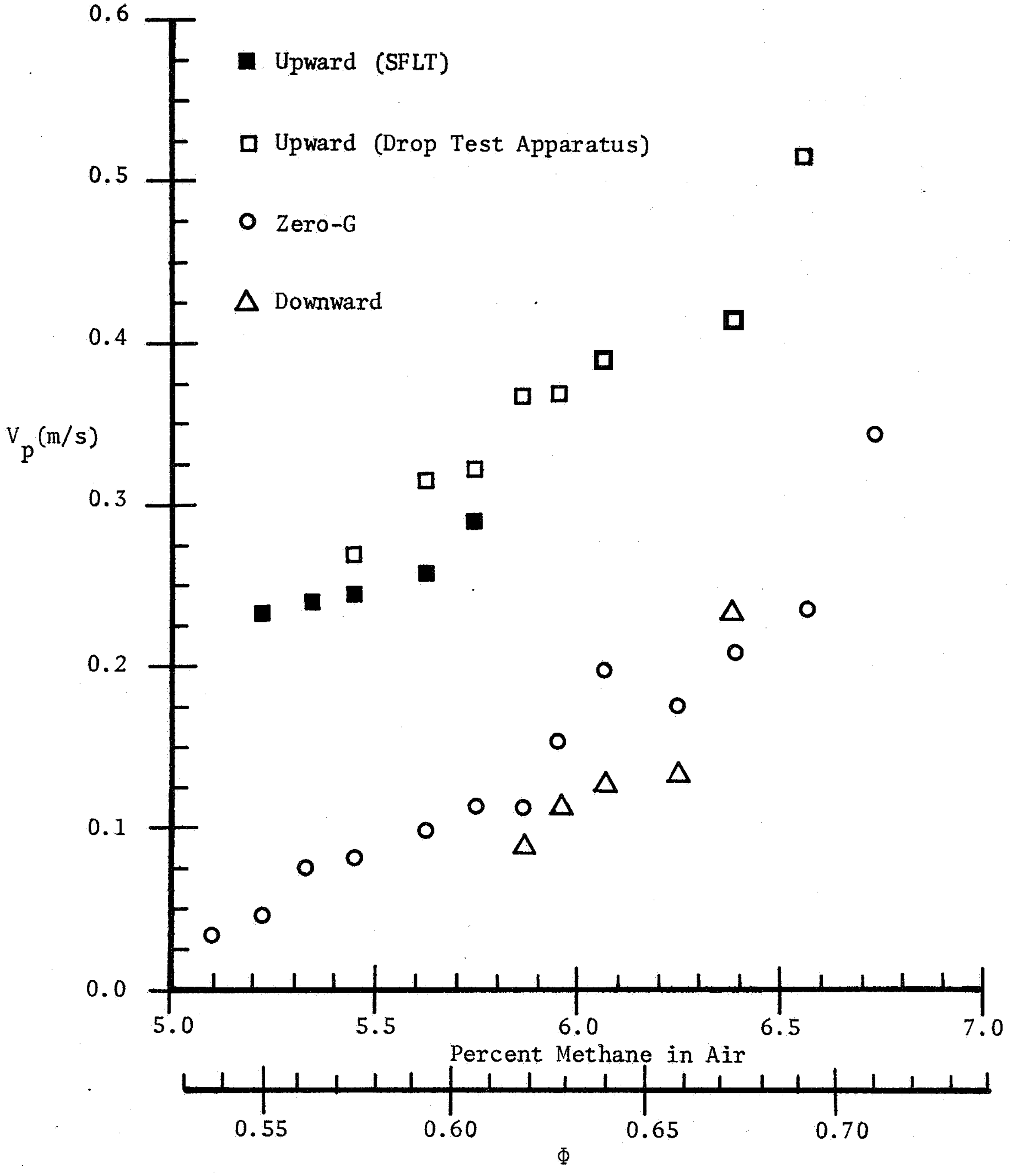

Flame Front Propagation Velocity
of Lean Methane-Air Flames
in 0-G and 1-G

Figure 4

must be available in order to verify this conclusion.

i. How flame shape and velocity changes under the zero g environment.

Figure 5 shows some flame photographs taken at the zero g facility at Lewis Research Center. The flame is seen to look somewhat like an upward propagating flame only with a much shorter skirt. Since the flame shape is a manifestation of the flow field and the flow field is affected by the presence or absence of gravity, a change in shape was expected. However, the fact that the highly curved 0-g flame and the flat downward 1-g flame propagate at about the same velocity for a given mixture (see Fig. 4) was not expected based on present conceptual models of flame propagation. The presence of this anomaly is just one more incentive for studying the velocity and density distributions in zero gravity.

2. Original scientific accomplishments.

The experiments performed during the feasibility study show that a laser Doppler anemometer can be used with a standard flammability tube apparatus and also show that the motion of the laser Doppler test region due to refractive indices changes associated with the flame passage must be interpreted in order to properly evaluate LDA signal records. The LDA results showed that, as viewed in the stationary (laboratory) coordinate, on the center line the motion ahead of an upward propagating flame is upward and away from the flame; the motion inside the flame sheet is everywhere downward; near the walls the primary motion ahead of the flame is downward; and at about the edge of the flame's skirt the downward velocity of the hot product gases near the wall is higher than the downward velocity in the central region of the flow. The axial velocity distribution, as viewed in the flame's coordinates, are presented in Fig. 6. In this coordinate system the velocity distribution is steady. The solid line is the position of the luminous flame zone. The arrows represent the magnitude of the axial velocity at their respective origin. One important result is the fact that unlike a steady 1-D flame, the velocity along the centerline first decreases and then increases as a fluid element passes through the flame. Secondly, the fluid motion occurs 15 mm upstream from the luminous flame zone. These

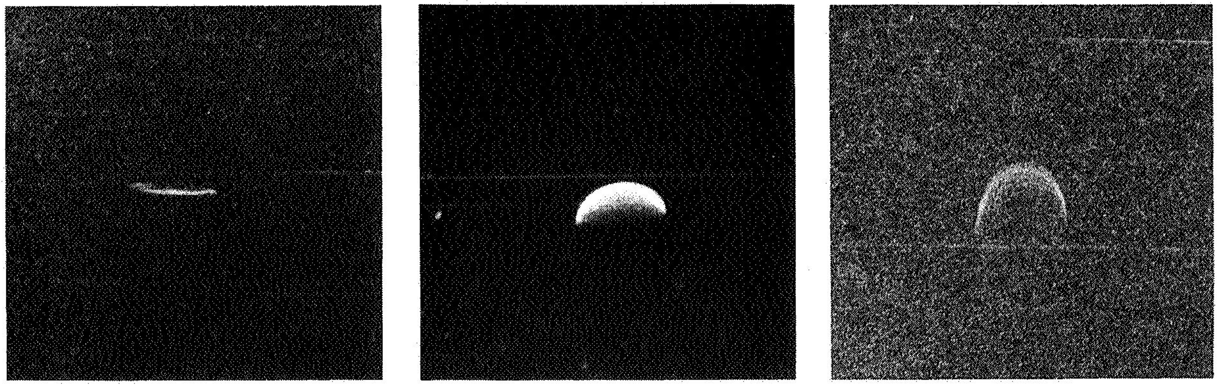

1-G 0-G 1-G

5.87%

0-G

5.33%

Photographs of Lean Methane-Air Flames

Figure 5

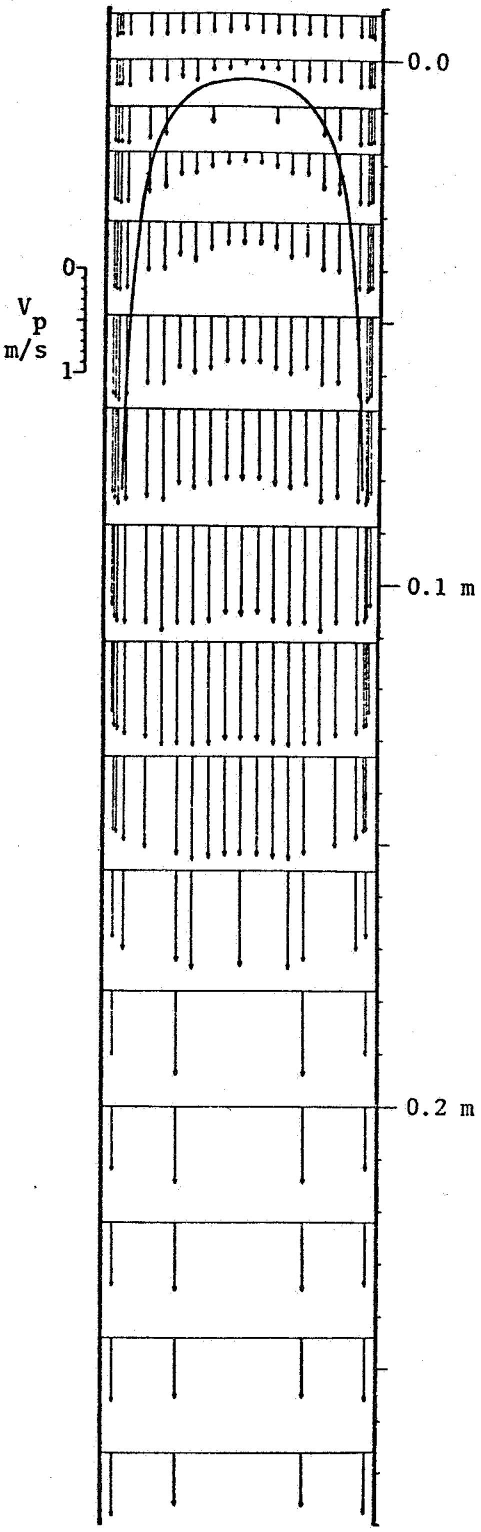

Axial Velocity Distribution
In Coordinates that Move with the Flame

Figure 6

results are all new and their observation should ultimately contribute to a better understanding of the mechanism of lean limit extinction. See the microfiche supplement for a more detailed discussion.

Holographic interferometric records were obtained of both the lean limit flame and the hot bubble that exists just after flame extinction. It was found that the inversion technique used to determine temperature distribution from these records was inaccurate primarily because the exposure time using our laser was such that the flame moved a considerable distance during exposure when compared to the width between the fringes that were produced on the interferograms. Two of these records are shown in Figs. 7 and 8. Calculation of the temperature distribution from these interferograms was fruitless due to the inadequacy of the equipment available for the feasibility study. A more powerful laser than is presently available in the Space Lab combustion facility will be necessary in order to make useful interferograms.

3. Publications or theses generated.

One Ph.D. thesis by David L. Reuss entitled "The Effect of Gravity on Lean Limit Flame Propagation", thesis advisor, Roger A. Strehlow, was generated under this feasibility study. Additionally, it is anticipated that this work will lead to a publication in the archival literature in the near future.

C. Conclusions

The study of the limit behavior of lean methane flames under zero g conditions and additionally, the study of the flow associated with such a flame using a laser Doppler anemometer is quite feasible in so far as the Space Lab environment is concerned. Furthermore, the length of the test time required as well as the delicacy of the instruments that must be used leads one to the conclusion that Space Lab is the only experimental tool that may be used to perform such a zero g study. The results of such a study will have a decided impact on the development of a sound theoretical model for the extinguishment of lean limit flames.

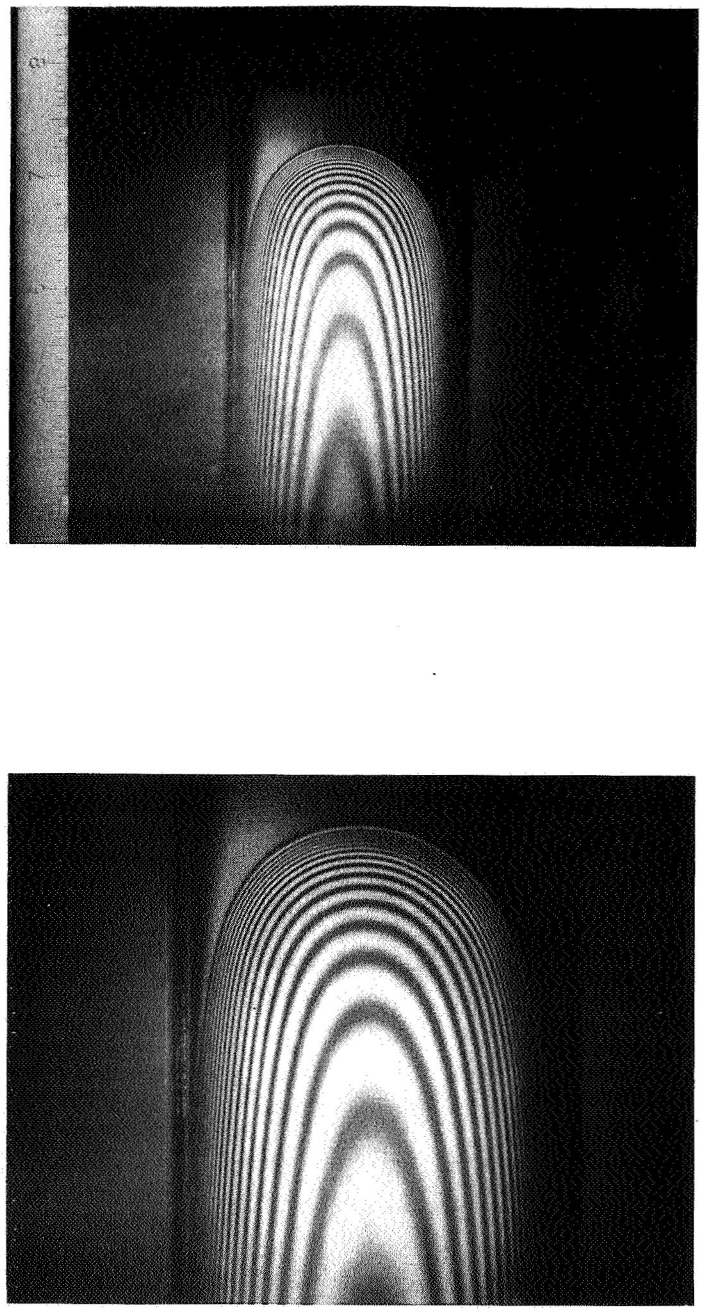

Holographic Interferograms
of Lean Limit Methane-Air Flame

Figure 7

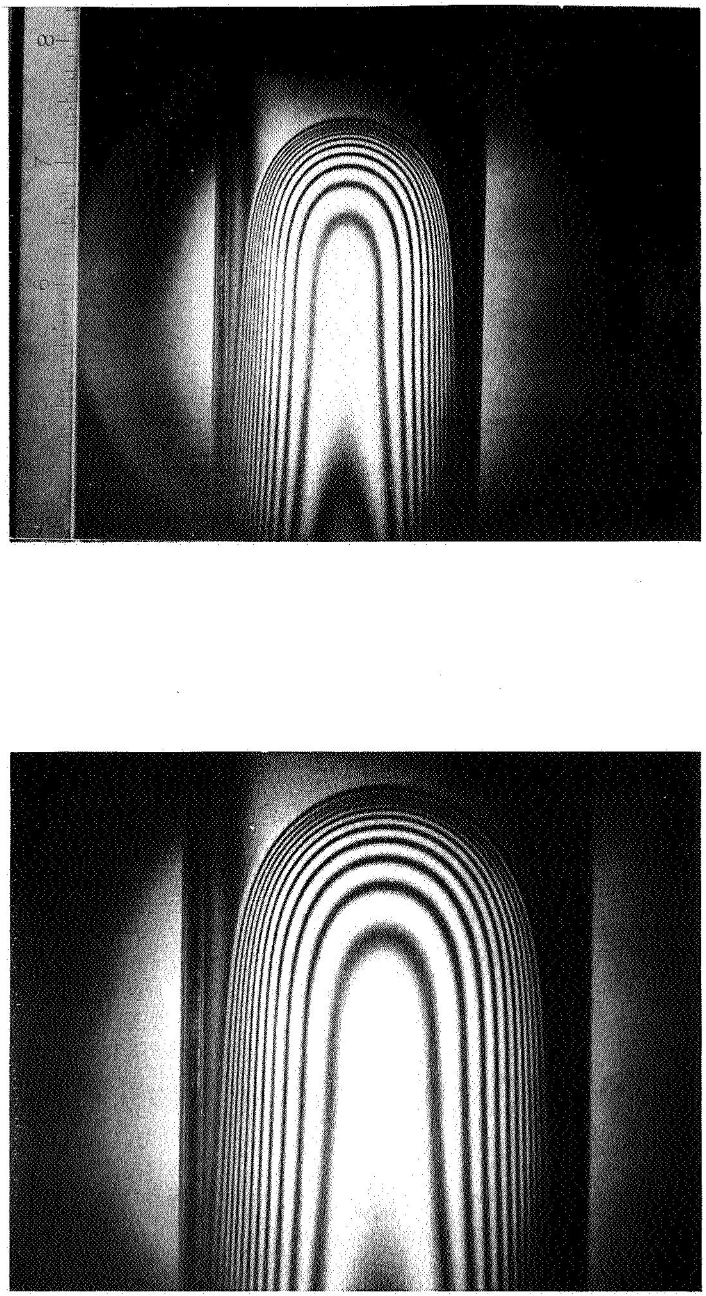

Holographic Interferograms
of Hot Bubble After
Flame Extinguished

Figure 8

IV. CONCEPTUAL DESIGN

A. Objectives

The objectives of the Space Lab experiment using a standard flammability tube would be to:

1. Determine the lean limit of methane-air mixtures in zero gravity.
2. Measure the propagation velocity of the flames in near lean limit methane-air mixtures.
3. Measure the fluid velocity distributions associated with the flame's passage.
4. Measure the heat transfer from the flame to the wall.
5. Measure the fluid density distribution associated with the flame's passage.

The above information will yield a complete characterization of the flame system under zero g conditions. It is anticipated that the same information will be developed in the same apparatus under 1-g conditions for an upward propagating flame. The comparison of data taken in the same apparatus on the same flame system under both zero and 1-g conditions will prove to be very useful in the development of a theoretical model of the extinguishment process for lean limit flames.

B. Apparatus

Figure 3 is a plan view of the combustion facility showing the location of the LDA relative to it. Figure 9 is an elevation view of the same apparatus showing its position relative to both the flammability tube, the cameras, and the beam referencing system which is used to determine the velocity of the flame propagation, as well as the relation between the location of the visible flame and the location of the density gradients in the flame. In addition to this the following support equipment will be needed:

1. The gas supply system to prepare and introduce the combustible mixtures into the flammability tube.
2. A particle-feed system to place fine alumina particles in the test gas mixture so that LDA signals may be obtained.
3. A cathotometer-telescope for alignment.

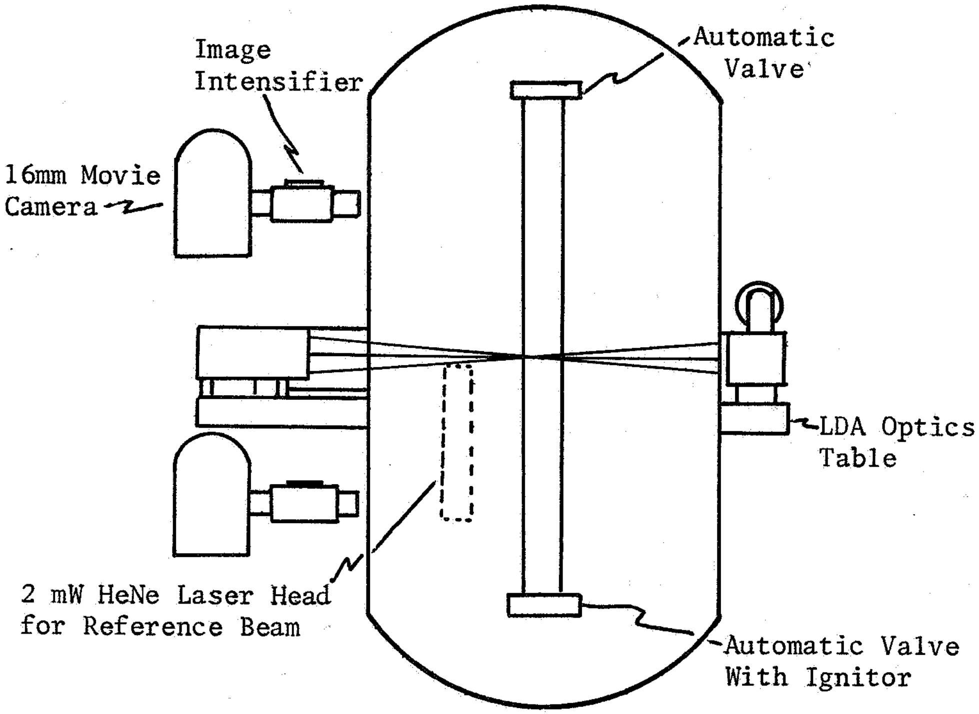

Illustration of Proposed
Experimental Equipment
Front View

Figure 9

4. A tube cleaning system (details of this have not yet been worked out).
5. A syringe system to introduce a quantity of methane near the igniter.
6. An igniter system as well as remote operating valves to place the valves in the filling and firing position.
7. Electronic support systems for the LDA and various timing circuitry needed to measure the velocity of flame propagation.

A detailed listing of suggested components to meet these requirements is included in this report as the appendix.

The gas-handling system is very important to this experiment as well as to other possible combustion experiments. There are a number of trade-offs that one must be aware of when designing the gas-handling system. First and foremost is the question of safety. By far the safest way of mixing the gases is to handle the gases as pure fluids in storage and to mix them as needed through critical flow orifices. With proper design, critical flow orifices can be used to meter a fixed composition mixture into a vessel either by flowing the mixtures through the vessel at constant pressure or by filling the vessel from zero pressure to the desired pressure. In the experiment that is being described in this report we will have to fill the vessel by displacement at constant pressure because of the need for seeding the gas. Thus, in this system we will meter air through a critical flow orifice and pass this metered air through the particle-dispersal system before mixing it with methane to make a combustible mixture. Under these circumstances the combustible mixture will exist in only a very short length of tubing and the chance for an accident involving combustion will be very slight.

It must be pointed out that it is almost impossible to mix the gases by an introduction technique where one introduces gas A and later gas B, particularly if the apparatus under question is of any size. The reason for this problem is that convective or buoyant mixing cannot occur under zero g conditions and only simple diffusion can occur. Thus, after preparing a mixture, one must either stir the mixture physically with a fan system or wait an extremely long time for normal diffusion processes to cause the mixture to reach a uniform composition. Therefore, the only viable technique is to premix the gases in a flow system and use that flow system to fill the vessel of interest. Storing the gases as a combustible mixture at high pressure is extremely dangerous and should not be done under any circumstances.

C. Measurements

The measurements that are planned are:

1. Composition of the lean flammability limit for zero g methane-air flame.
2. The speed of propagation of such a limit flame and of near limit flames in the 51 mm diameter tube.
3. The flow field associated with near limit flames in the tube.
4. Heat transfer to the wall surface.

It is anticipated that these measurements will be compared to similar measurements made for upward propagation under 1-g conditions in the same apparatus.

These comparative measurements will allow us to uniquely define the flammability limit under zero g conditions and to learn how the structure of the flame and the flow associated with the flame changes due to the effect of buoyancy forces. Heat transfer measurements will show how the gravity force affects heat losses to the wall in this particular experiment. Since it is well known that both the flows associated with the flame and the heat loss to the wall is important to the limit behavior of these flames, these pieces of information will be very important in formulating analytical description of the mechanism of extinction.

It is still considered desirable to measure the density distribution as discussed in Section III. f. Since the present combustion facility is not capable of accepting a holographic interferometer, it is hoped that a modified combustion facility will be considered in the future.

V. CONCLUSIONS

A definitive experimental study has been carried out in order to develop an understanding of the effect gravity has on lean limit flame propagation and the extinguishment process. The research conducted under this contract has demonstrated that the basic experimental apparatus needed for performing this reseach in Space Lab is feasible. The new 0-g and 1-g experimental results have added to our knowledge of the lean limit flame phenomenon and demonstrated that the effect of gravity has on the lean limit flame propagation is not as well understood as previously thought. For this reason there is a strong justification and motivation for conducting the proposed program in the 0-g environment of the Space Lab experimental laboratory.

VI. REFERENCE

1) DeWitt, R. L., "Preliminary Concept, Specifications, the End Requirements for a Zero-Gravity Combustion Facility for Space Lab", NASA TM 78910, June 1978.

VII. APPENDIX -

DEFINITION OF HARDWARE AND SERVICES FOR SPACE LAB COMBUSTION EXPERIMENTS

Lean Limit Flammability Study

1. Kodak 2475 Recording Film: Estar-AH Base. Cat #179-3900.
2. A. A standard flammability limit tube (SFLT) with end valves. A capability for injecting 4 cc of CH_4 near the igniter wire must be included.
   B. Tube-cleaning swab, e.g., chamois.
   C. Electric igniter (nichrome wire coated with nitrocellulose).
      12 → 30 VAC or VDC
      10 → 25 Amps < 40 msec duration
   D. CH_4 and air metering systems.
      3 to 7% CH_4 in air, continuously variable
   E. Aluminum oxide particle-feed system with air only feed and mixing.
   F. System to mix CH_4 and particle-laden air before entering tube.
   G. Image intensifier for each camera, e.g., Javelin High Viewing Device.
   H. Flame detector reference system.
      i) 2mW HeNe laser head and power supply with 1-D translational movement, e.g., Spectra Physics 145 head, 248 power supply.
         110/115/220 VAC ±10%
         50-60 Hz single phase
         23 watts
      ii) Beam splitter optics integrated with laser.
      iii) Two beam deflection reference systems with 2-D translational and rotational adjustment. Each detector consists of a 100 μm aperture in front of a phototransistor, e.g., MRD 450.
      iv) One shielded lead from detector to each associated electronic circuit.
      v) Electronics, 10 VDC, 100 mA.
      vi) One shielded lead from electronics to data acquisition system.
   I. Product gas sampling syringes. This also requires that chromatograph carrier gas (e.g., helium) be available to sample as a control sample.

J. i) Heat transfer gage in wall of SFLT, e.g., Medtherm Film thermocouples.

   ii) One shielded lead from thermocouple to amplifier.

   iii) Constant temperature reference junction, e.g., Kaye Instruments Thermocouple Reference System.
   117 v 60 HZ
   220/240 V 50 HZ
   100 watts

   iv) One shielded lead from reference to amplifier (could be hard wired)

   v) One differential amplifier - 1000 x
   ≥ 200 MΩ input impedance
   e.g., Teledyne/Phil Brick
   requires ±150 DC 50 mA

   vi) One shielded lead from amplifier to data acquisition system
   Note: System must resolve 0.01°C.

K. i) Holographic Interferometer - ≥ 15 mW HeNe Laser
   - 1) beam splitter
   - 2) expansion lens and special filter assemblies
   - 1) diffuse glass screen
   - 1-3) front surface mirrors
   - 1) holographic plate holder
   - 1) electronically triggered shutter

   ii) One shielded lead from flame detector electronics to shutter electronics.

   iii) Kodak Type 131 high speed holographic plates, 4" x 4" (6 required) OR
   Kodak high speed holographic film 50-253 (ESTAR Base), 4" x 5" sheets.

L. Laser Doppler Anemometer

   i) ≥ 25 mw HeNe Laser

   ii) Optics
   - a) fringe mode for longitudinal velocity component (V_z).
   - b) reference beam mode for radial velocity component (V_r).

- iii) Two photomultiplier assemblies with power supplies and electronic amplifier.
- iv) Frequency shifter with power supply and two signal mixers.
- v) Two LDA Frequency Counters with a signal validation circuit and digital interface.
- vi) Leads (coax cables)
    - a) leads to power photomultiplier tube (1 each)
    - b) 1 lead to power frequency shifter
    - c) 2 leads for signal from photomultipliers to frequency mixers (1 each)
    - d) 2 leads from mixers to frequency counters (1 each)
    - e) digital data lines from counters to data acquisition system

M. Data Acquisition System

- i) One A-D converter for thermocouple
    - 12 bit words
    - 0 → 25 mV in 0.1 sec
    - 0.2 mV resolution
- ii) Two A-D converters for flame detector signals
    - 12 bit words
    - must resolve time of voltage spike peak to 0.5 msec. The spike rises from 0 to -10 VDC in 10 msec.
- iii) Digital buses treating each counter as a device. Each counter outputs one 16-bit word and one data ready pulse. An IO data interface with buffer memory is available on TSI counters.
- iv) Digital tape accepting all 5 data words simultaneously.

N. Data verification system, e.g., CRT computer terminal with graphics capability to plot stored data in order to verify successful runs.

3. The anticipated maximum total time for a burn will be less than x/3 seconds, where x is the length of the tube in centimeters. 5×10^{-4} g is acceptable for our work.

4. Since it is not obvious what to expect in these tests, it is imperative that observations be made of the combustion process. The PI could then

make sure the tests are appropriate so that slight schedule modifications could be made, e.g., what mixtures need to be looked at or redone. This would allow the PI to effectively trouble shoot any problems that might arise. The TV camera might also require an image intensifier.

5. Effluents

Compound	Molecular Wt.	State	Quantity/run % of total volume
During filling (10 tube volumes total)			
CH_4	16	gas	6
N_2	28	gas	74
O_2	32	gas	20
After burn (total fuel conversion & complete combustion)			
CH_4	16	gas	0
N_2	28	gas	74
O_2	32	gas	8
H_2O	18	gas & liquid	12 (gas)
CO_2	44	gas	6

There is a possibility that CO may be present after a burn due to incomplete combustion. An extreme maximum would be 3%. There may be less than total fuel conversion so that the after burn values may vary, i.e., less H_2O and CO_2 and much more CH_4 and O_2.

1. Report No.
NASA CR-3259

2. Government Accession No.

3. Recipient's Catalog No.

4. Title and Subtitle
EFFECT OF A ZERO G ENVIRONMENT ON FLAMMABILITY LIMITS AS DETERMINED USING A STANDARD FLAMMABILITY TUBE APPARATUS

5. Report Date
June 1980

6. Performing Organization Code

7. Author(s)
Roger A. Strehlow and David L. Reuss

8. Performing Organization Report No.
None

9. Performing Organization Name and Address
University of Illinois at Urbana-Champaign
Urbana, Illinois

10. Work Unit No.

11. Contract or Grant No.
NSG-3043

12. Sponsoring Agency Name and Address
National Aeronautics and Space Administration
Washington, D.C. 20546

13. Type of Report and Period Covered
Contractor Report

14. Sponsoring Agency Code

15. Supplementary Notes
Final report. Project Manager, Thomas H. Cochran, Space Propulsion and Power Division, NASA Lewis Research Center, Cleveland, Ohio 44135. The microfiche supplement at the back of the report was taken from a thesis submitted in partial fulfillment of the requirements for the degree Doctor of Philosophy to the University of Illinois at Urbana-Champaign in 1979.

16. Abstract
A study was conducted over a three year period in which fundamental experiments on flammability limits in a zero gravity environment were defined. Initially, the need for this research was justified on scientific, as well as, societal grounds. A feasibility study was carried out in which key aspects of a possible spacelab experiment were investigated analytically, experimentally on the bench, and in drop tower facilities. Finally, a conceptual design for a spacelab experiment was developed.

17. Key Words (Suggested by Author(s))
Combustion; Flammability limits; Zero gravity; Spacelab

18. Distribution Statement
Unclassified - unlimited
STAR Category 25

19. Security Classif. (of this report)
Unclassified

20. Security Classif. (of this page)
Unclassified

21. No. of Pages
28

22. Price*
A03

* For sale by the National Technical Information Service, Springfield, Virginia 22161

SUPPLEMENT TO NASA CR-3259

EFFECT OF GRAVITY ON LEAN LIMIT FLAME PROPAGATION

by David Lee Reuss

This supplement was taken from a thesis
submitted in partial fulfillment of the requirements
for the degree of Doctor of Philosophy
to the University of Illinois at Urbana-Champaign in 1979

EFFECT OF GRAVITY ON LEAN LIMIT FLAME PROPAGATION

David Lee Reuss, Ph.D.
Department of Aeronautical and Astronautical Engineering
University of Illinois at Urbana-Champaign, 1979

A literature survey was conducted in order to learn what has been accomplished in the past 100 years in determining and understanding the occurrence of flammability limits. The knowledge acquired in this survey was used to determine the best test procedure for studying the effect of gravity on lean flammability limits and to determine how the occurrence of the limit is modeled. Upward and downward lean limit methane-air flames were studied and photographed in a 50 mm diameter tube open at the ignition end and closed at the other. A laser Doppler anemometer was constructed and used to measure the axial velocity profiles of an upward propagating lean limit flame and of flames during extinction in sub-lean limit mixtures. Diffuse illumination holographic interferograms of an upward propagating lean limit flame and a post-extinction hot bubble were made. However, attempts to calculate the temperature distribution were fruitless due to the inadequacy of the available equipment. Photographs from a still camera were made using a light beam deflection detector to trigger the exposures. These referenced photographs were used to determine the relative positions of the luminous flame zone, velocity distribution and interferograms of upward propagating lean limit flames. Movies were made of near lean limit flames propagating through a 50 mm tube in the zero gravity environment of the 2.2 s drop tower facility at NASA Lewis Research Center. The propagation velocity, flame shape and calculated burning velocity of the 0-g and 1-g flames are compared.

TABLE OF CONTENTS

LIST OF SYMBOLS

A	area	
A_ω	area of tube wall	
$A_{cs,g}$	cross-sectional area of gas	
c	component (atom)	Chapter II
c	speed of light	Chapter VIII
c_o	speed of light in a vacuum	
C_p	heat capacity	
d_c	characteristic cell diameter	
$d_{e^{-2}}$	diameter where the irradiance = $1/e^2$	
d_{part}	particle diameter	
d_{pv}	diameter of the LDA probe volume	
d_t	tube diameter	
D	diameter	
D_i	diffusion coefficient	
E	activation energy	
f_{Dop}	Doppler frequency	
FL	focal length	
FN	fringe number	
g	acceleration due to gravity	
g(r)	arbitrary function (Chapter VIII)	
H_i	sensible enthalpy	
i	current	
I	indices	
[I]	concentration of i^{th} species	

K	reaction rate
K'	Karlowitz number
ℓ_{pv}	length of LDA probe volume
L	geometric path length
Le	Lewis Number
m	mass
M	mass flow
MW	molecular weight
n	index of refraction
p	pressure
q	heat flux
q_{cond}	heat loss due to conduction
q_{loss}	heat loss
q_{rad}	heat loss due to radiation
Q_{rad}	volumetric heat loss due to radiation
r	radius
R	gas constant
s	species
S	average fluid velocity
S_c	rise velocity of flame kernel in closed bomb
S_b	velocity of burned gas
S_u	velocity of unburned gas
t	time
Δt_{exp}	exposure time
Δt_{mech}	mechanical delay time
Δt_{sh}	shutter delay time

T	temperature
T_{ad}	adiabatic flame temperature
T_b	burned gas temperature
T_{df}	temperature at point of maximum light beam deflection
T_f	maximum flame temperature
T_{IM}	temperature at point of maximum chemiluminescence intensity
T_{max}	maximum flame temperature
T_u	unburned gas temperature
U_∞	upstream fluid velocity
V_i	individual species velocity
V_p	translation velocity of flame
V_r	radial velocity component
V_{set}	settling velocity
V_z	vertical (longitudinal) velocity component
x_{frng}	LDA fringe spacing
Δx_{be}	distance between reference beam and back edge of image
Δx_{exp}	distance flame traveled during the exposure
Δx_{fe}	distance between reference beam and front edge of image
Δx_{im}	image thickness
X_i	mole fraction of i^{th} species
Y_i	mass fraction of i^{th} species

Subscripts

i	indices
k	indices
K	indices
ℓ	indices
m	indices

Greek Symbols

α	angle between the normal to the flame and the approach velocity vector
α	exponent
β	Gladstone-Dale constant
δ	reaction zone thickness
Δ	overall flame thickness
ε	non-dimensional activation energy
η	preheat zone thickness
κ	thermal conductivity
λ	wavelength of light
Λ	optical path length
μ	species flow rate
ν	frequency
ξ	LDA beam intersection half angle
ρ	density
τ	non-dimensional temperature
τ_{part}	characteristic time response of particles to flow variations

Acronyms

BDFD	beam deflection flame detector
HI	holographic interferometer
LDA	laser Doppler anemometer
MZI	Mach-Zehnder interferometer
NASA	National Aeronautics and Space Administration
PLL	phase-locked loop
PMT	photomultiplier tube
SFLT	standard flammability limits tube
0-g	zero gravity
1-g	earth's gravity

CHAPTER I

INTRODUCTION

A flame propagating through a homogeneous gaseous mixture of fuel and air is called a premixed gas flame. It is well known that as the amount of fuel in such a mixture is reduced a point is reached where a premixed flame will not propagate through the mixture for long distances from an ignition source. The leanest mixture composition that will support flame propagation in any particular apparatus is called the lean flammability limit for that apparatus. The premixed flame that is of interest here is not of the type that occurs as a steady-held flame such as a Bunsen burner flame. In that case the ability (or inability) of the flame to propagate is controlled by the flame holding process itself. The determination of flammability limits is based instead on the ability of a flame to propagate a considerable distance from an ignition source, usually in an initially quiescent mixture.

Historically, flammability limits have been of interest for determining whether or not mixtures are hazardous, and safety has remained as a major concern (see Coward and Jones, 1952). In recent years emissions and combustion efficiency standards have precipitated an interest in lean combustion practical systems (see Calcote, 1974). In practical systems the study of flammability limits is important in order to determine which mixtures are useful and to learn what factors are important in causing the limit.

The flammability limits are affected by the initial conditions of the mixture, for example, the initial temperature, pressure and dilution with an inert gas. For a given set of initial conditions, the limits are also dependent on both the apparatus used to determine the limits and the direction the flame is propagating with respect to the earth's gravitiational field. A review of the many effects is given by Lovochev et al. (1973). It is the effect gravity has on flame propagation near the lean limit that is the subject of this study.

The purpose of this study is to determine how gravity affects flame propagation which subsequently affects the leanest mixture through which the flame can propagate. It is expected that this information will reveal which, if any, of the theories available are adequate to predict the flammability limits. In order to answer these questions, a series of experiments were performed in which flame propagation was observed both in the earth's gravity field (1-g) and in the absence of a gravitational force (0-g). Experiments to measure the velocity and temperature profiles of a flame propagating in 1-g were also performed.

Laminar premixed flames were used in this study since laminar flames have the simplest and best understood structure. Methane was used for the fuel since historically it has been studied more than other hydrocarbons, and therefore there is more background information available. Also, methane is the only hydrocarbon for which a rather complete kinetic mechanism is available. This is useful when one is constructing flame propagation models. The flames were propagated through an initially quiescent mixture contained in a 50 mm diameter, vertical tube 1.8 m long, open at the ignition end and closed at the other. Originally it was felt that a flame propagating upward through the tube was most affected by gravity. Therefore, the emphasis of this study will be directed toward an understanding of how an upward propagating flame is affected by gravity on earth.

In order for the reader to understand how flame propagation is currently perceived, a number of experimental observations of laminar premixed flame propagation will be presented as well as current theoretical models. The various methods used for determining flammability limits will then be discussed along with the reason for choosing the methods used in this study. Theoretical models used for predicting the flammability limits will then be discussed and critiqued.

The experimental portion of this study is classified into four phases. In the first phase, flame propagation in 1-g was observed and photographed. A flame passage detector was developed in order to provide an electronic reference signal. This detector was used to compare the position of the visible flame with the velocity and temperature distributions. In the second phase, flame propagation in a 2.2 s 0-g drop tower facility (at the NASA Lewis Research Center in Cleveland, Ohio) was photographed. In the third phase, a laser Doppler anemometer was constructed and used to measure the fluid velocity associated with an upward propagating flame. In the fourth phase, a diffuse illumination holographic interferometer was constructed in an attempt to measure the temperature distribution of the upward propagating lean limit flame. The results of each of the four phases are discussed separately. Subsequently, a discussion will be presented integrating the results of all four phases.

CHAPTER II

FUNDAMENTALS OF PREMIXED FLAMES

Laminar premixed flames have been found to propagate through a given combustible gas mixture with a characteristic burning velocity (S_u). This is not necessarily the speed at which a flame propagates relative to the laboratory coordinates even in an initially quiescent mixture. Rather, S_u is the velocity at which the flame propagates relative to the fluid velocity. Conceptually one can think of a flat flame propagating normal to and toward a premixed fuel-oxidizer flow with a uniform velocity profile. In Fig. II-1a, the burning velocity is just equal and opposite to the fluid velocity (U_∞) so that the flame's propagation velocity in the laboratory coordinates (V_p) is zero. If, as in Fig. II-1b, $U_\infty > S_u$ the observed propagation velocity would be in the positive x direction and would be equal to $U_\infty - S_u$. Because flat flames are hard to stabilize, it is more common to observed steady flame sheets that are oblique with respect to the incoming flow direction. In this case, the flame is often conceived as an infinitely thin wave propagating with S_u = constant over the whole flame. As illustrated in Fig. II-1c, the wave propagates only normal to itself at S_u and an element of the flame moves parallel to the flame at $S_{||}$. In the ideal case a flame sheet, in a uniform flow, will relax to an angle α such that

$$S_u = U_\infty \sin\alpha \qquad \text{(II-1)}$$

is satisfied. It should be realized that the 1-D wave concept of a flame is only valid for certain configurations. Flames that are thick compared to their radius of curvature or the physical size of the apparatus violate the above assumption. Experimental methods for measuring the fundamental burning

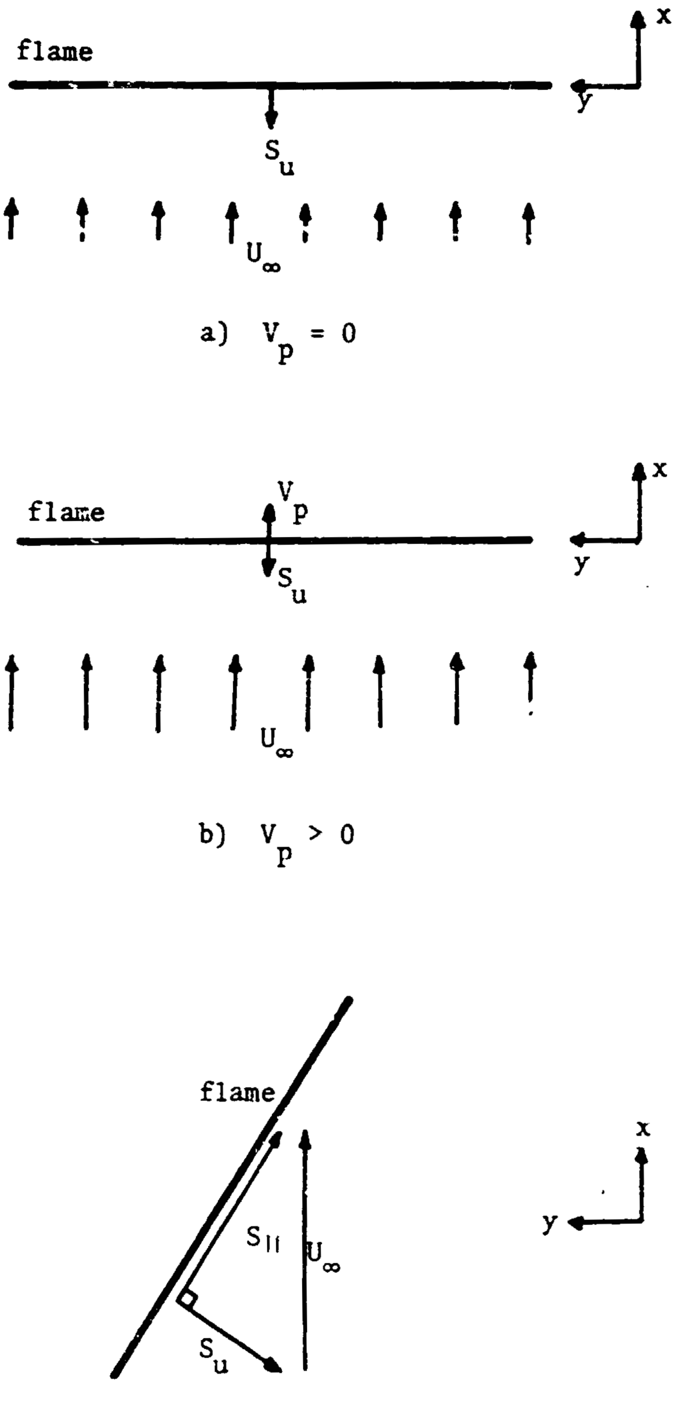

a) $V_p = 0$

b) $V_p > 0$

c)

Fig. II-1. Illustration of Flame Propagating as a Wave.

velocity are discussed and sources of error are critiqued by Gaydon and Wolfhard (1975).

The wave concept is useful when undertaking a phenomenological study of laminar premixed flames. The dependence of S_u on the mixture composition for a methane-air flame is shown in Fig. II-2. The absolute values are of course different for different fuel-oxidizer systems but the basic shape of the curve is the same. In Fig. II-2 the equivalence ratio is defined by

$$\Phi = \frac{X_{fuel}/X_{ox}}{(X_{fuel}/X_{ox})_{stoichiometric}}$$

where X is the mole fraction. By definition $\Phi < 1$ is a (fuel) lean mixture and $\Phi >$ is a (fuel) rich mixture. One can observe that it is a maximum near $\Phi = 1$ and decreases for other values of Φ.

The adiabatic flame temperature of a flame is, strictly speaking, the temperature that would be attained by the given combustible mixture if it were allowed to approach chemical equilibrium at constant pressure with no heat loss to the surroundings. A plot of T_{ad} vs Φ is shown in Fig. II-3.

Another macroscale parameter characteristic to flame structure is the thickness of the flame (Δ). Typically it is determined from the measured or calculated temperature profile of the flame as shown in Fig. II-4. T_u is the unburned or ambient temperature far ahead of the flame and T_{ad} is the adiabatic flame temperature. The reaction zone thickness δ is that region of the flame where the major portion of the reaction takes place. In the abscene of a reaction rate vs x curve, δ is determined from the temperature profile as that region from the inflection point to the point where $T = 0.99$ T_{ad} or by the intercept method shown in Fig. II-4. The preheat zone is that

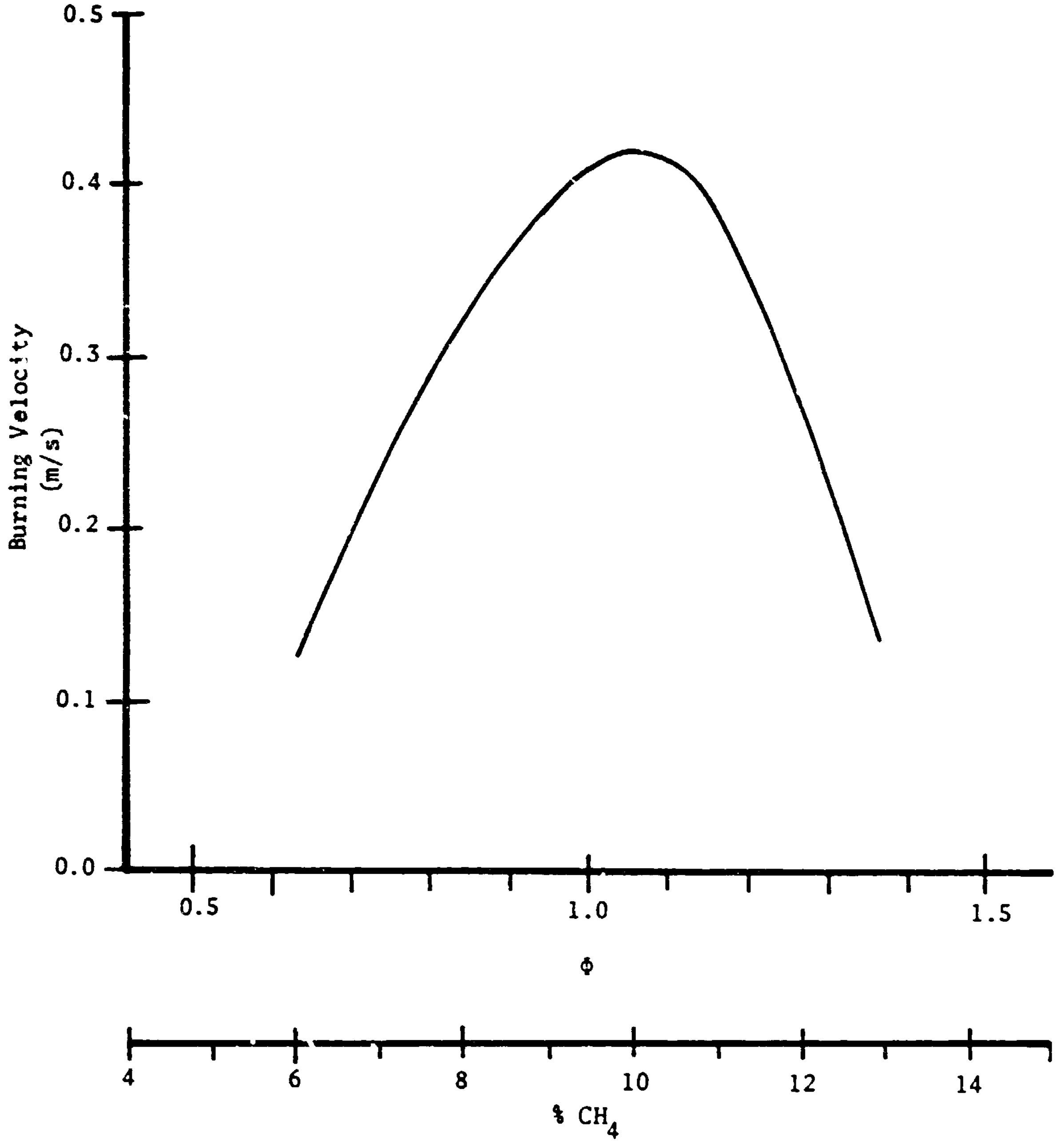

Fig. II-2. Measured Burning Velocity vs Mixture Strength for CH_4 in Air. (From Günther and Janisch, 1972).

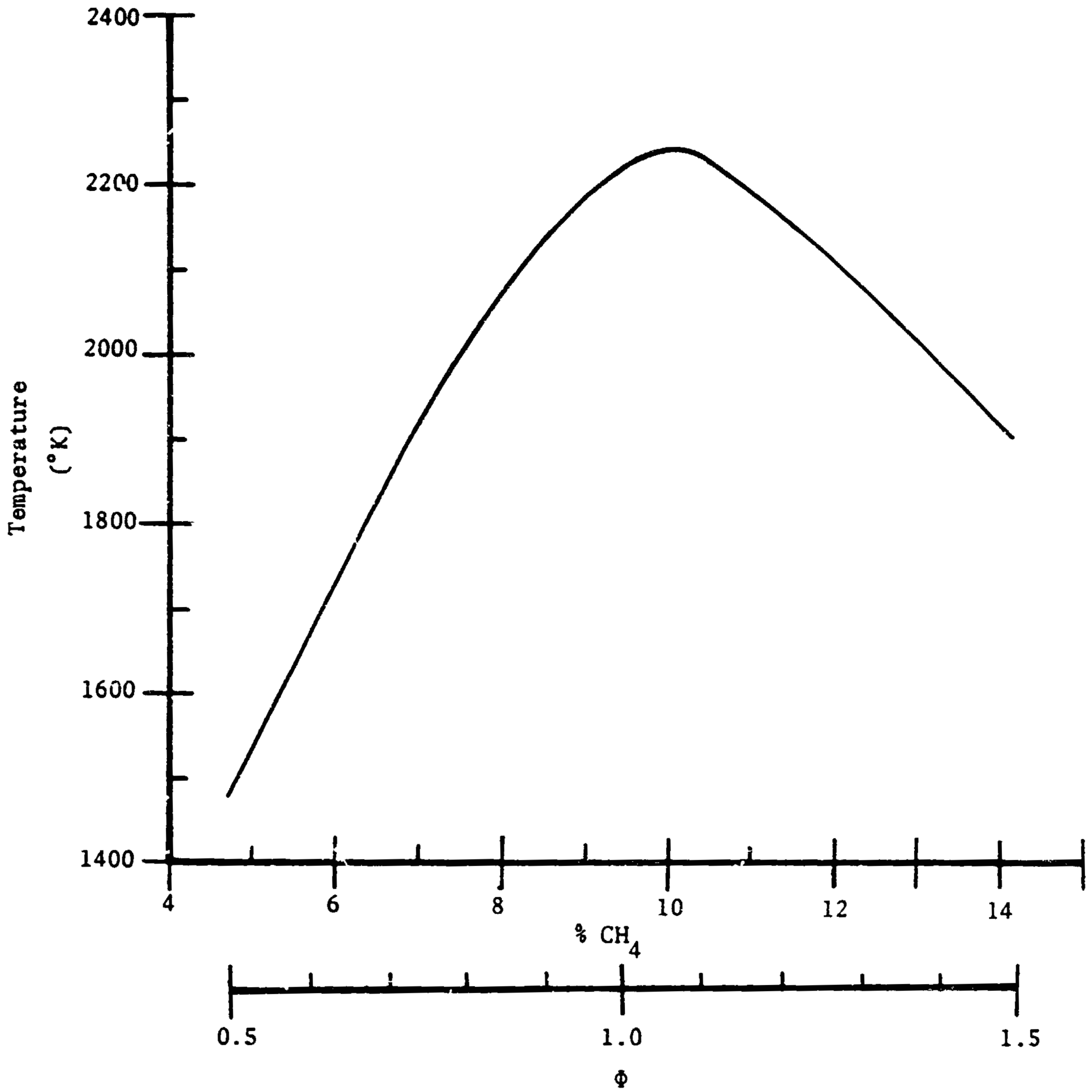

Fig. II-3. Adiabatic Flame Temperature versus Mixture Strength. (From Steffensen et al., 1966).

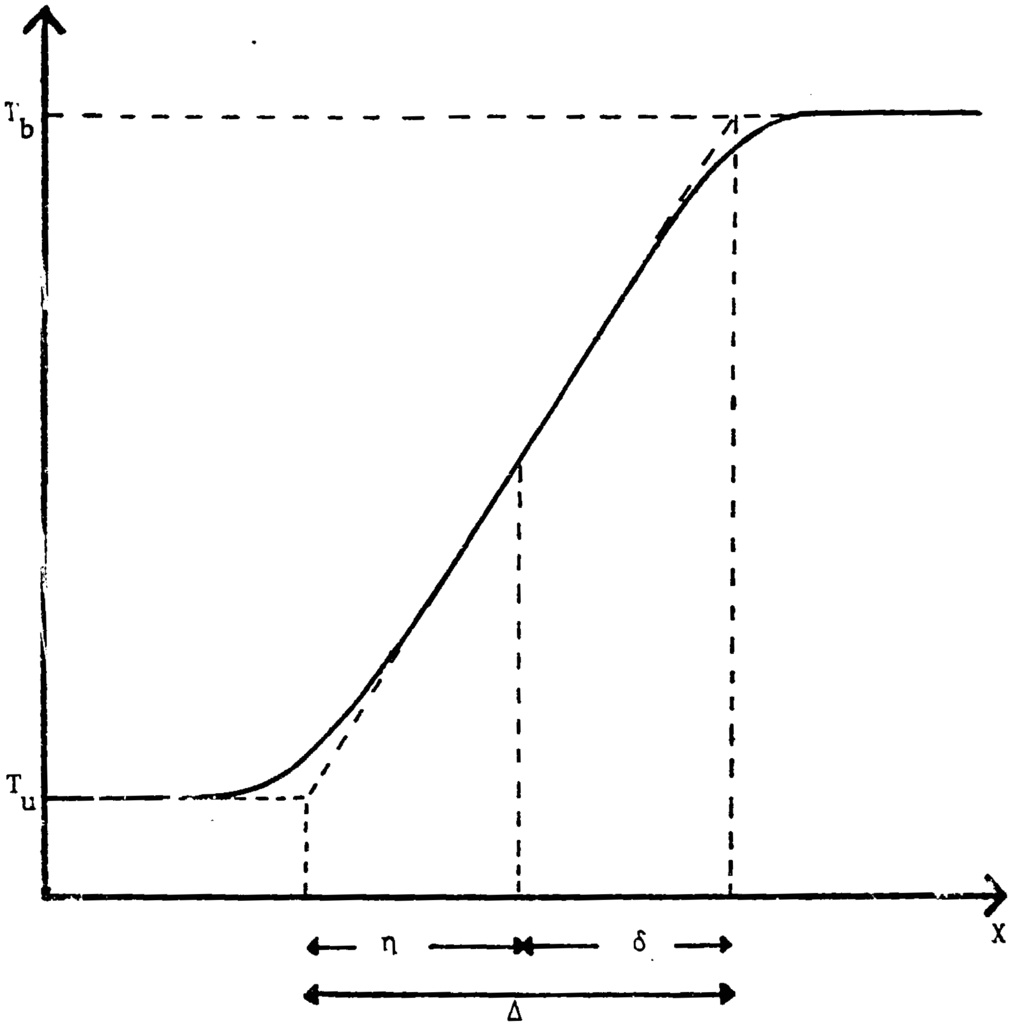

Fig. II-4. Temperature Structure of a One Dimensional Flame.

region ahead of the reaction zone defined by the thickness η. In this region very little heat release from reaction occurs. The increase in temperature is due to energy transport from the reaction zone.

A plot of flame thickness vs Φ is shown in Fig. II-5. These were measured using an interferometric method in a closed bomb for methane-air mixtures at STP on a flame with a 60 mm radius of curvature. It should be noted that the flame thickness is on the order of 10 mm near the flammability limits. Also plotted is the parallel plate quenching distance as a function of equivalence ratio for a methane-air flame. The parallel plate quenching distance is defined as the largest channel dimension for a given fuel-oxidizer mixture that will just keep a flame from propagating through the channel. A quenching diameter is defined in an analogous manner for a tube. In general it has a larger value because of the cylindrical geometry.

The phenomenological behavior of the above parameters provide useful information concerning macroscopic behavior of laminar premixed flames. In order to understand which mechanisms are thought to be important in flame propagation, it is necessary to look at the classical laminar premixed flame models.

Laminar premixed flame theories at first attempted to predict only the burning velocity. These theories were based on intuitive reasoning supported only by physical observation. Mallard and Le Chatelier (1883) developed a theory of burning velocity based entirely on heat conduction. In 1947 Tanford and Pease observed that there was a strong correlation between the calculated equilibrium hydrogen atom concentration and the burning velocity in CO-air flames at various equivalence ratios. In a subsequent paper by Tanford (1947) a theory based on diffusion of hydrogen atoms was compared with a thermal

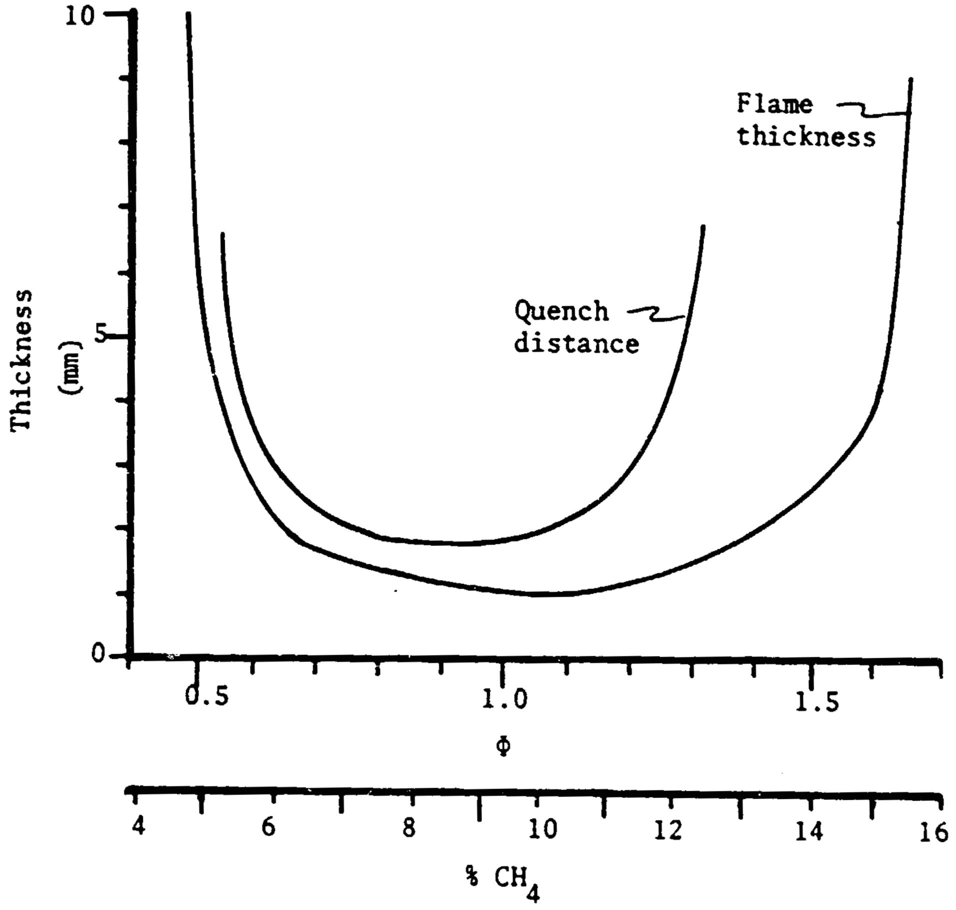

Fig. II-5. Flame Thickness and Parallel Plate Quench Distance versus Mixture Strength. (From Andrews & Bradley, 1972b).

theory based on conduction, convection and heat release by chemical reaction. Tanford concluded that heat conduction was not important compared to the diffusion of hydrogen radicals.

The first attempt to model a laminar premixed flame from a continuum mechanics point of view was undertaken by Hirshfelder and Curtis (1949). They first generalized the hydrodynamics equation to include diffusion and chemical kinetics and then simplified the equation by looking at a one-dimensional steady flame. In this case the global mass balance equation may be written as

$$\sum_{i=1}^{s} \rho_i (S + V_i) = M \qquad \text{(II-2)}$$

where S is the mass average flow velocity, V_i is the diffusion velocity of the i^{th} species and M (= ρS) is the overall mass flow. The steady one-dimensional species equations are written

$$\frac{d}{dx} \{[I](S + V_i)\} = \omega_i \qquad \text{(II-3)}$$

where ω_i is the net rate of production of species i and one equation exists for each of the s species considered in the reaction mechanism. It is also required that

$$\sum_{i=1}^{s} MW\omega_i = 0 \qquad \text{(II-4)}$$

where MW is the molecular weight.

The momentum equation is ignored in this model because the pressure drop across the flame is very small and since it is assumed that the effects of gravity and viscosity are negligible. For example, in a methane-air flame at atmospheric pressure (100 kPa), the presure drop across the flame is approximately 1 Pa and for an acetylene-oxygen flame it is about 100 Pa

(Lewis & von Elbe 1961). The chemical and transport processes are not directly affected by this pressure change. The pressure gradient is, of course, great enough to affect the motion of the gases and can affect the shape of a multidimensional flame. Ball (1951) was able to theoretically predict the shape of a flame in a duct by assuming a constant burning velocity and that the shape is controlled only by the aerodynamics (i.e., using only the continuity and momentum equations). This result supports the premise that flame shape is affected by the pressure gradient.

When writing the energy equation, Hirshfelder and Curtis assumed that the flame is adiabatic and that kinetic energy storage is negligible so that all chemical energy is transferred only to the potential energy of the fluid. Proceeding from the hot boundary (b) the energy equation becomes

$$q = \Big[\sum_{i=1}^{s} [I]SH_i\Big]_b - \Big[\sum_{i=1}^{s} [I]SH_i\Big] \qquad \text{(II-5)}$$

Assuming the heat flux is due only to thermal conduction and energy transport by diffusion (no radiative transfer) (II-5) may be written

$$\sum_{i=1}^{s} [I]SH_i\Big]_b = \sum_{i=i}^{s} [I]SH_i + \sum_{i=1}^{s} [I]H_iV_i - \kappa \frac{dT}{dx} \qquad \text{(II-5a)}$$

where the enthalpy is

$$H_i = H_o\Big)_i + \int_o^T c_{p_i} dT$$

and $H_o\Big)_i$ is the heat of formation. The equation of state is written

$$p = \rho RT \sum_{i=1}^{s} (Y_i/m_i)$$

The net rate of production of species i may be found (as in Williams 1965) from

$$\omega_i = \sum_{k=1}^{n} \omega_{i,k} \qquad i = 1 \ldots s$$

where there are n simultaneous elementary reactions and $\omega_{i,k}$ is the net rate of production of species i in the k^{th} reaction. It may also be written as

$$\omega_{i,k} = \nu_{i,k}\hat{\omega}_k$$

where $\nu_{i,k}$ is the stoichiometric coefficient for the i^{th} species in the k^{th} reaction as that reaction is written. The law of mass action requires

$$\hat{\omega}_k = K_k \prod_{i=1}^{s} [I]^{\nu_{i,k}}$$

For a constant volume process the temperature dependence of the reaction rate for the k^{th} reaction is empirically found and fitted to the Arrhenius expression

$$K_k = A \exp(-E/RT)$$

and in general

$$A = BT^{\alpha}$$

where $0 \leq \alpha < 1$.

Substituting, we may finally write

$$\omega_i = \sum_{k=1}^{r} \nu_{i,k} BT^{\alpha} \exp(-E/RT) \prod_{i=1}^{s} [I]^{\nu_{i,k}}$$

The diffusion velocities are found (as in Strehlow 1968) using

$$[I]V_i = - ND_i \frac{dX_i}{dx} \qquad \text{(II-7)}$$

where N is the total number of moles, D_i is the diffusion coefficient of the i^{th} species in the local mixture and X_i is the mole fraction given by

$$X_i = \frac{Y_i/MW_i}{\sum_{i=1}^{s} Y_i MW_i}$$

D_i is generally found using the expression from Reid and Sherwood (1966)

$$D_i = \frac{1-X_i}{\sum\limits_{i=1}^{s} X_i/D_{i_s}}$$

This assumes the pressure gradient, temperature gradient and body forces present do not affect the diffusion.

The boundary conditions at the hot boundary, from which integration begins, are now definable. As x approaches b the temperature, mass fraction and individual species flow rate ($\mu = [I](S+V_i)$) asymtotically reach a finite value. Therefore

$$\left.\frac{dT}{dx}\right)_b = 0 \qquad \left.\frac{dY_i}{dx}\right)_b = 0 \qquad \left.\frac{d\mu}{dx}\right)_b = 0$$

also

$$V_i = 0$$

For numerical solution it is necessary to iterate to find the eigenvalue M so that the solution satisfies the physical conditions imposed at the cold boundary. The cold boundary does propose a problem since here the reaction rate equations give a finite rate for T_u (initial temperature) and therefore it is necessary to start the solution at a first value of x. Because of the finite reaction the concentration gradients are finite and therefore products tend to diffuse back past the initial point. An artificial flame holder is inserted at the cold boundary such that it must pass fuel and inert gases but will not pass product gas. Because of this there is a slight jump in concentration. The holder is also a heat sink so that there is a finite energy flux at the cold boundary. Resolving this problem mathematically is complicated but realizeable.

The cold boundary problem can be circumvented by using a technique introduced by Friedman and Burk (1953). They look at the case of a simple one step reaction where species I_1 reacts to form species I_2 according to the kinetic law

$$\omega_{I_2} = k_o[I_1] \exp(-E/RT_b\tau)$$

where

$$\tau = \frac{T-T_u}{T_b-T_u}$$

and subscript u and b refer to the unburned and burned states respectively. In this case the reaction rate at the cold boundary is zero and $\tau \rightarrow 1$ at the hot boundary where the reaction rate is high. In order to develop a mathematically simple problem, Friedman and Burk further assumed I_1 and I_2 are ideal gases with constant heat capacities (C_p) and $M\omega_1 = MV_2 - MW$. In order to solve the H-C equations, they were simplified by defining new variables and rewriting them using T as the independent variable. The derivation and form of the simplified H-C equations can be found in Hirshfelder and Curtis (1949). It is, for the purposes of this paper, more instructive to look at the simplified equation after the Friedman and Burk assumptions have been incorporated, yielding

$$\frac{dz}{d\tau} = \beta\left(\frac{1-X_{I_2}}{\tau-z}\right) \exp(-\varepsilon/\tau) \tag{II-8}$$

and

$$\frac{dX_{I_2}}{d\tau} = \frac{1}{Le}\left(\frac{X_{I_2}-z}{\tau-z}\right) \tag{II-9}$$

with B.C.

$$X_{I_2} = z = \tau = 1 \qquad \text{at } x = x_b$$

$$X_{I_2} = z = \tau = 0 \qquad \text{at } x = x_u$$

The new parameters are defined as

$$z = \frac{(S+V_{I_2})X_{I_2}\rho}{S_u\rho_u} = \text{fraction of mass due to } I_2$$

$$\varepsilon = E/RT_b$$

$$\beta = \frac{k_o M\omega\rho}{S_u^2\rho_u^2 C_p}$$

$$Le = \frac{C_p D\rho}{\kappa} = \text{Lewis number}$$

All other parameters are as previously defined. Experimental data allows one to assume that $D \propto T^2$ and $\kappa \propto T$ and therefore Le is assumed constant through the flame. If k_o is assumed independent of temperature β is also constant through the flame.

The equations are easily integrated for the special case where Le = 1 which is a physically good assumption and equations (II-8) and (II-9) may be written

$$\frac{dz}{d\tau} = \beta_c \frac{1-\tau}{\tau-z} \exp(-\varepsilon/T)$$

For Le = 0, which corresponds to D = 0 (and ∴ $V_A = V_B = 0$), $X_{I_z} = z$ and

$$\frac{dz}{d\tau} = \beta \frac{1-z}{\tau-z} \exp(-\varepsilon/\tau)$$

These must be integrated numerically by assigning a value to ε and starting from the $x = x_b$ using an asymtotic formula, as the equations are independent with the given boundary conditions. β_c is the eigenvalue and must be found by iterating until it satisfies the boundary condition at $x = x_u$.

It should be noted that a nonsteady state model for a 1-D adiabatic flame was introduced by Spalding (1956,1971) using the same hydrodynamic equation as before but in the time dependent form. These equations are numerically integrated using a finite difference volume and assuming initial profiles for fast convergence. In this method the flame is propagating in a region of uniform initial conditions and in a region far from the boundaries which cause heat and mass transfer. This results in no cold boundary problem and therefore a complicated multi-reaction mechanism is easily accepted. A steady flame may be modeled with this theory by integrating through time long enough for steady state profiles to be attained.

Although the Friedman-Burk model is rather simple it does provide a useful description of flame structure. Figures II-6 and II-7 are solutions to the Friedman-Burk model for Le = 1 and Le = 0 respectively. These solutions indicate that there is a preheat zone with very little reaction and a reaction zone in the high temperature region where almost all the reaction occurrs. It may also be observed that with diffusion included (Le = 1) the flame is thicker and has a lower burning velocity. According to Friedman and Burk this is physically consistent (at least with the model) as the back diffusion of products would dilute the reactants in the reaction zone and therefore reduce the reaction rate. As pointed out by Strehlow (1968), if radicals were allowed in the flame model, S_u would be enhanced by allowing them to diffuse into the preheat zone. Friedman and Burk also found that the the effect of diffusion increases with increasing ε which corresponds to

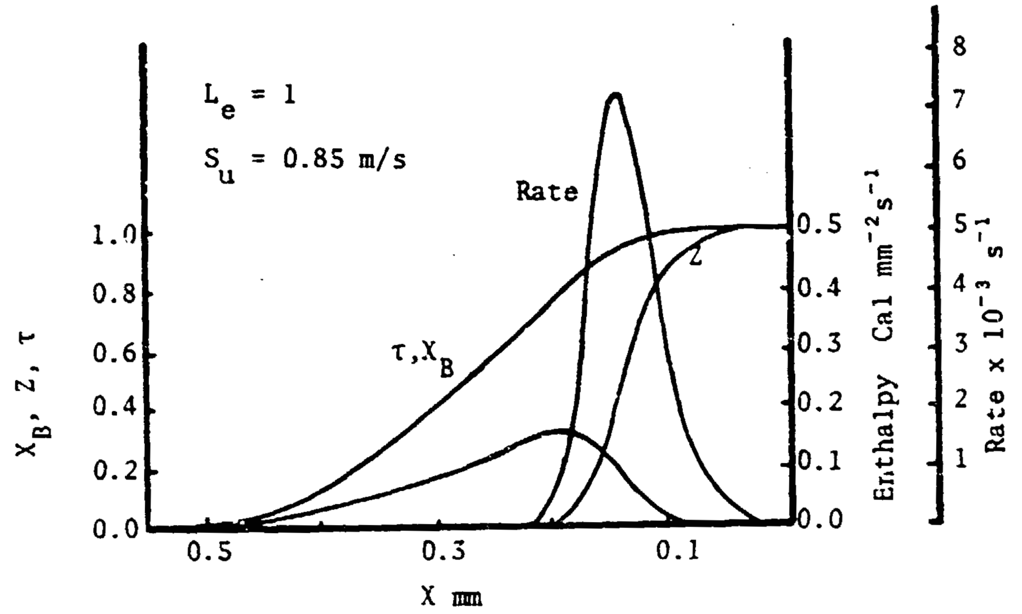

Fig. II-6 Solution to the Friedman-Burk Problem.
(From Strehlow, 1968).

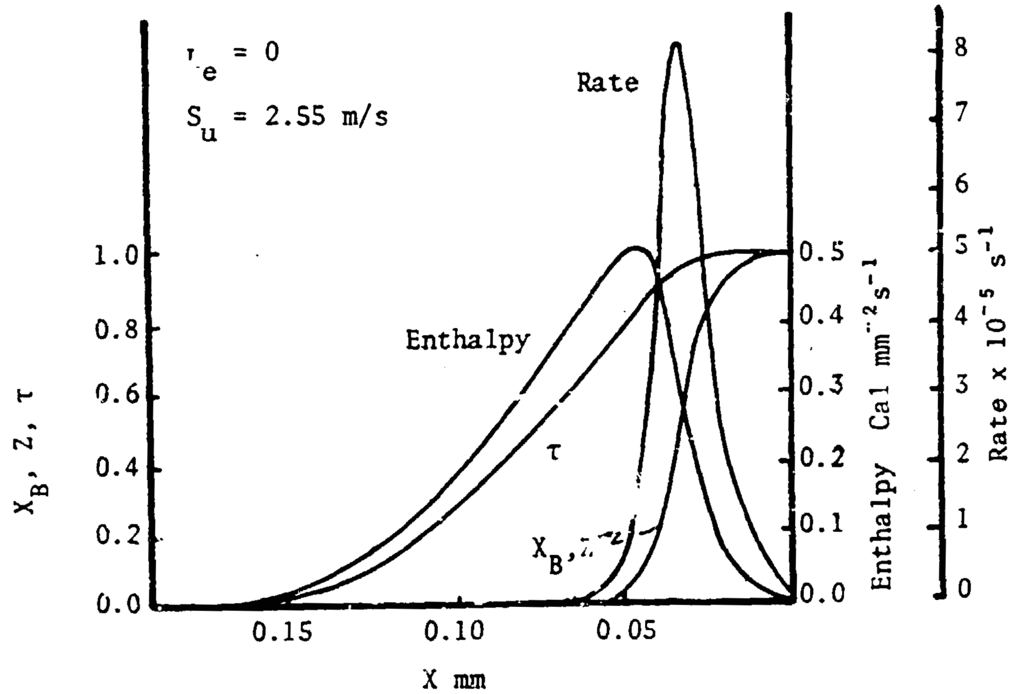

Fig. II-7. Solution to the Friedman-Burk Problem.
(From Strehlow, 1968).

increasing activation energy, E, or decreasing flame temperature, T_b.

Figure II - 8, 9 & 10 represent data taken by Fristrom and Westenberg (1965) in a methane-oxygen flame at 10 kP_a ambient pressure. Lowering the ambient pressure serves only to increase the thickness of the flame making direct probing techniques applicable. Figure II-8 shows that in real flame there exists a preheat zone, primary reaction zone and a secondary reaction zone where equilibrium is slowly reached. Figure II-8 confirms the existence of the secondary reaction zone.

Figure II-9 reveals that the reaction mechanism is far from a single step reaction. Smoot et al (1976) reviewed the literature and subsequently proposed a reaction scheme containing 15 species and 28 reactions for the methane-oxygen system (no N_2 reactions). This reaction scheme was then tested in the previously described nonsteady 1-D adiabatic flame model to compare the steady state macroscopic flame structure with experimental results. The major and minor species concentration profiles were also compared with molecular beam sampling in a flat flame from Peeters and Mahnen (1973). It was concluded that 23 reactions are important.

It has often been assumed that there is one rate determining reaction and therefore the Friedman-Burk model is reasonable. In the work by Smoot et al. it was found that there are at least 3 and in some cases 7 important reactions. This means that when using the Friedman-Burk model one must take care in extrapolating kinetic parameters. Further, Levy and Weinberg (1959) found experimentally that in the low temperature zones of the flame the one step reaction mechanism is not valid. Fristrom and Westerberg also calculated the diffusion velocities of species using equation (II-7). These are recorded in Fig. II-10 and confirm the importance of diffusion in a premixed

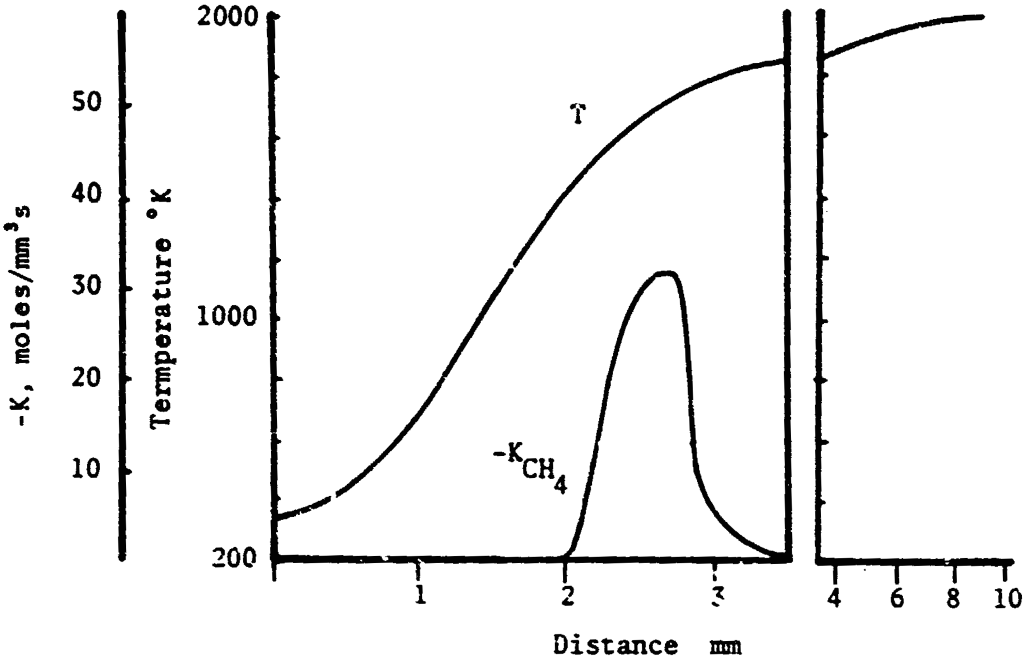

Fig. II-8. Temperature and CH_4 Reaction Rate in CH_4-O_2 Flame at 10.1 KPa. (From Fristrom and Westenberg, 1965).

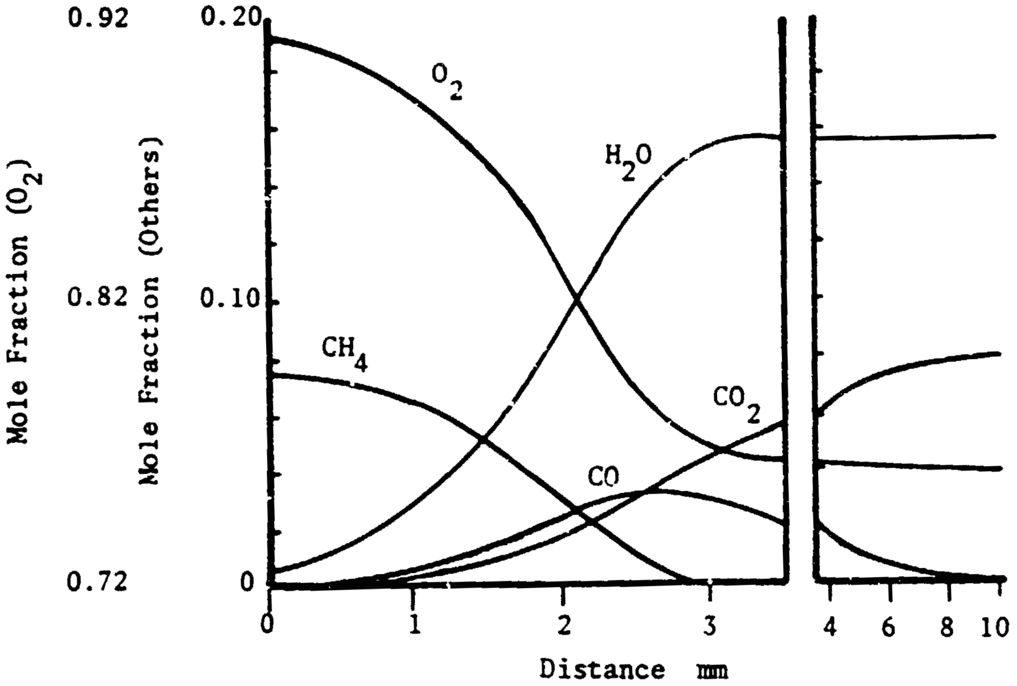

Fig. II-9. Concentration Profiles in Flame of Fig. II-8.

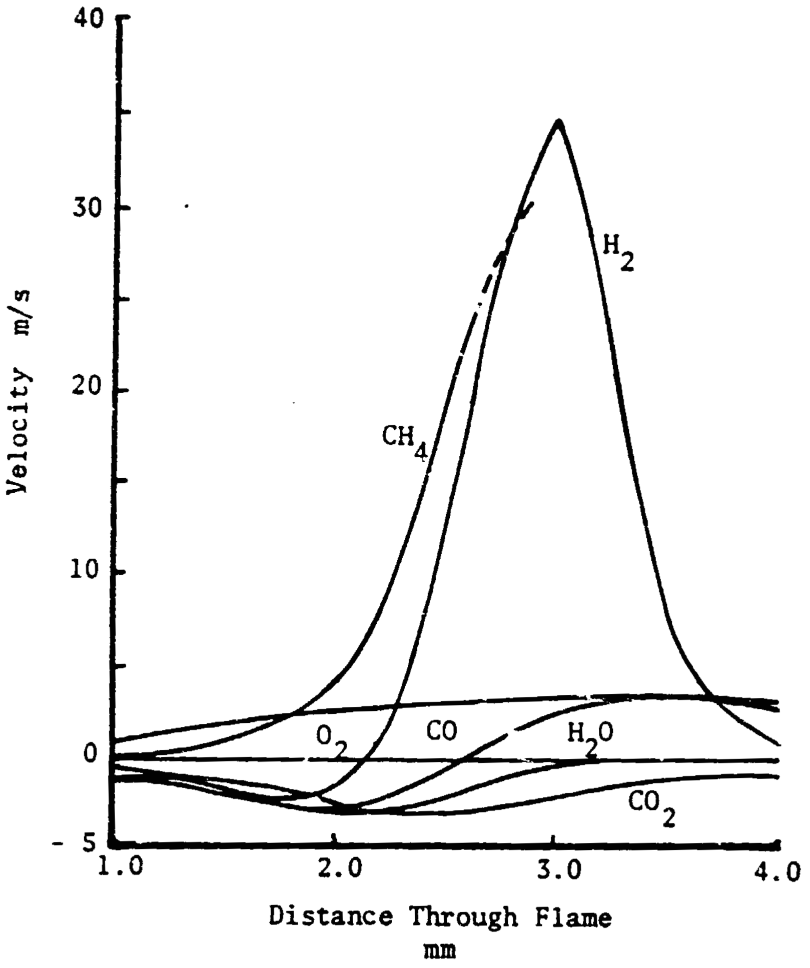

Fig. II-10. Diffusion and Gas Velocities in a 1-D CH_4 Flame @ 10.1 KPa. (From Fristrom and Westenberg, 1965).

flame. In Fig. II-10 the diffusion velocities of the major product species are negative and greater than the local mass average velocity in the preheat and primary reaction zone adding further confirmation to the Friedman-Burk model. Thus there is little doubt but that flame propagation is caused by a complex interaction of heat conduction, species diffusion and a homogeneous exothermic reaction.

CHAPTER III

EXPERIMENTAL DETERMINATION OF FLAMMABILITY LIMITS

Historically, flammability limits have been found by visual observation of a flame to determine its ability or failure to propagate as the composition of the fuel-oxidyzer mixture becomes successively lean or rich. The behavior of the burning velocity, flame temperature and flame thickness as a function of mixture strength give some insight into what happens to a flame as the limit is approached. However, these measured properties are inadequate by themselves to allow one to deduce why a limit exists. Discussion of that question will be reserved until after the presentation of experimental results. This section contains a review of experimental techniques used for determining flammability limits. In each case a description of the flame propagation process near the limit is given. Finally, reasons are given for choosing the flammability apparatus used in this experimental study.

There are four major types of apparatus that have been used for measuring flammability limits. They are the standard flammability limit tube (SFLT), closed bomb, flat flame burner and shrouded tent flame. There is a certain degree if inconsistency between limits taken on the various apparati as shown in Table III-1. It is important to note that in early experiments the method of manufacturing the specific gases that were to be tested and metering the mixture was a major task. In this review no effort has been made to account for this possible source of error. In order to understand why the limits are apparatus dependent one must know exactly what the various apparati are and how they are used to determine the limit in each case. In all reported experiments the mixtures are initially at STP unless otherwise noted.

TABLE III-1

EXPERIMENTAL FLAMMABILITY LIMITS OF METHANE AND AIR (%)

		Lean	Rich
Coward & Jones (1952)	open end 50 mm tube upward propagation	5.24	14.02
White (1924)	" "	5.40	14.25
Payman	" "	5.8	13.3
Levy (1965)	35 mm	5.3	---
Coward & Jones (1952)	open end 50 mm tube horizontal propagation	5.39	14.28
White (1924)	" "	5.65	13.45
Coward & Jones (1952)	open end 50 mm tube downward propagation	5.85	---
White (1924)	" "	6.12	13.25
Parker (1914)	bomb	5.97	---
Andrews & Bradley (1972)	bomb	4.5	15.5
Bone _et_ _al_. (1928)	bomb	5.6	14.3
Egerton & Thabet (1952)	flat flame burner	5.10	---
Badami & Egerton (1955)	" " "	5.31	---
Sorenson _et_ _al_. (1975)	shrouded tent flame	4.00	15

The Standard Flammability Limit Tube

The flammability limit tube was standardized by Coward and Jones (1952) at the U. S. Bureau of Mines as the most appropriate technique for determining the safety of gas mixtures. The report cited is a compendium of flammability tests undertaken up to that time. It includes tube and closed bomb studies for over 140 individual fuels in various oxidizing atmospheres and over 70 fuel mixtures. In order to understand why the SFLT was chosen by Coward and Jones, one must first know how a flame propagates through a tube.

The first major study of flames propagating in a tube was undertaken by Mallard and LeChatelier (1883). They established that there are three major tube configurations through which a flame can propagate, namely:

1) Both ends of the tube closed with ignition at one end or the middle.
2) One end open with ignition at the closed end.
3) One end closed with ignition at the open end (the SFLT configuration).

The direction the flame propagates with respect to the gravity vector is important in all three cases.

Photographs of nonlimit flames propagating through tubes in various configurations were recorded by Ellis (1928, Part VIII). He illustrated that for case 1,as the length of a 50 mm ID tube was varied from 90 mm to 195 mm the time for a flame to develop to a steady shape remained constant but that the distance traveled during that time changed. In fact, the propagation distance for a downward propagating flame doubled as the tube length increased indicating that the pressure build up does affect the propagation speed. For case 2 propagation, a "jerky movement" was observed by Mallard and LeChatelier and was also photographed by Ellis. For case 3 the flame motion was observed to have "uniform movement" after a short time. However, for a certain mixture strength and tube length a "vibratory movement" occurs. This vibratory movement does not usually occur at the limit for tubes shorter than 1.5 m. (See Coward and Jones 1952.)

Because of the above nature of flame propagation in tubes, Coward and Jones defined the SFLT to be a 50 mm ID tube, 1.5 m long, open at the ignition end and closed at the other. The 50 mm diameter was chosen since it was found empirically that flames in smaller diameter tubes exhibit significantly narrower limits and that there was generally no significant change in limits for larger diameters. The effect of the smaller diameter is reasonable in light of the flames quenching behavior defined in Chapter II.

The direction of propagation with respect to gravity affects the limits, the propagation speed, V_p, and the shape of the flame. The effect on the limit mixture is documented in Table III-1. The change in shape and V_p are just as dramatic.

An upward propagating flame of 5.3% methane and air in a SFLT will travel at $V_p = 0.23$ m/sec (Levy 1965). For that mixture the fundamental burning velocity is on the order of 0.05 m/sec indicating that natural convection is augmenting the propagation. In fact, Levy found that lean limit C_3H_8 and CH_4 flames propagate up the SFLT at the same speed as an air bubble (that fills the tube cross section) moves up a water filled tube of the same diameter. The upward flame is highly curved but with a longer skirt than a stoichiometric flame. Photographs are presented in Chapter V.

Coward and Hartwell (1932) observed that for downward propagation from an open end (case 3), the flame is flat in tubes as large or larger than 0.24 m ID for both lean and rich limit mixtures of methane and air. For near stoichiometric mixtures the flame takes on an approximately parabolic shape. The downward propagation velocity of the near limit (6% CH_4 in air) flame is approximately equal to the fundamental burning velocity of 0.10 m/sec. Because of this it was concluded by Coward and Hartwell that "...if convection is ever absent in explosives of methane-air mixtures, initiated at the open end of the tube, it is only so when the flame travels downward..."

The horizontal propagating flame (case 3) travels at a velocity somewhere between the upward and downward flame velocities (Coward and Hartwell 1932). The shape is still curved but very asymmetric with the leading edge traveling near the top of the horizontal tube.

Because of the effect of propagation direction, Coward and Jones further defined the standard test to be for the upward propagating flame as in this case the limits are the widest and therefore are best for determining whether or not a mixture is hazardous. In summary, a gas mixture is defined by Coward and Jones as flammable if a flame can propagate upward the full length of a vertical 50 mm ID tube, 1.5 m long, open at the bottom (the ignition end) and closed at the top.

A flame propagating in a standard flammability limits tube has two stages of propagation. In the first stage (immediately after ignition) the flame develops from a small flame kernel to one which fills the cross section of the tube. In this stage the flame is unsteady or the kernel is expanding and simultaneously translating at an increasing speed up the tube. In the second stage the flame has attained a constant propagation velocity and shape as it proceeds up the tube. In stationary (laboratory) coordinates the motion of the gas ahead of the flame is away from it (upward) at the center region of the tube and downward near the wall. Behind the flame, in the hot gas region, the flow is downward throughout the tube. This is depicted in Fig. III-1.

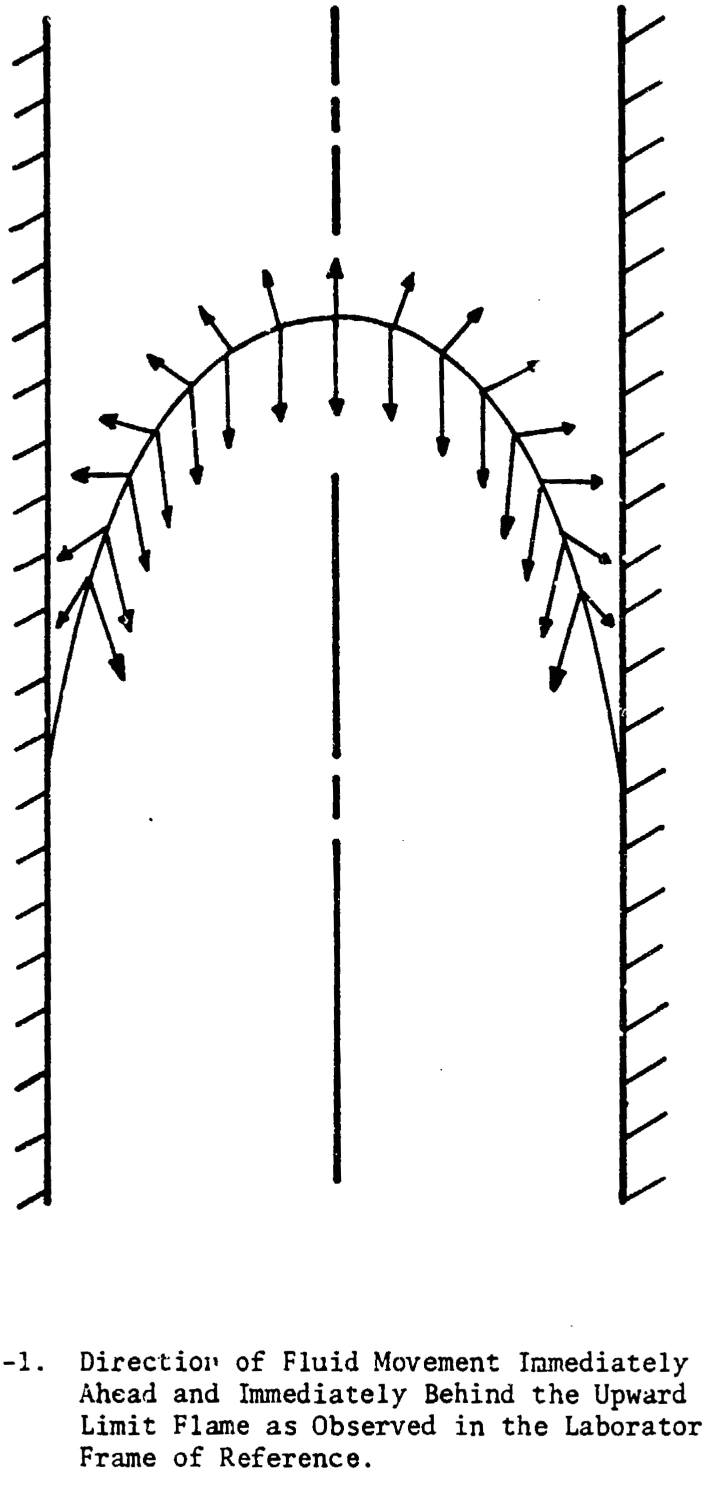

Fig. III-1. Direction of Fluid Movement Immediately Ahead and Immediately Behind the Upward Limit Flame as Observed in the Laboratory Frame of Reference.

This means the flow is unsteady since a fluid element at the centerline will initially be at rest, move upward, go through zero velocity and then move downward. If one can consider this flame to propagate as a wave, a transformation into coordinates that follow the flame will render the flow steady.

The manner in which a flame is extinguished is not clearly described in the literature. However, Levy (1965) observed the extinguishment process of an upward propagating lean limit methane-air flame using a schlieren system. He forced the flame to fail at a given region of the tube by propagating the flame from a slightly rich region into a mixture just outside the normal lean limit. He found that a hot bubble would continue to rise undeformed for 0.15 m (3 tube diameters) after the visible flame failed. According to his description the bubble then broke up.

The Closed Bomb

A closed bomb is either a constant volume sphere or circular cylinder with the height equal to its diameter. Ignition is generally at the bottom or center of the vessel. Early experiments used glass vessels that allowed visual inspection of flame propagation. Burgess and Wheeler (1914) used a 2.5 liter glass sphere for their experiments and made the following observations using CH_4, O_2 and N_2:

> "In all the limit mixtures the manner in which the flame travelled was the same. So soon as the igniting spark had been passed a flame shot up to the top of the vessel, bent over, and, after thus filling the whole of the top quarter of the globe, travelled downwards to the bottom as a uniform layer of light blue color."

Experiments using the same apparatus were undertaken by Parker (1914) and he made the following observations on lean CH_4 and O_2 flames:

> "...it was found that a mixture containing 5.94% of methane did not inflame throughout, the flame only filling the upper three-quarters of the bulb. A 6.01% mixture was then made, and was found to inflame throughout."

Photographs of this behavior were taken by Ellis (1928) and are shown in Figs. III-2 a & b. These were taken in a 2.4 liter sphere filled with CO in air and ignited at the base. The mixture strength in Figs. III-2a and 2b are 11.6% and 11.8% respectively. Since Coward and Jones found the lean limit mixture to be 12.5% in the SFLT, these are assumed to be near lean limit mixtures. Figure III-2a illustrates that the toroidal shape forms very early near the limit. These photographs further illustrate that *near the limit* a spherical flame never exists and, in fact, a very complicated flow pattern exists due to natural convection. Further, the limit itself is not well defined since partial propagation exists for a wide region of mixture strength. The flame may go out while the flame kernel is still small and translating upwards, or it may go out after it has filled the top of the vessel and only the lower downward propagating flame surface exists. The latter behavior appears to be occurring in the second exposure of Fig. III-2b. This region of limit ambiguity was presented quantitatively by Lovachev *et al.* (1973). He reported that for mixtures of CH_4 and air in a 0.18 m diameter sphere with center ignition, the fraction fuel consumed smoothly falls from 1.0 starting at 6.5% CH_4 to 0 at 5.5%. Although no visual observations were reported, this helps to identify mixtures that support only partial propagation.

The Flat Flame Burner

The use of a flat flame burner for determining flammability limits was first suggested by Powling (1944). The burner consisted of a 60 m diameter

a

Exposure 0.204 s After Ignition

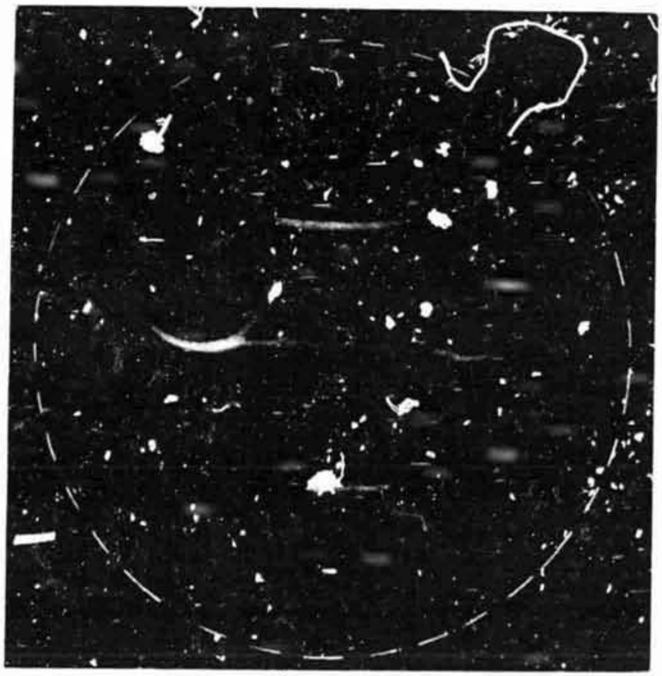

b

Exposures 0.408 s and 1.63 After Ignition

Fig. III-2 Photographs Taken by Ellis (1928).

tube with a wire gauze burner head producing a uniform flow. The burner was shrouded by a 100 mm glass jacket with a curtain of inert gas between the jacket and burner flow. A screen (top plate) was used at the exit of the jacket to stabilize the flow. The flame can be made to appear flat and therefore it is thought that the flame approximates a 1-D (nonadiabatic) flame. Egerton and Thabet (1952) observed that as the matrix and rim of the burner heat up, the flame has a complex shape. They also found that the heat radiated from the top plate affected the distance the flame would stand off the burner head, i.e., when the top plate was closer to the burner head so was the flame. In fact the top plate had to be moved closer to the head to stabilize low burning velocity flames. The flow at the edge of the burner head was probably hotter than at the centerline as the rim was 30°C hotter. Since the flow in this region diverges around the edge of the flame in this region, the temperature increase near the rim was felt to be a stabilizing factor. The gas near the centerline was preheated by a burner head to 140°C for near limit flames. To correct for this, the measured value of the limit mixture was decreased by an amount of fuel "thermally equivalent" to the heat provided by the preheating.

Dixon-Lewis and Isles (1957, 1959) used a flat flame burner with an electrically heated top plate and the head matrix heated only by radiation. Thermocouples were used to measure the temperature profiles in limit ethalene air flames and are shown here in Figs. III-3 a and b. In the high temperature case there is no well defined limit but in the low temperature case there is. They also found $T_{max} - T_{ad}$ increases as the flame gets closer to the top plate indicating that heat loss in the downstream direction as well as the upstream direction is important. Finally, they found when only the head matrix was

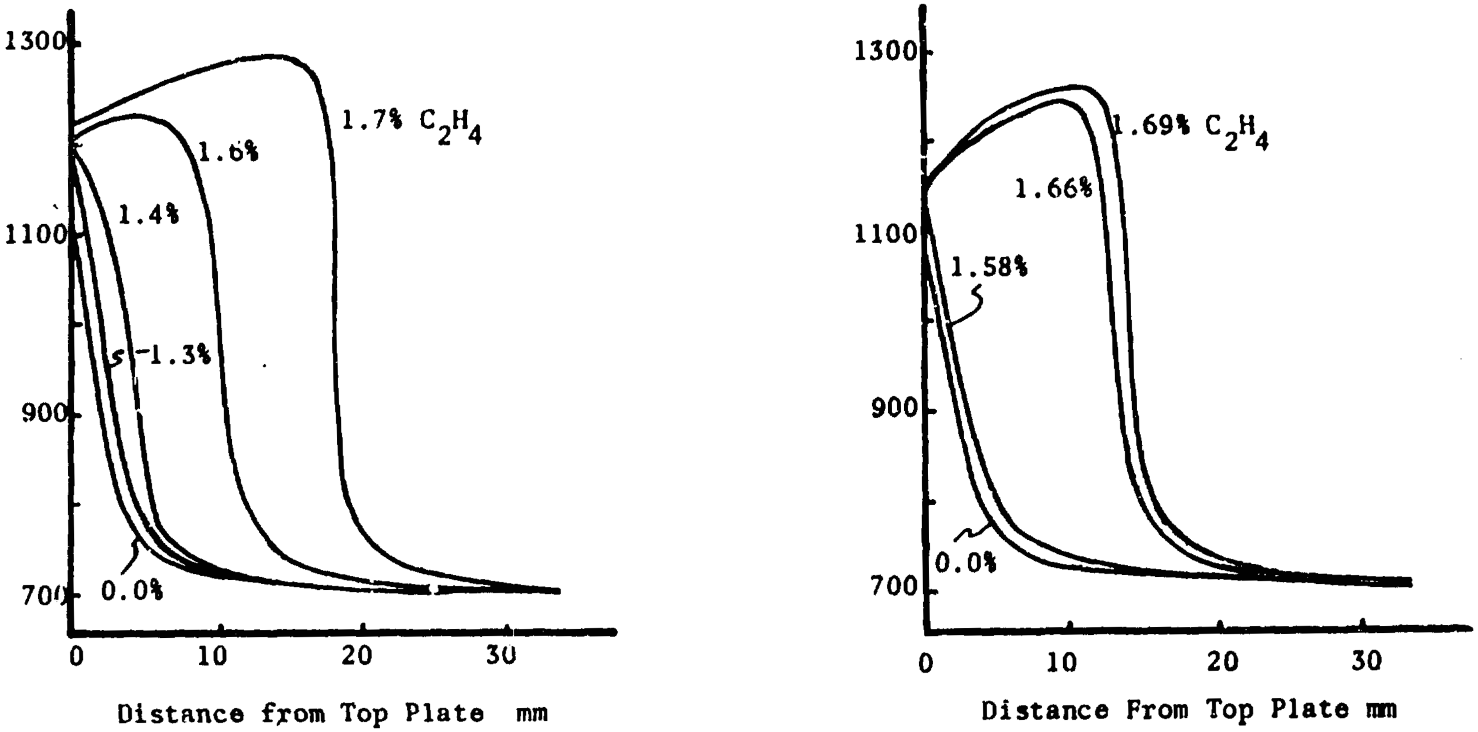

a) Top Plate Temperature = 1200°K

b) Top Plate Temperature = 1140°K

Fig. III-3. Temperature Structure of Lean Limit Ethylene-Air Flames on a Flat Flame Burner for Different Mixtures. (From Dixon-Lewis & Isles, 1954).

electrically heated, that for a given matrix temperature "the slower flames had a larger diameter and took up a higher stable position in the chimney." This indicates that the flame took a position which allowed more upstream divergence and a larger flame area so that the mass average fluid velocity was lower at the stable position than at the burner head. Further, the limit on a flat flame burner was described by Dixon-Lewis and Isles to occur when

> "...they (the flames) are unable to
> recover from chance disturbances."

It is reasonable to assume that aerodynamic stability plays a major role in determining limits on a flat flame burner.

Instability behavior was also reported by Kydd and Foss (1964). In their study CO-air and C_3H_8-air test flames were maintained on a flat flame burner 0.25 m in diameter surrounded by a 25 mm annulus with a lean hydrogen-air flame to stabilize the test flame (see Fig. III-4). In some tests a hot boundary diffusion flame was provided by injecting methane through the screen and therefore producing an artificially high temperature downstream boundary. As expected, this resulted in wider limits (1% CO-air) than a "cool" downstream boundary. When a cooled metal plate was inserted "above the test flame", three-dimensional instabilities occurred. In lean flames "holes" formed in the flat flame with reversed flow (opposite to the incoming test fuel-air stream velocity). It is implied that these holes move radially outward in the test flame. The holes are larger for leaner mixtures until they are so large that the entire flame fails. Kydd and Foss also reported that in

> "Flames of near stoichiometric mixtures
> burning at low velocity...these holes
> are smaller and move more rapidly than
> those due to flow reversal."

They conclude that the "holes" result from Taylor instabilities due to the

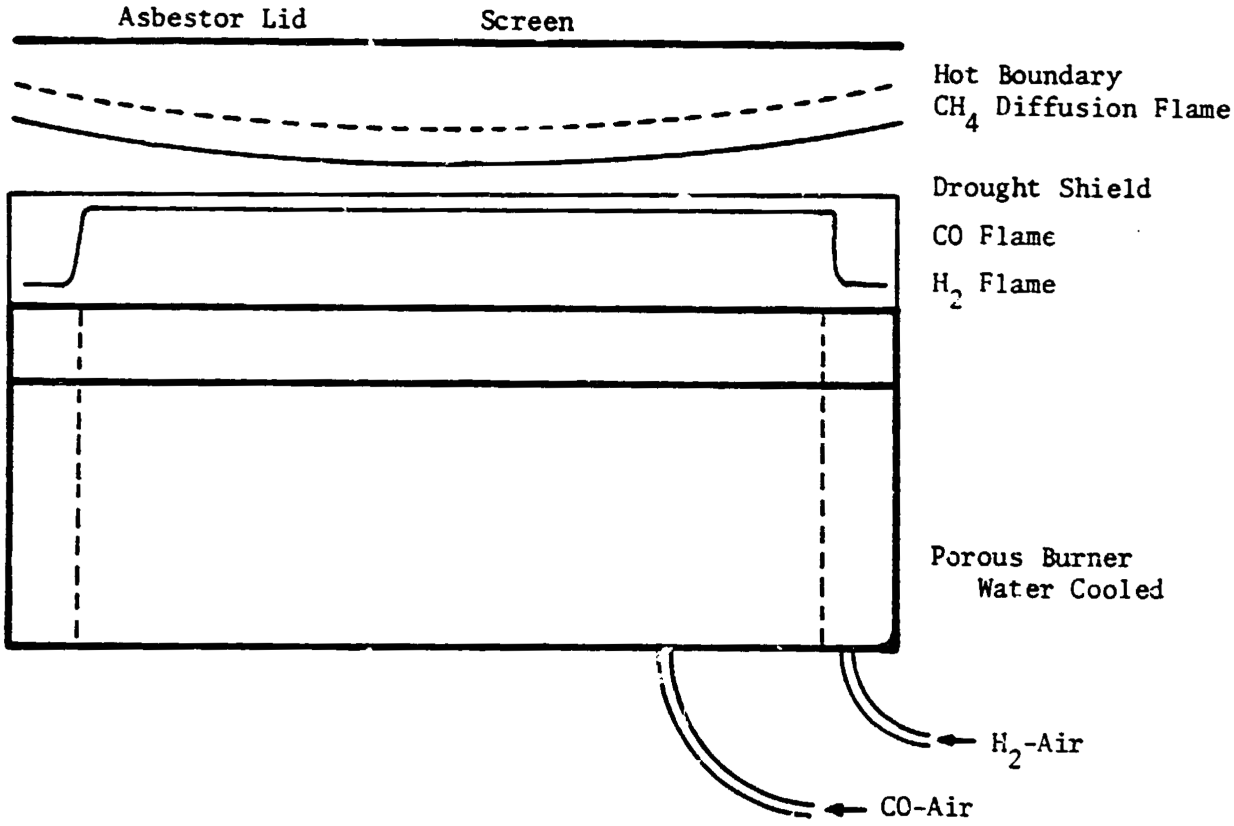

Fig. III-4. Flat Flame Burner of Kydd & Foss (1964).

negative temperature gradient with respect to the gravity vector.

The apparatus of Kydd and Foss is very complicated from an aerodynamic point of view, however, very little discussion was given concerning this aspect. Since a nonporous plate is placed downstream from the flame, a stagnation point must exist at some vertical position on the centerline of the burner. All the incoming gas mixture has a predominately vertical velocity while the gas must exit in an axial direction. Because of this complex flow field, it is not clear that the instabilities observed by Kydd and Foss are the same instabilities observed by Dixon-Lewis and Isles. It is possible that the instabilities are a result of gravity in both cases but that the steeper temperature gradient in the work of Kydd and Foss resulted in a considerably different aerodynamic behavior.

The flat flame burner is very attractive for varifying 1-D flame models of nonlimit mixtures. However, the occurrence of aerodynamic instabilities make limit determination very complicated in this type of apparatus.

The Shrouded Tent Flame

The shrouded tent flame technique for flammability limits was conceived by Sorenson *et al.* (1965). The burner head consists of a matrix of 2.7 mm ID tubes, 50 mm long. There is a rectangular test stream 51 mm by 75 mm surrounded by a rectangular annulus 25 mm wide in its major length and 38 mm wide in its major length and 38 mm wide in its minor length. The annulus supplies what is termed the "ignitor flame" which provides a stabilizing heat source for the holding point of the flame (see Fig. III-5). A rich ignitor flame is used for a lean test flame and vice versa. As the test mixture nears the limit for a given flow rate, the included angle formed by the test flame

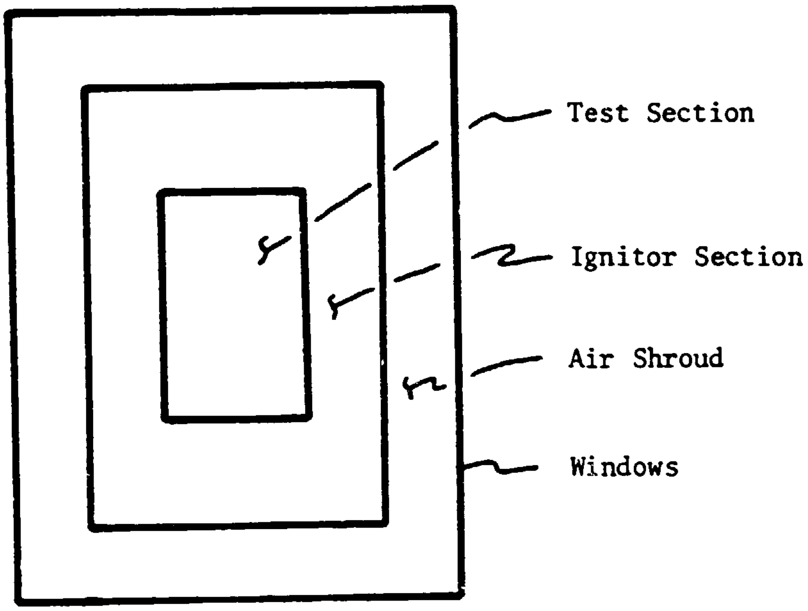

Top View of Burner Head

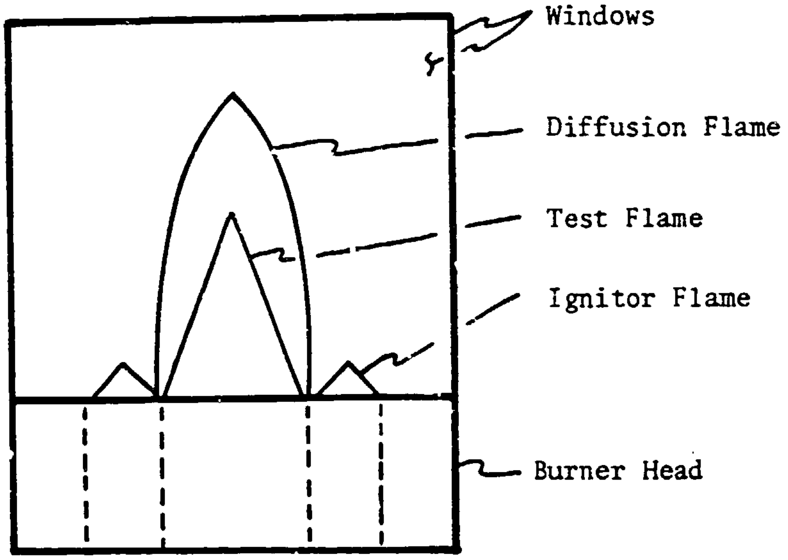

Fig. III-5. Illustration of Shrouded Tent Flame Burner used by Sorenson *et al.* (1975).

becomes smaller until at the limit the top opens up and two nearly vertical flame sheets exist. It was shown in Table III-1 that the limits using this technique are wider than those using other techniques.

In a later study on this burner (Mehi 1977) it was found from schlieren photographs and gas sampling that a diffusion flame exists between the test flame and the ignitor flame. The gas sampling resulted in a horizontal mapping of the species concentrations in the burner just above (downstream from) the peak of the test flame (refer to Fig. III-5). Gas samples were extracted at various horizontal positions but all at the same height. It was concluded that H_2 and CO (products of the rich ignitor flame) were reacting with excess O_2 from the lean test flame. The resulting diffusion flame would produce an excess of CO_2 and H_2O which then diffuse away from the diffusion flame (see Fig. III-6). The presence of this diffusion flame and the steep concentration gradient in the horizontal direction could affect the position of the test flame. As $\Phi \rightarrow 0$, the test flame merged with the diffusion flame. This would mean that values of S_u using Eq. (II-1) and the angle α are incorrect. Therefore, the criterion for the limit mixture was defined as that mixture for which there was a sharp change in the flame angle vs Φ curve. Even though a meaningful value of S_u could not be calculated from the experimental data, it was concluded that:

> "...the only factor that could have an
> effect on the limits observed in this
> burner are the rapid reduction in
> burning velocity as the composition
> becomes nonflammable."

As was noted in the introduction, the major purpose of this thesis is to study the effect of gravity on lean limit flame propagation. There is no easily defined gravitational effect in the case of the flat flame burner or the shrouded tent flame and therefore these two techniques are not useful to the

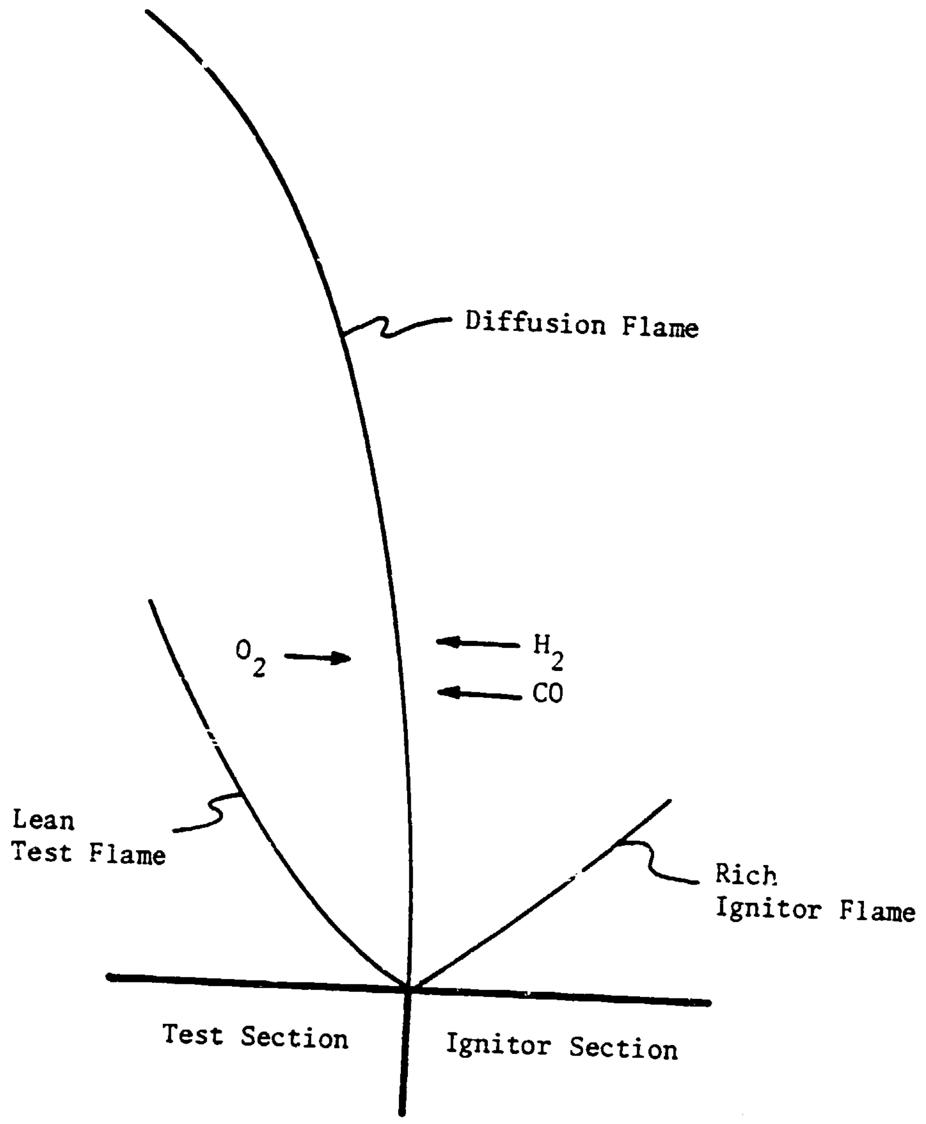

Fig. III-6. Illustration of Diffusion Flame (From Mehl, 1978).

above purpose. It is obvious from the above discussion that gravity is greatly affecting the fluid mechanics of the flame in a tube and the closed bomb. One could of course attempt to develop a totally new technique (or apparatus) for determining the effect of gravity on limits. However, using an established technique aides in verification and evaluation of any new 1-g results.

The similarities and differences between flame structure in the SFLT and the closed bomb lie in the nature of the fluid mechanics. First of all, they both represent flame propagation far away from an ignition source into initially quiescent mixtures and are somewhat dependent on the ignition source. Far away from the ignition source the fluid mechanical forces are not a result of externally forced convection as they are in flames held on burners. Instead there is forced convection as a result of the expansion due to chemical reaction as well as natural and/or free convection due to gravity.

In the case of the closed bomb one might surmise from the previous observations thatthe free convection exists some time after ignition but before the flame becomes large with respect to the vessel. This was demonstrated by Andrews and Bradley (1972). Although natural convection still exists, the influence of the walls on the flow field at later times precludes the existence of free convection. After the flame kernel fills the top of the chamber, only downward flame propagation exists and gravity acts to form a hydrodynamically stable thermal convection field. The complicated flow fields and continual transition from one regime to another does not make the closed bomb attractive for a well defined experimental investigation intended to separate physical phenomena. Likewise it is not attractive for the development of a reasonable analytic model.

The standard flammbility limit tube, on the other hand, produces a limit flame that becomes constant in propagation speed, has a constant symmetric shape and has well defined physical boundaries. This is not to say that it is a simple system to model but relative to the closed bomb it has far more potential. The SFLT also permits total separation of the upward and downward propagating flame front and therefore one can be studied independent of the other. For a first investigation of the importance of gravity on near limit flame propagation the SFLT is far more tractable. This is why it was chosen for this investigation.

CHAPTER IV

MODELS FOR THE THEORETICAL PREDICTION OF FLAMMABILITY LIMITS

Beginning in the early 1950's, a number of analytic theories were developed attempting to predict flammability limits. They all assume non-adiabatic flames in which heat loss is the only important limit criterion. Recently, models attempting to explain the effect of natural convection have been developed. From the material presented so far, the reasons for taking these two avenues of approach are obvious. This section will first review and critique the above theories. Finally, a presentation will be made reviewing other limit criterion based on conceptual models developed from observations on the behavior of near limit flames. A critique of the latter concepts will be presented after the results of the current experimental study are described.

The Limit Predicted by Heat Loss

Spalding (1957) attempted to predict limits using the steady state, constant pressure, constant C_p, 1-D flame equations with an $A + B \rightarrow C$ reaction scheme. The solution technique required that the flame be divided into two regions:

1) $x < 0$ where the reaction was allowed to occur with no heat loss
2) $x > 0$ where heat loss occurred with no reaction

For this technique to be used, he further required that $[A] = 0$ at $x = 0$.

In the flame region ($x < 0$), Spalding wrote the energy equation assuming the heat generation had a $[A]T^n$ dependence. The species conservation and energy equations were then integrated (in nondimensional form) from $x = -\infty$ to $x - 0$ assuming

$$[A] = [A]_{-\infty} \quad , \quad T = T_{-\infty} \quad @ \quad x = -\infty$$

and

$$\left.\begin{array}{ll} [A] = 0 \quad , & \dfrac{d[A]}{dx} = 0 \\ T = T)_{-} \quad , & \dfrac{dT}{dx} = \left.\dfrac{dT}{dx}\right]_{-} \end{array}\right. \quad @ \quad x = 0$$

In order to further simplify the solution he assumed that $T)_{-} \simeq T_{ad}$ and $\frac{d[A]}{dx} \simeq 0$. The final form of the solution is valid only near $x = 0$, for low heat loss and contains no dependence on concentration.

In the post-reaction zone $(x > 0)$ the energy equation was rewritten with no heat addition due to reaction and therefore no species conservation equation is required. Heat loss is included by assuming a T^m dependence and assumes $T^m \simeq (T)^m_{x=0}$. The equation is integrated assuming

$$T = T_{+} \quad , \quad \frac{dT}{dx} = \left.\frac{dT}{dx}\right\}_{+} \quad @ \quad x = 0$$

$$\frac{dT}{dx} = 0 \quad @ \quad x = +\infty$$

$x = 0$ is then used in the solution. The solution for the flame zone and the solution for the post-reaction zone are then matched at $x = 0$ by requiring

$$T)_{+} = T)_{-} = T_{max}$$

and

$$\left.\frac{dT}{dx}\right\}_{-} = \left.\frac{dT}{dx}\right\}_{+}$$

In essence Spalding has solved for a 1-D flame with 1-D heat loss at the hot boundary.

In order to determine the character of the solution, he assumed the heat loss had a T^n dependence to simulate radiative losses. The bulk heat loss due to radiation was acquired from engineering data for a CO_2 and H_2O mixture at 1500°K in an infinitely long tube. He then assumed that the heat generation was characterized by $n = 11$. The solution is shown in Fig. IV-1. The model predicts that two burning velocities exist for each value of heat loss. As the heat loss increases a critical value of heat loss is reached such that only one value of burning velocity exists. As the heat loss is increased beyond the critical value only imaginary eigenvalues exist. The higher value for burning velocity was shown to be stable based on mathematical arguments while the lower value of the velocity was not. Spalding further submitted that the flammability limit is determined by the heat loss and therefore occurs when the critical value is reached.

It is evident that, even assuming the heat loss assumptions are good, the simplifying assumptions used to make the equations easily integrable have mathematically restricted the solution to the region of T_{max} at $x = 0$. Further it is not reasonable to assume that $T_{max} \approx T_{ad}$ near extinction. It is not clear that this model adquately describes a flame.

Mayer (1957) attempted to explain the flammability limits by a simpler model. He assumed one can make a distinction between the quench condition, which is controlled only by convective heat loss, and the composition (flammability) limit. The latter is assumed to be controlled only by radiative losses from the post reaction gases and subsequent conduction losses from the reaction zone to the post-reaction zone. Mayer wrote the energy equation for the flame as

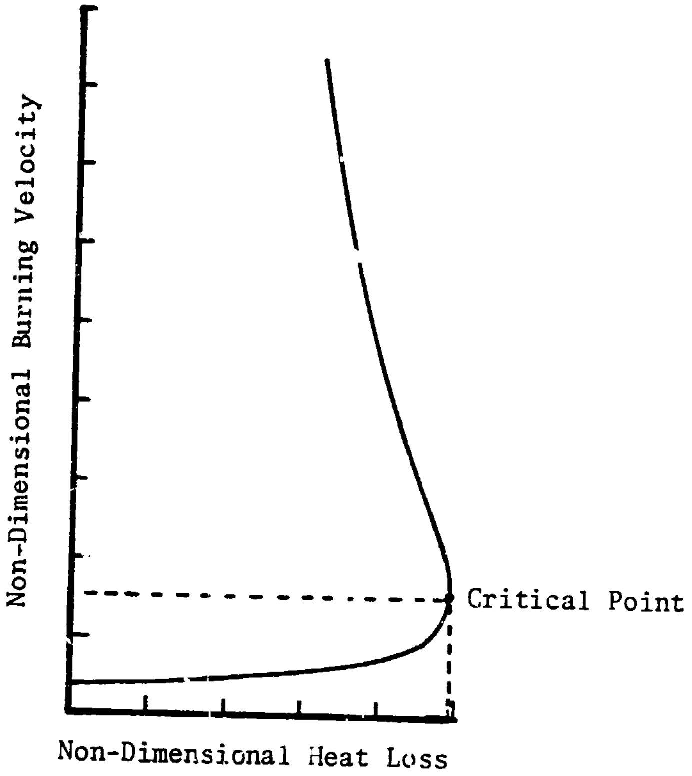

Fig. IV-1. Solution to 1-D Nonadiabatic Flame Equations of Spalding (1956).

$$\begin{aligned} q_{loss} &= \rho_u S_u [\bar{C}_p T_u + H_{ad}] \\ &\quad - \rho_u \bar{C}_p S_u T_f \\ &= \rho_u \bar{C}_p S_u (T_f) [T_{ad} - T_f] \end{aligned} \qquad \text{(IV-1)}$$

where

$$\begin{aligned} S_u(T_f) &= B \exp(E/RT_f) \\ &= S_u\Big]_{ad} \exp(E/2R) \left(\frac{1}{T_{ad}} - \frac{1}{T_f}\right) \end{aligned} \qquad \text{(IV-2)}$$

The radiative heat loss was given by

$$q_{rad} = \frac{K_b Q_{rad}(T_f)}{\rho_u \bar{C}_p S_u (T_f)} \qquad \text{(IV-3)}$$

where $Q_{rad}(T)$ is the volumetric heat loss rate given by

$$\begin{aligned} Q_{rad}(T) &= C^a (T_f^2 - T_u^2) \\ &= 4.1 \times 10^{-7} \{p_{CO_2} + 0.18\ p_{H_2O}\} (T_f^2 - T_u^2) \end{aligned} \qquad \text{(IV-4)}$$

Equation IV-4 was derived from a T^4 flux dependence and a T^{-2} dependence of gas emissivity. A plot of q_{loss} and q_{rad} is given in Fig. IV-2. The composition limit at point p was found analytically by substituting

$$\frac{dq_{loss}}{dT_f} = \frac{dq_{rad}}{dT_f}$$

into the equation

$$q_{loss} = q_{rad}$$

given by equation VI-1 and VI-3.

The kinetics are included in this model through Eq. (IV-2). This

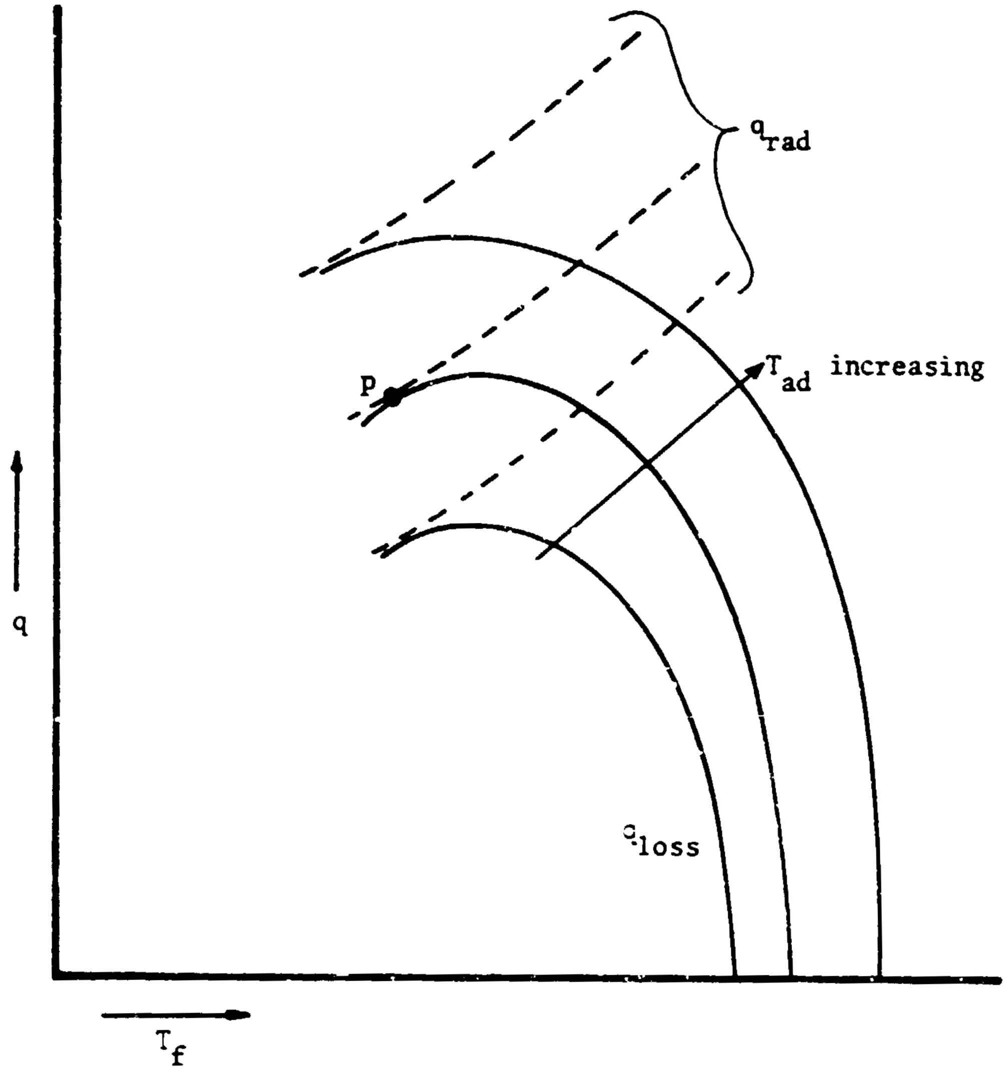

Fig. IV-2. Heat Loss versus Final Flame Temperature for Flammability Limit. (From Meyer, 1957).

relation for burning velocity is a correlation based on a 1-D adiabatic flame model where $S_u = S_u(T_{ad})$, not T_f. In this model, the heat loss is the difference between the adiabatic energy available and the energy required to raise a nonreacting fluid to T_f. It is not at all clear that Eq. (IV-2) is valid under the conditions at extinction.

Berlad and Yang (1960) tried to predict the flammability limit by including both conduction and radiation in the heat loss term. Again the 1-D non-adiabatic flame equation with constant C_p and simple kinetics were used. The conduction loss was defined by

$$q_{cond} = (g\kappa/2D^2)(T - T_u)$$

where g is a geometric factor. The radiative loss was given by

$$q_{rad} = N\varepsilon T^4$$

where $N\varepsilon$ is assumed to be constant with temperature and composition. The equations are integrated for $X = -\infty$ to $x = 0$ ($T = T_{max}$) for Le = 1 and Le = 0. The temperature profile was assumed to be represented by a Gaussian error function. The main difference between this and the previous examples is that the heat loss occurs in the flame (reaction and pre-heat zone) and not to the hot boundary. A far more reasonable integration scheme is also used. In a later paper by Yang (1961) an analog computer was used for the solution. Using physical parameters for propane-air mixtures and Le = 0, it was found that for small diameters, conduction losses accounted for 99% of the loss. For a diameter of 50 mm, at atmospheric pressure, the losses due to conduction and radiation were approximately 60% and 40%, respectively at the limit. The flammability limit was defined in terms of the nondimensional solution. A physical translation is that a minimum initial mixture concentration is reached such that a positive value of T_{max} (maximum temperature) is not obtained.

Gerstein and Stine (1972) used the same set of flame equations and similar heat loss terms as were used by Spalding (1957) but used a numerical integration technique from $-\infty$ to $+\infty$ instead of using an intermediate boundary. This essentially allows heat loss in both the preheat, reaction and post-reaction zone. Again a quenching diameter is found, in a manner analogous to Meyer, and here the composition limit is defined as the diameter where the conduction and radiation losses are equal.

Since all of the above models used the steady state flame model, there is an implicit assumption that the limit mixture occurs when a steady state flame can not exist. The problem is that mixtures outside of limits defined in this manner would support non-steady flame propagation. It will be shown, that in finite enclosures non-steady propagation can be significant. The above model also assumed that only conduction losses determine the quenching diameter and that the limit mixtures are determined by radiative loss as well. The problem is that only overall reactions were considered. As a consequence, no effect on the competition in the chain reaction mechanism can be observed as it is not accounted for in the energy production. Levy and Wienberg (1959) present evidence to show that the overall reaction concept breaks down in the low temperature region of the flame. It is conceivable that formation of radicals may become increasingly important as the mixture strength decreases. Since the flame becomes thick and S_u is very low in limit mixtures, one would expect the residence time of a fluid element to increase. As a result of this, the relative importance of intermediate reactions might change.

It is also important to examine the proposed heat loss mechanism. All of the above theories (including Meyer's ill-conceived flat flame at the mouth of a Bunsen burner) model the heat loss as being analogous to the heat loss from a gas in a tube. In that case the conducted energy loss is controlled by the mass average temperature (so called bulk or cup mixing temperature) at a given cross-sectional plane in the tube. As a consequence, energy unit area (or volume) in a given cross-sectional plane loses the same amount of heat. In other words, if the flame fails, it fails everywhere at once. The heat loss mechanism is not consistent with the 1-D model since a 1-D flame can only lose heat through conduction in the x direction. If heat losses were important in the radial direction, a 1-D flame would not exist. For instance, if a 1-D flame (thin with respect to the diameter) does exist in a tube the conductive heat loss could only be important close to the wall where a very steep temperature gradient exists and (near the wall) the flame shape would become 3-D. If the heat loss to the wall was important everywhere in the cross section, a radial temperature gradient would extend to the center of the tube and a flat 1-D flame could not exist. Instead, a 3-D flame would exist and heat loss normal to the flame would be important. This argument is valid in any configuration. For this reason the heat loss mechanism in the flame, proposed by Berlad and Yang and by Gerstein and Stine, is not consistent with the 1-D model. If any reasonable heat loss in a 1-D flame is to be included, it should be a 1-D loss via the boundary after the reaction zone. Spalding's method was an attempt at this. However, attempting to add credence to a 1-D fictitious heat loss by using a number arrived at from unrelated conditions is not a valid approach. It would be more effective to have a variable parameter at the boundary, adjust it to affect the maximum temperature in the flame and observe the effect on a realistic kinetic volume. This would yield very useful information and would be as much as can be expected from a 1-D model.

The models given for the radiative loss mechanism are also ill conceived for the 1-D flame model. The most distinctive characteristic of radiative transfer in gases is that for a given species the radiative emission and absorption occurs at discrete wavelengths in the electro-magnetic spectrum and not continuously as from an ideal black body. In fact the emission and absorption bands of two different species do not necessarily overlap. From an engineering point of view this is not convenient to model and so a gas emissivity is defined for a given path length (see Hottel and Sarofim 1967). The gas emissivity only has meaning in reference to an isothermal gas shape radiating to a specific portion of its boundary surface. The standard emissivity is defined as the ratio of the radiation from an isothermal gas hemisphere to a spot on the center of the base, to the radiation emitted from an equivalent black body hemisphere. The standard emissivity was used in all the above theories.

In general, the radiative heat loss is a function of the species present, the concentration, the optical thickness and the temperature of the gas. As a result one cannot calculate the radiative emission and absorption at a point. Rather one must have a finite volume (or at least a finite length in the 1-D case) in order to calculate meaningful energy flux.

Further, when calculating gas-gas interchange the discrete emission-absorption spectrum and concentration of all species must be known.

The theories presented by Spalding and by Meyer do not include any of this detail. The objections raised in their use of conduction loss calculation also apply here.

Berlad and Yang's use of radiative transfer more severely violates physics. First of all, they are calculating the loss in the reaction zone where $[CO_2]$ and $[H_2O]$ vary from nearly zero to some finite value. Further, there are intermediate and fuel species present. In the region of the flame the effect of concentration would be greater than the temperature effect. In spite of these facts they only used a CO_2 and H_2O temperature variation of the emissivity. Secondly, the total heat loss per cross-sectional area of gas was calculated for an infinitely long tube using

$$\frac{q}{A_{cs,g}} = \frac{1}{\pi(D/2)^2} \int_{-\infty}^{0} \frac{q\pi D}{A_\omega}\, dx \qquad \text{(IV-5)}$$

where q/A_ω, in the integrand is the rate of heat transfer to a unit area on the wall of the tube. Equation (IV-5) says, in effect, that all the heat transfered to the wall of the tube from $x = 0$ to $x = -\infty$ is emitted through a cross-sectional area of the gas. Even when this integral is transformed, through the Gaussian error function, to a temperature that becomes 0 at infinity, Eq. (IV-5) is a gross overestimate. It is quite obvious that this model is physically invalid in a flame. The high radiative loss predicted by the model is not due to the nature of the flame but rather the nature of the model.

In the paper by Gerstein and Stine no value for ε_g or derivation of the radiative loss term was given and so little can be said with conviction.

In order to model the radiative heat loss mechanism in the reaction zone of the 1-D flame model, it would be far more realistic to deal with the loss in the x direction only. One would have to describe the spectrascopic nature and the concentration variation as well. This could be done by integrating through flames of finite thickness with known species and concentration and include emission and reabsorption of each cell with all others (see Hottel and Sarofim). If modeling a flat flame burner, the boundary conditions would be determined by the temperature and radiative characteristics of the up and downstream screens. For a flame in an infinite fluid, inserting a black body at T_u at both boundaries would be appropriate. In this way all emission not reabsorbed by the intermediate gas would be accounted for at the boundaries. No emissions from the boundaries to the flame would be allowed. This would give a physically realistic value of the radiative losses in flames. Finally, considering the shape of flames in a tube and closed bomb, one realizes that radiative transport between flame "surfaces" exist as they radiate toward each other.

It should be noted that one experimental investigation was undertaken by Egerton and Powling (1948) in order to determine the importance of radiative losses to tube walls. A SFLT was blackened and then silvered. They found no detectable change in limits for upward propagating hydrogen-air flames. Because of the fuel used and the fact that they did not report if the inside or outside of the tube was coated, these results are far from conclusive.

Another thermal flammability limit theory was presented by Burgoyne and Weinberg (1954) based on the excess enthalpy concept. This concept was first proposed by Lewis and von Elbe (1951, 1956). The energy equation (II-5) can be rewritten as

$$[\kappa \frac{dT}{dx} - \sum_i [I]V_iH_i] = (\sum_i^s [I]SH_i)_x - (\sum_i^s [I]SH_i)_b \qquad \text{(IV-6)}$$

The RHS is the difference in enthalpy per unit mass between some plane x and the hot boundary. For x = u the RHS becomes zero. The excess enthalpy arguments say that if on the average at some plane x in the flame (u < x < b) the energy transport by diffusion is less than that by conduction, then

$$\sum_i^s [I]V_iH_i < \kappa \frac{dT}{dx} \qquad \text{(IV-7)}$$

and the total enthalpy at that point is larger than at the boundaries. This was visualized as a wave of thermal energy traveling with the combustion wave. As pointed out by Savage (1978), this violates the first law of thermodynamics. Either relation (IV-7) is false or at least one significant mode of energy transport has been omitted from Eq. (II-6) rendering the excess enthalpy concept meaningless. For this reason the flammability limits theory proposed by Burgoyne and Weinberg will not be discussed in detail.

The Limit Predicted by Convection

In recent years several attempts have been made to theoretically determine the flammability limits based solely on convection. Lovochev (1971) equated the Archemedian force of a hot sphere and the aerodynamic drag force on that moving (and assumed solid) sphere. He submitted that this is the sole limit criterion. He further assumed the radius of the sphere to be equal to the flame thickness (Δ), where Δ was calculated from Spalding's flame equation (1957a). In the drag equation he assumed

$$U_\infty = S_b$$

The resulting equation gives a relation for the burning velocity at the limit, which is then used to calculate the heat release at the limit. Even in the most logical application (a closed bomb) there are several problems with this approach. The assumption that at the limit the buoyancy force and the drag force are equal means only that this ideal sphere would no longer accelerate. Assuming that in the presence of gravity a spherical shape exists, which is a false assumption, it would still move upward and still continue to expand. This by no means is a valid criterion for flame extinction. Further, at the time when the sphere radius equals Δ, the drag force is not important. Andrews and Bradley (1972a) calculated that for a hot sphere $F_g \simeq 39F_b$ under the conditions stated by Lovachev. For a radius $\simeq \Delta$, the 1-D equations are not valid. Finally, velocity measurements made by Andrews and Bradley (1972b) show that $U_\infty \neq S_b$.

Andrews and Bradley (1972a) attempt to determine the limits in a closed bomb by equating the rate of change of momentum of the kernel to the buoyancy force by

$$\frac{dmS_c}{dx} = mg(\rho_u/\rho_b - 1) \qquad \text{(IV-8)}$$

where S_c is the convective rise of the flame kernel. From Eq. (IV-8) they calculated the vertical distance of the kernel as a function of time and found good agreement with experiments. This means that the flame kernel indeed translates upward as described by the Archimedian force. They defined limit criterion for only the downward propagating flame surface. The downward limit is assumed to occur when the convective rise velocity equals the propagation velocity of the side surface of the kernel.

$$\frac{\left.V_p\right)_{\text{side}}}{S_c} = 1$$

It was illustrated in Chapter III that the only time the downward propagating flame is limit determining is after the flame has filled the top of the closed bomb. In this case, however, the vertical rise of a hot bubble no longer exists and therefore the theory does not address the physical nature of the phenomenon. Andrews and Bradley did allude to this discrepancy in the paper but did not carefully discuss it. Further, no attempt was made to determine failure of the upward propagating portion of the flame kernel.

Hertzberg (1976) attempted to theoretically predict the limits based on convection for upward, downward and horizontally propagating flames in tubes. To this end he first defined a "combustion force" as

> "....the gradient of the kinetic energy increases per unit volume across a propagating flame zone."

and said that it was given by the equation

$$F_{\text{comb.}} = \frac{\Delta KE}{\Delta x} = \frac{\frac{1}{2}\rho_b S_b'^2 - \frac{1}{2}\rho_u S_u^2}{\alpha S_u}$$

where αS_u is some characteristic dimension Δx which means α has the dimensions of a diffusivity (cm^2/sec) but is undefined in his paper. It is conveniently divided out of the equation before a value is needed. He then defines a buoyancy force/unit volume

$$F_g(\rho_u - \rho_b)g$$

He equates the two forces resulting in a limit burning velocity for a horizontal flame in a tube. This is improper since F_{comb} and F_g are vectors and, for a horizontally propagating flame, are orthogonal, as Hertzberg admits.

For the downward propagating flame Hertzberg calculates a limit velocity for the case where the rise velocity of a heated sphere is equal to the ideal burning velocity. Since he is trying to model a downward propagating flame in a tube the F_g term does not apply as there is no hot bubble rise due to gravity as described by his relation. The flame ingests nearly all of the fluid ahead of the flame and appears to propagate at nearly the fundamental burning velocity. As shall be discussed later, gravity does affect the downward flame but not as modeled by Hertzberg.

The most fundamental failure of Hertzberg's theory is his introduction of the concept of a combustion force. The fact is, the flame is not a solid surface which is being pushed through the fluid by a pressure differential. The pressure gradient through the flame acts on the fluid elements, causing net motion of the fluid from the cold to the hot region. The energy transport mechanism of Eq. (II-5) still exists in the flame and, in fact, the flame behavior is predicted without the use of this force (see Chapter II).

The major fault of all the theories based on convection is that they assume the Archimedian force is acting on the hot bubble as a whole and, in the last two theories, that the subsequent lack of translation of this bubble is the sole cause of flame failure. It will be demonstrated that the energy transport mechanisms are still occurring regardless of whether or not there is an overall "bubble" translation. In order to deal with the effect of convection on the energy transport mechanism, if there is indeed a direct effect, one needs to take a detailed look at how the forces act on a fluid element and the subsequent and coupled change in thermal structure.

Empirical Hypotheses

Other hypotheses for predicting flammability limits have been proposed based solely on physical observations. They include:

i) Flame Stretch
ii) Preferential Diffusion
iii) $S_u \to 0$

A description of the phenomena and their relation to predicting flammability limits will be discussed in this section.

The concept of flame stretch was proposed by Karlovitz et al. (1953) and recently extended by Strehlow and Savage (1978). Flame stretch provides a means of extending the 1-D flame concept into two or three spaces. An understanding can be gained by observing a 2-D curved flame sheet as illustrated in Fig. IV-3. As an element of the flame moves along the flame front in the positive ξ direction, $S_{\parallel}$ increases due to the velocity gradient $\frac{dU_\infty}{dy} > 0$, according to Karlovitz

> "As a consequence of this stretching of the flame surface, the amount of heat flowing from the reaction zone of the flame into the unburned gas is distributed over increased volumes of gas, which means that the burning velocity must decrease."

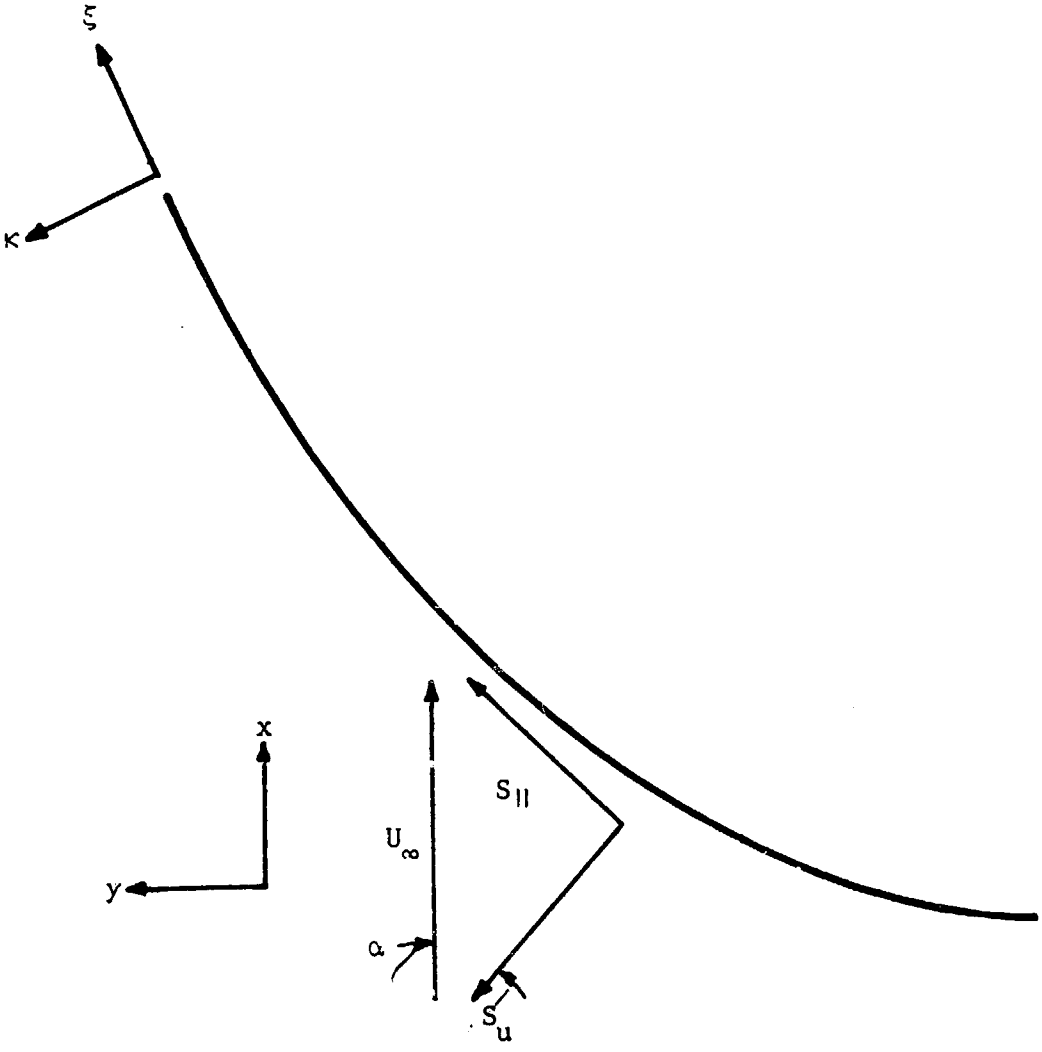

Fig. IV-3. Illustration for Flame Stretch Concept.

The flame illustrated in Fig. VI-3 is said to have positive stretch. A flame where $\frac{dU_\infty}{dy} < 0$ (e.g., the tip of a bunsen burner flame) is said to have negative stretch.

Karlovitz et al. defined the rate of flame surface production by the velocity gradient for the case $\cos\phi \simeq 0$ ($\sin\alpha \simeq 1$) or

$$\frac{1}{A}\frac{dA}{dt} = S_u \frac{1}{U_\infty}\frac{dU_\infty}{dy}$$

Strehlow and Savage solved for the more general case (arbitrary α) and found

$$\frac{1}{A}\frac{dA}{dt} = S_u \frac{1}{U_\infty}\frac{dU_\infty}{dy}\frac{1}{\sin\alpha}$$

which reduces to the form of Karlovitz et al. as $\alpha \rightarrow 90°$. Strehlow and Savage further defined a dimensionless number to characterize the stretch as

$$K' = \frac{\partial \ln \Delta A}{\partial t}\frac{\eta}{S_u}$$

where η/S_u is a characteristic time which is in essence the residence time of a fluid element in the preheat zone assuming $dS/dx = 0$ through the preheat zone. K was then solved for in cylindrical coordinates to approximate the upward propagation near limit flame in a SFLT with U_∞ being parallel everywhere. They then solved for the special case of flame "cap" propagating through a tube. Assuming that the radius [illegible] curvature at the centerline is constant, they found

$$K'_{℄} \simeq \frac{2\eta}{R}$$

at the "skirt" of the flame "cap" ($R \rightarrow \infty$) and

$$K'_{SK} \simeq \frac{\eta}{r}$$

where r is the radial coordinate value and R is the radius of curvature. Consequently since $R_{\mathbb{C}} = r_{SK}$,

$$K'_{\mathbb{C}} > K'_{SK}$$

Stretch is therefore greater at the leading edge of the flame "cap" and therefore if the flame fails by this mechanism it would fail first at the leading edge. If stretch is a valid concept as developed and K' is a non-dimensional number characteristic of the system, K' should predict flame failure. This type of correlation has not been established.

Preferential diffusion is believed to be the mechanism responsible for cellular flames. In essence, preferential diffusion is local stratification of a premixed flame. A cellular flame is illustrated in Fig. IV-4 as it would appear in a lean CH_4-air mixture. At the leading edge of a cell (point a) the mixture is locally rich and therefore $S_u]_a$ is locally higher. In the region between the cells, the mixture is locally leaner than the bulk average. The local concentration gradients are due to the fact that CH_4 has a higher diffusion velocity than oxygen. Therefore the CH_4 moves more rapidly in the preheat zone near the hot region of the cell. If the fuel has a lower diffusivity than the oxydizer, the cells will occur predominantly in overall rich mixtures (Markstein 1953). Cells concave with respect to the upstream direction do not occur as that is an unstable configuration and always relaxes to a flat flame.

The first attempt to predict flammability limits based on preferential diffusion was presented by Bregeon <u>et al</u>. They were observing the downward propagation limit behavior of mixtures of H_2-O_2 and CH_4-C_2 in different

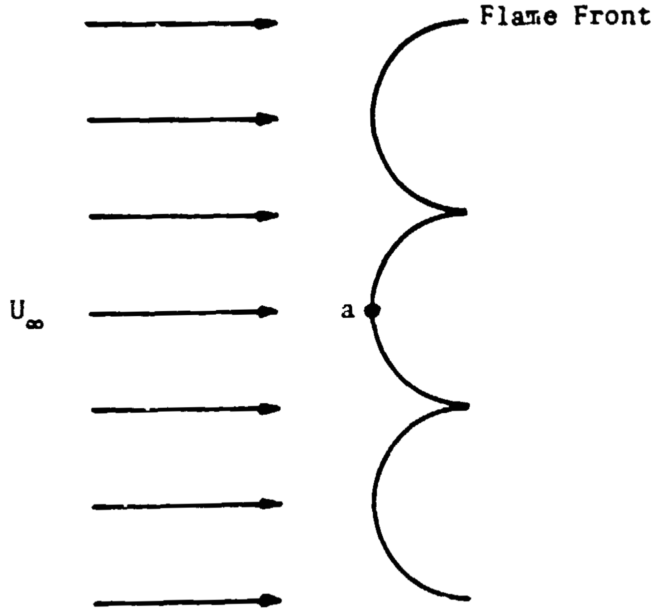

Fig. IV-4. Cellular Flame Front due to Preferential Diffusion.

dilutions of N_2 in a vertical flammability tube. They observed that the flammability limit of H_2-O_2-N_2 flames in 25 and 50 mm tubes is independent of tube diameter. The thermal theories assumed that in large tubes ($S_u \neq f$ (Dia)) radiation loss dominates and therefore is the limit determining mechanism. Some simple calculations by Bregeon et al. indicate that the rate of radiative loss is 10^{-3} of the rate of heat generated by the reaction. They concluded that neither radiative nor conductive heat loss to the walls are important. They hypothesized that instead the limit is determined by the cellular structure. Bregeon et al. felt that once the cells were established, the heat was lost to the boundary between the cells. Since between the cells the mixture is locally leaner than the overall lean mixture, the fluid between the cells acts as an inert sink. They further conclude that the cell size (d_c) and not the tube diameter (d_t) is important. Specifically

$$V_p d_c > B\alpha$$

for propogation to be allowed. Here, B is a constant of proportionality and α is the thermal diffusivity. The downward lean limit flame propagation in CH_4-O_2-N_2 mixtures seemed to support this hypothesis. CH_2-O_2 mixtures of $\Phi < 1$ would support downward flame propagation in a 25 mm tube with more N_2 dilution than in a 50 mm tube. Their explanation was that cells occurred in the 50 mm tube and not in the 25 mm tube. Since the cells were smaller than 25 mm in diameter, the heat loss was greater in the larger tube. They also found that for all limit H_2-O_2-N_2 mixtures, $V_p d_c/\alpha$ was approximately constant.

The concept that the fundamental limit mixtures occur when $S_u = 0$ is a logical conclusion from the S_u vs Φ behavior illustrated in Fig. II-2. If the curve is extrapolated far enough, S_u would become zero at a nonzero mixture composition on the lean side. This concept has been supported by the paper of Sorenson <u>et</u> <u>al</u>. (1975), but has not been established as a universal criterion.

CHAPTER V

BEHAVIOR OF LEAN LIMIT METHANE-AIR FLAMES IN A STANDARD FLAMMABILITY LIMIT TUBE

The first phase of the four phases of experimental investigation entailed simple observations of lean limit methane-air flame propagation at 1-g and only in a vertical tube. A standard flammability limit tube (SFLT) was constructed and an experimental technique was developed for producing repeatable near limit flames. The major objectives of the first phase were to:

1) Determine the upward and downward lean limit mixtures in this particular apparatus.
2) Verify that a constant propagation velocity is attained and measure its value.
3) Photograph near limit flames.
4) Observe the extinguishment process.
5) Make a referenced photograph of an upward lean limit flame by releasing the camera shutter from a high resolution flame detector.

In this chapter the experimental equipment needed for the first phase will be described. Observations made during the determination of the downward and upward lean limits are then discussed. Finally, the technique used to make referenced photographs is detailed.

The Experimental Methods

The SFLT used in the 1-g study is illustrated in Fig. V-1. In the first two phases of the study a Plexiglass tube was used. It had a 50.8 mm ID, 3.2 mm thick walls and was 1.83 m long. For the laser Doppler anemometry

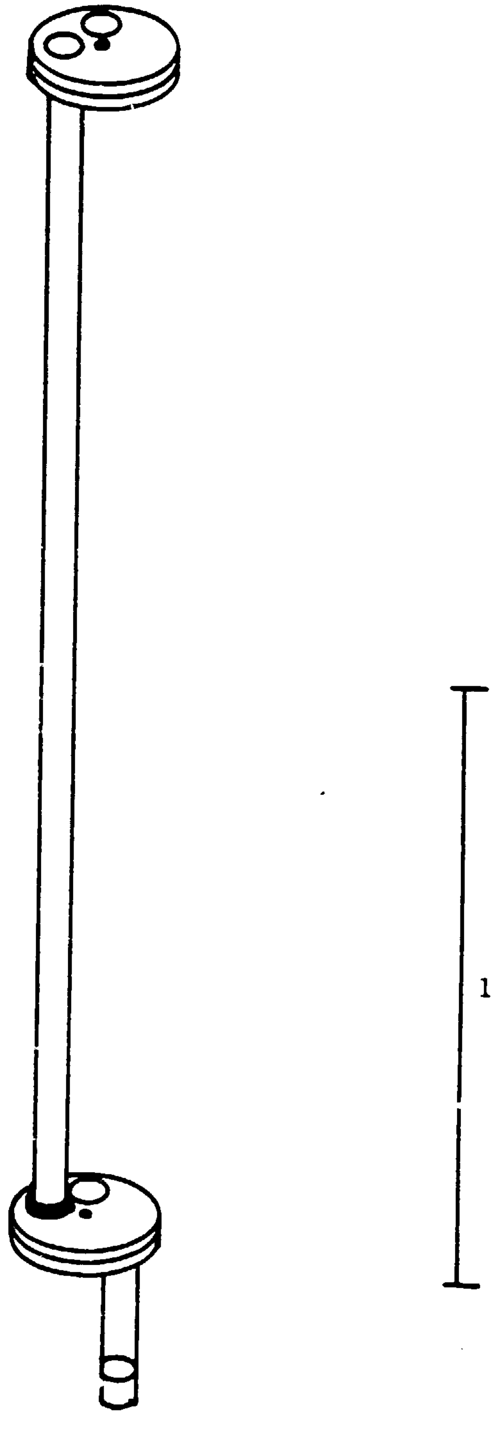

Fig. V-1. Standard Flammability Limit Tube.

(LDA) and interferometric studies a Pyrex tube of the same length with a 52 mm ID was used. Two pieces of tubing 1.22 m and 0.61 m long were fused together since only short lengths were readily available. The Plexiglass rotary valves were copied from Levy (1965). The valve on the filling end of the tube had four positions (see Fig. V-2). One position placed the plenum in position for filling the tube, one sealed the tube and one opened the tube for venting and ignition. The fourth position sealed the tube but vented the plenum chamber to the exhaust system. This allowed a flow of the desired mixture to be established in the plenum. The valve could then be quickly rotated to fill the SFLT with minimum disturbance to the established flow. The plenum chamber had two screens of 2.54 mm mesh size 3 mm apart and 0.25 m ahead of the entrance to the tube. The screens were used for producing a uniform flow with minimum particle extraction from the particle seeded mixtures used in the LDA experiments. The methane and air flows were first mixed in a "T" just outside the plenum. The valve at the exhaust end of the tube had only two positions, open and closed. The valve plates had a silicone oil film between them and an o-ring for a seal. Plexiglass flanges were glued to the ends of the tube and bolted to the valves with a soft rubber gasket in-between. Mixtures could be mainained for 0.5 hr with no evidence of contamination.

The SFLT was mounted on an optical table constructed for this study. It was mounted vertically with the filling end at the bottom for all studies.

The optical table was made from a 400 Kg cast-iron machinery table with a 0.61 m x 2.4 m machined surface. This was placed on top of a 550 Kg concrete slab 0.23 m x 0.76 m 2.4 m. The whole table assembly could be isolated from room vibration by "floating" it on five inner tubes. The SFLT

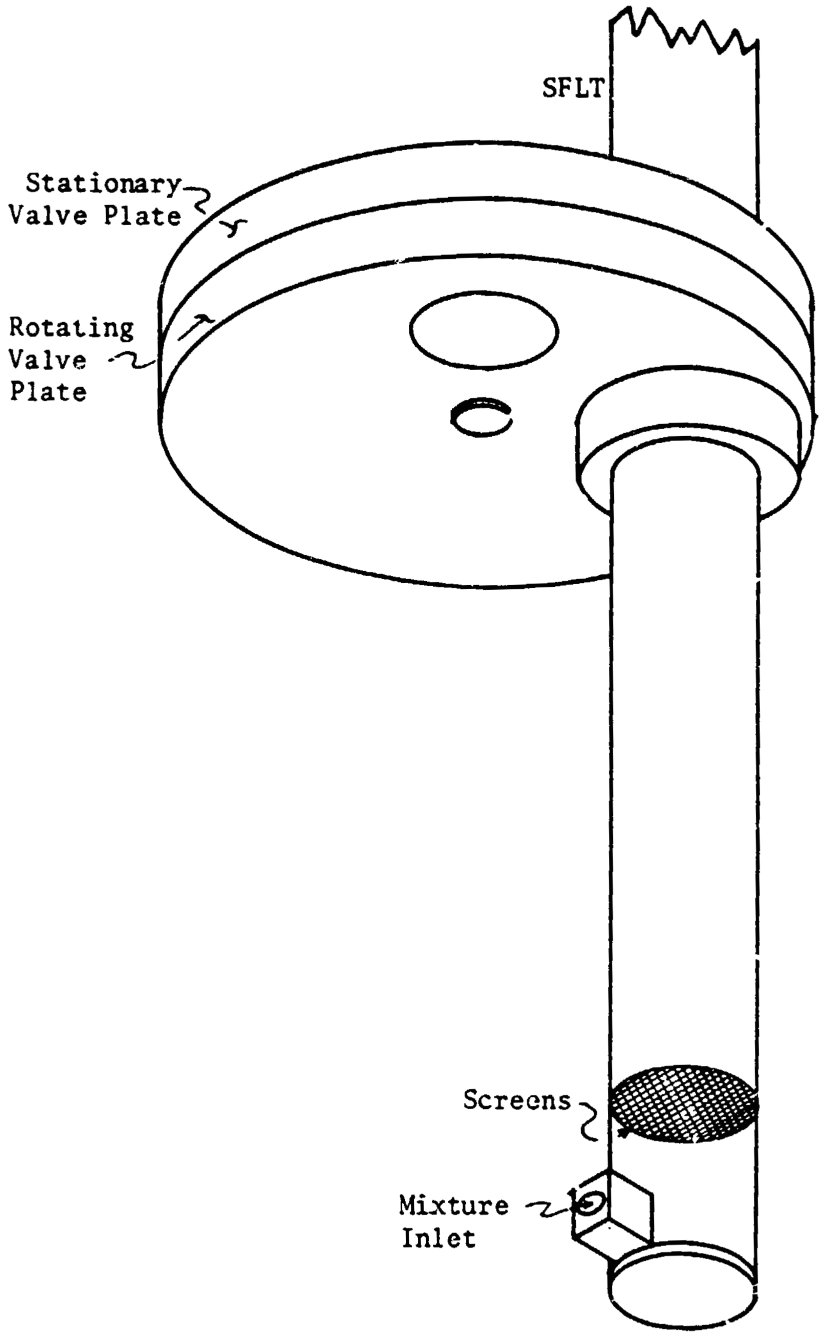

Fig. V-2. Standard Flammability Limits Tube (Lower Valve).

was mounted to the optical table so that it was isolated from the room except for the 10 mm polypropolene gas feed lines. The isolation is necessary for holography. The table also provided a stable base for the LDA facility.

The methane and air flow rates were metered using Matheson 602 and 604 rotometers respectively. They were calibrated using a gasometer and measuring the time necessary to fill the known volume at a given rotometer setting. These same two rotometers were used for all four phases of this study. The accuracy of the absolute value of the flow rates is at least ±2%.

Two types of flame detectors were developed for this study. They were required to measure the flame propagation velocity, to reference the LDA velocity profiles and to reference the interferometric density profile. The first system detected the visible flame emission whereas the other detected the line integrated maximum deflection of the 3-D refractive index field.

The visible light flame detector is illustrated in Fig. V-3. A 35 mm x 40 mm selenium solar cell (American Science Center No. 30728) was used as a photo transducer. A gas filled photo diode was also tried. The solar cell was used in the final design since it had equal sensitivity, adequate time response, is more compact and required no external power supply. From Fig. V-3 it is obvious that the aperture is very large. This was necessary because the lean limit flame has such a low level of light emission. Ideally a photomultiplier should have been used, but the cost was prohibitive. The voltage output of the solar cell was input to a 1000X DC amplifier. The circuit diagram of the amplifier is shown in Appendix B, Fig. B-1. Four visible flame detectors were constructed and positioned 0.20 ±0.005 m apart (see Fig. V-4). They were positioned such that the midpoint between the

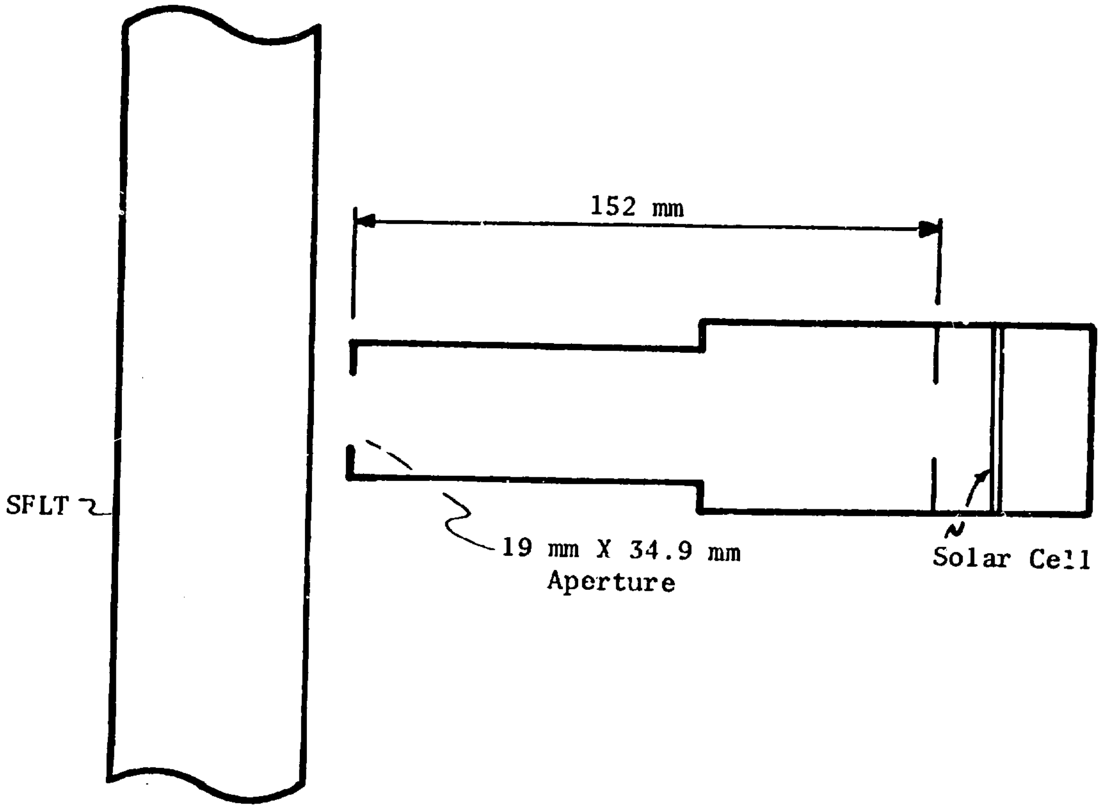

Fig. V-3. Visible Light Flame Detector.

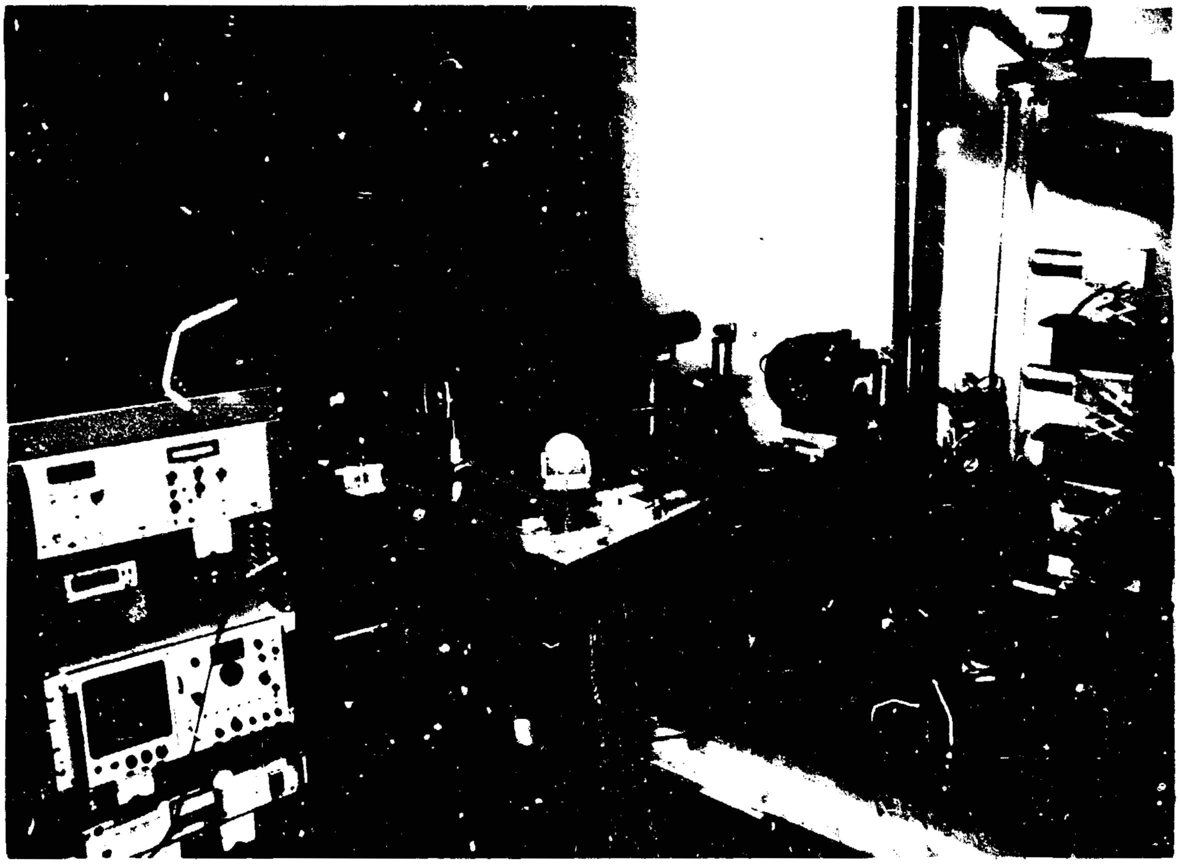

Fig. V-4 Photographs of Visible Light Flame Detectors in Relation to SFLT.

second and third detectors was 1.15 m from the lower end of the tube (0.45 m above the table top). This point coincides with the vertical position of all the LDA measurements. All four detectors were input to the DC amplifier and then recorded on a Century light beam oscillograph. Using time of flight information, three average velocities could be calculated and compared to determine if the flame propagated at a constant velocity.

The second type of flame detector (beam deflection flame detector) depends on the fact that light is refracted as it passes through the index of refraction gradient associated with the preheat zone of a flame. An illustration of the system is shown in Fig. V-5. A 2 mW laser beam was split into two beams 113.2 ±0.2 mm apart forming a vertical plane. The two beams were each passed through their respective aperture and onto the photo transistor. The aperture and phototransistor were integrated into a single unit and mounted on an x-y positioner. The undeflected and deflected output voltages were +15 VDC and 0 VDC respectively (see circuit of B-1). AC coupling was used so that both detector outputs could be recorded on one channel. With the AC coupling, there were of course two peaks, the first at about -4 VDC and the second at about +? VDC. The first peak was measured to occur 2 ms later in time than the DC coupled pulse. The filter had a 2 Hz cutoff frequency. This system offers several advantages over the visible light detectors. The position of the detector is well defined in space by measuring the position of the 1 mm diameter laser beam. Due to the steep temperature gradient in the flame, a relatively sharp spike results. In short, the beam deflection flame detector system has far better resolution. It also has the advantage that it does not depend on visible light. It is therefore capable of detecting the hot bubble that exists after the flame has extinguished

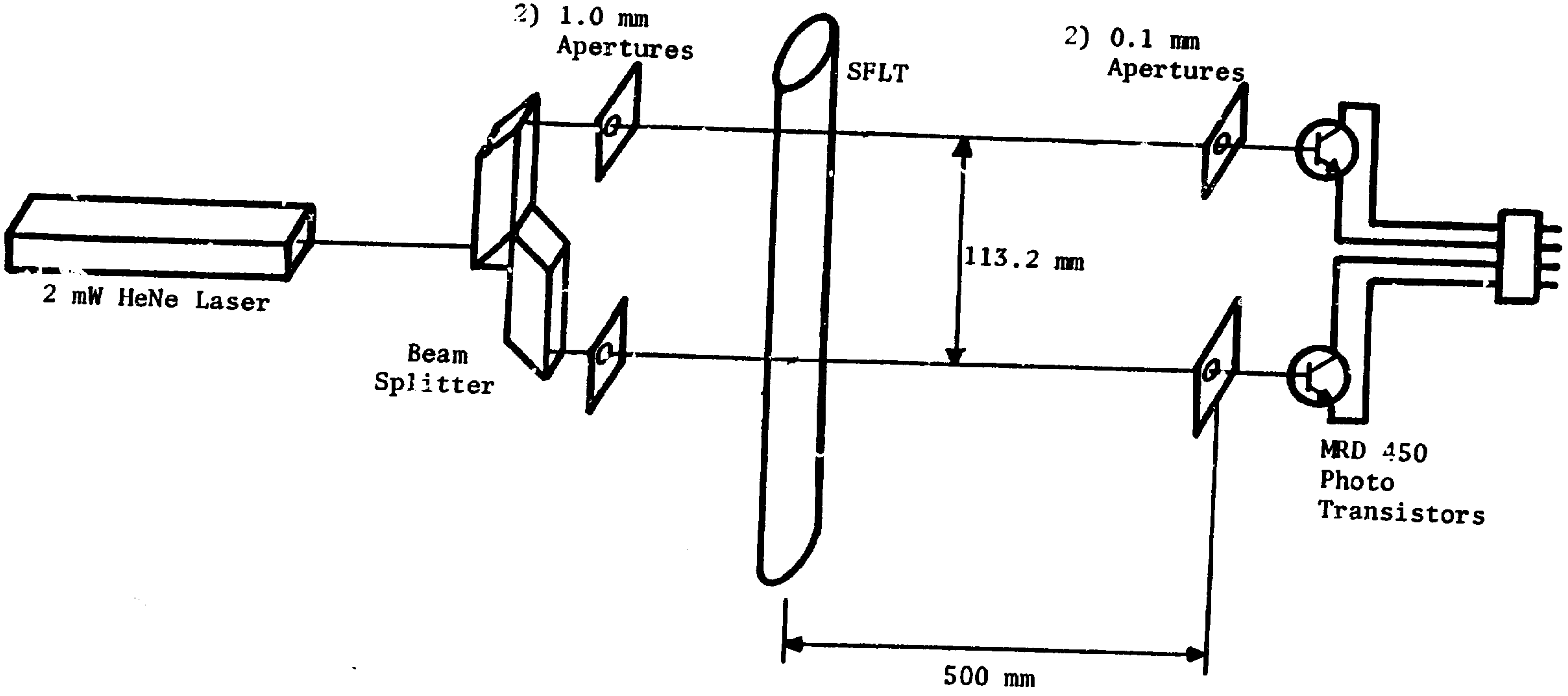

Fig. V-5. Schematic of Beam Deflection Flame Detector.

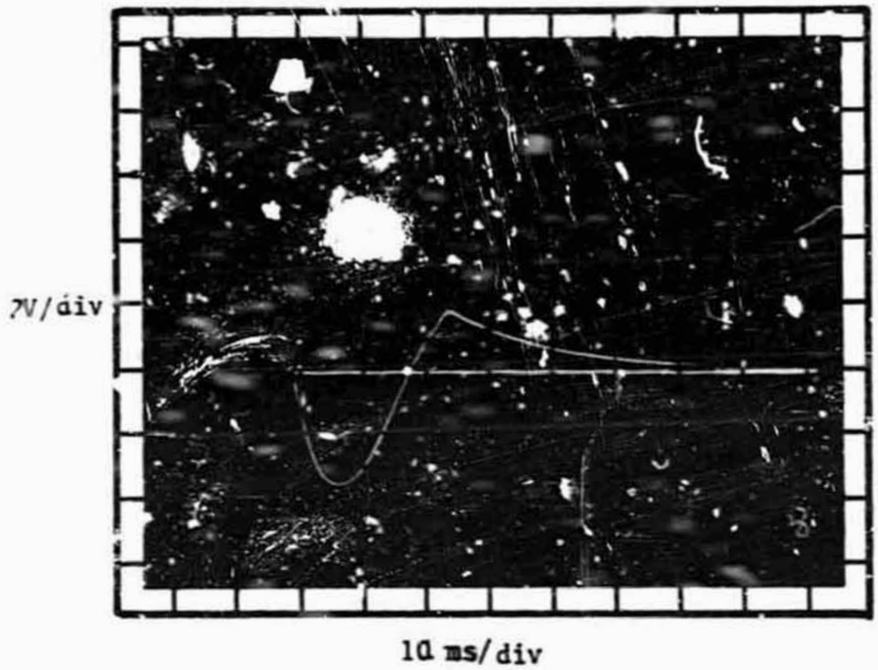

Fig. V-6. Oscilloscope Trace of AC Coupled Output from Beam Deflection Flame Detector.

(refer to Chapter III and Levy). The only disadvantage is that only two detection points were available and therefore the question of constant propagation velocity could not be addressed with this technique.

To photograph the lean limit flames, a Miranda 35 mm single lens reflex camera was used with a 50 mm f/1.9 lens. The film used was Kodak 2475 High Speed Recording Film ASA 1000. The film was pushed just into fog by developing it in Acufine at 34°C for 10 min. The flame shapes are distorted due to the lens effect of the tube and the focal plane shutter of the camera. The latter effect was minimized by orientating the camera such that the focal plane shutter moved opposite to the direction of flame propagation. The method used to fill and ignite the mixture in the SFLT is similar to that used by Levy (1965). The following procedure was used for the limits determination of upward propagating flame.

1) Open top valve and position plenum to fill.
2) Adjust rotometers to establish desired test mixture and allow the flow to purge the tube for approximately 10 tube volumes.
3) Clo top valve.
4) Close bottom valve and establish slightly enriched mixture in exhausting plenum by readjusting CH_4 rotometer.
5) Reposition plenum for filling of tube.
6) Open top rotary valve for 2 s.
7) Close top valve and shut off rotometers.
8) Close bottom valve and let stand for 4 min.
9) Open bottom rotary valve and ignite mixture with 75 mm Ohio stick match.

For downward propagating flames steps 4 through 6 were eliminated and the top valve was open for ignition. The 4 s enrichment of the ignition end (steps 4 through 6) was necessary for upward flame propagation to provide consistent ignition of limit mixtures. This technique was only necessary for igniting mixtures leaner than 5.37% CH_4 in air. This procedure inserted a rich slug approximately 0.1 m long.

The Downward Propagating Flame

The downward lean limit mixture was found to be 5.87% methane. The limit flame propagated at about 0.086 m/s with a standard deviation of 0.002 m/s for 10 trials. This is about equal to the extrapolated burning velocity measured on other burners (see Fig. II-2). The visible light flame detectors were used to measure V_p. A typical record is shown in Fig. V-7a. V_p is assumed to be constant for this flame since variance between detectors did not correlate. The limit mixture was the one for which the flame propagated the full length of the tube for about 80% of the tests. Flames traveling through mixtures of 5.81% never traveled more than 0.15 m down the tube.

The manner in which the flame propagates down the SFLT changes right at the limit. For a 5.93% methane mixture, the flame is cellular and stable in the sense that the "plane" of the flame was always horizontal. This is shown in the photographs of Figs 8a and 8b. For Fig. 8a the camera was placed horizontal, while [illegible] Fig. 8b the camera was viewing up toward the downward propagating flame at about a 45° angle. A shutter speed of 1/250 was used. In 5.87% methane mixtures, the flame would tend to "walk" (tip from side to side) down the tube. One point on the edge of the tube would stay stationary while the rest of the flame would propagate. Then a point

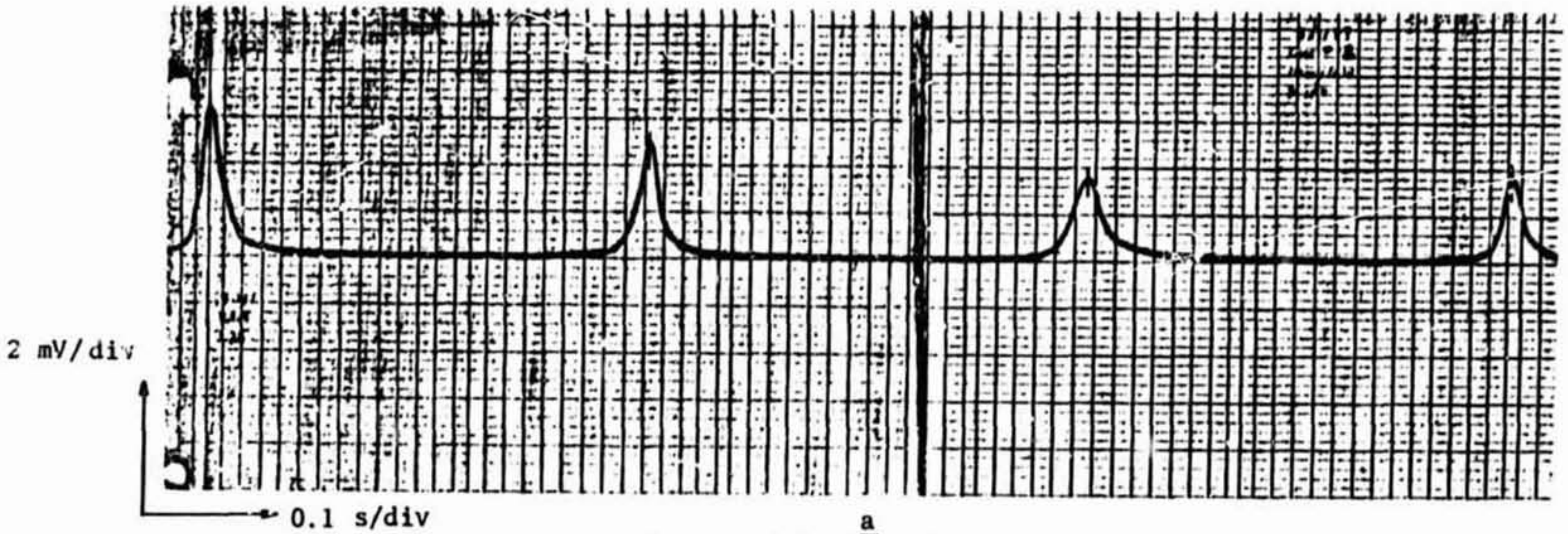

a
Downward Propagating Flame

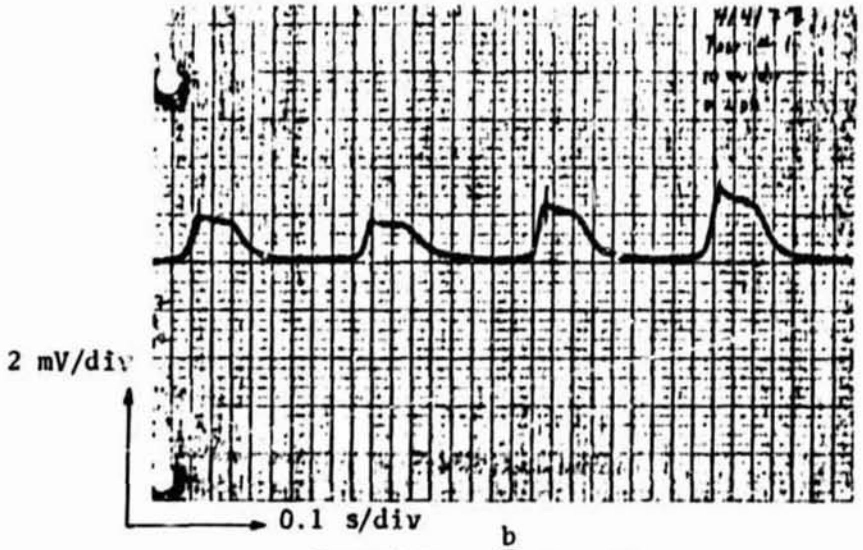

b
Upward Propagating Flame

Fig. V-7. Records of the Visible Light Flame Detectors.

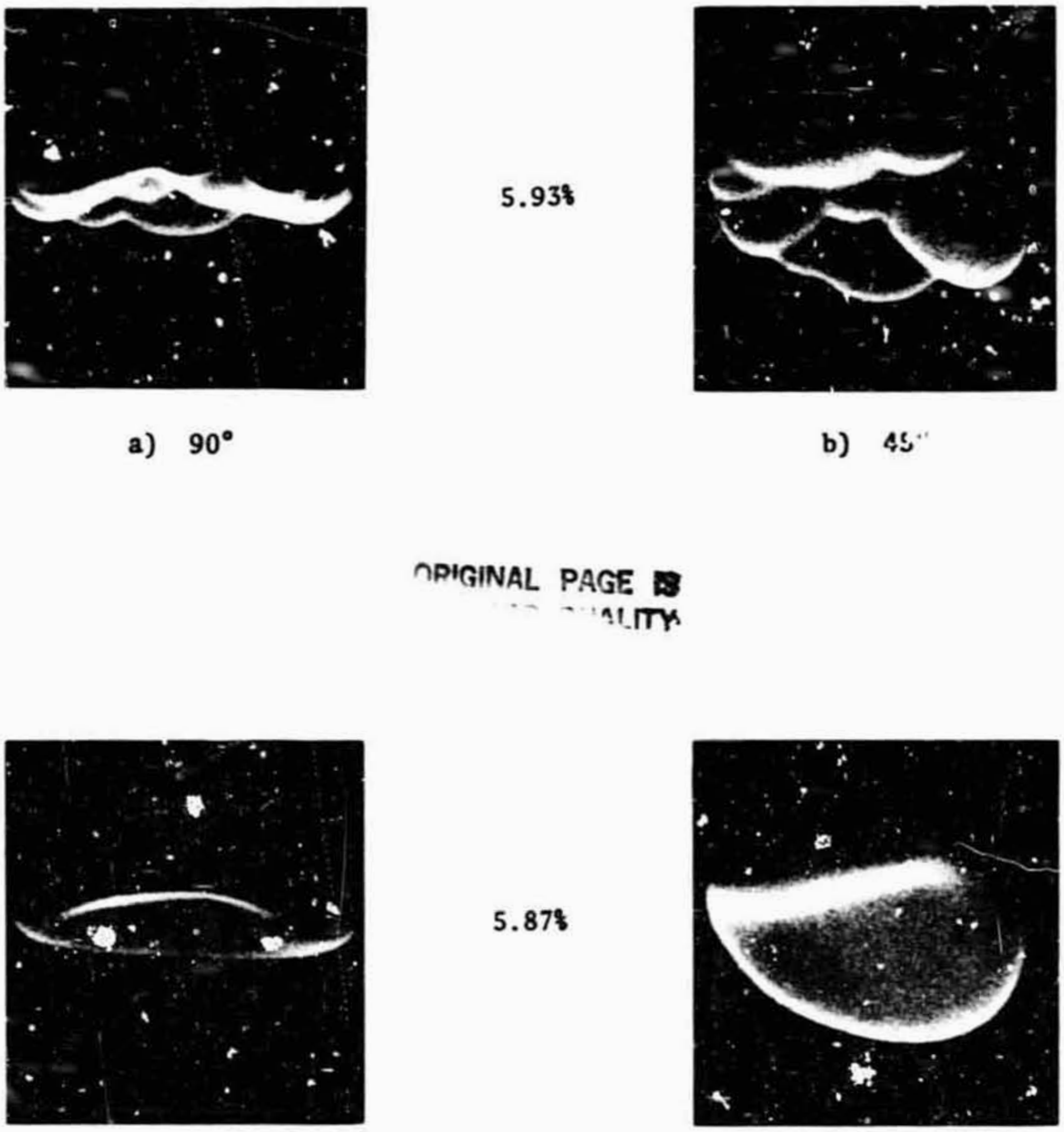

5.93%

a) 90°

b) 45°

5.87%

c) 90°

d) 45°

Fig. V-8 Downward Propagating Flames in Lean Limit and Near Limit Mixtures

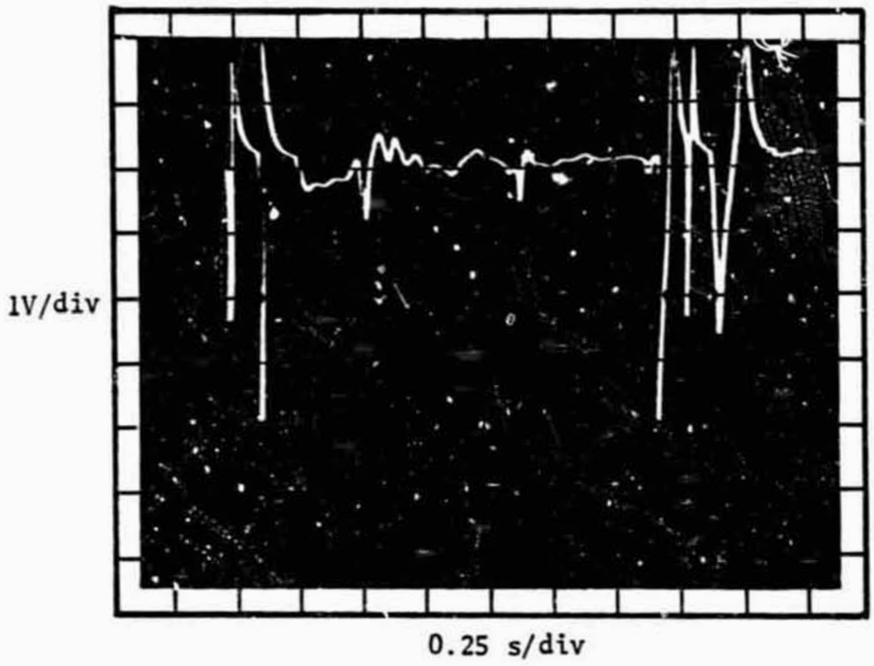

a Downward Flame Propagation

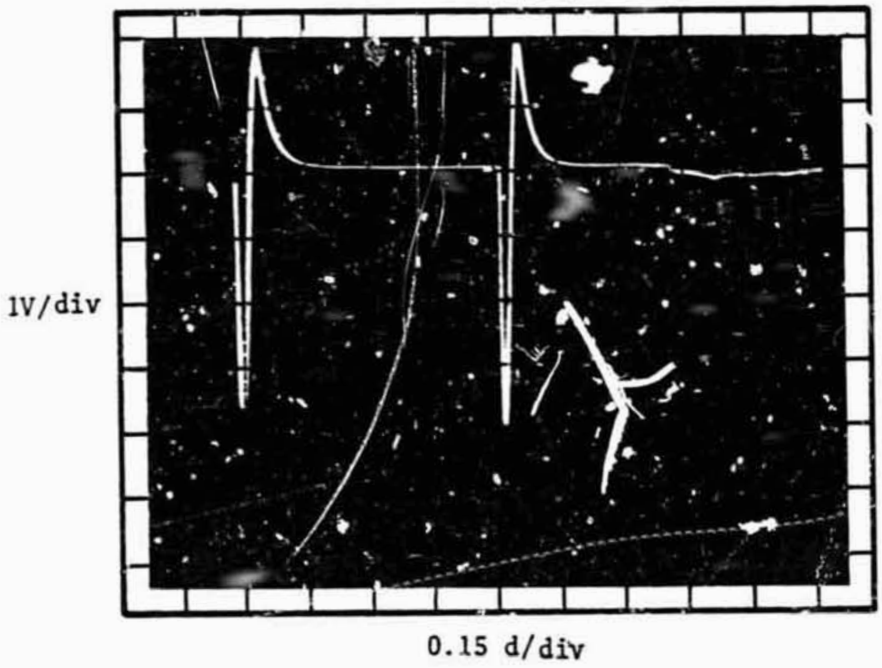

b Upward Flame Propagation

Fig. V-9. Typical Records from Beam Deflection Flame Detector.

on the "leading" edge would be stationary and the "trailing" portions of the flame would propagate. This behavior has also been observed by Levy (1965) and by Jarosiński (1978). For the 5.87% mixture, no well defined cell structure is ever present. This is shown in Figs. 8c and 8d.

The beam deflection flame detector could not be used to measure the propagation velocity of downward propagating lean limit flames. A typical oscilloscope trace is shown in Fig. V-9a. It is obvious that because the limit flame has a "walking" motion, it is impossible to measure propagation velocity using this technique.

The Upward Propagating Flame

The behavior of the upward propagating limit flame was perplexing at first. Sometimes a flame would travel the full length of the tube in a 5.22% mixture, and sometimes it would not. V_p varied between 0.23 m/s and 0.26 m/sec. Levy (1965) reported the limit mixture to be 5.3% and the limit V_p to be 0.235 m/s with a standard deviation of 0.006 m/s for 10 trials. This composition discrepancy of the limit mixtures is within the experimental error of the rotometers used. The discrepancy in V_p was troubling as one would expect the propagation velocity to be a fundamental property of the limit mixture and tube diameter. After careful investigation a strong correlation was found between the propagation velocity and the trial number for a given day (see Fig. V-10a). At the time these trials were made, trial number 1 was the first trial for which a flame propagated the full length of the tube in a 5.22% mixture. Figure V-10a also shows that waiting 15 min between trials lowers V_p some but not to values as low as the first trial of the day. It was later discovered that a 5.27% mixture was required for the first trial of the day to ensure that the flame would propagate the full length of the tube. If

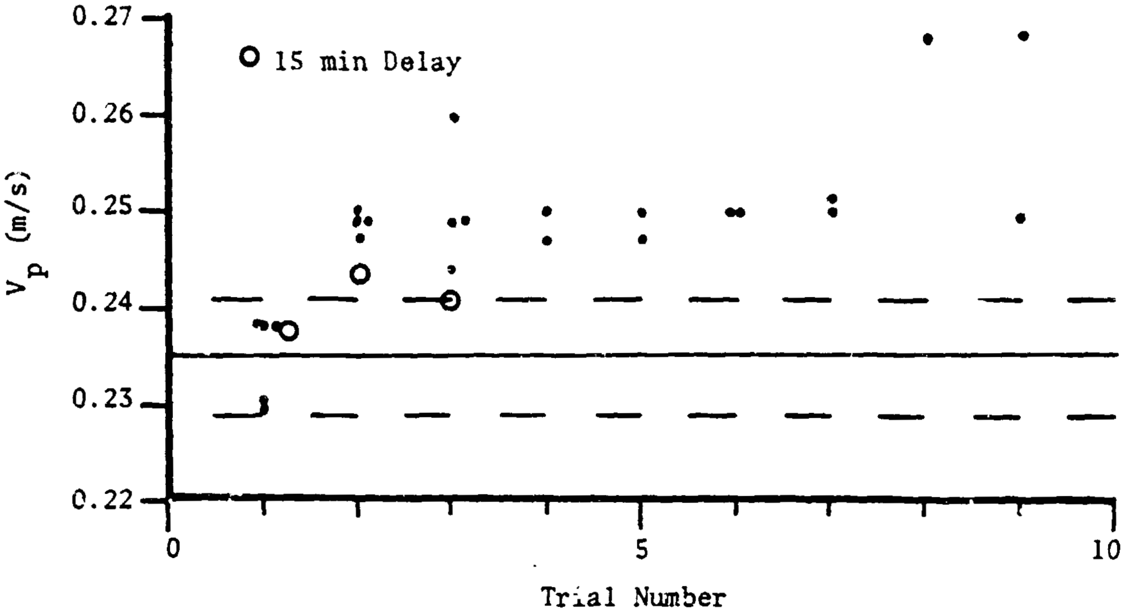

a Trials from Many Different Days, 5.22% CH_4.

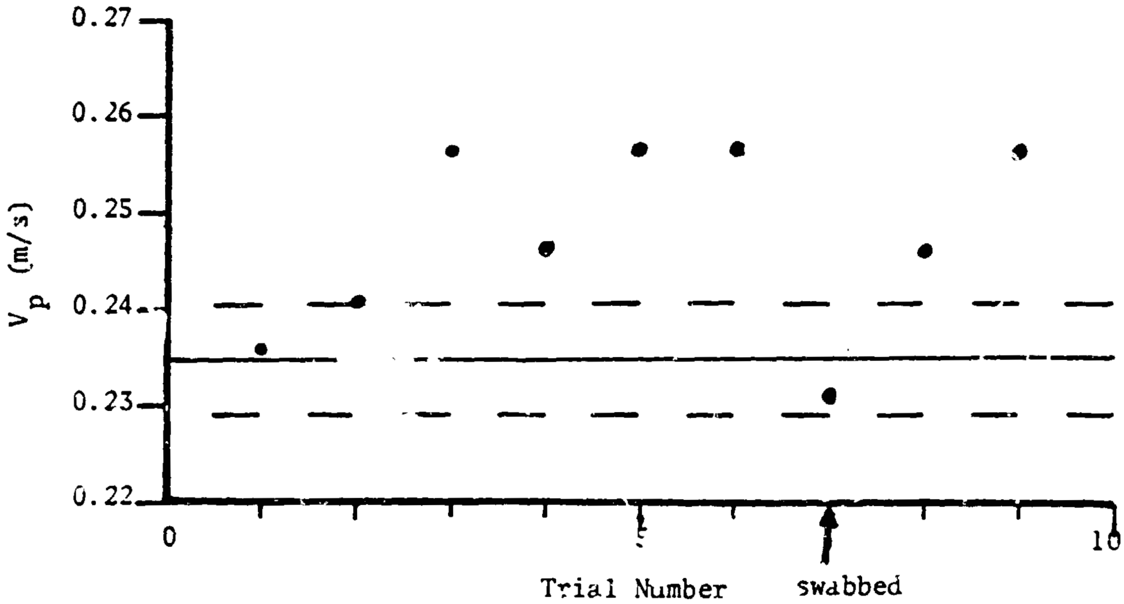

b Trials from One Day, 5.27 % CH_4.

Fig. V-10. Flame Propagation Velocity versus Daily Trial Number.

5.22% mixtures were used, the first trial would allow the flame to propagate only 1/3 of the way up the tube, the second trial 2/3 and the third run the full length of the tube.

Some insight into the cause of this phenomenon was gained during preliminary LDA tests. As will be explained, it is necessary to artificially seed the test mixture with 1 μm aluminum oxide particles in order to measure fluid velocities using a laser Doppler anemometer. It was found that when the particle laden mixture was used to purge the tube after a flame had propagated the particles would accumulate on the tube wall. However, if the tube was swabbed with ethanol to remove the particles and purged with air to evaporate the ethanol, the next time particle laden air was introduced, the particles would no longer accumulate on the wall. Furthermore, the measured V_p of the next limit flame fell back to the same values as the first trial of the day. This behavior is illustrated in Fig. V-10b. It was also found that a water swab was just as effective as ethanol. Both the Plexiglass and Pyrex tubes illustrated the same effect.

Three hypotheses can be made to explain the behavior of the propagation velocity based on the above observations:

1) Heating of the tube walls.
2) An electrostatic charge build-up on the walls.
3) Some species build-up on the wall and subsequent transport to the flame.

Heating of the walls can be discounted for two reasons. For one, wall temperature measurements were made by Jarosiński and Strehlow (1978) using a surface temperature gage. They discovered that the maximum wall temperature was about 3°C and substantially decayed in five minutes. Secondly, the evaporation of the ethanol would be expected to lower the wall temperature to slightly below ambient. If V_p of the limit flame is sensitive to these small wall temperature changes, V_p, after swabbing, would have been less than the first trial. This behavior was not observed.

An electrostatic charge seemed to exist on the tube wall as this would account for the particle accumulation. It is well known that ions exist in a flame and that flame propagation can be affected by electric fields. Whether or not a static charge would, by itself, affect V_p was not tested. In retrospect this could have been tested by artificially charging the tube (possibly with rabbit fur).

The third hypothesis might at first seem unreasonable, but there is some supportive evidence. The tube used by Jarosiński had a 50 mm square cross section and was 1.83 m long. Each of the Plexiglass panels was made from two pieces so that there was a horizontal joint. The ends of the panels were machined so that one would expect no more than a 25 μm crack due to irregularities. A piece of plastic tape was placed over the joint on the outside of the tube. As upward and downward flame propagated past the joint, the flame would hesitate and the shape was perturbed. When a boundary layer trip wire was placed horizontally along the inside wall of the tube, Jarosiński observed that the flame would pass this wire unperturbed. Further, when the joint was sealed with glazing compound (window putty) instead of plastic tape, the flame would pass by the crack unperturbed. This evidence suggests that the joint did not present an aerodynamic disturbance to the flow field. Instead the entire limit flame was evidently sensitive to the presence of the crack. This evidence does not by any means prove the third hypothesis, but only allows it to be a viable possibility.

No further attempt was made to explain this phenomenon. Instead it was eliminated by cleaning the tube after every run, first using a water swab, then a chamois and finally by blow drying with air.

Due to the previously described behavior of upward propagating flames in 5.22% and 5.27% mixtures, 5.27% is defined as the limit mixture. The propagation velocity was measured to be 0.235 m/s with a standard deviation of 0.004 m/sec for 10 runs. This is in very good agreement with Levy's work. A typical time-position record for an upward propagating lean limit flame using the visible light flame detectors is shown in Fig. V-7b. No positive conclusion can be made about V_p being a constant. The time between detectors varied as much as ±3%, but no correlation was evident to suggest that the flame was accelerating or decelerating. More accurate detectors are required. The beam deflection flame detectors have the resolution required as can be seen in Fig. V-9b. Unfortunately it was not possible to make a 4 position detector for this study.

In an attempt to observe the extinguishment process of an upward propagating lean limit flame, a procedure (originally used by Levy 1965) was developed to effect failure at a given height in the tube. The SFLT was first filled with a 5.16% mixture, which is slightly leaner than the upward lean limit. The lower 0.6 m of the tube was then filled with a 5.27% mixture. Ignition would produce a flame that propagated approximately 1.2 m up the tube (0.6 ±0.1 m past the lean-rich interface). The failure of the flame was not instantaneous. Instead, the visible flame front would collapse inward before going out. Since the emission intensity decrease during the collapse, it was not possible to photograph this process. However, an intermediate flame shape is sketched in Fig. V-11.

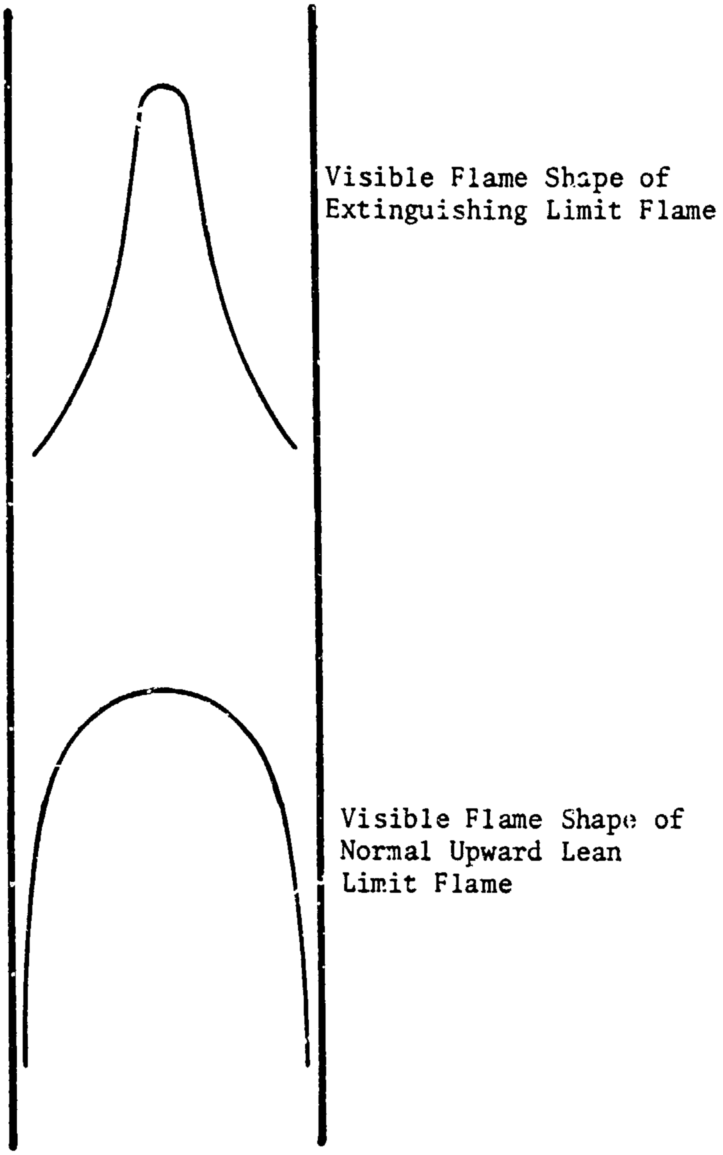

Fig. V-11. Extinction Process of Upward Propagating Flame.

Photographs of the Upward Propagating Flame

The beam deflection flame detector was used as a fiducial as well as for calculating propagation velocity. Therefore it was of interest to take referenced photographs by having the detector output trigger the camera shutter. This made it possible to calculate the position of the visible flame front with respect to the laser beam position at the time the beam was fully deflected. With this information it is possible to determine the position of the visible flame front with respect to the velocity profiles. No referenced photographs were made of a downward propagating flame. As previously described, multiple beam deflections occur as the downward propagating limit flame propagates past the detector. Consequently, a photograph of a downward propagating lean limit flame triggered by the beam deflection would have been no more meaningful than one triggered manually.

The first referenced photographs were made with a 4 x 5 Kodak Graflex and a 190 mm f/4.5 lens. The major advantages of this camera are that the lens shutter allows double exposure and does not distort the flame shape. It was hoped that the double exposure capability would allow exposure of the laser beam only (made visible by a particle seeded gas mixture) and the second exposure of the flame only in an unseeded mixture. The lens was found to be too slow to photograph an unseeded flame.

The shutter was released with a solenoid and an associated power circuit developed by Meagher (1978). A schematic of the equipment used to determine the shutter delay and the exposure time is shown in Fig. V-12. A laser beam was passed through the center of the Graflex lens and then through the aperture-phototransistor detector previously described. The detector output was recorded on a Tektronixs 7603 oscilloscope. The oscilloscope trace

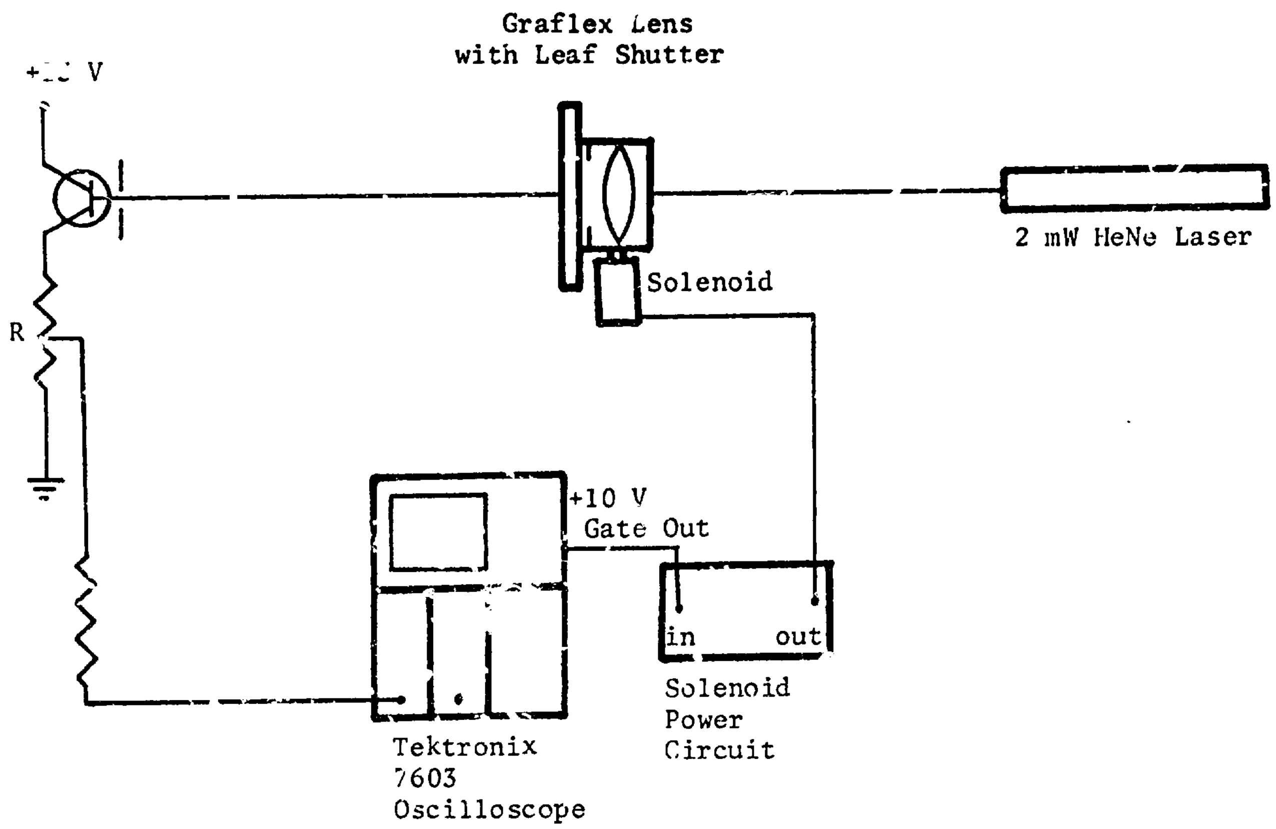

Fig. V-12. Equipment for Calibrating Graflex Lens with Leaf Shutter.

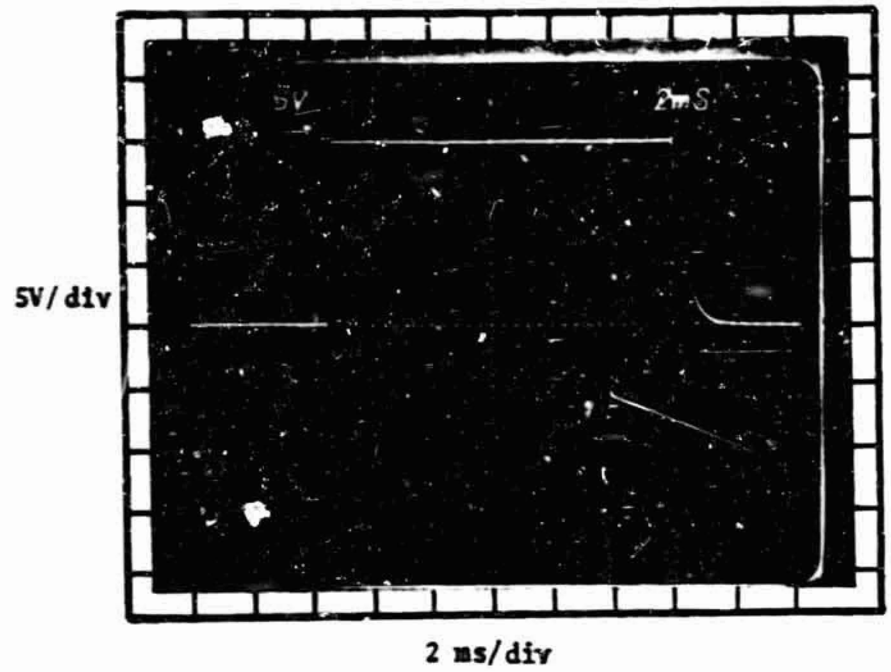

a Shutter Calibration at 1/200 s

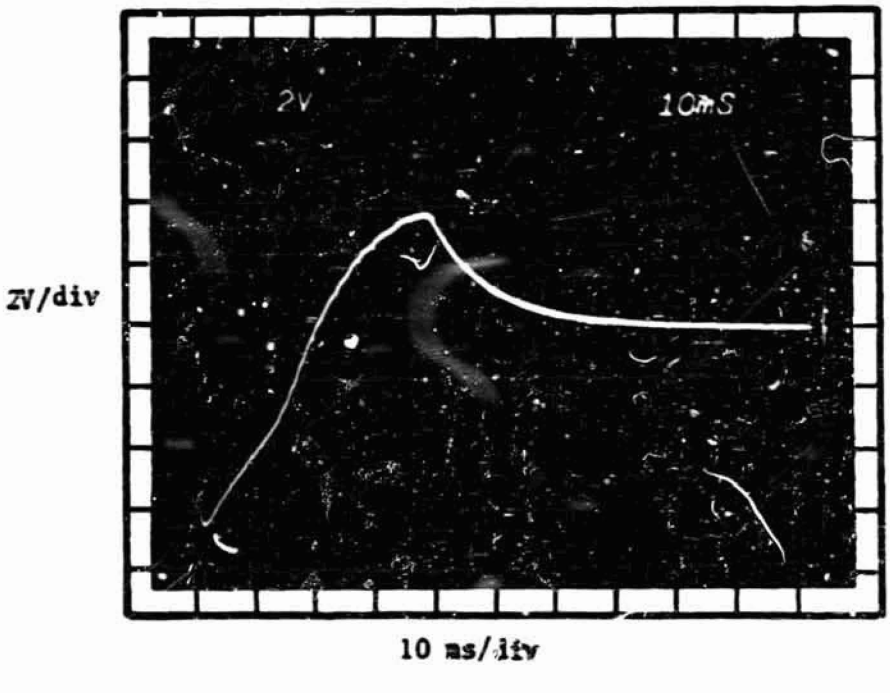

b Schmitt Trigger Setting of Beam Deflection Flame Detector Output

Fig. V-13. Oscilloscope Records of Graflex Shutter Calibration.

was triggered manually which simultaneously began the +10 VDC gate and subsequently triggered the solenoid power circuit. During the time the shutter was open, a +15 VDC signal was recorded on the oscilloscope (see Fig. V-13a). Consequently the mechanical delay time and exposure time may be read from the oscilloscope record. Shutter settings of 1/100 and 1/200 resulted in centerline exposure times of 24 ±0.7 ms and 12 ±0.5 ms respectively. The mechanical delay time was 4.3 ±0.1 ms for both shutter settings.

To take the referenced photographs the arrangement of Fig. V-11 was slightly modified. The laser beam (diameter = 1 mm @ $1/e^2$ point) was very accurately passed through the centerline of the SFLT. Accurate alignment was accomplished by positioning all the secondary reflections from the tube surfaces back on the original incoming beam. Once aligned, the laser beam was passed into the aperture-phototransistor assembly placed 0.5 m from the tube centerline. The AC coupled output of the beam deflection circuit was input to the scope as before. The Schmitt trigger was set for a negative slope and -2 VDC. As the flame propagated past the laser beam, it was deflected starting the oscilloscope trace at the -1/3 point of the reference pulse (see Fig. V-13b) and subsequently began the exposure sequence. It can be seen in Fig. V-13b that setting the Schmitt trigger at -2 VDC compensates for the 2 ms shift of the peak caused by the AC coupling.

Seven referenced photographs were made with Poloroid Type 410 film (ASA 10,000). The photographs shown in Figs. V-14a and V-14b were taken at shutter settings of 1/100 and 1/200 respectively and f/4.5. The horizontal line in the photograph is the laser beam made visible by particle scattering. The scale was placed alongside the tube but at the center plane parallel to the film plane. It was photographed separately from the flame. The numerals

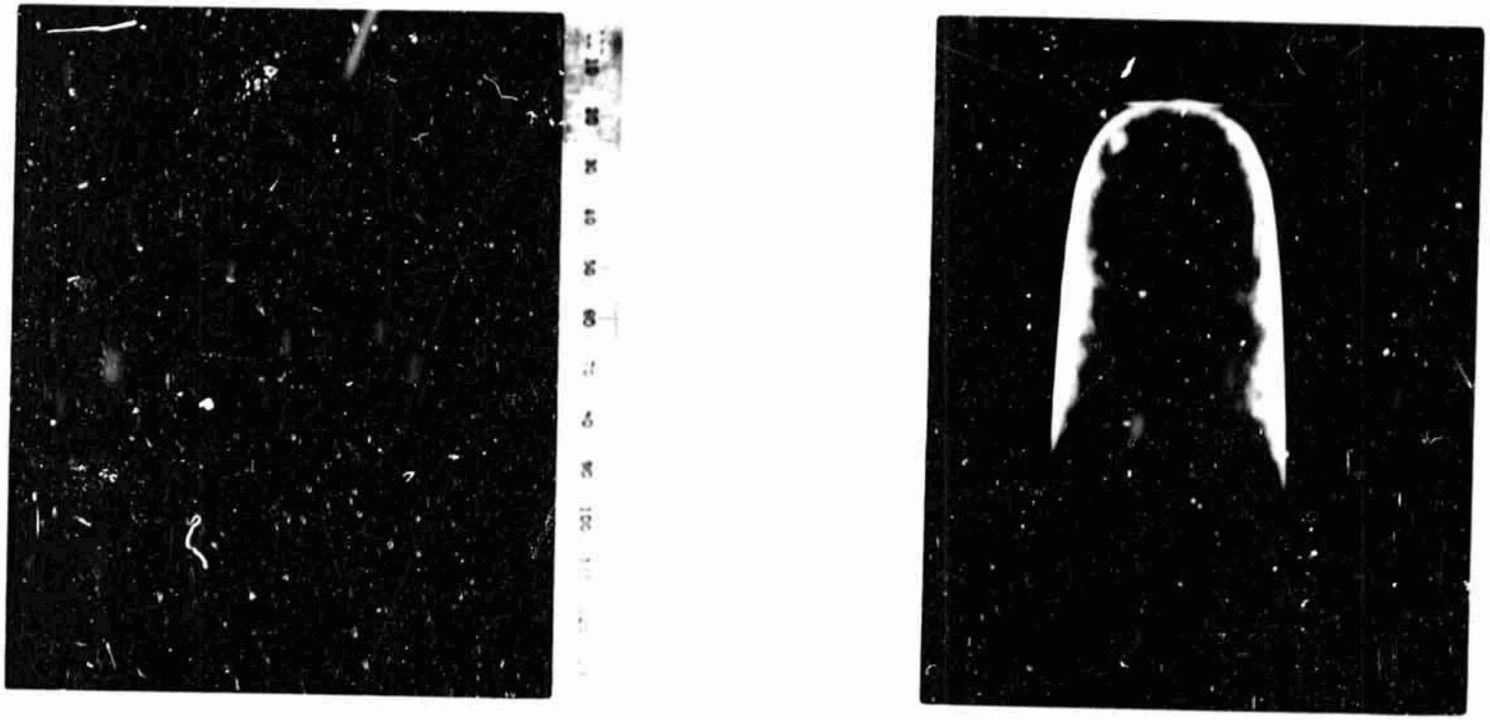

a) 1/200

b) 1/100

Fig. V-14 Photographs of Upward Propagating Flames in Particle Seeded Lean Limit Mixtures.

have units of mm. Of all the trials, the leading point of the upward propagating lean limit flame was always within ±0.5 mm of the laser beam.

A second set of referenced photographs were made of the upward propagating lean limit flames in unseeded mixtures. The previously described Miranda was used for these tests. Other 35 mm single lens reflex cameras were available with faster lenses, but only the Miranda's shutter could be released with the solenoid system. The major advantage of the Miranda over the Graflex is that unseeded flames could be photographed. However, the nature of the focal plane shutter required a new calibration technique to be used.

The focal plane shutter on the Miranda has two shades that move across the film plane. At high speeds (exposures ≤ 1/125 s) a slit moves across the film as illustrated in Fig. V-15a. This figure illustrates the Miranda as viewed from the open back of the camera. When the shutter is released, the first shade begins to move from right to left beginning the exposure. At the appropriate time the second shade moves from right to left ending the exposure. The shades always move at the same speed so that the exposure time is varied by changing the width of the slit.

In order to measure the exposure time and the rate at which the slit moves across the film, the camera shutter was calibrated using the equipment shown in Fig. V-15b. The camera lens was removed and two laser beams 12.45 mm apart were passed through the focal plane shutter in the positions shown in Fig. V-15a. The output from both aperture-phototransistors were input to separate channels of the Tektronix 7603 dual trace oscilloscope. The oscilloscope was triggered manually. A record from the calibration at a shutter setting of 1/125 is shown in Fig. V-16a. The shutter delay was read from

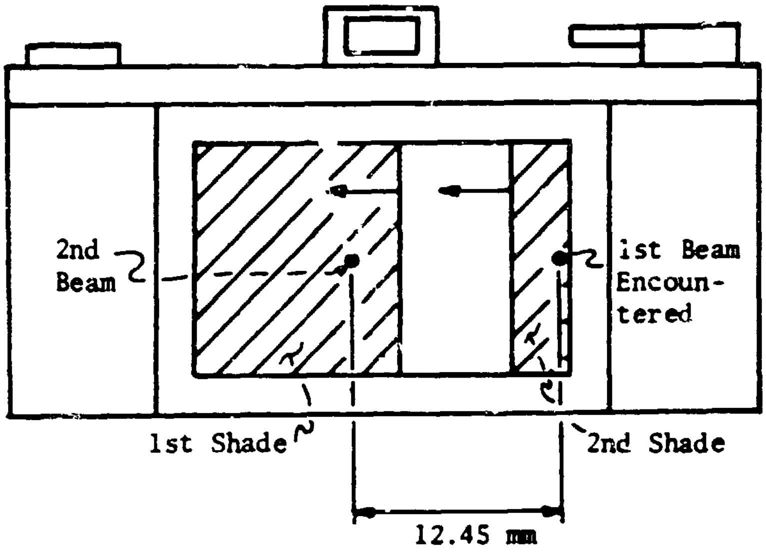

a Miranda Focal Plane Shutter

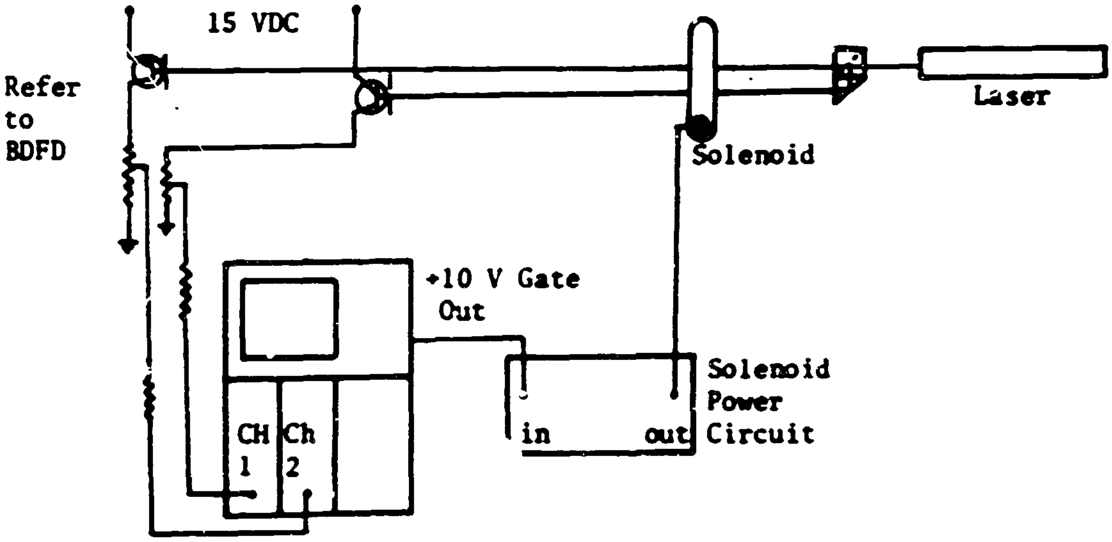

b Calibration Equipment

Fig. V-15. Illustration of Miranda Shutter Calibration Equipment.

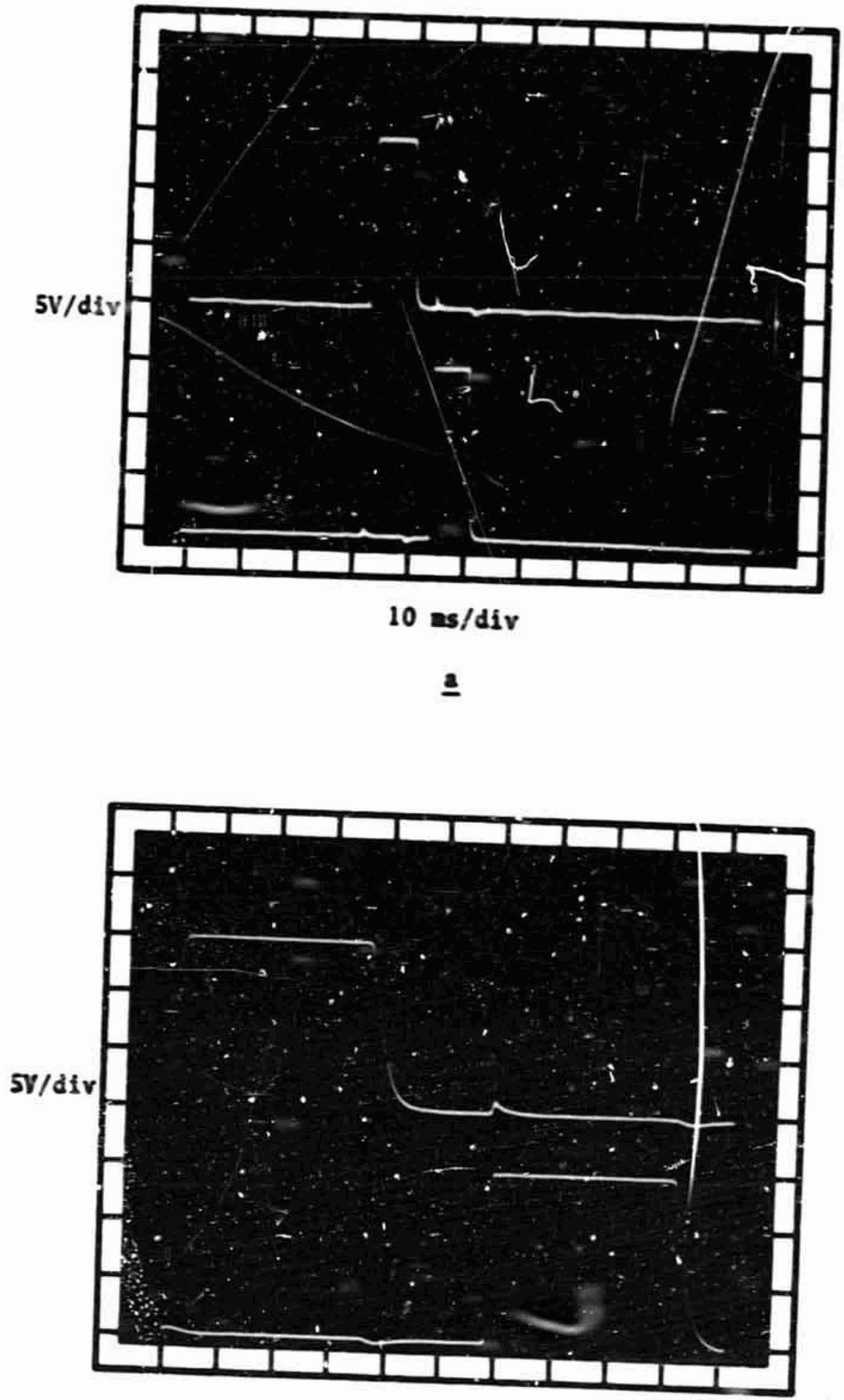

a

b

Fig. V-16. Oscilloscope Records of Miranda Calibration at Shutter Speed of 1/125.

this record. In order to increase readability, the time base was expanded for calibrating the shade speed and exposure time (see Fig. V-16b). A summary of the Miranda calibration results are shown in Table V-1. Six trials were made at each shutter setting (3 per time scale). All related trials were consistent within the readability of the scope. They are therefore considered to be accurate to 3%.

The same laser beam alignment procedure and equipment used for the seeded flame referenced photographs were used for these unseeded tests. The film and developing procedure used for photographs of Fig. V-8 were repeated. The aperture was set at f/1.9. The camera was mounted so that there was no movement from one exposure to the next. The camera was positioned so that the major axis of the film was vertical and the exposure slit of Fig. V-15a was moving opposite to the motion of the flame's image on the film plane. Originally an attempt was made to produce an image such that the leading edge of the flame was at the leading edge of the field of view. This would have provided the minimum delay time between the reference pulse and t beginning of exposure. However, the Miranda lens would not form a sharp image at that point. Consequently, the camera was positioned such that the reference beam was near the center of the field of view.

With a focal plane shutter there is a delay between the time when the 1^{st} shade begins the exposure at the leading edge of the field of view and the time the first shade begins the exposure at a distant point (refer to Fig. V-15a). Therefore it is necessary, for these tests, to measure the distance between the leading edge of the field of view and the image of the laser beam on the film. When the flame is photographed all the room light must be off. As a consequence, the edges of the field of view are not visible on the film.

TABLE V-1

RESULTS OF CALIBRATION OF MIRANDA 35 mm SLR

Shutter Setting	Mechanical Delay Δt_{mech}(ms)	Exposure Time Δt_{exp}(ms)	Shade Speed m/s
1/60	32.5	14.0	2.23
1/125	32.5	6.8	2.23
1/250	32.5	3.0	2.23

ideally one could produce the edge of the field of view and the flame on the same frame through double exposure. Since the Miranda is not equipped for double exposures, this was not possible. Instead, a scale was positioned in the plane parallel to the film plane and through the centerline of the tube. The 10 mm mark on the scale was placed coincident with the laser beam. The distance between the leading edge of the field of view and the 10 mm mark was then measured on a separate exposure. Care was taken so that the camera did not move between exposures.

A referenced photograph on an upward propagating lean limit unseeded flame is shown in Fig. V-17. For the purpose of manuscript reproduction it was necessary to print from a negative taken at a shutter speed of 1/60. Since the Miranda is not equipped for double exposure it was not possible to make the laser beam visible as previously suggested. Instead, the reference laser beam is visible only where it enters and exits the SFLT walls. Aluminum oxide powder was smeared on the outside of the tube walls to provide light scattering sources. These are visible as short horizontal lines in the photograph. The vertical lines are secondary reflections.

The referenced photographs from which the data were taken were exposed at a shutter speed of 1/125 (6.8 ms). All data were taken from the negatives using a Bausch & Lomb 20x comparator calibrated at 2.5 µm (0.0001 inch) increments. Close inspection of Fig. V-17 revealed that there is an apparent flame "thickness" associated with the image. This image thickness is not the flame thickness but mainly due to the movement of the flame during the exposure. The edges of the image had much better definition (not diffuse) on the negatives taken at 1/125 shutter speed. The position of the reference beam, the front edge and the back edge of the image at the centerline was

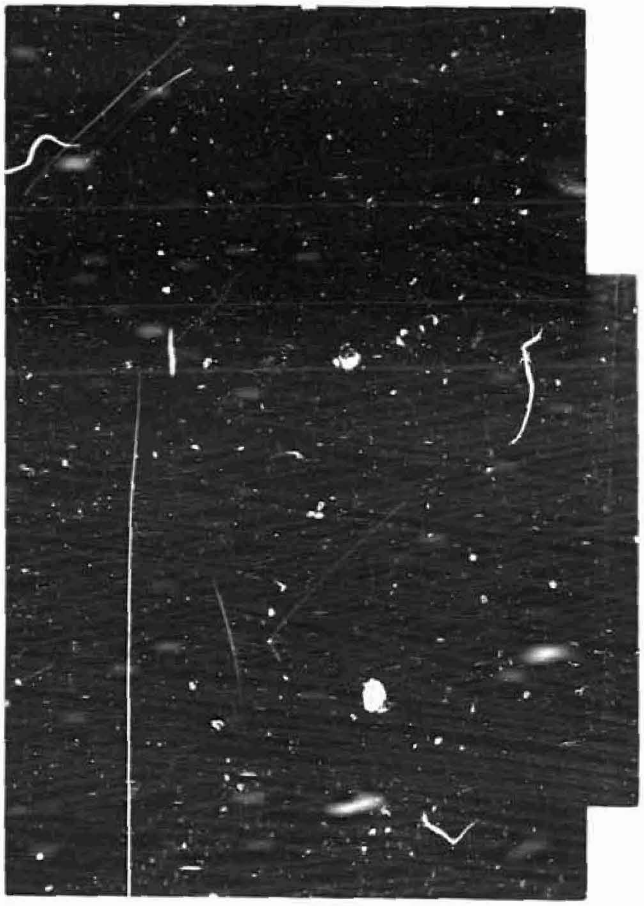

Fig. V-17 Photograph of Upward Propagating Flame in Unseeded Lean Limit Mixture.

measured on each negative (see Fig. V-18). The image thickness (Δx_{im}), the distance between the reference beam and the front edge (x_{fe}) and the d tance between the reference beam and the back edge (x_{be}) are tabulated in Table V-II. The major source of error in these measurements is the determination of the front and back edges of the image. The comparator projection surface is very bad, the negatives are very grainy and the actual image thickness on the negative is only 0.2 mm. The observed 8% variation is evidence of these problems.

In order to properly interpret the recorded image on the photograph, it is necessary to first consider the two possible sources of light emissions. The emissions that are visible in the lean limit methane-air flames have not been spectroscopically analyzed, however, the flame does appear blue-violet to the eye. Some generalizations can be made as to the sources of these emissions. Gaydon (1974) has compiled data on spectroscopic emissions from organic flames in various apparatus. Since the photographic emulsion used is not sensitive to infrared radiation, these sources will not be discussed. Intermediate species formed in the reaction zone of the flame do emit in the blue, violet and ultra-violet portion of the spectrum. According to Gaydon, CH has spectral bands with the strongest lines at 432 nm (blue) and 390 nm (violet). In weak mixtures and low temperature organic flames, HCO has been observed. HCO has bands from 250 nm to 400 nm with the strongest between 300 nm and 390 nm. OH has its strongest bands at 306 nm and below, into vacuum ultra-violet. The Swan bands of C_2 are at about 474, 517 and 564 nm. Since no green was observed (and the eye is a more sensitive detector than film) C_2 emissions are assumed to be absent. Although the photographic emulsion used is sensitive out to 250 nm, an inexpensive camera lens is

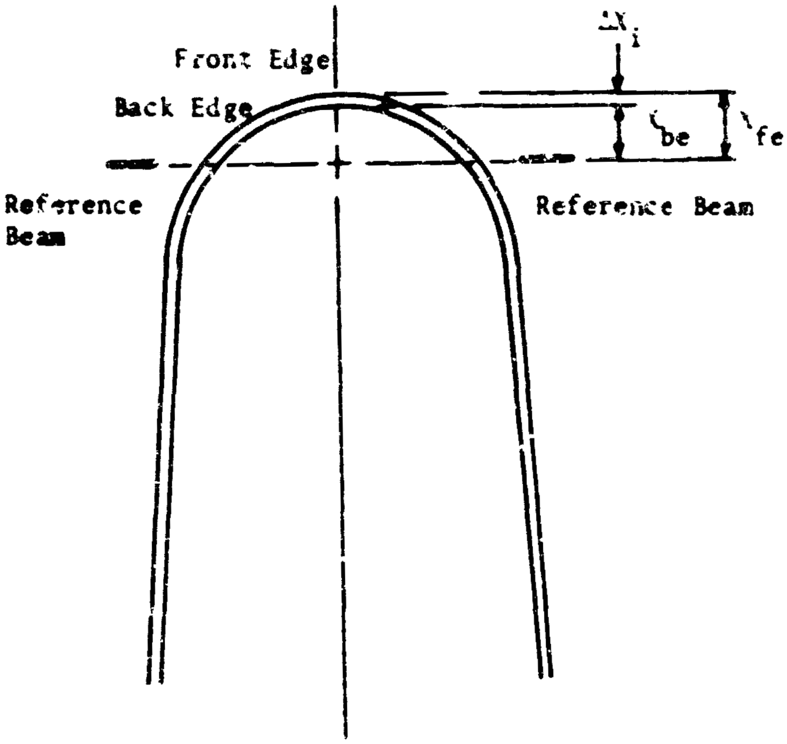

a Illustration of Unseeded Flame Image on Photograph

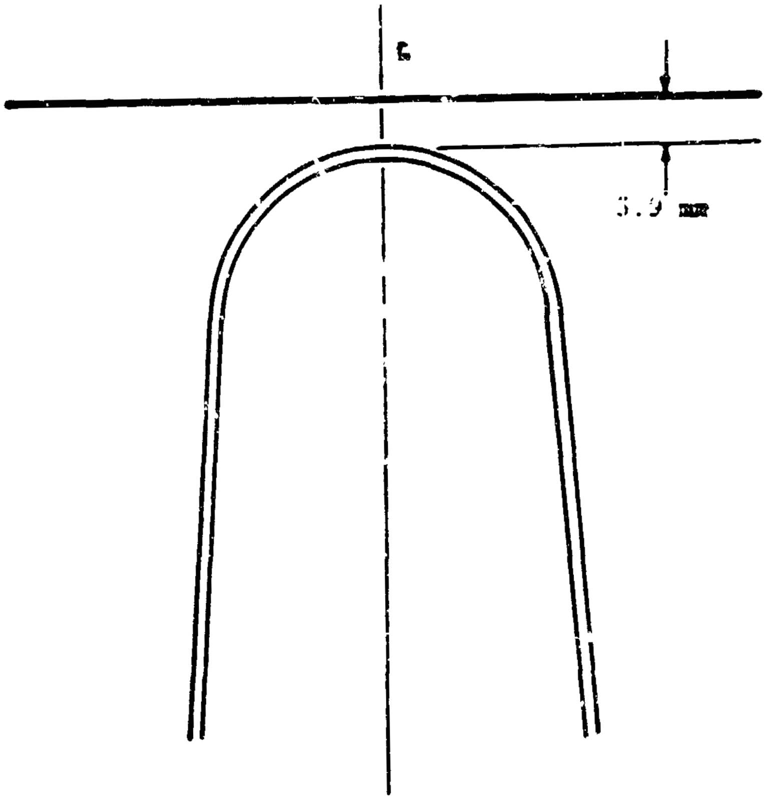

b Actual Position of Flame at Time When Beam was Deflected

Fig. V-18. Illustration of Unseeded Upward Propagating Lean Limit Flame.

TABLE V-2

REDUCED DATA FROM UNSEEDED FLAME REFERENCED PHOTOGRAPHS AT A SHUTTER SETTING OF 1/125

Test Number	Image Thickness ΔX_{im} (mm)	Back Edge to Ref. Beam X_{be} (mm)	Front Edge to Ref. Beam X_{fe} (mm)
1	1.68	5.41	7.09
2	1.43	5.29	6.72
3	1.55	4.97	6.52

typically transparent only to 320 nm. Therefore the OH emissions would not be recorded. Since CH and HCO are the major source of photographically recordable emissions and they have the highest concentrations in the reaction zone, the position of the visible near-UV emissions is a good indication of the position of the reaction zone.

The second source of emissions in the seeded flame is from the aluminum oxide particles. As the particles move through the flame, they heat up and individually emit as black bodies. The spectrum would be essentially continuous with the peak shifting towards the shorter wavelength as the temperature increases. As a consequence, a limit flame propagating through a particle-seeded mixture appeared yellow. The blue-violet color from the reaction zone could still be distinguished since the particle concentration was small.

It is obvious from the above discussion that the particles would produce the highest intensity at the region of highest temperature. If the particles were the sole or at least major source of emissions, the photographic image would have been essentially uniform, i.e., a solid white image on a black background. As is seen in Fig. V-14a and V-14b, this was not the case. Instead, there is an intense narrow band at the perimeter of the flame cap. The explanation for this is that the particle emissions do not, by themselves, expose the film. Both the particulate emissions and reaction zone emissions are required to expose the film at the specified aperture and shutter speed.

From the previous discussion it is valid to assume that for a flame propagating through a particle-seeded mixture, the maximum emission intensity is near the reaction zone. However, there is still some ambiguity in the

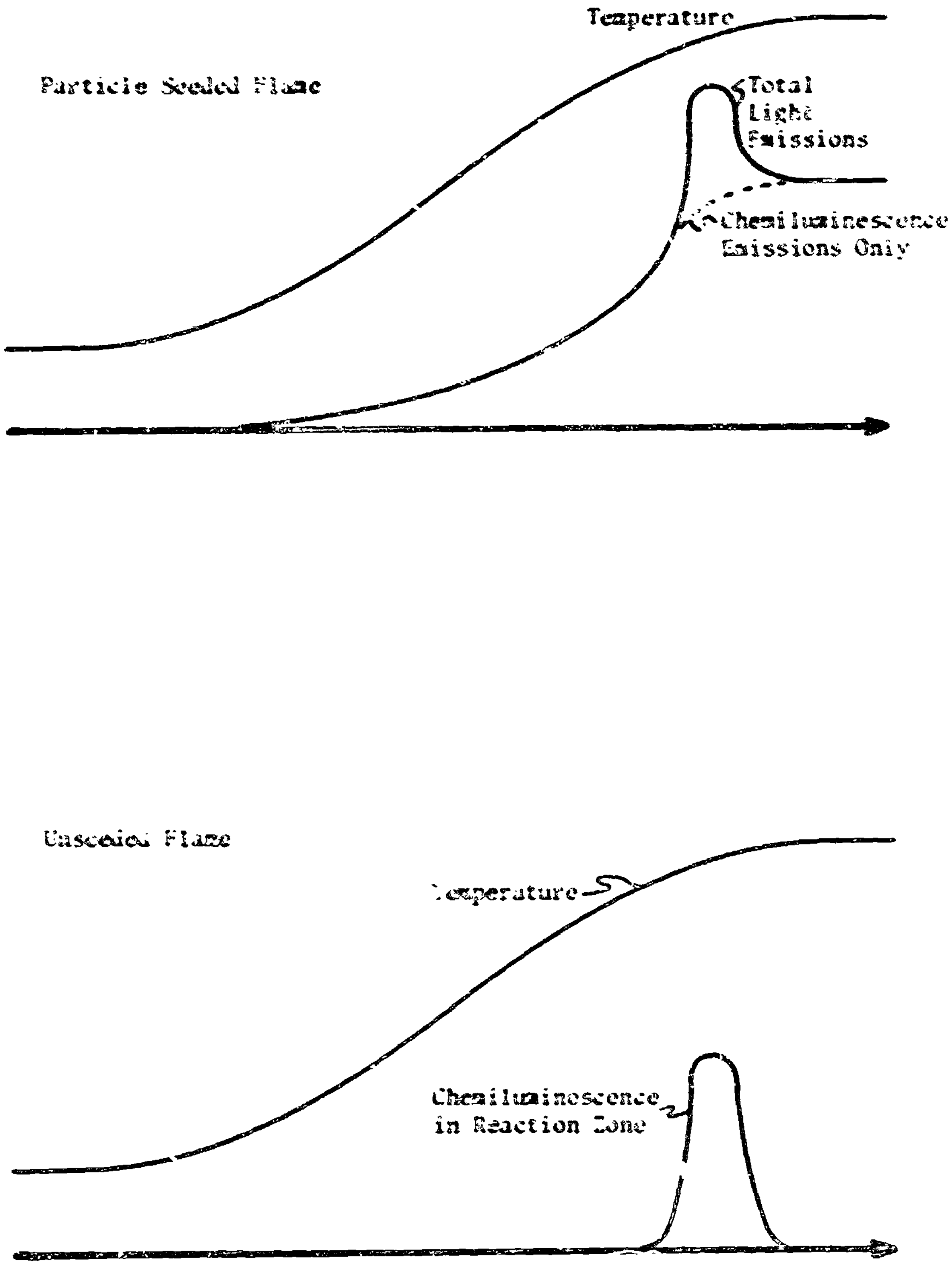

Particle Seeded Flame

Unseeded Flame

Fig. V-19. Hypothetical Light Intensity Distribution Through 1-D Flame.

interpretation of the photographs. The intensity as a function of distance (integrated over all wavelengths) along the centerline should look something like that shown in Fig. V-19a. A leaf shutter is essentially a variable aperture such that it moves from f/∞ (closed) to $f/4.5$ (open) and back. Since the transition is not a step function in time, the irradiance at the film plane is a complicated function. However, even with these complications it is still of interest to bracket the position of the visible flame in a seeded mixture.

By assuming that the position of maximum image intensity in the position of the flame at the beginning of the exposure, the position of the flame at the time of maximum beam deflection can be calculated. During the delay time between the beginning of the gate and the opening of the shutter (4.3ms), a limit flame traveling at V_p = 0.235 m/s would have moved 1.0 mm. During the 12 ms exposure (1/200) the flame would have traveled another 2.8 mm. Since the image of the flame was nearly coincident with the image of the reference beam, on the photograph, the flame would have been between 1.0 and 3.8 mm ahead of the reference beam at the time the reference beam was at its maximum deflection point.

The second set of referenced photographs made interpretation easier for two reasons. First of all, there were no particles present so that light emission was only from the reaction zone. Secondly, the exposure provided by the focal plane shutter was shorter and is essentially a step function in time. However, there were more sources of calibration error.

During the 6.8 ms exposure time (Δt_{exp})(refer to Table V-1), the lean limit upward propagating flame traveling at V_p = 0.235 m/s would have moved 1.6 mm (Δx_{exp}). This is on the order of the image thickness tabulated in

Table V-2. If the spacial intensity distribution (integrated over all wavelengths) is assumed to be a symmetric function as illustrated in V-19b, the image on the film represents a trace of only the maximum point of intensity. For this reason, the back edge of the image of the flame (at the centerline) is defined as the position of the flame at the time the exposure first began. The shutter had to travel 14.1 mm from the time it began to move until the time it exposed the image of the flame. Since the shutter is traveling at 2.23 m/s, there was a 6.3 ms shutter time delay, Δt_{sh}. Therefore a total of 38.8 ms elapsed ($\Delta t_{sh} + \Delta t_{mech}$) from the time the beam deflection triggered the gate until the time the image exposure began. This represents 9.1 mm of flame movement. Therefore at the time the beam deflection started the electronics, the flame (at the centerline) was 3.9 mm below the reference beam not the 5.2 mm above the reference beam as shown on the film (see V-18b). The uncertainty was calculated to be ±0.7 mm (Holman 1966).

Since the position of the visible flame is known at the time of maximum beam deflection, it is possible to reference it to the flow velocity profiles (to be discussed later under LDV measurements). However, it is of interest to know where the point of maximum deflection is on the flame temperature profile. According to Weinberg (1963) the point of maximum deflection in a 1-D laminar flame is at $T_{df} = 1.5\ T_u$ based on theory. This is in the preheat zone. It follows that this flame is at least 3.9 mm thick. This is the same order of magnitude as the 10 mm measured by Andrews and Bradley (1972b) but somewhat smaller. There are two reasons for this. It is presumed that Andrews and Bradley define the flame thickness as in Fig. II-4. This would account for some of the discrepancy since $T_{df} > T_u$ and the region of maximum light intensity $T_{IM} < T_b$. More important, the upward lean limit flame is not flat but three dimensional. In order to calculate the maximum deflection point indicated by the laser beam, it would be necessary to integrate the beam path through the index of refraction gradient across the whole tube diameter. From the shape of the flame, it is reasonable to assume that the maximum deflection point occurs when the beam is through a point at the centerline where $T > 1.5\ T_{u)_{℄}}$. Without the actual 3-D temperature profile, it is impossible to calculate exactly where the maximum deflection occurs.

CHAPTER VI

BEHAVIOR OF LEAN LIMIT METHANE-AIR FLAMES IN A FLAMMABILITY LIMIT TUBE AT 0-G

The second phase of the experimental investigation entailed observations of flame propagation in the 2.2s zero gravity environment of the small drop tower at the NASA Lewis Research Center. The major objectives were to:

i) Determine the lean limit methane-air mixture composition in zero gravity.

ii) Determine the shape of the flame in zero gravity.

iii) Determine the propagation velocity.

In this chapter the small drop tower facility is described along with the flammability limit tube used for the zero-gravity tests. The results of these tests are also presented.

The 2.2 second zero-gravity facility at the NASA Lewis Research Center in Cleveland, Ohio is illustrated in Fig. VI-1. In essence the 0-g environment is produced by dropping the experiment in an eight story tower. The dropped package consists of two separate parts, the bus which contains the experiment and the drag shield (see Fig. VI-2). In the ready-drop position, the package is hung on an 0.7 mm support wire which is attached only to the bus. There is a clearance hole in the drag shield for the support wire so that the drag shield is supported only by the bus. To initiate the drop, a pneumatically driven knife edge cuts the support wire allowing the bus and the drag shield to drop independently. As they fall, the aerodynamic drag slows the drag shield. Since there is negligible drag on the bus, there is a relative velocity between the two. A 0.2 m space between the bottom of the bus and the bottom of the drag shield allows for independent movement. The

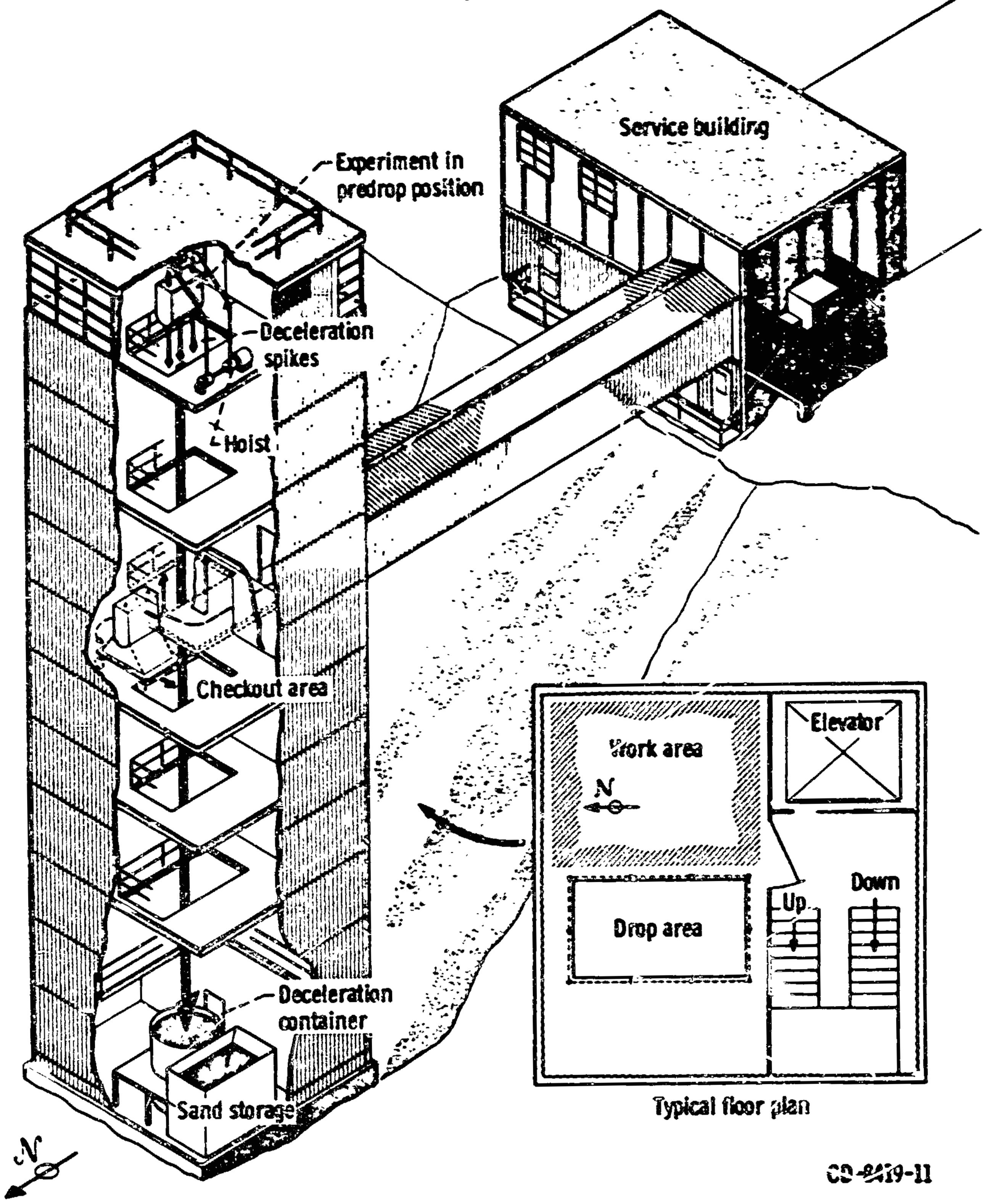

Fig. VI-1. 2.2-Second Zero-Gravity Facility at NASA Lewis Research Center.

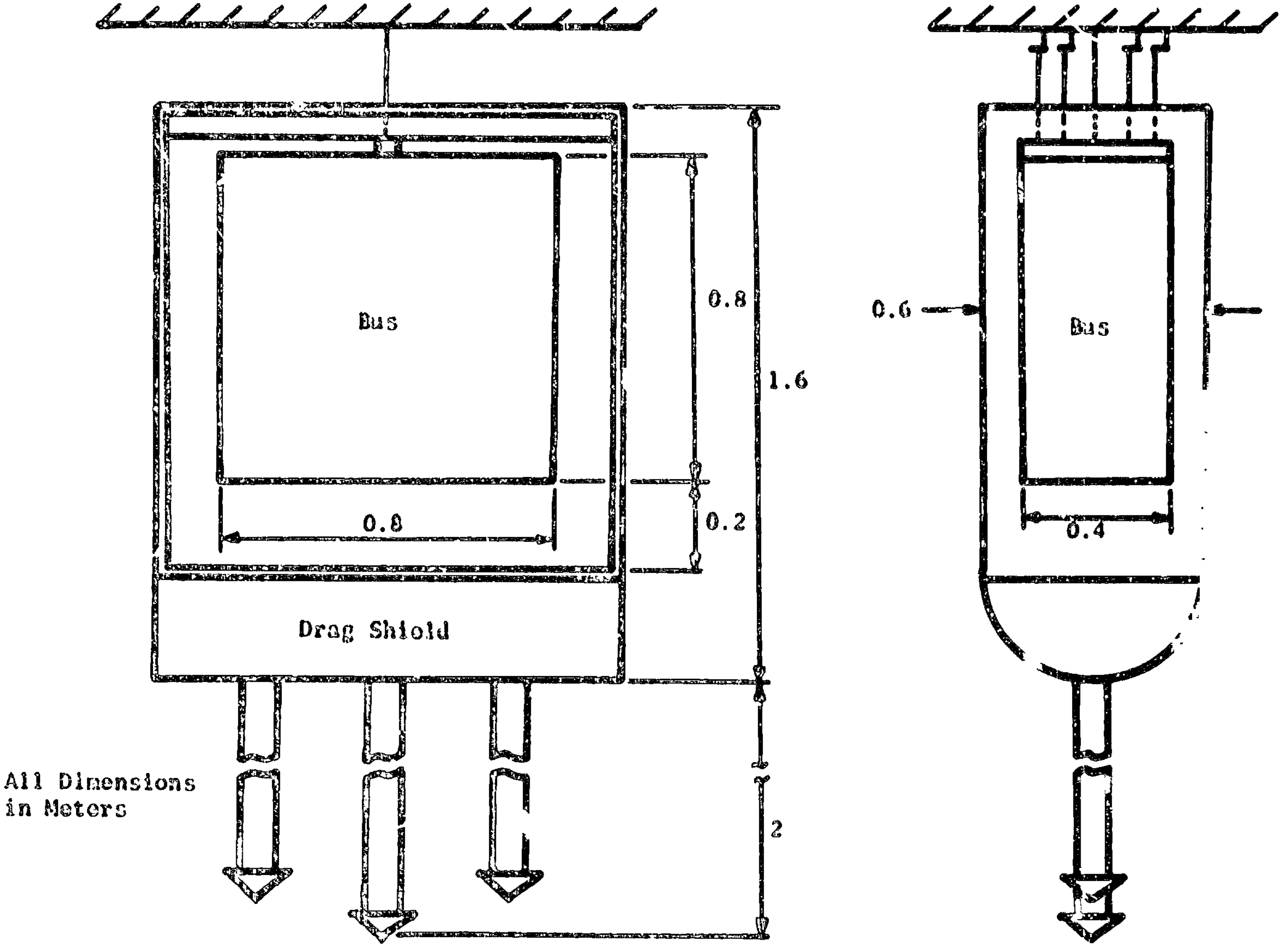

Fig. VI-2. Schematic of Zero-Gravity Package.

experimentally determined force on the bus is 10^{-5} g. The package is caught at the bottom of the tower by a deceleration container filled with fine dried sand which is aerated before each drop to prevent packing. The deceleration spikes attached to the drag shield have interchangeable conical tips to maintain proper penetration according to package mass. The bus contacts the bottom of the drag shield at approximately the same time that the spikes contact the sand. After the drop the package is hoisted to the fifth floor check-out area for servicing of the bus and preparation of the experiment for the next drop. The drag shield has easily removable side panels so that the bus can be removed between drops. When the experiment is ready for a drop, the bus is placed back in the drag shield and the package is hoisted to the eighth floor. The fastest cycle time for this experiment was 45 min.

Since the bus is totally inaccessible once it is in ready-drop position, the experiment must be run remotely. All experimental events can be automatically sequenced from both external and onboard timers. The external timer provides either +24 VDC or 0 VDC at a selectable point in time and for a selectable length of time. Several channels are available. A signal is simply set by dialing in the time of power on and time of power off using calibrated thumb wheels. These times are set relative to the time the external timer is started. The power from the external timer is brought on board the bus via umbilicals. The umbilicals are simply banana plugs attached to brass rods which are in turn externally clamped. The banana plugs fit through clearance holes at the top of the drag shield and into jacks in the bus (see Fig. VI-2). When the package drops, the plugs remain stationary and the bus pulls away breaking electrical contact.

The on board timer circuit provides sequencing from on board batteries. Either +15 VDC or +30 VDC are available. There is a single timer with several variable time delay relays for sequencing. The timed delay relays are calibrated with the on board timer. A calibration clock is zeroed and the on board timer is manually started. This starts the clock. When the relay changes mode (either on to off or off to on), the clock stops indicating the delay time. An uncalibrated set screw adjustment is made and the sequence repeated until the desired time delay is set. The relays may be started by the on board timer, by the external timer or at the time of the drop. The on board timer is started by the external timer. Once the package is in the ready-drop position, the external timer is started which subsequently sequences all the package events as well as the knife edge motion.

The photograph in Fig. VI-3 shows the bus used in this experiment inside the drag shield with the side panels removed. For this study a double bus was used so that a long tube and a larger photographic field of view were available. The control box with the timer and the timed delay relays is in the upper left-hand corner. The 16 mm movie camera had a 10 mm f/1.6 lens. This lens allowed viewing of the top 0.5 m of the flammability tube. The camera was operated at 24 frames per second with an 18.5 ms exposure per frame. The camera also had a neon light to provide timing marks on the film. Two umbilicals are visible at the top center of the bus. The batteries for on board power are at the bottom center just behind the calibration clock. The flammability limit tube used for this study is in view at the right-hand side. The ignition end (open during the test) is at the top of the bus. Not in view is a neon lamp at the vertical center of the tube. The lamp

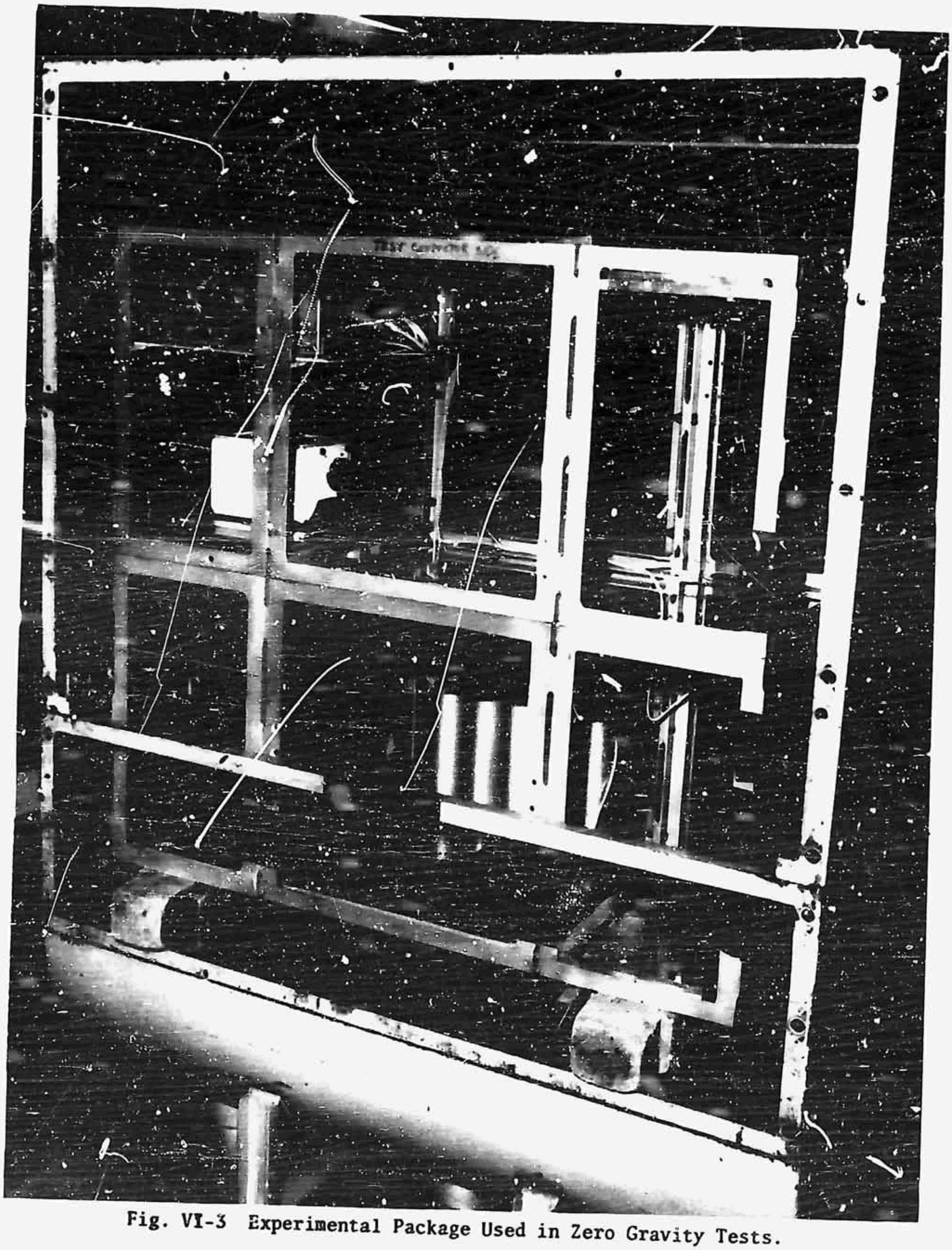

Fig. VI-3 Experimental Package Used in Zero Gravity Tests.

indicated when zero gravity began. The brass weights shown taped to the bus provided static balance.

The flammability tube used for these tests was 52 mm ID cylindrical Pyrex tube 0.74 m long. Plexiglass flanges were glued to the ends with GE RTV silicone glue. The valve back plates were rigidly mounted to the bus. The tube flanges were mounted with 3.2 mm rubber gaskets on both sides to damp any deceleration shock and to seal the tube (see Fig. VI-4). The bottom valve was a manually operated aluminum rotary valve used to vent and seal the tube during refilling. The top valve was manually closed and automatically opened (see Fig. VI-5). The valve is shown in its open position with the ignition ring and electrical leads in position. A free clearance was maintained between the sliding and the back plates. The valve was sealed with an o-ring. The valve was held closed by the plunger of a solenoid (not visible) on the bottom side of the back plate. When power was supplied to the solenoid, the plunger was retracted and the valve would open by the force of a rubber band.

The flammability limits tube and valves were designed and constructed in the AAE Departmental shop and taken to Lewis Research Center for mounting in the bus. The on board electronics were also customized at that time. The complete bus was then brought back to the University of Illinois for ground testing of the electronics, ignition and photographic procedure. The bus was then returned to Lewis Research Center where the zero gravity tests were conducted during a three week period. During the tests the film development, gas metering and ignition preparation were implemented by myself. Procedures concerned with the drop tower facility were implemented by NASA technicians.

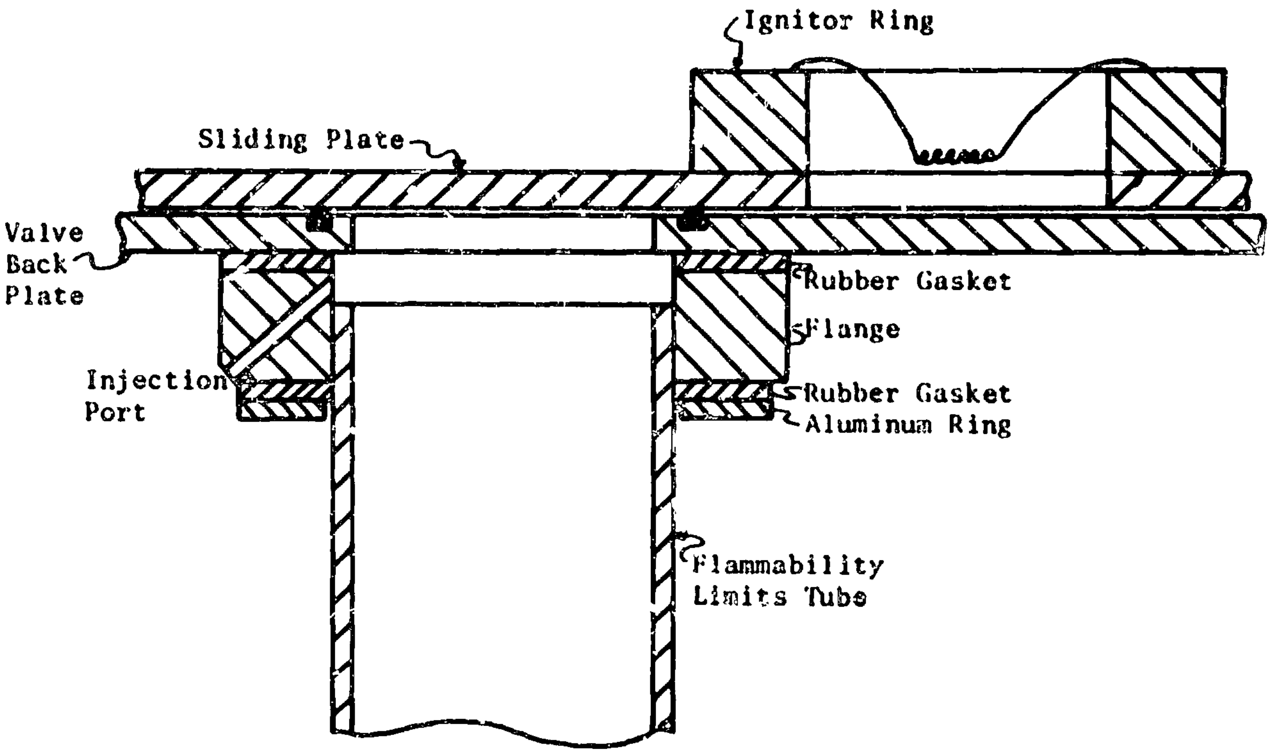

Fig. VI-4. Schematic of Automatic Valve.

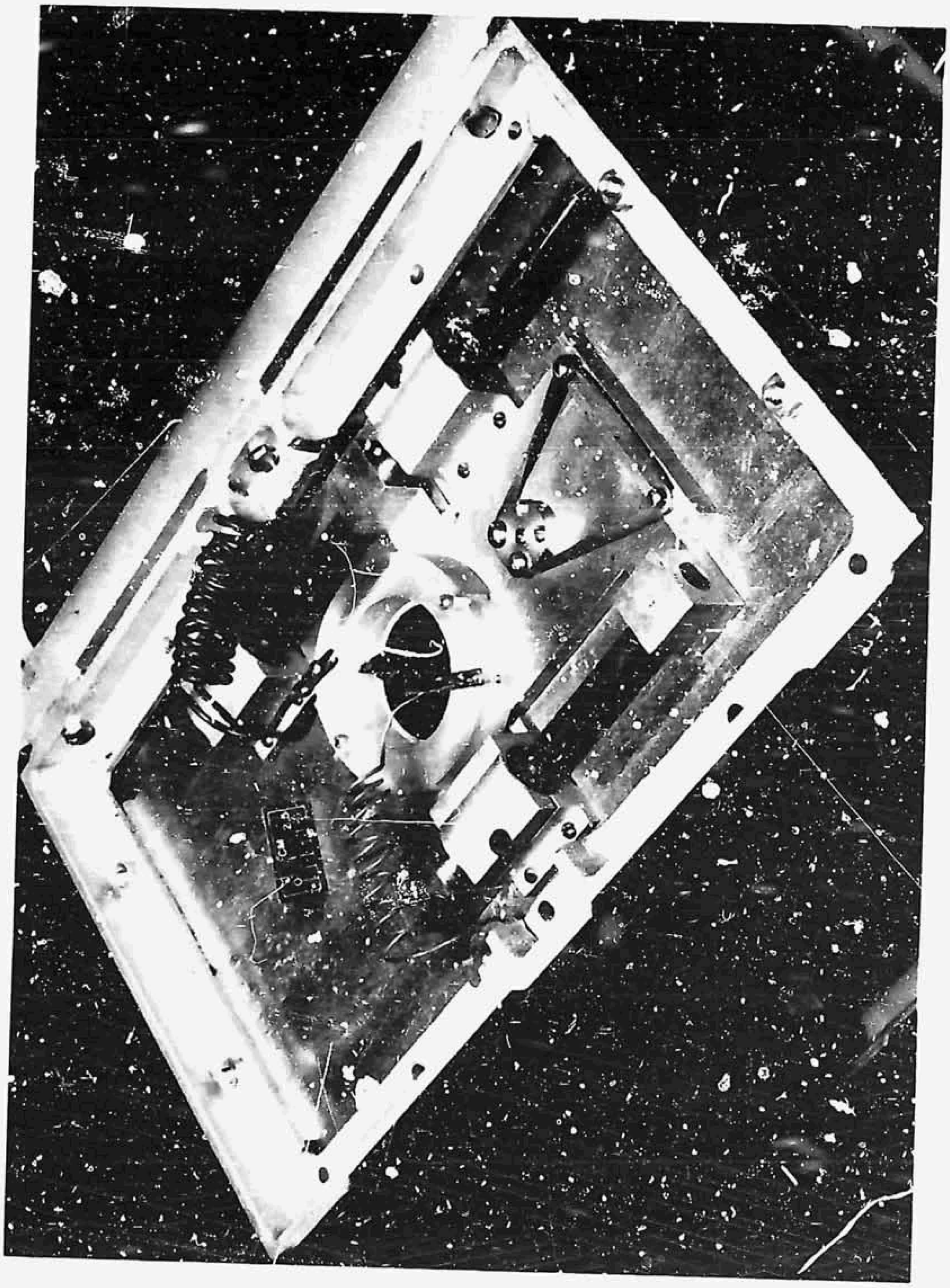

Fig. VI-5 Automatic Valve in Open Position.

The gases used for the 0-g tests were supplied by NASA. The methane was Airco Grade 2, 99% pure. The air was bottled "Breathing Quality". The same two calibrated rotometers used in the 1-g tests of Chapter V were taken to Lewis Research Center for the 0-g tests. For this reason, the mixture compositions reported in the 0-g tests and all 1-g tests are assumed to be self-consistent.

A new ignition procedure had to be developed for the zero gravity tests. There was a 20-min delay between the times when the flammability tube was filled with a test mixture and the time the package was in the ready-drop position. For this reason the insertion of a richer slug of methane-air mixture near the igniter that was used for the 1-g tests at Illinois could not be used in these tests. Instead a locally rich composition was produced at the ignition end by injecting 4 cc of pure CH_4 from a syringe. 4 cc of CH_4 would form a 40 mm long slug of 5% CH_4 if homogeneously mixed with air. The methane was injected through a 0.64 mm dia port drilled through the top flange (see Fig. VI-4). This was done manually just prior to drop.

An electric ignition source was made by wrapping 10 turns of 0.2 mm nichrome wire around a 1.9 mm rod and leaving 30 mm pigtails. The coil was then dipped in a nitrocellulose-acetone solution and allowed to dry. Care was taken so that only a thin coating of nitrocellulose was deposited on the wire. In this way all the nitrocellulose would burn completely without dripping (in 1-g). 30 VDC was established across the terminals for only 0.20 s so that the igniter wire would not melt. The wire was placed at the center of the tube and as near the valve as possible (see Fig. VI-4). The electric igniter and the amount of CH_4 was empirically determined to be the least required and still provide consistent ignition. As a further test, this ignition method was tried in the SFLT to determine if previous results were altered. It was found that the limit composition did not change and the propagation velocity was not altered.

The experimental package was prepared for each drop on the fifth floor of the tower. The procedure is given in Table VI-1. Approximately 20 min elapsed between steps 3 and 9. No more than 45 s elapsed between steps 7 and 9. Pressing the fire button started the automatically timed sequence given in Table VI-2. The ignition current did not start until 0.05 s after electrical contact from the umbilicals was broken. The bus had to fall at least 20 mm to break contact. Therefore there were no thermal gradients until after the zero gravity condition was established. The neon lamp went out when umbilical contact was broken so that the beginning of 0-g was marked on the film.

Two types of film were used to record the flame propagation during each drop, Kodak 2498 RAR ASA/250 and Kodak 4X negative ASA/500. The 2498 was used at first since it was readily available through NASA. It proved to be too insensitive for mixtures leaner than 5.63%. Consequently the 4X negative film was used for most of the 0-g tests (all lean mixtures). Both film types were developed as negatives in a Kodak Versomate continuous film developer. For normal developing the film is run through at 1.8 m/min. For these tests the film was pushed approximately 2 stops by processing it at 0.45 m/min. The film record length of each test was kept to approximately 3 m by removing the record after each drop. Each drop record was then processed separately.

The photographic record of each test contained several frames of a

TABLE VI-1

1) Open both valves and replace the igniter ring with the plenum chamber. Seal injection port with Apogon.
2) Purge tube with 10 volumes of test mixture.
3) Close valves and replace plenum chamber with igniter ring and new ignition wire.
4) Place bus in the drag shield; attach new support wire and hoist package to 8th floor.
5) While still held by the hoist, attach support wire, umbilicals and side panels to drag shield.
6) Activate external console and then onboard electronics.
7) Inject 4 cc of CH_4 into injection port through access door in side panel.
8) Hang package on support wire.
9) Sound alarm and start external timer.

TABLE VI-2

TIMED SEQUENCE OF ELECTRICAL FUNCTIONS

0.00 s	External Timer ON
	On Board Timer ON
	Camera ON
	0-G Indicator Light ON
0.30 s	Open End Valve
0.70 s	Cut Support Wire
T_1	Umbilical Contact Broken
	0-G Indicator Light OFF
T_1 + 0.05 s	Ignition Current ON
T_1 + 0.25 s	Ignition Current OFF

0.3 m scale, several frames of the identifying run number and the flame propagation itself. There were also timing marks along one edge of the film. The timer was not working during all tests and sometimes only intermittently. When it was working, there was excellent agreement between the timer and the framing rate. It is assumed that the framing rate was accurate for all tests.

The data were read directly from the negatives using a Vanguard 16 mm film analyser. One frame is projected on a screen at a time and an x-y calibrated crosshair is used to measure the coordinate of the desired point. The analyser was calibrated every 2.5 μm. The magnification was measured using the scale photographed before each drop.

A total of 35 0-g drop tests were made with mixture compositions ranging from 4.6% to 6.74% methane in air. In addition, while at NASA, 1-g tests were photographed in the 0.74 m tube using the same test procedure (Table VI-1) and the same timing sequence (Table VI-2) that was used in the 0-g drop tests. The 1-g results were used for comparing the flame shape, the propagation velocity and to determine if the limit composition was the same as in the SFLT.

Photographs of the flames at 5.85% methane are shown in Fig. VI-6a. The most striking feature of the 0-g flame is that the surface area of the flame is between that of the upward and downward propagating flame of the same mixture. The photograph in Fig. VI-6b is of a 0-g flame in a mixture near the 1-g upward lean limit composition. This was the leanest 0-g flame recorded that was suitable for reproduction. It was not possible t re-produce the photograph of an upward propagating flame at 5.37% using the technique described in this chapter. However, the photograph of an upward propagating lean limit flame shown in Fig. V -7 is a reasonable comparison.

Downward Zero Gravity Upward

5.87%

Zero Gravity

5.33%

Fig. VI-6 Photographs of Flames in Zero and Earth's Gravity.

The 5.37% 0-g flame of Fig. VI-6b has a much shorter "skirt" than the 5.27% upward propagating 1-g flame shown in Fig. V-17. This is consistent with visual observation made of 5.37% upward propagating flames in the SFLT.

Accurate determination of the 0-g lean limit was not possible in the drop tower. The propagation velocities of the lean flames are low and consequently the flames did not travel far in the 2.2 s available. Instead, a lower bound was found by testing progressively leaner mixtures until the flame was observed to fail during the drop. In order to assess approximately what the 0-g lean limit mixture composition is, it was necessary to determine how far flames would travel away from the ignition source in mixtures outside the upward and downward lean limits. It was expected that a flame would evolve even in sublean limit test mixtures due to the use of a rich ignition slug. From the earlier 1-g tests, the upward flame was known to travel up to 0.3 m away from the ignition source in a 5.22% CH_4 test mixture. This effect is assumed to be due to the fluid flow being augmented by gravity. Therefore, it was felt that a study of the downward flame ignition is a better comparison for the 0-g case. The results of the downward flame ignition tests are shown in Table VI-3. It was demonstrated that the downward propagating flame does not propagate far from the ignition source even in mixtures just outside the downward lean limit.

A summary of the 0-g tests is shown in Table VI-4. It should be noted that the flame did not attain a steady propagation velocity until 0.46 - 0.54 seconds (11 - 13 frames) after zero gravity began. It is apparent from Table VI-4 that the lower bound for the lean limit of methane-air mixtures in zero gravity is 5.10% It is the leanest mixture composition that would support combustion for the entire duration of the drop. The

TABLE VI-3

DOWNWARD PROPAGATING 1-G FLAME TESTS IN THE DROP TOWER APPARATUS

Φ	% CH_4	Distance Flame Traveled (m)
0.618	5.87	full length
0.611	5.81	0.08
0.611	5.81	0.08
0.605	5.75	0.05
0.605	5.75	0.09
0.605	5.75	0.10
0.599	5.69	0.05
0.599	5.69	0.05
0.592	5.63	0.06
0.592	5.63	0.05

TABLE VI-4

RESULTS OF 0-G TESTS IN NASA LEWIS SMALL DROP TOWER

Φ	% CH_4	0-G Run Number	Frame in Which Flame Failed	Total Distance Traveled m	Propagation Velocity m/s
0.709	6.74	35	--	0.37	0.326[a]
0.691	5.57	32	--	0.50	0.306
0.672	6.39	31	--	0.51	0.209
0.658	6.25	33	--	0.39	0.177
0.639	6.07	30	--	0.41	0.198
0.629	5.98	34	--	0.44	0.150
0.618	5.87	29	--	0.28	0.111
0.605	5.75	28	--	0.27	0.115
0.592	5.63	27	--	0.24	0.098
0.573	5.45	26	--	0.21	0.079
0.561	5.33	25	--	0.19	0.074
0.549	5.22	18	--	0.15	0.044
0.537	5.10	19	--	0.14	0.033[b]
0.524	4.98	20	34	0.09	
0.524	4.98	22	34	0.10	
0.511	4.86	21	30	0.08	
0.511	4.87	23	30	0.08	
0.502	4.77	24	26	0.08	

---

[a] Transitioned to vibratory motion.

[b] Unsteady motion.

propagation velocity for 0-g test 19 was calculated from the last 9 frames even though the flame was continually slowing down. It is suspected that this flame would have extinguished before propagating the full 0.74 m length if zero g conditions could have been maintained for a sufficiently long time. The flame in 0-g test 18 did appear to reach a steady state propagation velocity during the last 45 mm (≈ 1 s) of the run. It also propagated significantly further than the sublean limit downward propagating flames reported in Table VI-3. This might be called the limit mixture (5.22%) but this is a tenuous conclusion because of the short test time available.

A plot of flame propagation velocity as a function of mixture composition is illustrated in Fig. VI-7 for both 0-g and 1-g flames. The solid squares represent the average of 5 trials each from tests in the SFLT. The open symbols represent 1 trial each and all are from tests in the drop apparatus. As before, the 1-g tests in the drop apparatus used the same ignition procedure used in the 0-g tests. This figure, along with the previously discussed results, reveal three important properties of lean methane-air flames propagating in a 0-g environment. Namely,

1) Zero-gravity flames propagate further from the ignition source than downward propagating 1-g flames in mixtures outside the downward lean limit. It appears that the 0-g lean limit is closer to the upward than the downward lean limit.
2) The surface area of the 0-g visible flame is between those of the upward and downward propagating 1-g flames.
3) The 0-g flames propagate at nearly the same velocity as downward propagating flames in like mixtures.

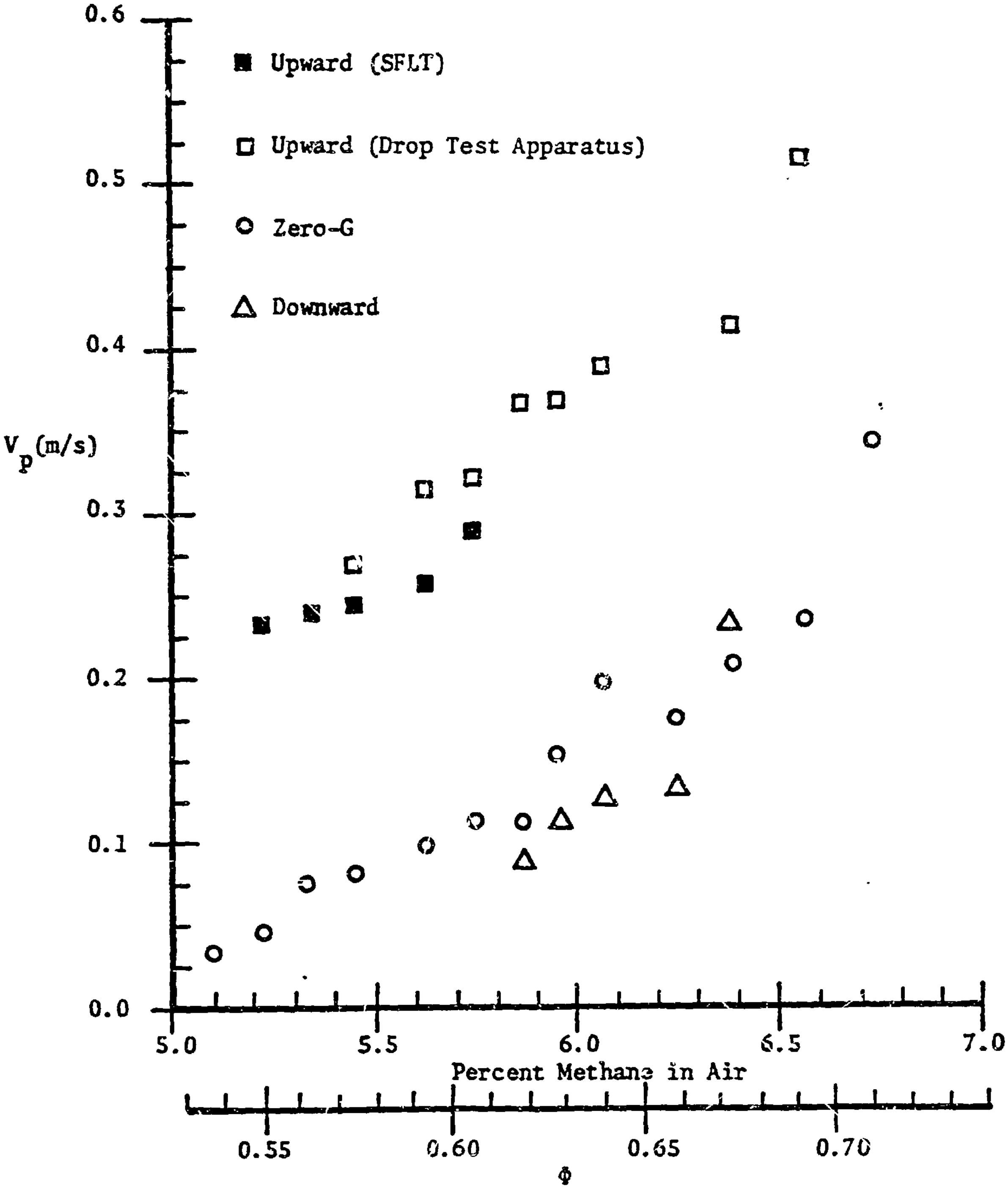

Fig. VI-7 Flame Front Propagation Velocity of Lean Methane-Air Flames in 0-G and 1-G.

CHAPTER VII

VELOCITY MEASUREMENTS THROUGH AN UPWARD PROPAGATING LEAN-LIMIT FLAME

The purpose of the third phase of this experimental study was to measure the velocity profile of an upward propagating lean-limit methane-air flame in the standard flammability limit tube. Measurements of both the longitudinal velocity component (V_z) and the radial velocity component (V_r) were made. Mechanical probes are not acceptable for this purpose since they would have introduced a heat sink as well as interfered with the flow and a lean-limit flame is very sensitive to both thermal and aerodynamic perturbations. Particle tracking with a high intensity flash lamp is far less intrusive but is, at best, tedious and prone to error due to frame to frame particle identification. It was felt that a laser Doppler anemometer (LDA) is best suited for this flame configuration. A LDA is relatively unintrusive and has good spacial and temporal resolution. This chapter contains a brief description of the apparatus used for this study and the results of its application.

The LDA Optical System

Laser Doppler anemometry is a technique for measuring the fluid velocity by measuring the Doppler shift of visible light scattered by small particles (0.5 → 10 μm). These particles are almost always artificially seeded into the fluid. Yeh and Cummins (1964) are credited with being the first to demonstrate this technique for measuring fluid velocities. Durst et al. (1972) demonstrated that it is possible to measure fluid velocities through a laminar premixed flame on a Bunsen burner. It has also been used in turbulent premixed flames (Durst and Klein, 1973) and in diffusion flames (Baker, Bourke and Whitelaw, 1973). However, a LDA has not previously been used for measuring fluid velocities in a medium through which a laminar flame is moving with respect to the LDA probe volume.

The system used for this study was a single-channel forward-scatter dual-beam LDA. The phenomenological description of LDA principles in this chapter will be limited to this simple configuration. A theoretical description of this simple system is given in Appendix A. More detailed information on this and other possible LDA configurations can be found in Durst et al. (1976) and in Adrian and Fingerson (1976). An engineering approach to the design criterion of a LDA is given in TSI Bulletin #25.

A schematic of the LDA optics system built for this study is illustrated in Fig. VII-1. A single laser beam is split into two parallel beams of equal intensity. The beams are then passed through the transmitting lens. This focuses the two beams at the LDA probe volume. The laser beams illustrated in Fig. VII-1 lie in a horizontal plane. Consequently the LDA measures the magnitude of the horizontal velocity component in the direction indicated by the arrow. However, this LDA system can not distinguish between a positive or negative velocity.

When a particle passes through the probe volume, the light from both beams is scattered, collected by the receiving lens and imaged on an aperture just ahead of the photomultiplier tube (PMT). The PMT converts the information contained in the scattered light into a time varying current i(t). Signal processing equipment (not shown in VII-1) then converts the PMT current into a voltage. Each time a particle passes through the LDA probe volume a single voltage pulse is output. The magnitude of this voltage is

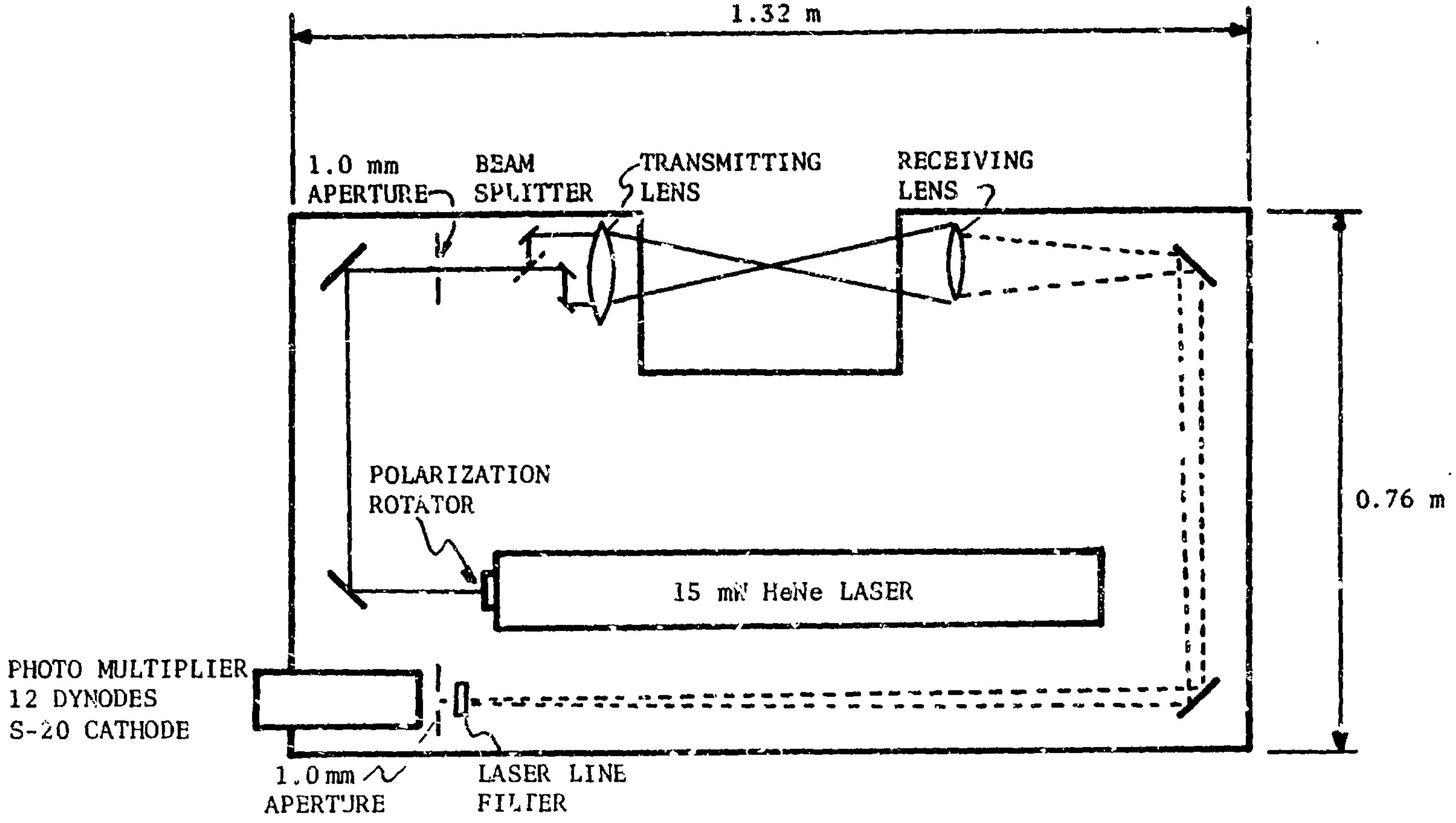

Fig. VII-1. Schematic of Single Channel Laser Doppler Velocimeter.

TABLE VII-1

LDA PROBE VOLUME POSITION ERROR FOR OFF AXIS MEASUREMENTS OF THE RADIAL VELOCITY

Y Translation of LDA Optics (mm)	Measured Position of Probe Volume (mm)	Error %
0.0	0.0	0.0
2.0	2.0	0.0
4.0	3.9	2.5
6.0	5.9	1.7
8.0	7.9	1.3
10.0	9.9	1.0
12.0	11.8	1.7
14.0	13.8	1.4
16.0	15.7	1.9
18.0	17.9	0.6
20.0	19.7	1.5
22.0	21.4	2.7
24.0	23.3	2.9
26.0	24.5	5.8

proportional to the magnitude of the particle velocity. Thus a time varying fluid motion is recorded as a series of discrete voltage pulses. It is assumed that the particles are small enough to accurately follow the fluid motion.

A magnified representation of the LDA probe volume is illustrated in Fig. VII-2. It is most frequently modeled as consisting of parallel and stationary fringes. These fringes are planer and are oriented perpendicular to the plane formed by the intersecting beams. The fringe spacing (x_{frng}) is given by

$$x_{frng} = \frac{\lambda}{2 \sin\xi} \qquad \text{(VII-1)}$$

where ξ is the beam intersection half angle and λ the wavelength of the light. The probe volume is characterized by its length

$$\ell_{pv} = \frac{d_{e^{-2}}}{\sin\xi} \qquad \text{(VII-2)}$$

and its diameter

$$d_{pv} = \frac{d_{e^{-2}}}{\cos\xi} \qquad \text{(VII-3)}$$

The beam diameter at the probe volume $d_{e^{-2}}$ is that region where the intensity is about 14% ($1/e^2$) of the centerline intensity. It is related to the beam diameter just ahead of the transmitting lens ($D_{e^{-2}}$) by

$$d_{e^{-2}} = \frac{4}{\pi} \lambda (F.L.)/D_{e^{-2}} \qquad \text{(VII-4)}$$

where F.L. is the focal length of the transmitting lens. As a particle passes through the probe volume it scatters the light. The electrical signal output from the PMT from a single particle (called a Doppler Burst) would

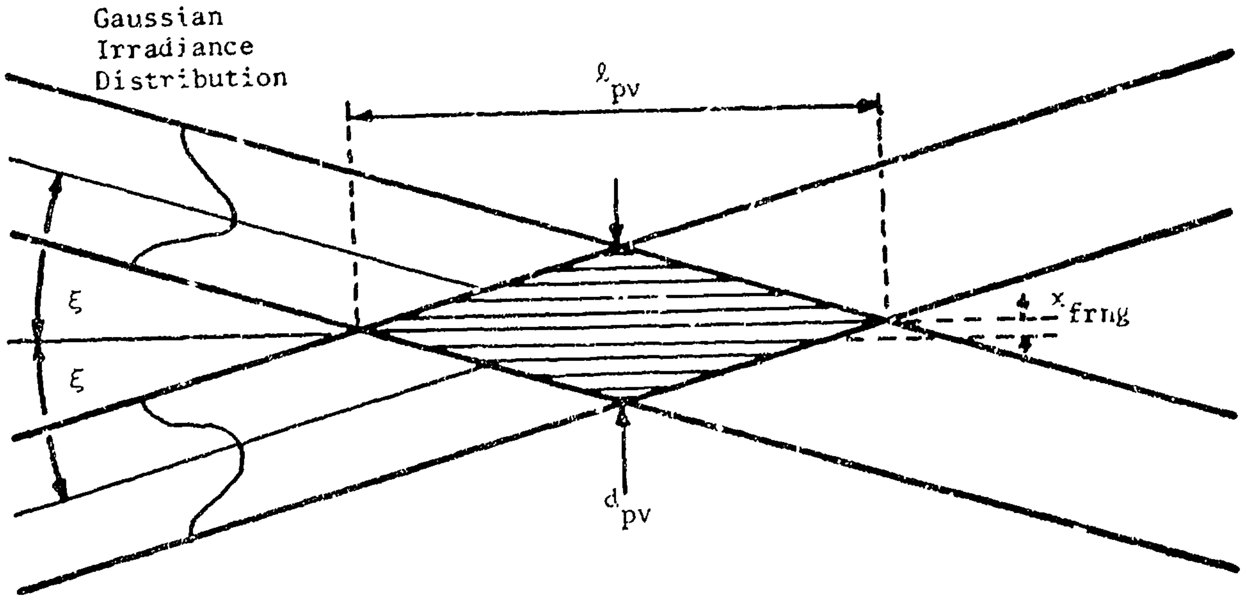

Fig. VII-2. Fringe Representation of LDA Probe Volume.

appear as illustrated in Fig. VII-3a. This signal consists of the Doppler frequency (high frequency component) modulated by the pedestal frequency (low frequency component) which can be separated and observed individually as illustrated in Fig. VII-3b. The Doppler frequency is simply related to the fringe spacing and the particle velocity component perpendicular to the fringes (u). Each Doppler burst results in a discrete frequency measurement (data point) which is linearly related to the particle velocity by the equation

$$f_{Dop} = \frac{u2\sin\xi}{\lambda} \qquad \text{(VII-5)}$$

In order to determine a velocity profile, enough particles must be present to provide a data rate sufficient to resolve the velocity changes.

The LDA system constructed for this study (Fig. VII-4) used a linearly polarized 15 mW Spectra Physics HeNe laser operating at 632.8 mm with $d_{e^{-2}} = 1.1$ mm. A polarization rotator was mounted on the laser output bezel to properly orientate the direction of polarization with respect to the dielectric beam splitter. The 1 mm aperture ahead of the beam splitter was used to eliminate the secondary beam reflections (refer to Fig. VII-1).

An alignable beam splitter was constructed (Fig. VII-5) providing two parallel beams 112 mm apart. A 145 mm plano-convex transmitting lens with a focal length of 250 mm (at $\lambda = 588$ nm) was used. This lens resulted in a beam intersection half angle of $\xi = 13.6°$ (@ $\lambda = 632.8$ nm). Both the lens and the beam splitter assembly were mounted to a 152 mm diameter rotator with stops orientating the plane of the beams vertically or horizontally. The large beam intersection angle was used because of the low fluid velocity to be measured (refer to Eq. VII-5).

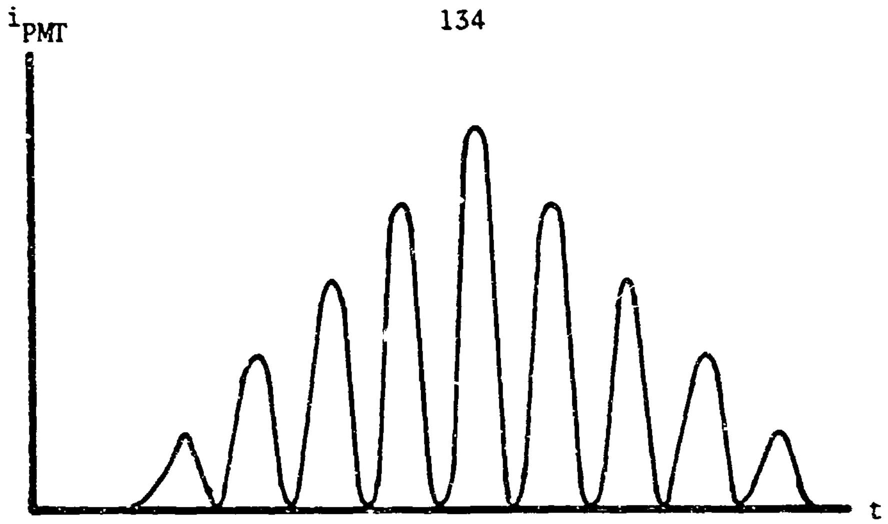

a PMT Current vs Time

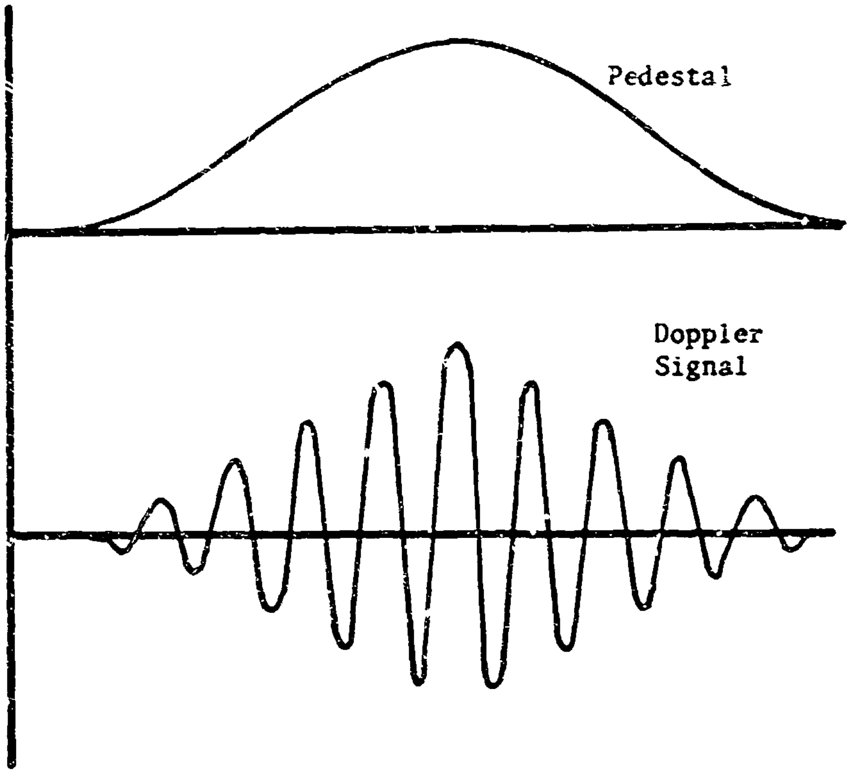

b Low and High Frequency Components

Fig. VII-3. Representation of an Ideal Doppler Burst.

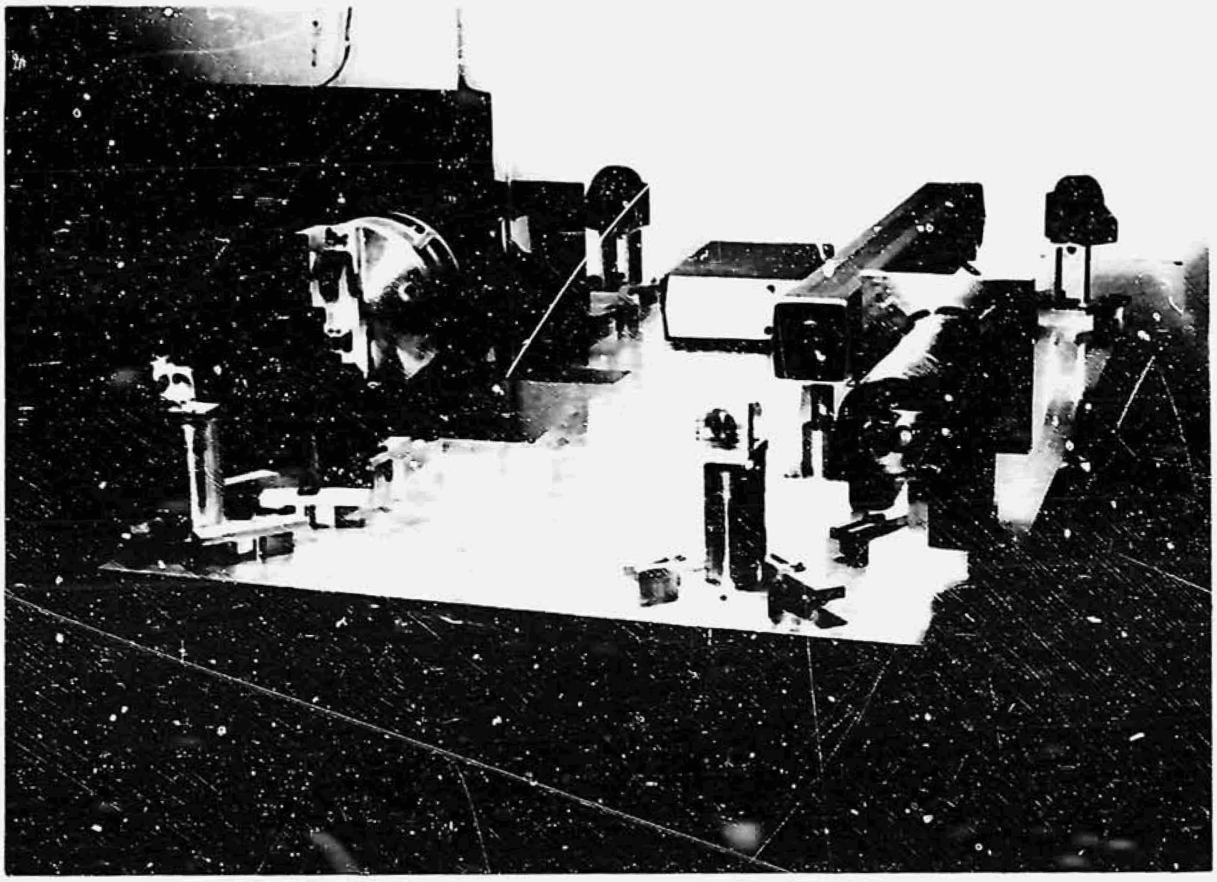

Fig. VII-4 Optical Components of Laser Doppler Anemometer.

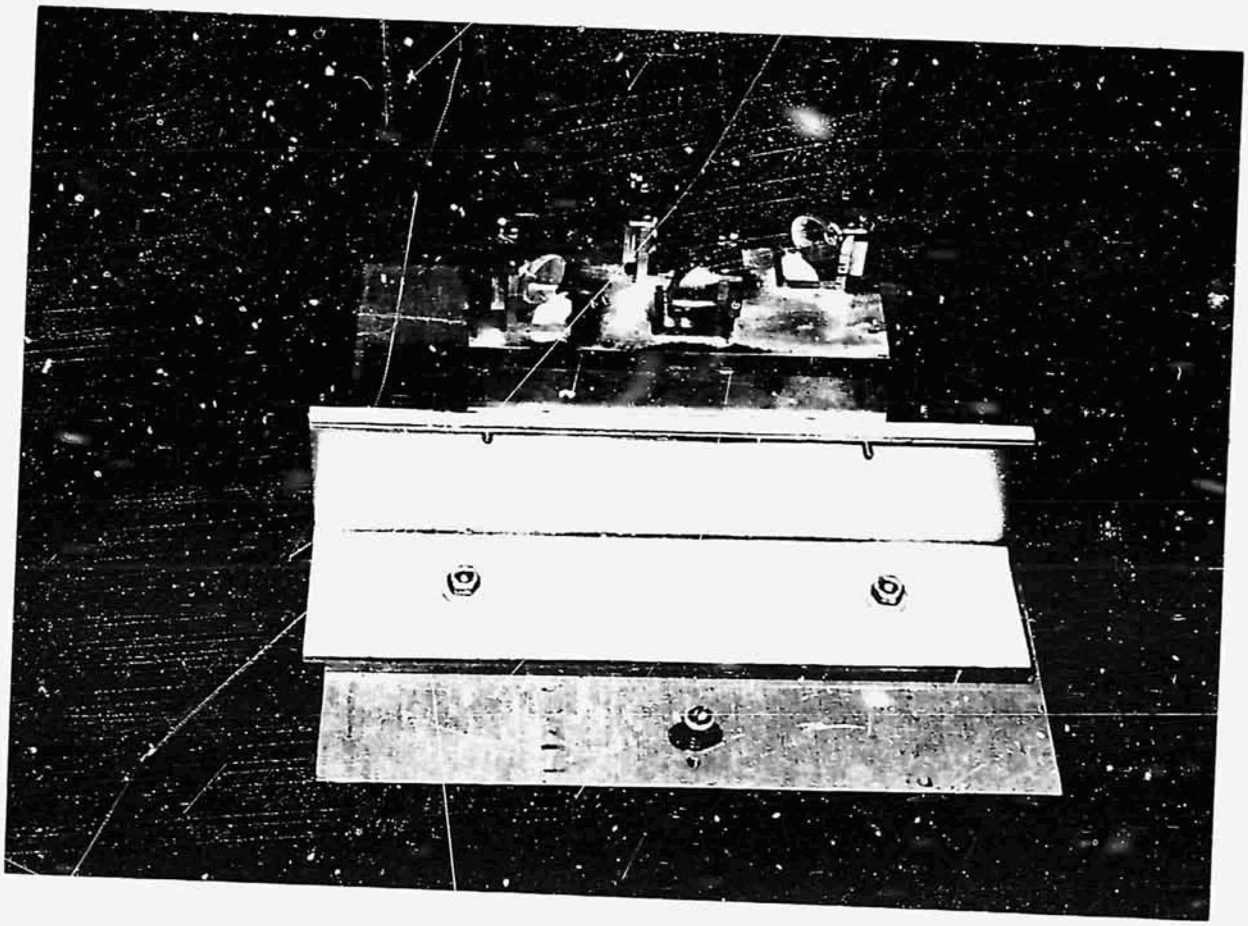

Fig. VII-5 Beam Splitter Assembly.

The receiving lens had a 70 mm diameter primary aperture and a 178 mm focal length. Two 50 mm plane mirrors (λ/10) were used to direct the forward scattered light around the table and subsequently focus the image of the probe volume on a 1.0 mm aperture just ahead of the PMT cathode. The receiving optics provided a 10x magnification of the probe volume. This magnification made possible the use of a large image aperture and therefore allowed more of the cathode surface to be illuminated. The laser line filter had a band width of 0.063 nm. It was used to attenuate room light and flame emissions.

The PMT used was an EMI 9558F with a 50 mm diameter S-20 cathode and 11 dynodes. It had a 20 mA/W sensitivity and 10 ns anode rise time. This particular tube was chosen because it had a large gain. This reduced the need for high gain electronic amplification. The cathode was operated at a high negative voltage so that the anode was at ground potential. This lessens the possibility of accidental grounding and precludes the necessity of AC coupling. A schematic of the linear voltage divider circuit for the dynode chain is given in Appendix B. The PMT, magnetic shield and voltage divider were mounted in a brass housing for light and electronic shielding. Series V ring adapters were used to hold the image aperture and laser line filter. A Glencom model 3000R regulated DC power supply was used for power to the PMT. Typically, the tube was operated at -1250 VDC resulting in a 0.1 mA anode current when measuring in a properly seeded flow.

The LDA optical components were mounted to a table which provided two dimensional movement in the horizontal plane (see Fig. VII-6). The table top and intermediate plates were 19 mm cast aluminum tool and jig plate guided by linear ball bushings. The cast iron base was cast in the

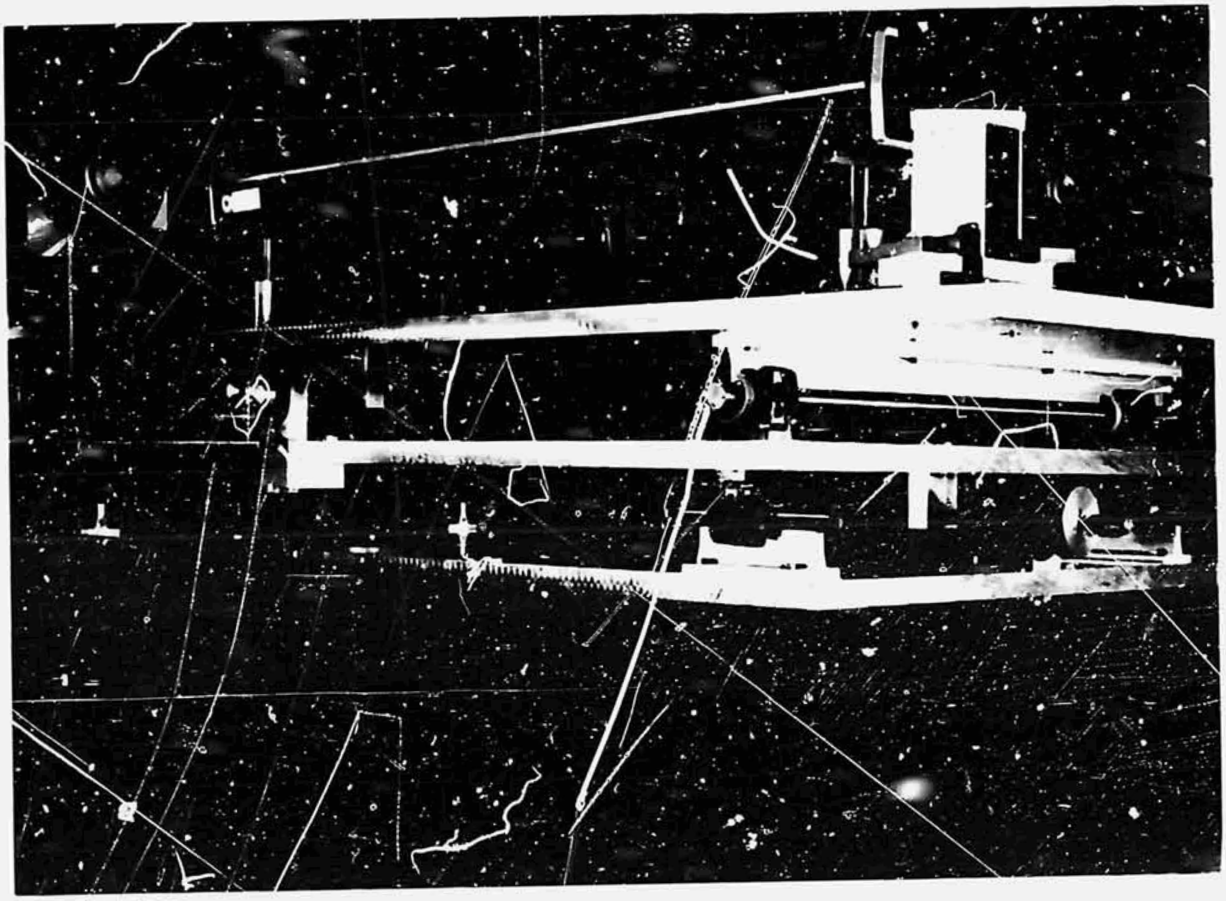

Fig. VII-6 LDA Translating Table.

ORIGINAL PAGE IS
OF POOR QUALITY

Mechanical Engineering foundry and subsequently heat treated by the Ceramic Engineering Department. The LDA table could be positioned on the holography optical table using a dolly. It could also be positioned on a vertical driver assembly to provide 3-D movement for studies on an existing stationary burner. The LDA table and all optical hardware was constructed in the shop of the Aeronautical and Astronautical Engineering Department. The linear motion of the table was controlled by manually operated, uncalibrated screws. The position of the table was monitored by metric dial gages.

Once the LDA optical system was constructed, it was necessary to calculate the proportionality constant between the Doppler frequency and the fluid velocity. It is only necessary to know the wavelength of the laser light and the beam intersection angle as dictated by Eq. (VII-5). The laser wavelength is known to within 0.1% accuracy. Therefore it is only necessary to measure the beam intersection angle. To accomplish this, the light beams were made visible in the region of the probe volume by scattering the light with a silicone oil-air jet. The beams were then photographed with a 35 mm SLR camera. In order to photograph the correct beam intersection angle, it was necessary to accurately align the camera's film plane parallel to the plane formed by the intersecting beams. This was accomplished by situating a front surface mirror such that the light beams just scattered off the mirror surface as shown in Fig. VII-7. The camera was then positioned to view itself via the mirror. The camera was then adjusted so that the image of its own lens was concentric with the circular focusing spot on the viewer. Using this method, the angle between the film plane and the plane formed by the LDA beams is considered to be less than 5°. This results in an error of $\sin\xi$ less than 0.35%. The beam intersection half angle (ξ) was measured

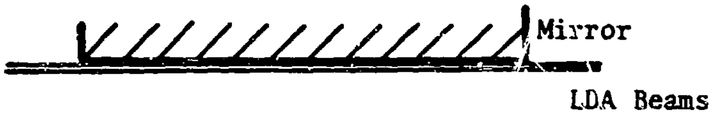

Top View

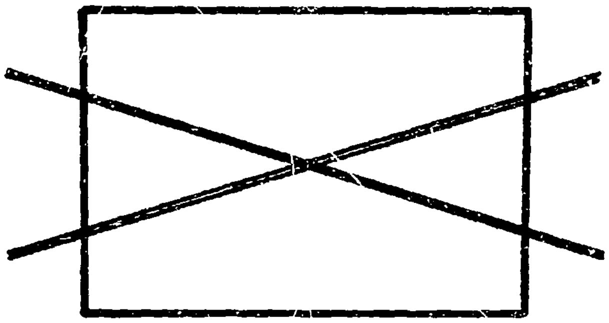

Front View

Fig. VII-7. Configuration for Accurately Measuring LDA Beam Intersection Angle.

from the negative using the Bausch and Lomb 10x optical comparator and found to be 13.6°. From equation (VII-5),

$$u = 1.35 \times 10^{-3}\ f\ (m/s) \qquad \text{(VII-6)}$$

where the Doppler frequency (f) is in KHz. The dimension of the probe volume can be calculated from Eqs. (VII-2 and 3) to be 0.72 mm in diameter and 1.74 mm long.

The Pyrex tube used for this study acts as a cylindrical lens. Consequently the LDA beams were deflected and altered as they passed through the tube walls. Therefore, it was necessary to estimate the amount of change in the beam intersection angle, the probe volume position and the shape of the probe volume for all LDV positions relative to the tube's position.

In order to measure the longitudinal velocity (V_z) the LDA beams form a vertical plane. To measure off-axis components the probe volume was translated in the -x direction, as illustrated in Fig. VII-8a. As a result, the only effect on the probe volume (as viewed from the side) was a displacement as illustrated in Fig. VII-8a. The intersection angle (ξ) was unaltered. This position error was eliminated by direct calibration. The LDA probe volume was first translated in the +x direction until a single spot was formed on the inside of the tube wall. The probe volume was translated in a -x direction until a single spot formed diametrically opposed to the first. The center of the tube was assumed to be at the midpoint of these two positions. The inside wall positions could be found to within ±0.1 mm. This precision is sufficient when compared to the natural asymmetry of the flame. This will be demonstrated in Chapter VIII.

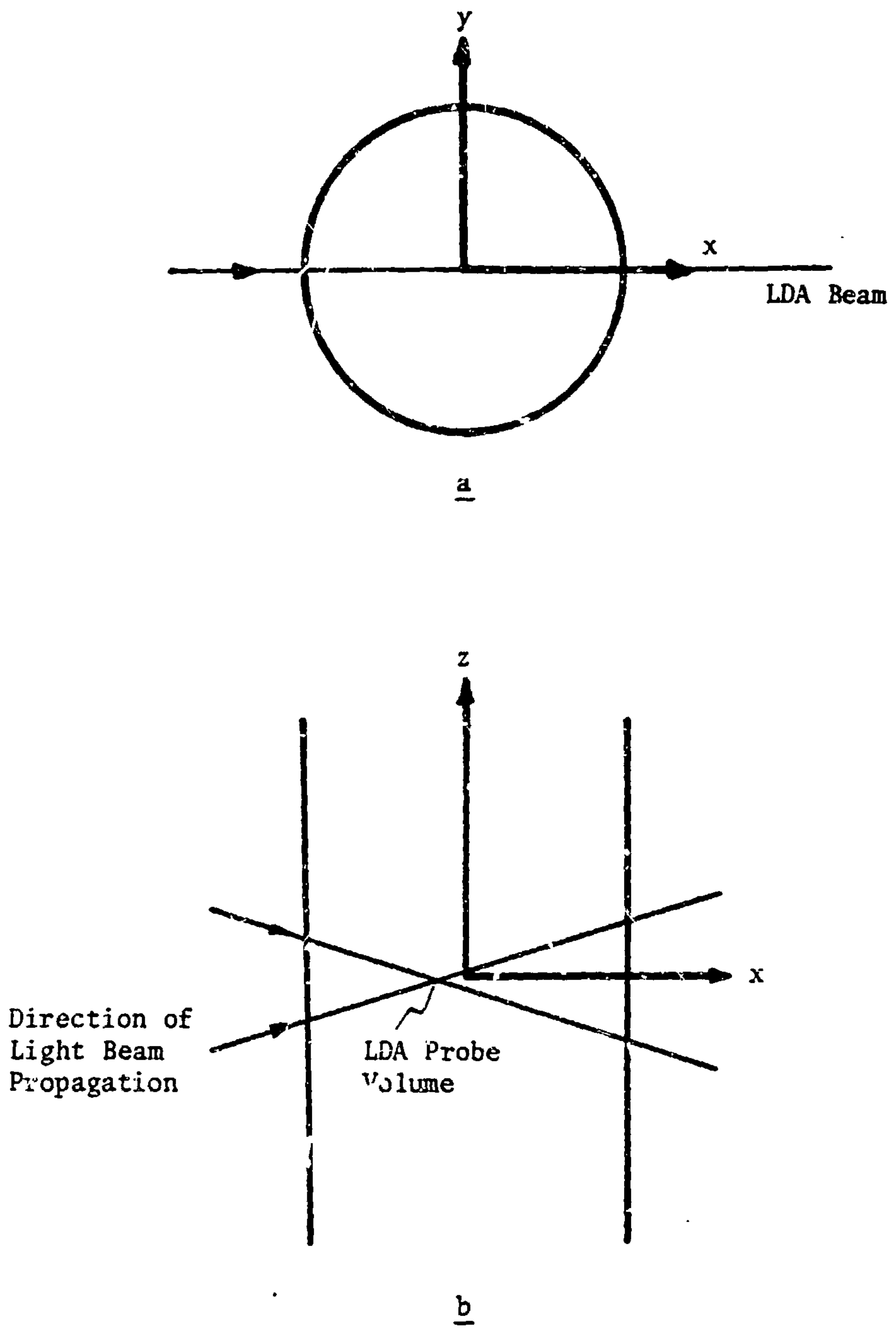

Fig. VII-8. Off Axis Measurement of the Vertical Velocity Component.

The tube does tend to expand the probe volume in the x direction, as illustrated in Fig. VII-8b. The focal length of the semicircular cross section of the tube is approximately 1.5 m according to the thick lens formula (Born and Wolf, 1975). Therefore the tube tends to expand the probe volume by less than 2% in the y direction.

In order to measure the radial velocity component (V_r) the LDA beams formed a horizontal plane and were translated in the y direction, as illustrated in Fig. VII-9a. As the LDA probe volume was moved the bisector of the beam angle was rotated, the beam intersection angle changed and there was nonlinear translation of the probe volume in both the x and y direction. Because of the complexity, these changes were photographed instead of calculated. The camera was aligned as previously described. A 50 mm long section of the Pyrex tube was then mounted on an x-y positioner with its axis perpendicular to the film plane and translated about the LDA probe volume. Photographs were taken at known positions. No detectable changes in beam intersection angle or rotation were found. The error in position is tabulated in Table VII-1. This table was used for correction during the tests.

It should be noted that the presence of the tube does not affect the magnitude of the Doppler shift of the scattered light. However, it may act to degrade the signal to noise ratio. The electronic signal processing equipment used for this study will now be discussed.

The Electronic Processing System

In this study a TSI model 1090 frequency tracker made by Thermo-Systems Inc. was used for signal processing. This frequency tracker performs two functions,

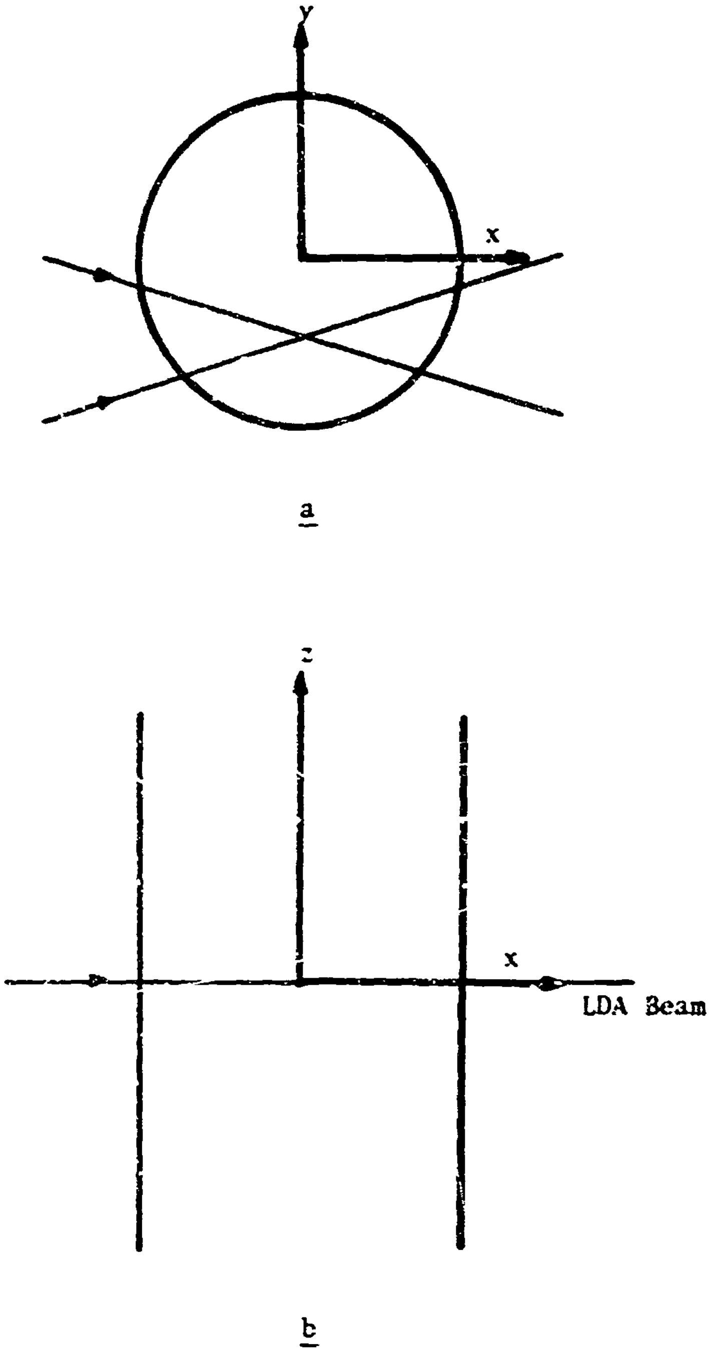

Fig. VII-9. Off Axis Measurement of the Radial Velocity Component.

TABLE VII-1

LDA PROBE VOLUME POSITION ERROR FOR OFF AXIS MEASUREMENTS OF THE RADIAL VELOCITY

Y Translation of LDA Optics (mm)	Measured Position of Probe Volume (mm)	Error %
0.0	0.0	0.0
2.0	2.0	0.0
4.0	3.9	2.5
6.0	5.9	1.7
8.0	7.9	1.3
10.0	9.9	1.0
12.0	11.8	1.7
14.0	13.8	1.4
16.0	15.7	1.9
18.0	17.9	0.6
20.0	19.7	1.5
22.0	21.4	2.7
24.0	23.3	2.9
26.0	24.5	5.8

1) It measures the frequency of a given Doppler burst and converts it to a voltage.

2) It verifies that the measured frequency is a Doppler burst and not the pedistal frequency or noise.

The frequency tracker has a phase locked loop (PLL) which locks onto the Doppler signal and a frequency to voltage converter to transform the Doppler frequency to a proportional voltage. To validate that the measured frequency is from a Doppler burst, the PPL must remain locked for 8 cycles and then for an additional 2 consecutive cycles. Only then is the measured frequency allowed to be output to the recording system.

The frequency tracker also has an outside frequency locked loop. Essentially this is a constant width bandpass filter (10% of full scale) with an automatically variable center frequency. This creates a capture window which is centered about the most recent Doppler frequency. Therefore, the capture window moves up and down the frequency range as the input frequency changes. Consequently, the tracker only accepts new Doppler frequencies that fall within this capture window. The tracker is said to be "locked onto the signal" when the capture window is properly following the frequency variations.

The frequency tracker outputs an analogue voltage signal for each new Doppler burst and holds that voltage until the next validated signal is output. Therefore, a time varying flow is recorded as a series of step functions. If the Doppler burst rate is large compared to the time scale of the flow, the signal will appear continuous in time.

The frequency tracker has three ranges, but only the 2 KHz to 500 KHz range was used in this study. Besides providing the processing functions described above, the tracker contains a variable gain 100x DC amplifier ahead of the processor and a sample rate meter (Doppler bursts/second).

A schematic of the complete electronic system used for this study is given in Fig. VII-10. The PMT output can go to either the ammeter, spectrum analyzer, oscilloscope or the frequency tracker. The ammeter is grounded and measures the PMT anode current. It was used for coarse alignment of the receiving optics and to set the gain on the PMT so that the anode current does not exceed 1 mA. Typically 0.1-0.2 mA anode current was used with a properly seeded flow and 1.3 kV DC input to the PMT. The spectrum analyzer could be used to verify the existence of a Doppler signal and for accurate optical alignment. However, it was better to use the sample rate meter on the frequency tracker for the final adjustment.

The analogue signal of the frequency tracker was recorded on a Midwest Industries LCR, two-channel light beam oscillograph with a 2 kHz frequency response. The oscillograph had DC amplifier with discrete values of gain. Therefore a continuously variable gain DC amplifier was constructed. This allowed the first channel of the oscillograph to be calibrated to frequency/division. The tracker-recorder system was calibrated by inputing a sine wave of known constant frequency into the frequency tracker. This results in a DC voltage proportional to the input frequency at the output of the tracker. The tracker and the oscillograph were zeroed with a 2 KHz signal. The span was set with a full scale input frequency. The system was calibrated before every series of tests. The linearity of the system was checked by inputing various frequencies corresponding to fractions of full scale. Linearity was better than 2% (accuracy of standard) from 50-500 KHz. Below 50 kHz an empirical correction factor was used during the data reduction. The correction for nonlinearity is given in Table VII-2.

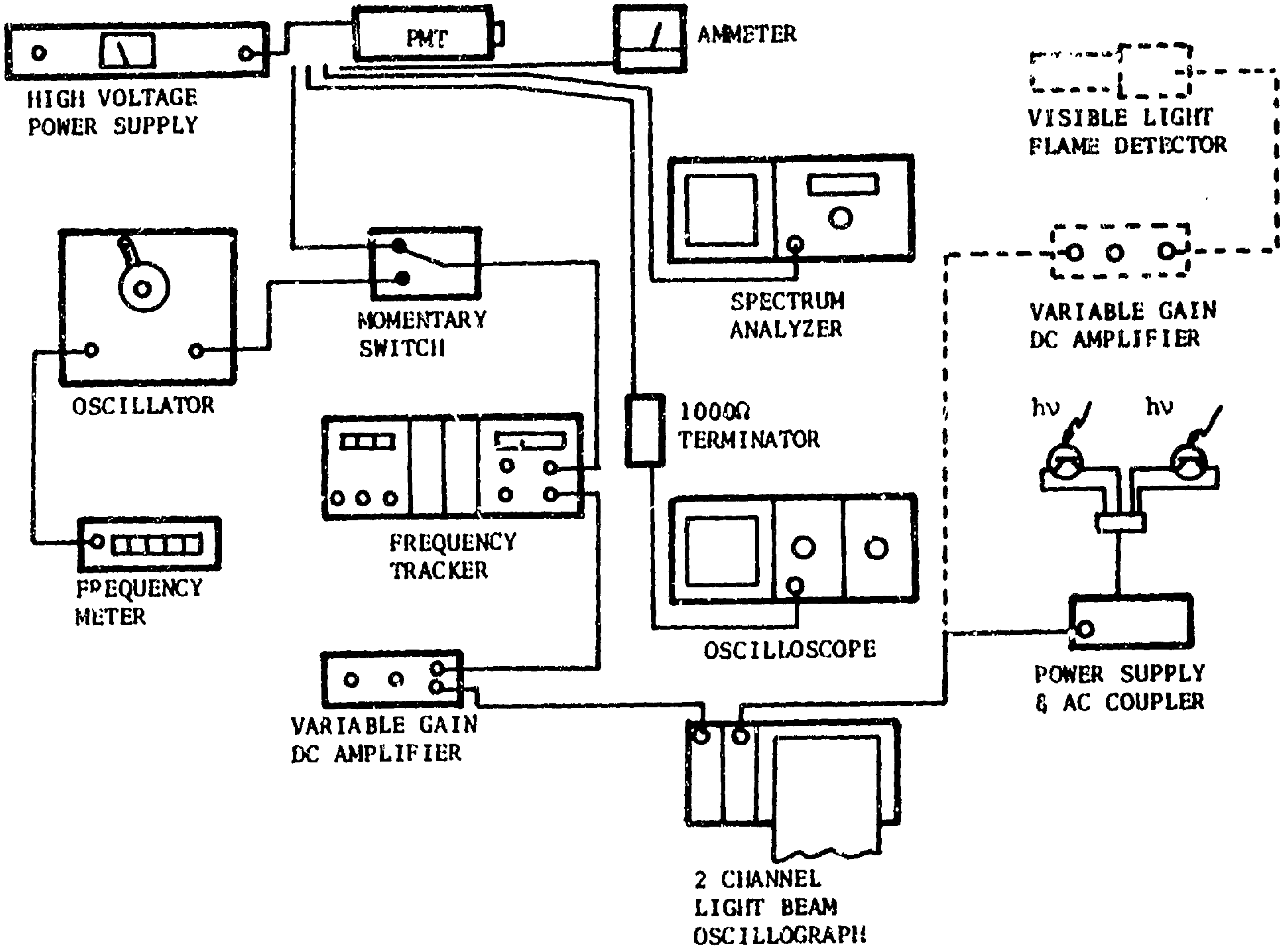

Fig. VII-10. Schematic of LDA Electronic Processing Equipment.

TABLE VII-2

NONLINEARITY OF RECORDING SYSTEM

Input Frequency (kHz)	Recorded Frequency (kHz)
0.0	2.0
12.5	14.2
25.0	26.4
37.5	38.5
50.0	51.9
62.5	63.9
75.0	76.7
87.5	87.4
100.0	100.0

As illustrated in Fig. VII-10, a momentary switch was used so that the frequency tracker input could be rapidly varied from the PMT or the oscillator. This was necessary because the capture window of the tracker, in absence of a Doppler signal, would drift to higher and higher frequencies. This would mean that the first frequency seen by the tracker would have to be high in order for the tracker to lock on to the signal. Since the fluid velocity in the tube is zero initially, the slower velocity regions (low frequency) were not accepted by the tracker as the flame approached the LDA probe volume. To correct this problem, the oscillator was set to 2 KHz and the momentary switch depressed there by holding the capture window in the low frequency region. Just before the flame reached the probe volume, the switch was released so that the tracker would lock onto the PMT output. In this way the frequency tracker would record the full range of the velocities as the lean limit flame passed the measuring volume.

The LDA Particle Seeding

Thus far the particles have been ignored. However, the quality of LDA scattering by the particles is at least as important as the optics and signal processing system. Unfortunately the physical nature of the particles required for this system is hard to quantify and the least understood portion of this LDA system.

There are several criteria that one must consider when artificially seeding a fluid for LDA probing. Those considered to be most important for this study are:

1) Material composition
2) Particle size
3) Particle density (number concentration) in the fluid

4) Method of dispersion

For this flame study it was necessary to choose a material which would not be destroyed in the flame and which was inert. For this study, aluminum oxide (AL_2O_3) polishing powder was used since it met the criteria and was readily available.

LDA probing requires a particle size that is small enough to accurately follow the flow and large enough to be a good scattering source. The upper limit of the acceptable particle size can be estimated by calculating a settling velocity (due to gravity) and the characteristic time response to a change in fluid velocity. According to Adrian and Fingerson (1976), the settling velocity of a particle in a fluid is given by

$$V_{set} = \frac{\Delta\rho d_p^2 g}{18\mu} \qquad \text{(VII-7)}$$

and the time constant given by

$$\tau_{part} = \frac{d_{part}^2 \rho_{part}}{18\mu} \qquad \text{(VII-8)}$$

For a 1 μm aluminum oxide particle in air at STP

$$V_{set} = 0.1 \text{ mm/s}$$

$$\tau_{part} = 10 \ \mu s$$

In this size range, the larger the particle the better the quality of the Doppler signal. Therefore, the largest particle with an acceptable time response and settling velocity was used. The aluminum oxide powder used for this study was Microgrit GB supplied by Micro Abrasives Corporation. Three size distributions were tried (see Table VII-3). The distributions listed

TABLE VII-3

SPECIFICATION OF POWDER USED FOR PARTICLE SEEDING

Microgrit GB, Aluminum Oxide Polishing Powder, 98% Al_2O_3

From: Micro Abrasives Corporation, Westfield, MA

Specific Gravity: 3.6

Particle Size (μm)	#2000	#2500	#3000
Average Size	1	0.5	0.1
Distribution Range	0.05-2	0.05-1.4	0.05-1
Distribution Peak	0.7	0.5	0.37

are based on number concentration. This powder was chosen because it was about the correct size and because the shape was approximately spherical (as opposed to oblong-like lapping powders). It is possible that the velocity of single particles was measured. However, it is more likely that the velocity of agglomerates was measured. This is supported by the fact that there was no detectable difference between the signals from the three powders tried. Melling and Whitelaw (1973) used a fluidized bed to disperse 0.25 μm TiO_2 particles and found that agglomerates on the order of 2 μm were formed. Because of this fact, it was decided that the Micro-grit #3000 should be used in all tests. It is hoped that agglomerates less than 4 μm were formed which would result in

$$\tau_{part} < 0.16\ \mu s$$

and

$$V_{set} < 1.6\ mm/s$$

Ideally one would like a truly monodispersed powder. This would result in one time constant and settling velocity. Secondly, since the larger particles scatter more light, only the largest particles will be observed. This would necessitate an overall higher seeding density with polydispersed particles to achieve the same data rate since the small particles would be present but not contribute to the measured Doppler bursts.

For the purpose of optimizing the LDA signal, the particle number density is dictated by the nature of the flow. The upper limit is set as that density, flow rate and probe volume diameter such that no more than one particle is in the probe volume at any one time. The lower concentration is set by the need to have a data rate (Doppler bursts/unit time) sufficient to achieve the needed time resolution. For this study there was a further stipulation that the concentration be as low as possible in order to minimize the disturbance to an already sensitive lean limit flame. It is possible to quantify the upper and lower particle concentration in terms of optimizing the LDA signal. However, no means was available to measure the concentration so that the theoretical information would be useless. Instead an empirical method was used to determine the proper seeding density. A description of the method will be given later.

Dispersing the aluminum oxide powder into single particles in air is difficult, if not impossible. Even if it is possible, the forces acting to form agglomerates of 1 μm particles are very important. Further, the powder "cakes" if any mechanical means is used in an attempt to disperse the powder. For these reasons, fluidized beds or air jets are usually used for dispersion. In this study, the problem was further compounded by the low mass flow rates of the air and particles. Consequently the shear forces necessary to break up the powder were harder to achieve.

A schematic of the particle feed system used for this study is illustrated in Fig. VII-11. This system was developed through trial and error. It uses a fluidized bed 20 mm Dia x 140 mm long for breaking up large agglomerates (≈ 2 mm Dia) that form in the powder. The particle laden air then passes through a settling tube into a hypodermic tube 1.25 mm ID x 0.1 m long. This is presumed to classify the material into agglomerates less than 1 mm. The jet formed at the hypodermic tube exit creates a region of high shear to further break up the agglomerates. The jet emptied into a large chamber for further classification. The four impinging air jets right at the hypodermic tube exit were not used due to the low air flow rate. In this study the

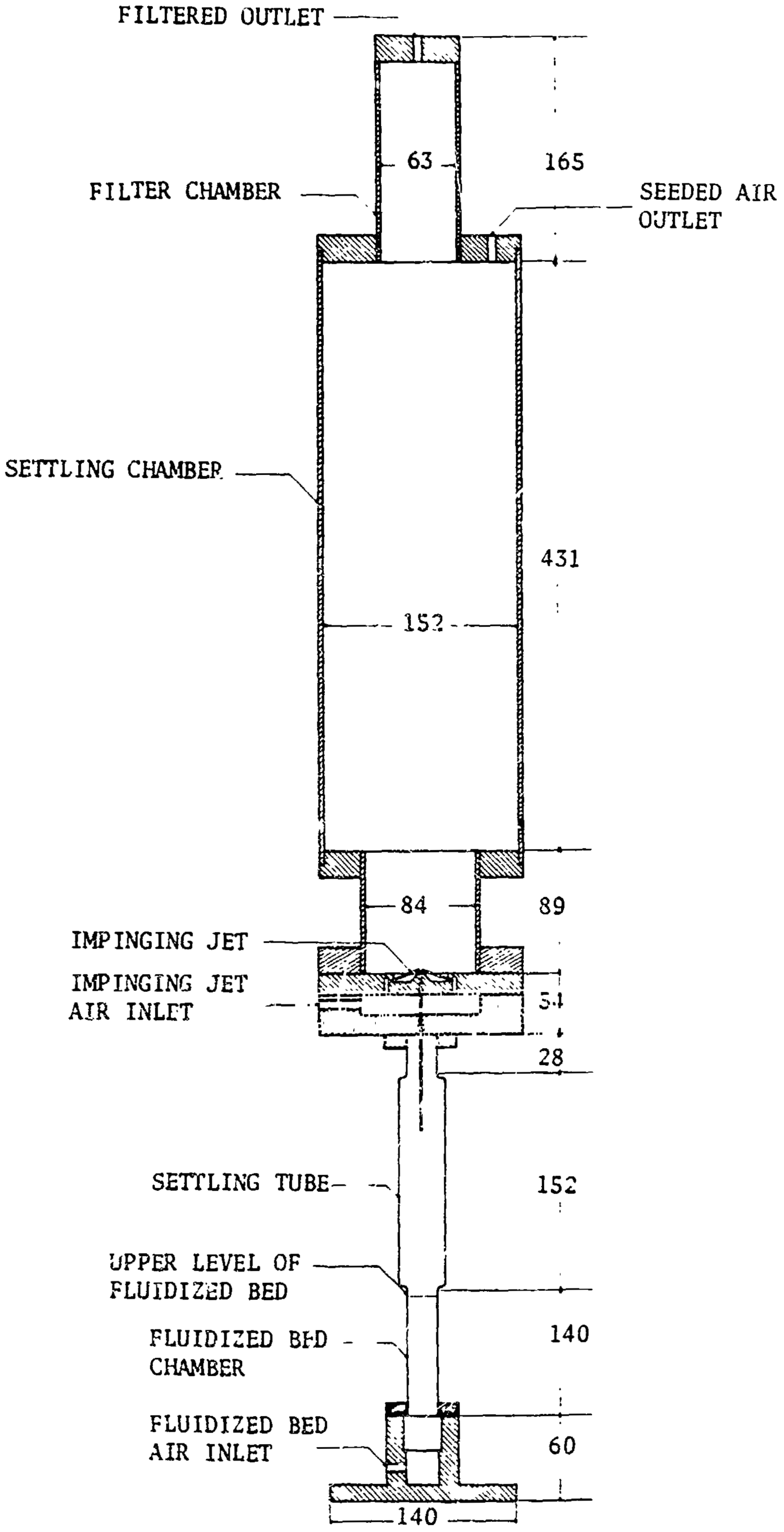

Fig. VII-11. LDA Particle Feed System.

filter at the top of the large settling chamber was not used. All of the air which passed through the fluidized bed exited through the outlet at the top (right) of the large settling chamber. The particle laden flow then passed through a piece of 6.4 mm polypropylene tubing 1 m long. The air flow was mixed with methane just before it entered the SFLT plenum as described in Chapter V. All the air required for the test mixture was passed through the particle feed system. The same rotometers used for the tests described in Chapters V and VI were used for the LDA tests.

An empirical method was used to determine the air flow rate necessary to properly seed the mixture for this study. The LDA optical system was situated to properly measure the vertical velocity component at the centerline of the tube (see Fig. VII-12). Several lean limit flame trials were conducted until the lowest air flow rate was found which would produce a continuous velocity record. A flow rate of about 125 ml/s was used. Since the particle concentration resulted in a nearly continuous signal, one might assume that more than one particle is present in the probe volume in regions of high velocity. However, in the low velocity regions of the flame the gas is cold and therefore the gas and particle density is high. In the high velocity region of the flame (burned gas region) the opposite is true. Consequently the increase in velocity is partially compensated by the decrease in particle concentration. Further, since the flow was not turbulent, if signal dropout occurred, the velocity between Doppler bursts could be interpolated. Therefore some signal dropout was tolerated at lower velocities.

After the required particle seeding rate was determined, it was of interest to find out whether or not the particles are nonintrusive. A

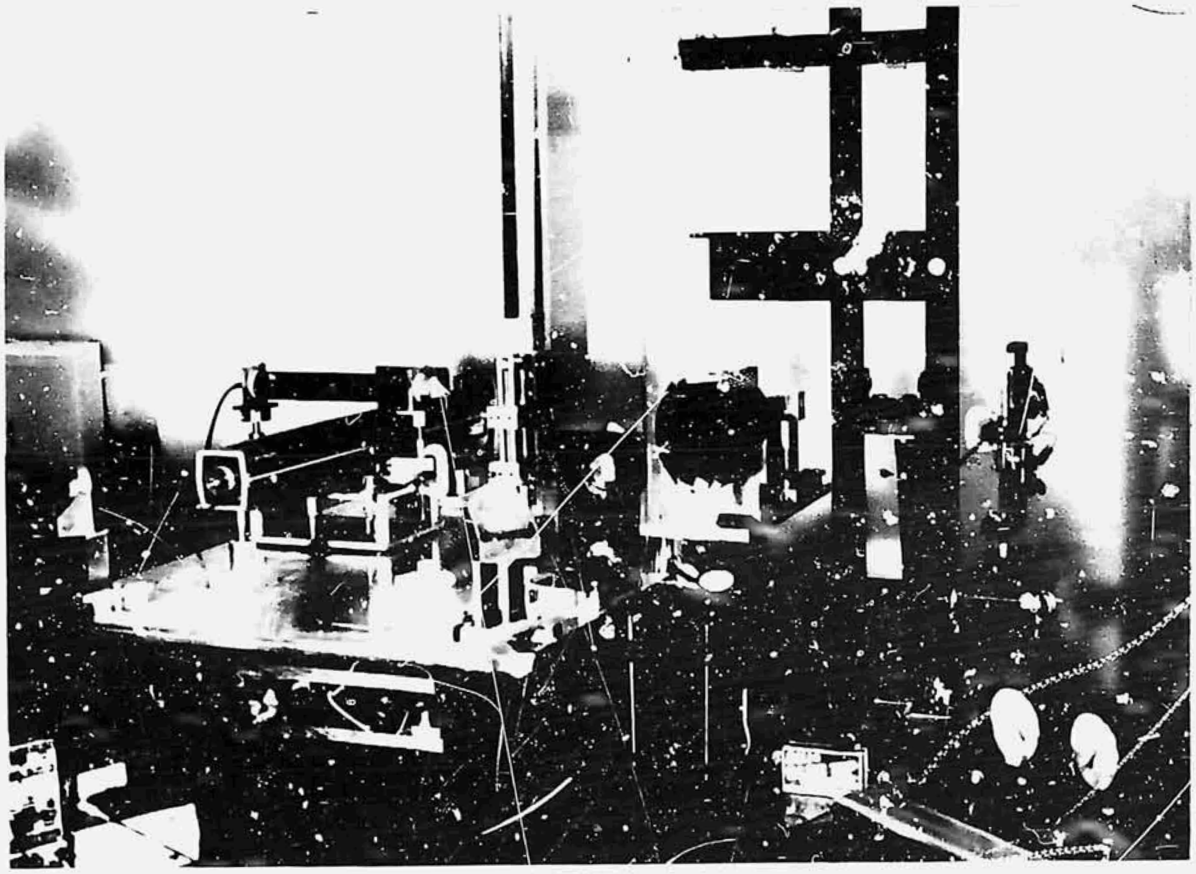

Fig. VII-12 LDA and Beam Deflection Flame Detector in Position for a Test.

separate series of tests were conducted to determine if the lean limit of a CH_4-air flame is altered by the presence of the particles. For these tests the lean limit was determined with particle seeded mixtures using the same procedure described in Chapter V but with the new air flow rate. During these tests, the presence of the fluidized bed caused a back pressure in the air feed line. A Wallace and Tiernan precision manometer was used to measure the pressure at the outlet of the air rotometer to be 20 kPa. After the seeded lean limit was determined, the particle feed system was thoroughly cleaned. The lean limit was then determined with the unseeded flow but with the particle feed system in the air supply line. The air flow was established by setting the same rotometer reading as in the seeded limit tests and artificially creating the back pressure by a valve between the rotometer and the particle feed system. Using the pressure correction for the flow rate, the unseeded and seeded lean flammability limits were calculated to be 5.34% and 5.44%, respectively. This error in the unseeded limit composition is assumed to be due to the new air flow rate used. It is within the 2% accuracy of the rotometers. In any case, the tests indicate that the seeded lean limit mixture composition is slightly richer than the unseeded mixture. This is reasonable since the presence of the particles increases the effective heat capacity of the fluid and therefore lowers flame temperature. The propagation velocity of the seeded flames was found to be 0.228 m/sec with a standard deviation of 0.00[illegible]. This is within 3% of the unseeded value.

The Velocity Measurements

The LDA system used for this study can only measure one component of the velocity at one position in the tube during a single flame passage.

Therefore, it was necessary to perform many tests and use a fiducial mark in time and space to superimpose the many velocity records in order to reconstruct the complete velocity distribution. The beam deflection flame detector (BDFD) described in Chapter V was used to produce the fiducial mark. The lower beam of the BDFD was passed through the centerline of the tube in a plane coincident with the horizontal plane passing through the LDA probe volume and perpendicular to the vertical plane formed by the LDA beams. This is shown in Fig. VII-13. In this way, even when the LDA probe volume was off axis, a fiducial mark was created relative to the leading adge of the upward propagating flame at the centerline. The output of the beam deflection flame detector was input to the second channel of the light beam oscillograph shown in Fig. VII-10. The probe volume and BDFD were 1.15 m from the ignition end of the tube for all measurements.

The procedure used to measure a single velocity component through the flame at a given radial position is listed in Table C-1 of Appendix C. The complete procedure was repeated for each trial. If the flame for a given trial was observed to be significantly asymmetric, the velocity record of that trial was disregarded. The trials were repeated at each radial position until three records were obtained for which the flame appeared to be symmetric. Each time the probe volume was moved to a new radial position, the receiving optics were realigned to achieve a maximum signal rate during purging of the tube.

A record of the Doppler frequency corresponding to the vertical velocity component (V_z) versus time is shown in Fig. VII-14. This record was made while the LDA probe volume was at the centerline. Therefore the probe volume and the beam from the BDFD are coincident in this experiment. The

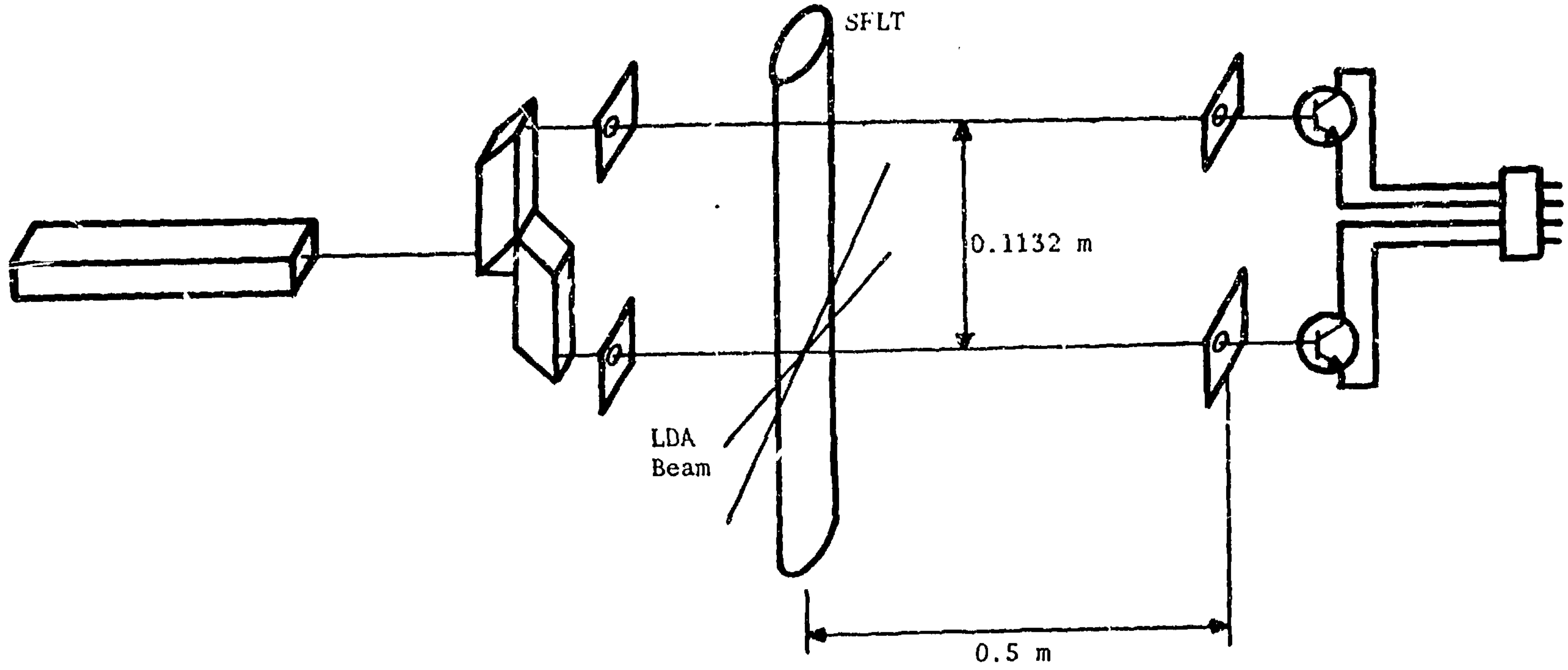

Fig. VII-13. Orientation of LDA Beams and BDFD

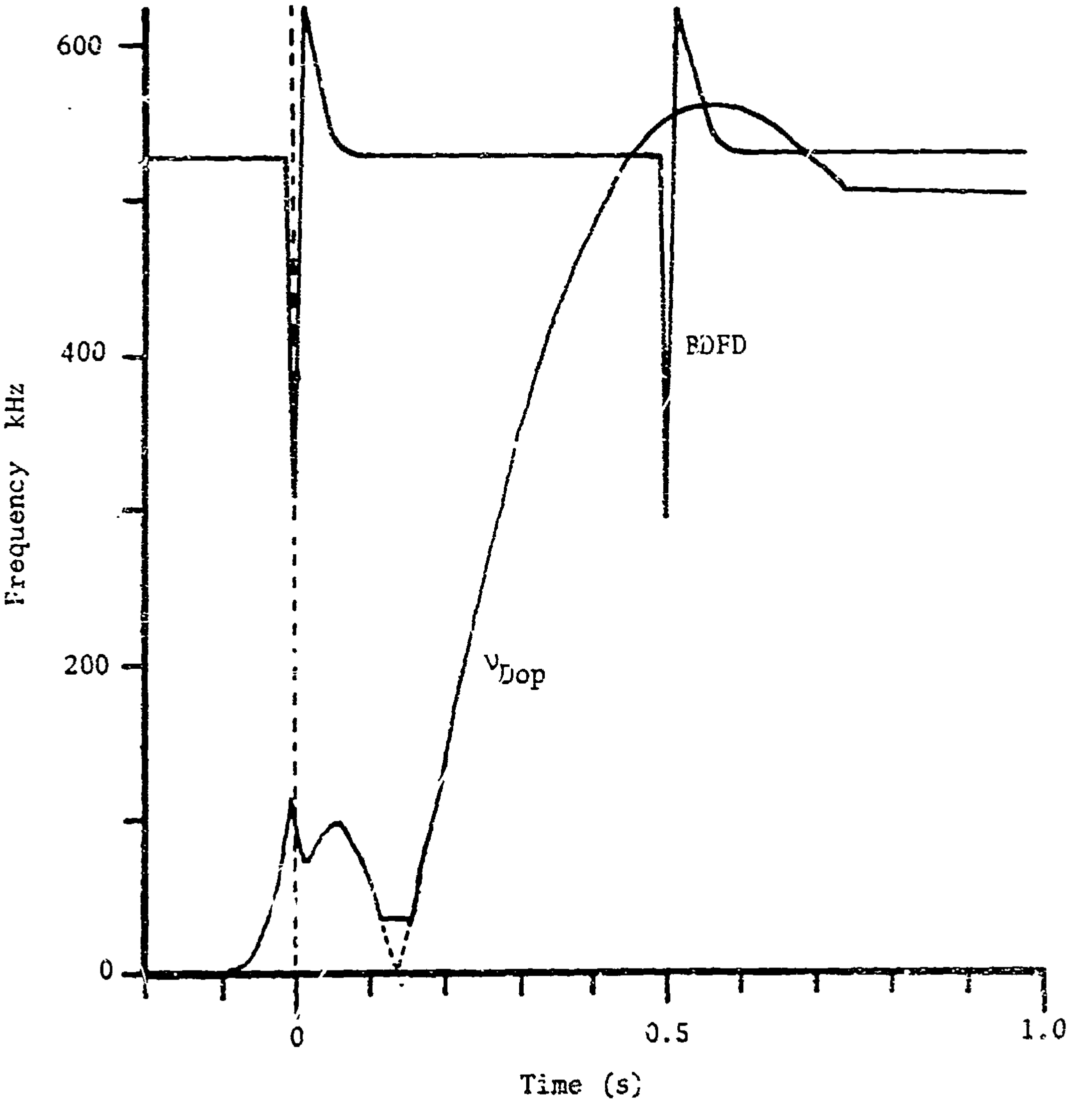

Fig. VII-14. Doppler Frequency versus Time at the Centerline of the SFLT.

BDFD remained at the centerline in all experiments. In this and all other records, t = 0 is defined to occur at the time of maximum deflection as determined by the BDFD record. The correct interpretation in terms of the Eulerian velocity is given in Fig. VII-15. No Doppler signal was recorded during the time at which $V_z \simeq 0$, since the tracker always looses signal under these conditions. However, if the slopes of the curve are extrapolated to $f_{Dop} = 0$, they always intersect as shown by the dotted lines in Fig. VII-14. Additionally, in all but two trials, the frequency tracker looses signal soon after the peak downward velocity was reached. This was due to condensation of water on the tube walls from the products of combustion. The water droplets rescatter the particle scattered light so that the intensity at the PMT was too weak to detect.

As shown in Figs. VII-14 and 15, the velocity was not a smooth function of time between $-0.2 < t < 0$. This is because the refractive index gradient in the flame had a significant effect on the LDA beams. This effect is expected, however, it is usually considered to be negligible. The sudden decrease in the measured frequency could be caused by three phenomena,

1) A sudden change in fluid velocity
2) Deflection of the LDA beams
3) A phase change in the incident beams.

One would not expect this kind of a change in fluid velocity through the flam since there are no forces acting on the fluid that would cause a rapid deceleration followed by a rapid acceleration in the manner the f vs t record indicates.

Deflection of the LDA beams is believed to be the most likely cause

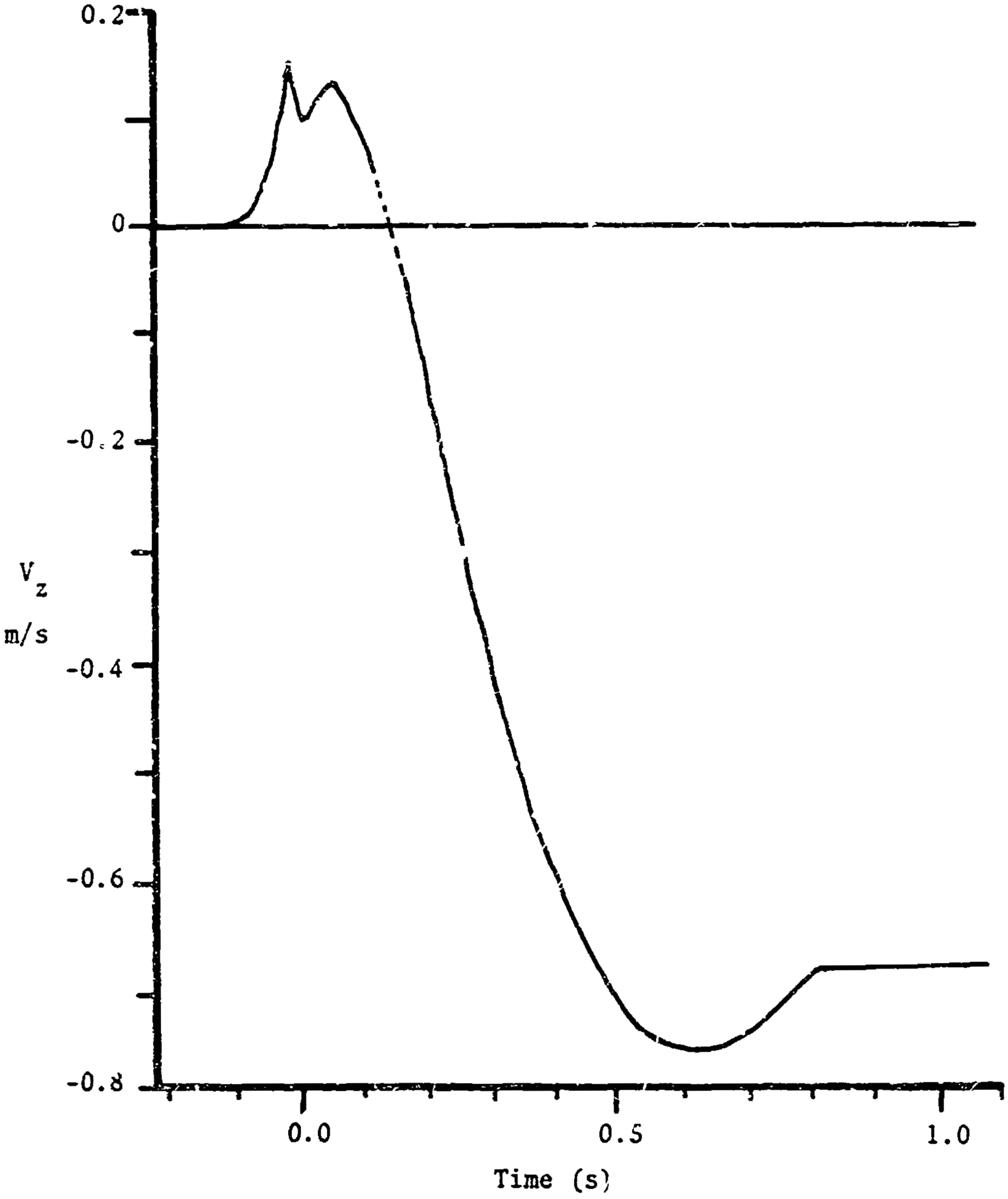

Fig. VII-15. Fluid Velocity with Respect to the Laboratory Coordinates at the Centerline of the SFLT.

of the frequency perturbation. Especially since it is coincident with the beam deflection of the BDFD. One possible explanation is that the sudden change in measured frequency is due to a change in the magnitude of ξ in Eq. (VII-5). However, the total deflection of the BDFD was measured to be on the order of 0.01°. This results in an error in sinξ of less than 0.1%. The phenomenon can be explained in terms of the rate of beam deflection. As the flame moves up the tube, it first encounters the lower beam deflecting it upwards. At some time later, the top LDA beam is moving upward and the lower beam downward. Lat· the lower beam is stationary and the upper beam moves downward. This behavior is illustrated in Fig. VII-16. The net result is that the probe volume is moving vertically and, to some degree, radially. Therefore, the velocity measured is a relative velocity between the probe volume and the particles. Similarly, the Doppler shift (as described in Appendix A) is due to the velocity of the particle relative to the velocity of the beam.

There is also a possibility that there can be a change in the frequency due to a phase shift of the incident LDA beams. As the refractive index gradient (flame) moves upward the optical path length changes first in the lower LDA beam and then in the upper beam. If there were no beam deflection, the probe volume would be stationary with moving fringes. In this study, one would expect both beam deflection and phase changes in the incident beams. There is a question of how important the rate of place change is relative to the rate of beam deflection and the relative magnitude of each could be quantified. However, that problem is beyond the scope of this work.

The vertical velocity component was measured as a function of time at

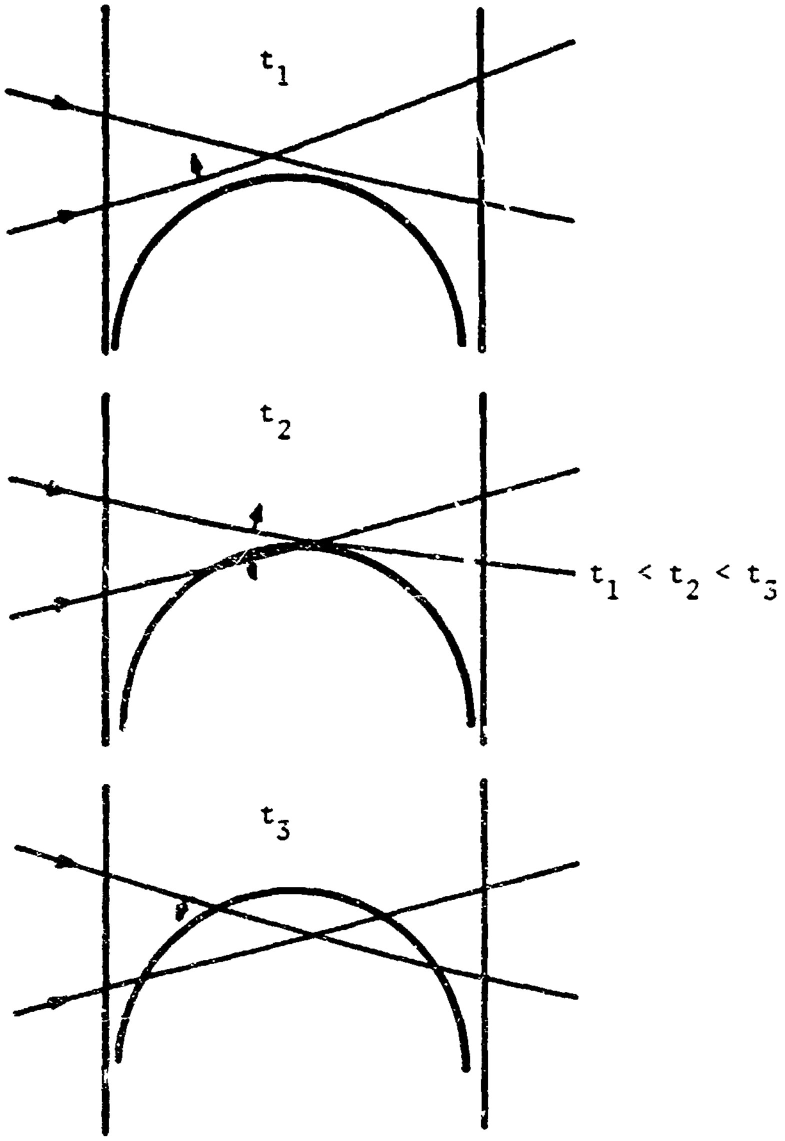

Fig. VII-16. Representation of LDA Beam Motion with Flame Passage.

several different radial positions from the centerline to the outside wall. Since the flame was assumed to be axisymmetric, the positions were all in the -x direction as defined in Fig. VII-8a. One record from each of eleven positions is included in Appendix C. Each record is the best of the three symmetric records taken at the respective position. These records were used to construct the velocity distribution (relative to the flame) shown in Fig. VII-17.

The criterion used for choosing the velocity profile to represent each radial position was quite qualitative. For those trials near the centerline, the agreement between the three records (from the symmetric flames) was good. However, away from the centerline some disagreement occurred. In those cases, the record that appeared to be the best average of the three was chosen. It should be noted that the representative velocity profile for each position was chosen before the complete velocity distribution was constructed. No attempt was made to go back and pick different records that might produce a distribution with better agreement.

The velocity distribution in Fig. VII-17 was constructed by determining the frequency from the records in Appendix C at several different times. The frequencies were converted to velocity using Eq. (VII-6). This in turn was converted to the fluid velocity relative to the flame by adding the flame propagation velocity (0.235 m/s) to each value. The time at which each velocity measurement occurred was converted to a position relative to the stationary flame. To accomplish this each time was multiplied by V_p and recorded relative to the position of the BLFD. The origin of each velocity vector in Fig. VII-17 is plotted at the position at which it was recorded. A list of the velocities relative to the stationary (laboratory) coordinates

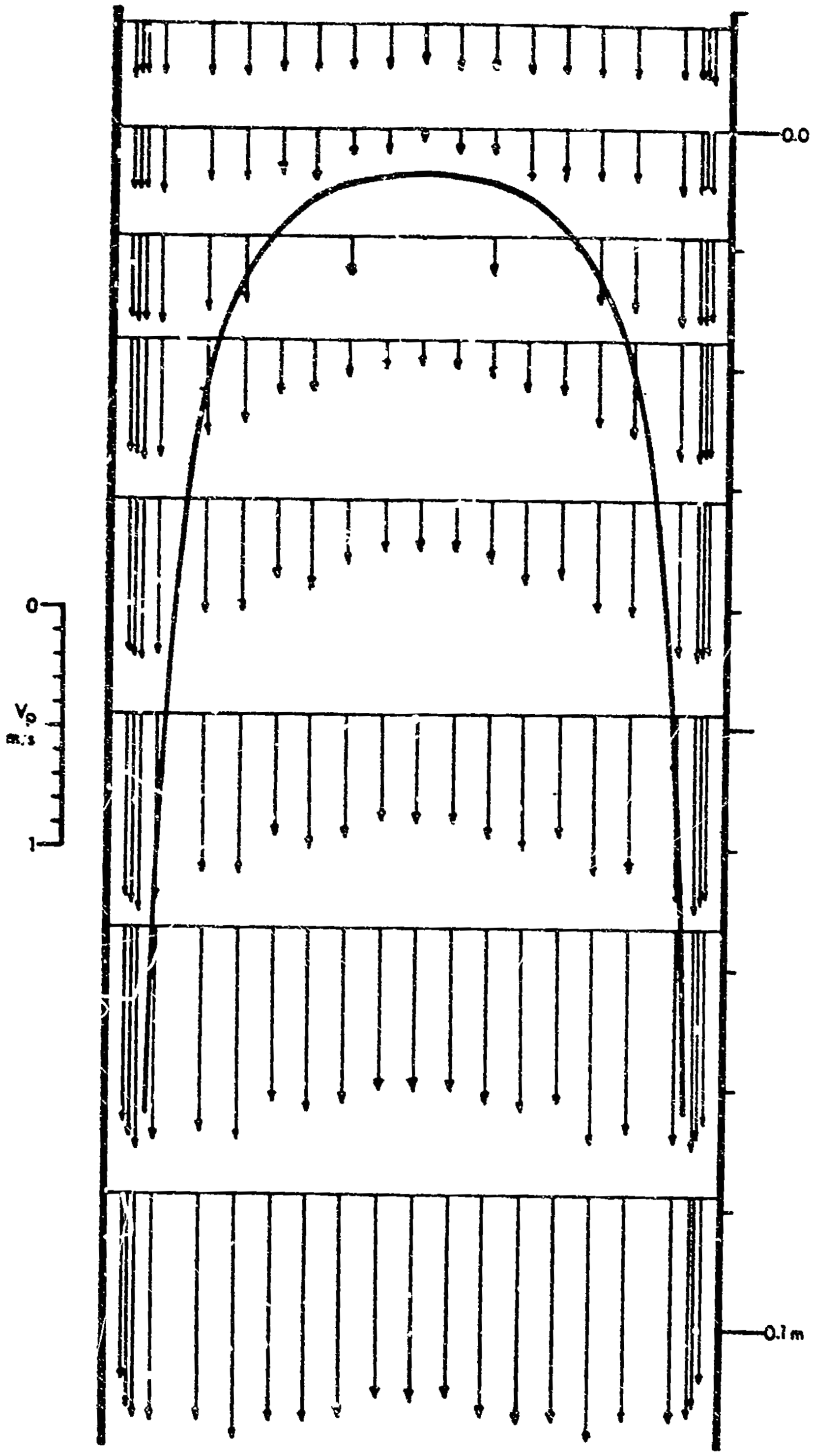

Fig. VII-17. Axial Velocity Distribution in Coordinates that Move with the Flame.

is listed in Table C-1 of Appendix C. A positive velocity is defined as upward.

The heavy solid line in Fig. VII-17 represents the photographic image of the flame in Fig. V-18. The leading edge of the flame image was placed at the position calculated in Chapter V. All other positions are as they appeared on the photograph. No correction was made for radial position error due to refraction by the tube or longitudinal position error due to the focal plane shutter.

The velocity distribution shown in Fig. VII-18 not only includes the data from Fig. VII-17, but also data in regions further downstream from the flame. As illustrated, all but two of the velocity versus time records end at about 0.155 m. In fact, the two records illustrated in Fig. VII-18 are the only two of more than 100 trials for which a signal was recorded that far downstream. In spite of numerous attempts to repeat the records, none were obtained. The reason these two were obtained is still a mystery and therefore these two velocity records may not be truly representative of the flow velocity at their respective positions. The velocity record at $r = 24$ mm appears to be consistent with the rest of the velocity distribution. The record at $r = 12$ mm seems to reflect slightly lower velocity than the nearby records through most of the distribution. The other two records at $r = 12$ mm were more self-consistent and may have been more consistent with the rest of the distribution. However, this record was chosen for the downstream information it provided.

An attempt was made to measure the radial velocity components in the hope that a 2-D axisymmetric velocity distribution could have been constructed. Unfortunately this was not possible for several reasons. Near the centerline

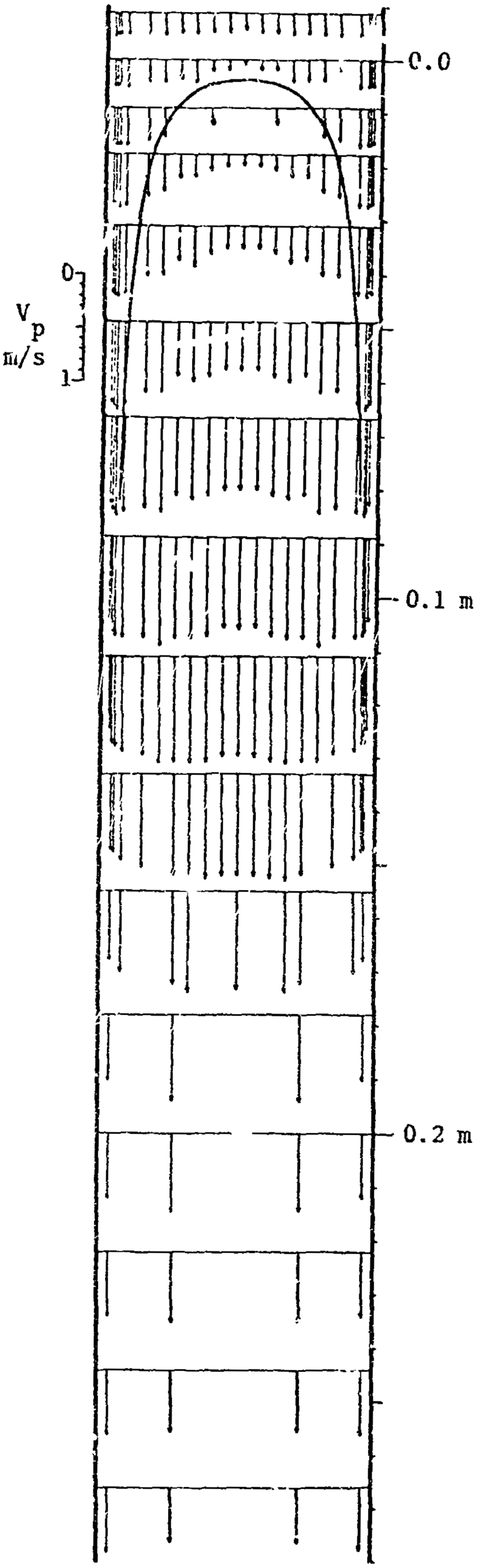

Fig. VII-18. Axial Velocity Distribution in Coordinates that Move with the Flame.

of the tube, the radial velocity components are too small to measure. In the intermediate regions where some Doppler signals were obtained ($9 \text{ mm} \leq r \leq 22 \text{ mm}$) the radial velocity components are only significant near the flame zone. In the flame zone region, no Doppler signal occurred for much of the time. This is probably due to the incident LDA beams becoming uncrossed. Further, frequency error due to the beam deflection and phase change, as previously described, occurs. Therefore, when a frequency was recorded, the accuracy was unknown. Near the wall, $r > 22$ mm, the radial component again becomes too small to measure.

As a result of these problems, great care had to be taken to get any signal at all. When signals were obtained, the data points were sparse since much signal dropout occurred. The records that were obtained are illustrated in Fig. VII-19. The velocity record at each radial position in Fig. VII-19 is a composite of three separate records due to the scarcity of available data points. As the flame approached the probe volume, one would expect the fluid to move radially outward, go to $V_r = 0$ and then move back toward the centerline. The dotted lines in Fig. VII-19 are fictitious profiles reflecting this behavior. In all cases, the data are too inconclusive and inconsistent to be useful. Therefore, the radial velocity was not included as part of the velocity distribution in Figs. VII-17 and 18.

As was discussed in Chapter V, extinction could be made to occur at various vertical positions of the tube. To characterize what happens to the flow at extinction, several centerline velocity profiles were measured for extinction at different vertical positions. These velocity profiles are illustrated in Figs. VII-20, 21 and 22. In each case, extinction was defined to occur when no visible light was detected by eye. The position was

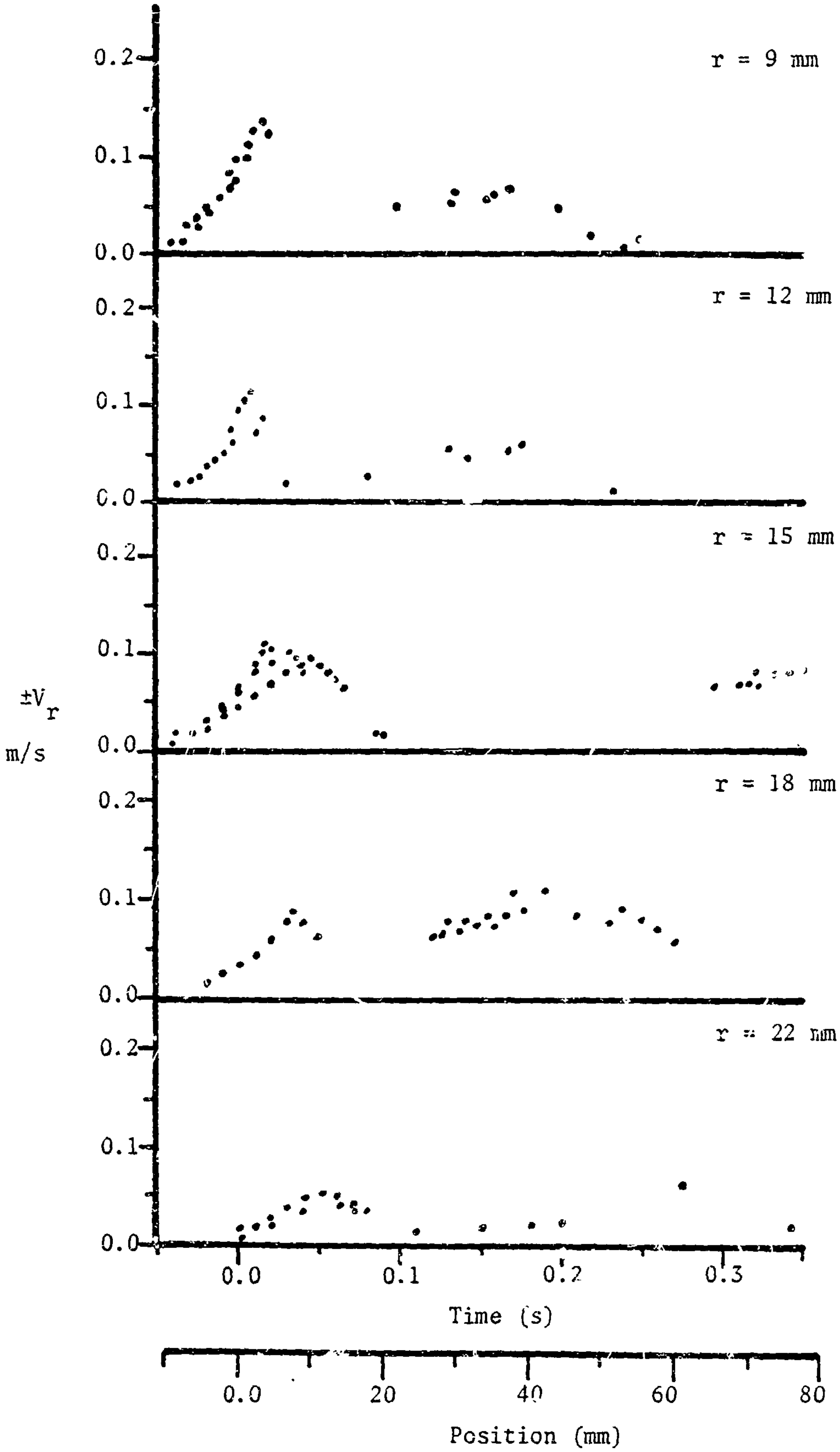

Fig. VII-19. Composites of Radial Velocity Profiles.

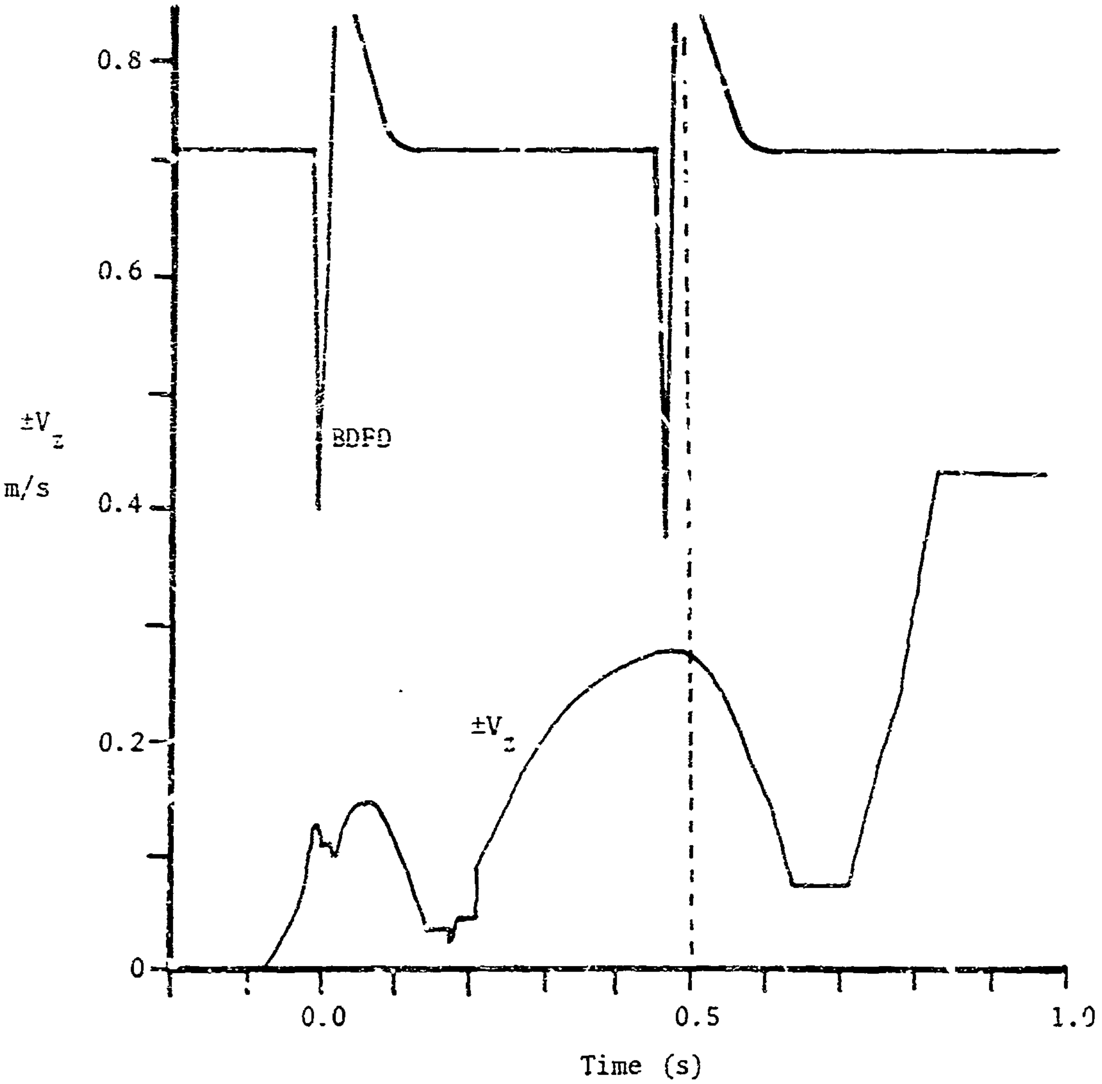

Fig. VII-20. Centerline Velocity Profile with Extinction at t = -0.5 s.

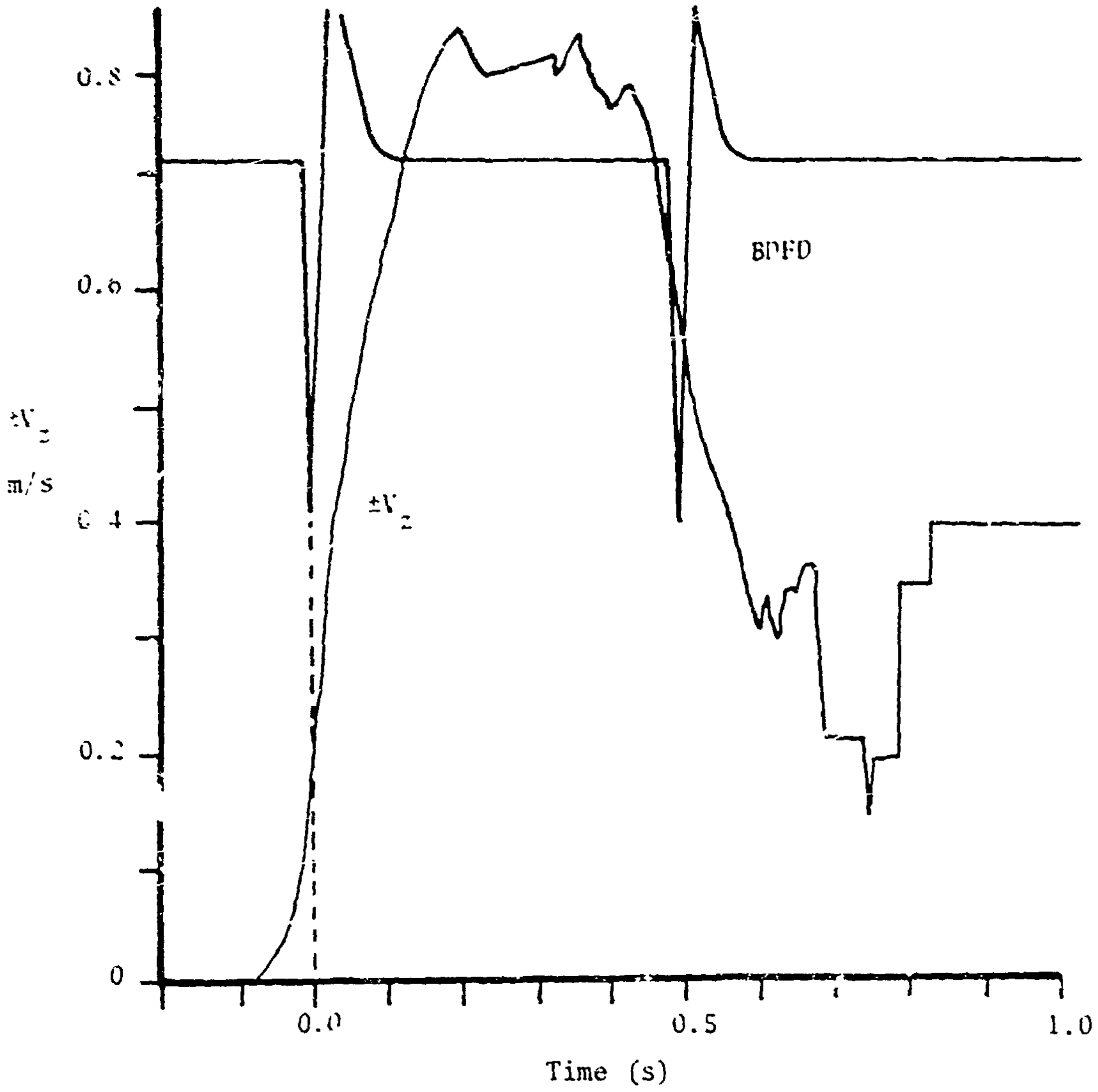

Fig. VII-21. Centerline Velocity Profile with Extinction at t = 0.

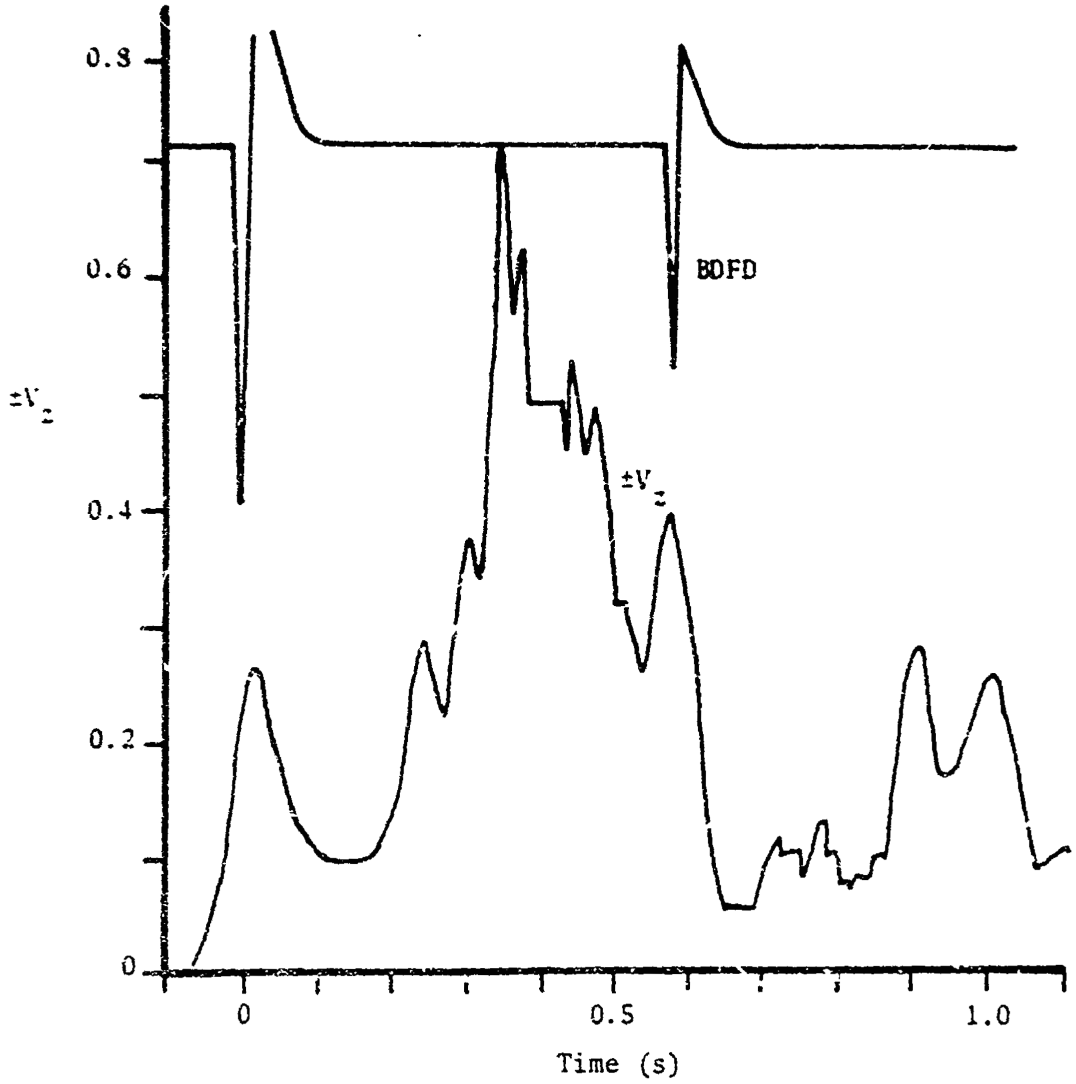

Fig. VII-22. Centerline Velocity Profile with Extinction at t = 0.5 s.

noted. The accuracy of this position is estimated to be within ±10 mm (±0.055s). The extinction position is illustrated by the dotted line in Fig. VII-20. A positive velocity component is defined as being upward. A detailed discussion of the velocity distribution during propagation and extinction will be left for Chapter IX.

CHAPTER VIII

THE TEMPERATURE DISTRIBUTION IN A LEAN LIMIT FLAME

The purpose of the final phase of this experimental study was to measure the temperature distribution of an upward propagating flame in a SFLT. With a complete temperature distribution it would be possible to determine the flame thickness, the maximum flame temperature and the temperature distribution of an extinguishing flame. Holographic interferometry was chosen for this purpose because it is completely nonintrusive and because of the advantages it has over classical interferometry. Perhaps the most familiar interferometer used in fluid mechanics is the Mach-Zender interferometer (MZI). For this reason, the Mach-Zender interferometer will be used for illustrating the principles of interferometry and as a basis of comparison for holographic interferometry.

A MZI is illustrated in Fig. VIII-1. This type of interferometer compares a reference plane wave with an initially planar object wave which passes through some region of interest. These two beams are then superimposed producing an interference pattern which is a result of local phase changes in the object beam. The superimposition is accomplished by recombining the reference and object beams with a beam splitter and imaging the beams on a photographic plate. If the intersection angle of the two beams is zero and no phase changes occur in either beam, a uniform irradiance (no fringes) will occur at the image plane. If a refractive index change occurs in either beam, fringes will appear which are a function of the path integrated change in refractive index. This is known as an infinite fringe interferogram (sometimes called a single fringe). Only

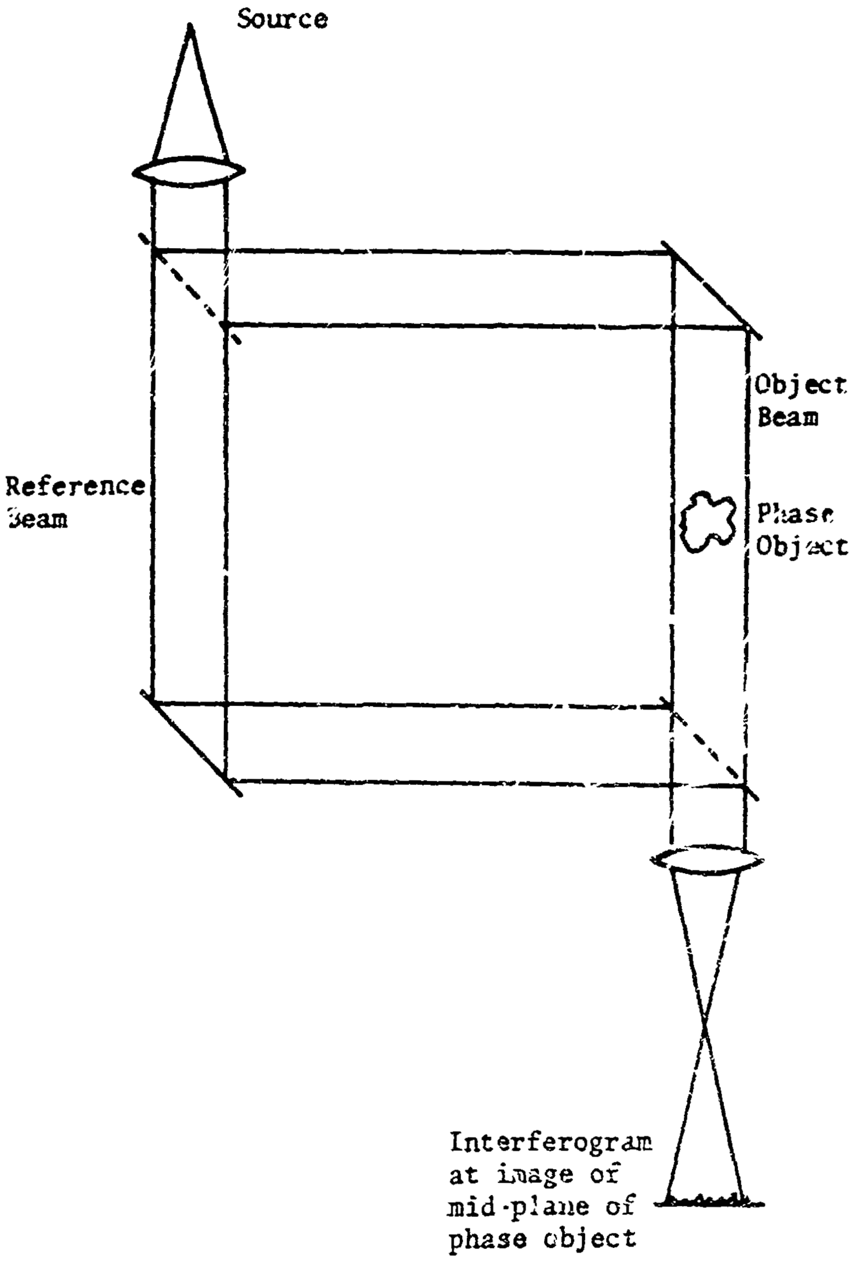

Fig. VIII-1. Mach-Zender Interferometer.

infinite fringe interferograms were created in this study and therefore they will be the object of the subsequent discussion.

The MZI has been used for flame structure studies. For example, Schultz-Grunow and Wortberg (1961) measured the temperature distribution through a 5.4% premixed methane-air flame on a flat flame burner. In that study, it was only necessary to have fringe shift information in one direction (perpendicular to the flame) since the flame was essentially 1-D and the geometric distance through the flame was known. However, for this study a 2-D interferogram is required since the flame is assumed to have a 2-D (radially symmetric) temperature distribution. This requires a more complex data reduction technique. Further, since the flame is confined by a refracting cylinder, holographic interferometry is required. The ability of holographic interferometry to produce interferograms in combustion systems has been demonstrated by Trolinger (1976). However, few quantitative studies have been undertaken.

In this chapter, the concepts of interferometry and their application to radially symmetric phase objects will be discussed. The apparatus used for this study and the resulting interferograms will then be presented. Finally, the temperature calculations and a critique of the results will be given.

Interferometry of Phase Objects

From a fundamental point of view, interferometry is an optical technique for measuring the path integrated speed of light. However, the speed a monochromatic light wave propagates through a transparent medium can often be expressed as a function of density alone.

As a wave passes through a medium with a change in density, it acquires a phase shift relative to a wave that did not pass through that density change (see Fig. VIII-2a). This is due to the relative propagation velocities of the two waves. As a wave passes through a medium with a density gradient normal to the direction of wave propagation, the wave is refracted as illustrated in Fig. VIII-2b. In this case the phase shift at the exit plane is due to the change in geometric path length as well as wave propagation velocity. If these two waves are superimposed constructive or destructive interference occurs depending on the relative phase. A transparent object which causes a phase shift with no refraction is known as a phase object. Interferometry has had its greatest utility when studying phase objects.

The speed of light in a medium is expressed as the index of refraction (n_r), which is the ratio of the speed of light in a vacuum (c_o) to that in the medium of interest,

$$n_r = \frac{c_o}{c} \qquad \text{(VIII-1)}$$

The refractive index of the medium can be linearly related to its density by

$$n_r - 1 = \beta\rho \qquad \text{(VIII-2)}$$

The phase shift of a light wave is expressed in terms of the fringe number (FN) which is the ratio of the change in optical path length (Λ) to the wave length of the wave (λ),

$$FN = \frac{\Lambda}{\lambda} \qquad \text{(VIII-3)}$$

Λ is not the geometric path length (L) but rather

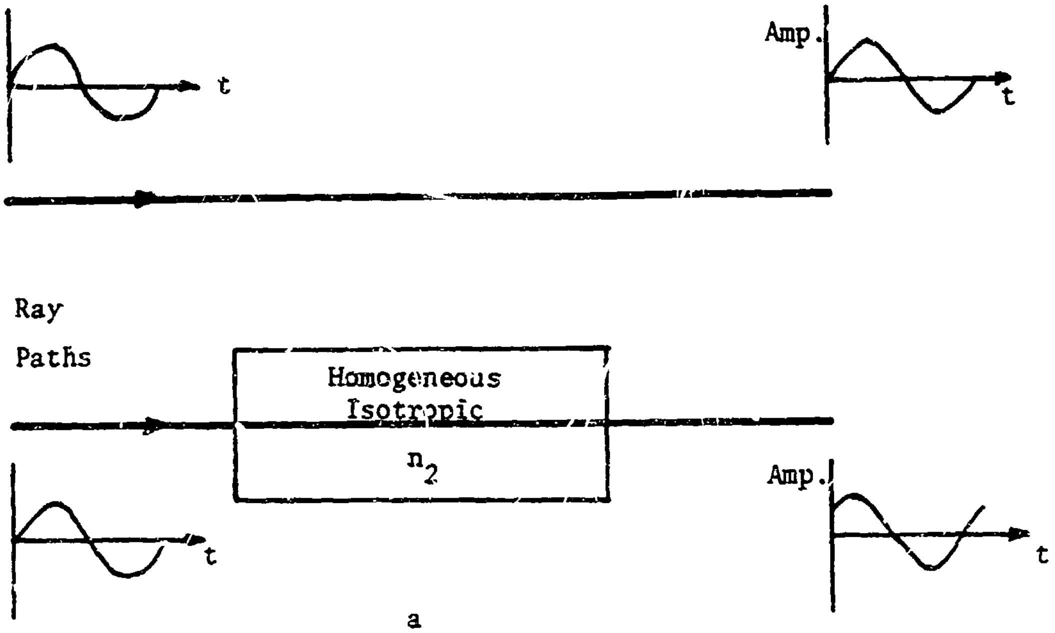

a

Phase shift due to change in optical path length

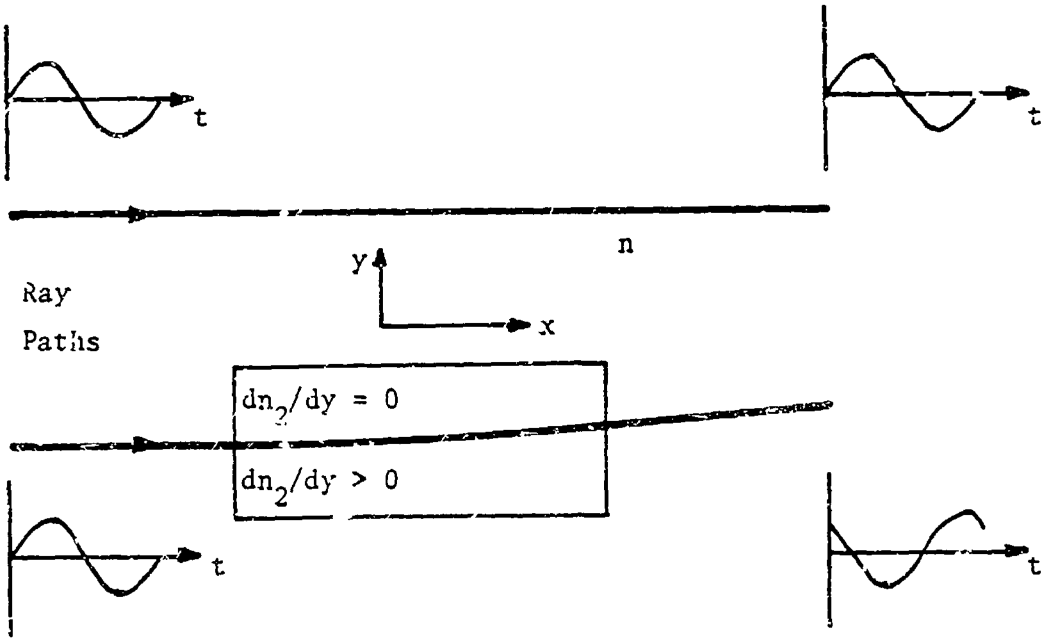

b

Fig. VIII-2. Phase Shift Due to Changes in Optical and Geometric Path Lengths.

$$\Lambda = c_o \Delta t$$

$$= L[(n_r)_2 - (n_r)_1] \qquad \text{(VIII-4)}$$

where Δt is the additional time needed for a wave to propagate through medium 2 relative to medium 1. A change of one fringe number is equivalent to a 2π radian phase shift. From Eq. (VIII-2 and 4, Eq. (VIII-3) can be rewritten

$$FN = \frac{L}{\lambda}(n - n_o)$$

$$= \frac{\beta L}{\lambda}(\rho - \rho_o) \qquad \text{(VIII-5)}$$

Here ρ_o is the density at some reference state and ρ is the density of a homogeneous phase object. For an arbitrary density distribution and arbitrary geometric path (s), Eq. (VIII-5) becomes

$$FN = \frac{\beta}{\lambda}\int_{S_1}^{S_2} [\rho(x,y,z,t) - \rho_o]\, ds \qquad \text{(VIII-6)}$$

For the MZI of Fig. VIII-1, ρ_o is normally the density of the surroundings, and Eq. (VIII-6) need only be integrated between the bounds of the phase object. In all cases the MZI uses a plane wave object beam. Therefore the s direction is constant in cartesian coordinates. In the refractionless limit (a phase object) the integration can be simplified since the change in fringe number is due only to changes in propagation velocity and not due to geometric path changes. Further, the path of the ray producing the fringe number at any point on the interferogram is known since there is a one-to-one correspondence between any x-y position on the interferogram and that in the phase object.

Before discussing holographic interferometry, it is necessary to understand conceptually what a hologram is. To this end a simple holographic apparatus is illustrated in Fig. VIII-3a. To create a hologram of a transparent object, a photographic plate is simultaneously exposed by the object and reference beams. The plate is then developed becoming the hologram. If the holographic plate is illuminated by the original reference beam (Fig. VIII-3b), the original object beam is reconstructed from the holographic plate on. If one looks through the hologram, a 3-D virtual image of the object appears in its original position. Therefore, a hologram is simply a means for storing the information contained in a light beam.

At this point there are two major concepts that must be introduced. First, there is a difference between the holographic object and reference beams, and the interferometric object and reference beams. This distinction will be clarified. Secondly, unlike a conventional photograph which records only amplitude information, the hologram contains the phase information of both the holographic object and reference beams. Likewise, the reconstructed holographic object wave contains all of the phase information contained in the original object beam. The theory explaining the manner in which the information is stored in the hologram and the object wave recreated has been treated rigorously (see Collier et al., 1971). It is sufficient for the purpose of this paper to realize that the reconstructed wave exists and contains all of the phase information that was in the original wave.

Holographic interferometry differs from classical interferometry in that in the former case one compares the change in the optical path lengths in time instead of in space. This difference is revealed by understanding how a holographic interferogram is made. For double exposure holographic

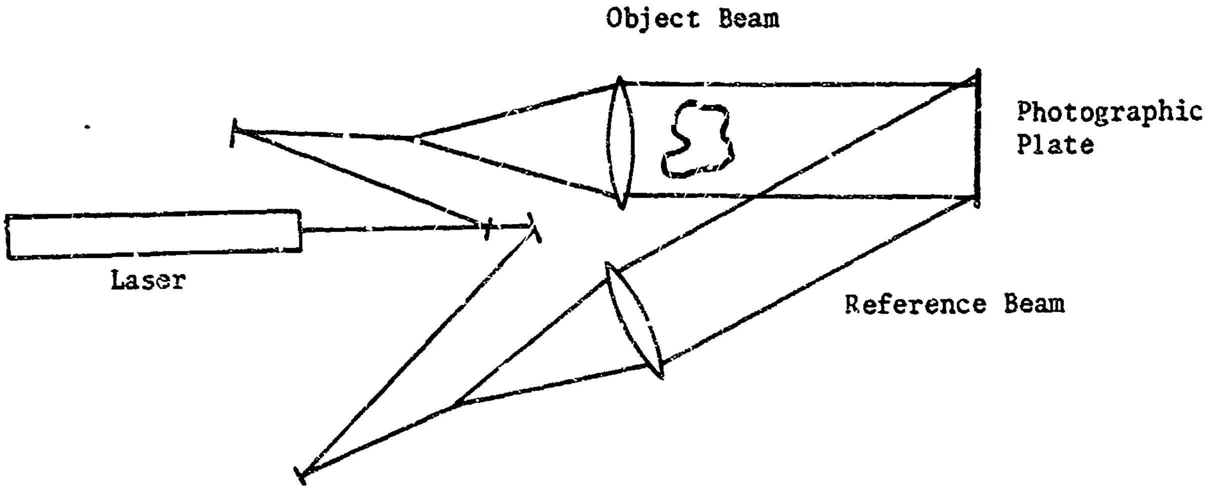

3a

Creation of Hologram

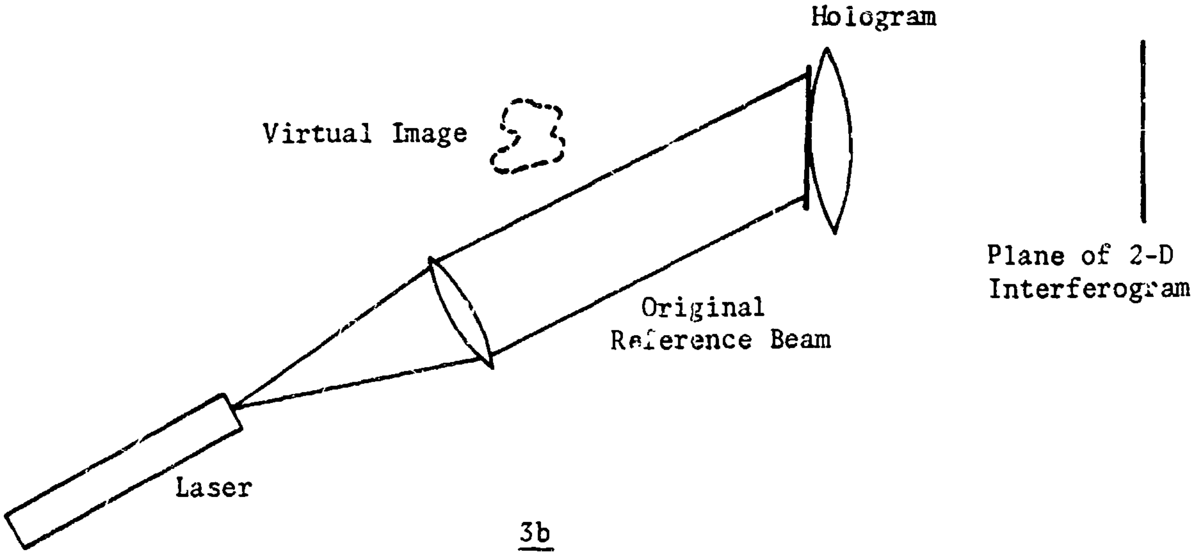

3b

Formation of Interferogram

Fig. VIII-3. Experimental Apparatus for Holography.

interferometry, the holographic plate is first exposed while the object is in its reference state. The second exposure is made when the desired refractive index change occurs. When the hologram is illuminated by the holographic reference beam, the holographic object beams from both exposures are simultaneously reconstructed and consequently interfere at the image plane of the observation system.

This interference can be understood in terms of the MZI. The holographic object beam from the first exposure is equivalent to the interferometric reference beam. The holographic object beam from the second exposure is equivalent to the interferometric object beam. Since, in holographic interferometry, the interferometric reference and object beams use common optics, any phase changes due to imperfect optical components are canceled. Further, there are no stringent alignment requirements. The only requirement is that the optics remain stationary between exposures. Another important feature of double exposure holographic interferometry is that all the phase information of the two holographic object beams is stored in the hologram. Therefore, the original beams can be reconstructed and viewed at will.

Probably the best known quality of holography is its ability to create 3-D images. This feature can be utilized in holographic interferometry by including a diffusing screen in the holographic object beam just ahead of the phase object (Fig. VIII-4). In practice, this diffusing screen can be made of opal or ground glass. In effect, the diffusing screen creates an infinite number of spherical wave sources. Therefore, every position of the hologram is illuminated from every position on the diffusing screen. The only requirement of the diffusing screen is that the longest and shortest distances between the diffusing screen and the hologram differ by a distance less than

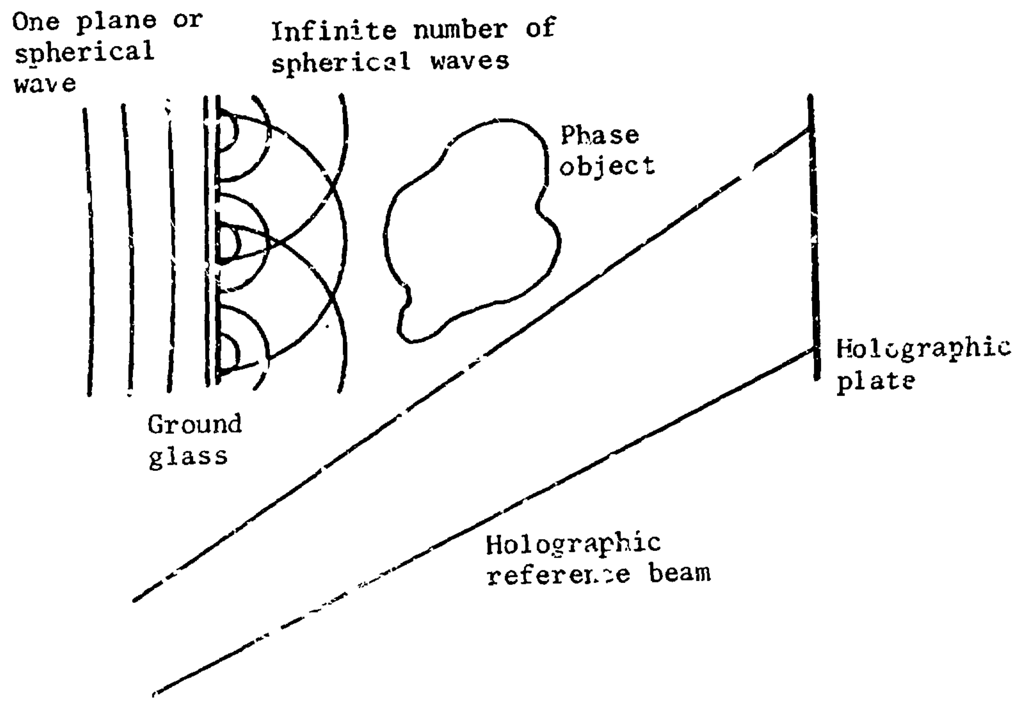

Fig. VIII-4. Diffuse Illumination Holographic Interferometry.

the coherence length of the light. The major utility of the diffuse screen in terms of interferometry is that this method creates a 3-D interferogram that localizes in the region of the phase object. As one views the interferogram from any given direction, a fringe pattern appears that is the same as the one that would have been created by a parallel beam interferometer in that same direction. A symmetric phase object creates an interferogram at the mid-plane of the object and is the same at every viewing angle. A diffusely illuminated holographic interferogram has no analogue in the realm of classical interferometers.

Heflinger et al. (1966) were the first to demonstrate the usefulness of diffuse illumination for holographic interferometry. In their work, they made a diffuse illumination double exposure holographic interferogram of the flow about a 22 caliber bullet. In fact, they were able to predict the fringe pattern by assuming that the fringe pattern was created by a plane wave. In a later paper by Witte and Weurker (1969), the density field behind a supersonic projectile was calculated from the interferogram using the same plane wave assumption.

No rigorous theory is available that predicts why diffuse illumination interferograms occur as they do.* In particular, there is no rigorous explanation as to why they can be interpreted in the same way as interferograms that have been created using a parallel light beam. Heflinger et al. did offer a conceptual explanation. The following explanation is taken directly from Heflinger et al. (1966).

"...consider a test object consisting

---

*A book by C. M. Vest will be available in 1979 which includes this theoretical treatment.

C-3

> of a sphere whose refractive index is slightly greater than air so that the path length change through the center of the sphere is, say, 7/2 wavelengths. For this object the path length change through the center of the sphere is independent of direction. For rays passing off center through the sphere the path length change will be less than 7/2 wavelengths. As shown in Fig. 3 (Fig. VIII-5 in this text), the path length is almost independent of direction for bundles of rays focused on the midplane of the sphere. Thus if one views the sphere by focusing even a low f-number lens on the midplane, one will see a set of concentric interference bands centered on the sphere. Focusing at other positions does not maintain the independence of path length change with direction and hence the bands tend to disappear. Hence in this case, the interference bands depend on position but not on direction, standing in direct contrast to the parallel glass plate case previously discussed..."

The major disadvantage of diffuse illumination holographic interferometry is that one cannot resolve as small an interferometric fringe spacing as is possible with plane wave illumination. This was demonstrated by Vest and Sweeney (1970). They found that 1 fringe/mm was the best possible in the former case while 15 fringes/mm could be resolved with nondiffuse light. The reason is that the diffuse screen causes a so-called "speckle" pattern which limits the resolution.

The theory predicting where fringes occur in the MZI (Eq. (VIII-6)) applies equally to the plane wave holographic interferometer (HI) and the diffuse illumination HI. The latter interferometer was used in this study. The advantage of holographic interferometry over classical interferometry for this study lies in the ease of set up. The advantage of diffuse over

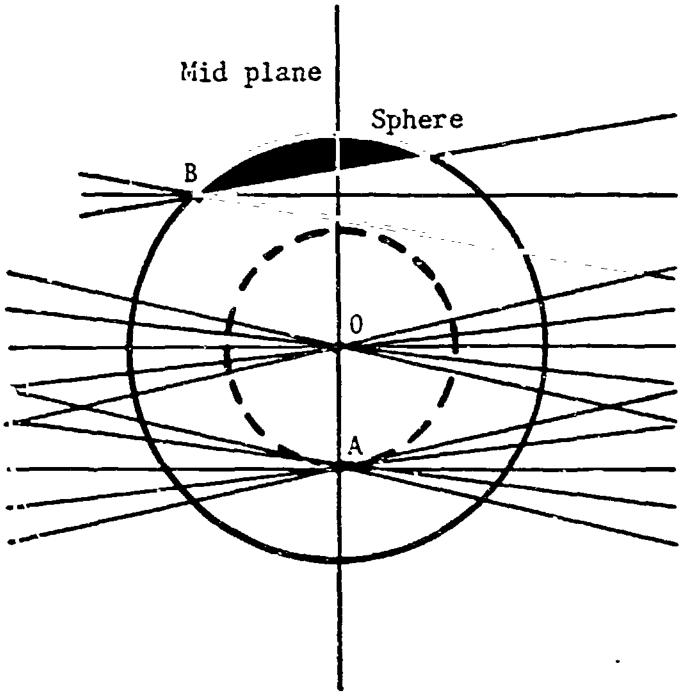

Fig. VIII-5. Sphere of index slightly greater than the surrounding medium showing path length changes for different focused bundles of rays. The rays through 0 all have the same pathlength, independent of direction. All rays tangent to the dotted sphere have the same path length and hence the bundle through A has nearly constant path length. For the bundle through B the path length is not independent of direction. (From Heflinger et al. 1966) plane wave illumination HI is that refraction, caused by the SFLT, is minimized by diffuse illumination. This refraction makes interpretation of the interferogram difficult in interferometry with plane waves. An explanation of the problems caused by refraction will now be discussed.

The Pyrex tube used for this study acts as a cylindrical lens as illustrated by the rays shown in Fig. VIII-6. As a result, even in the absence of the flame, the MZI would produce a fringe pattern. This is because the refraction causes a phase shift at the image plane due to the change in geometric path lengths. When the flame is present, the phase shift due to the refractive index field would be superimposed on the fringe pattern caused by the SFLT. Interpretation of such an interferogram is exceedingly difficult.

For a plane wave HI, no fringes would appear due to the presence of the SFLT since both the interferometric object and reference beams follow the same geometric path. Therefore, all the fringes are due to the flame alone. However, the fringe pattern is still altered by the refraction. Since the rays passing through the tube spread in the horizontal direction (see Fig. VIII-6), a positional error will occur at the image plane. Even if one images at the midplane of the SFLT, the path of the ray producing the fringe number at any point on the interferogram would have to be traced back through the tube (see Vest, 1975). This is possible, however, it requires the use of an imaging lens large enough to collect all of the refracted rays.

A diffuse illumination HI minimizes the effect of refraction. The position of the diffuse screen is immaterial to the creation of the interferogram as long as the coherence requirements are met. In fact, using a flat ground glass screen is equivalent to grinding the surface of the tube. Therefore, the side of the SFLT upon which the light beam is incident does not affect the

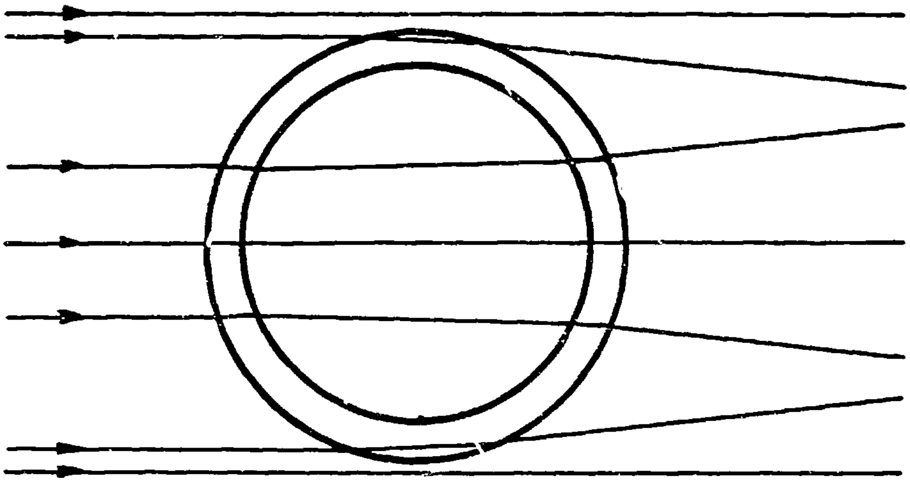

Fig. VIII-6. Refraction by the Standard Flammability Limit Tube.

formation of the interferogram. Further, if one can accurately focus on the midplane of the tube, the conceptual explanation for fringe localization by Heflinger et al. still holds. Therefore, the side of the tube from which the object beam exits simply acts as part of the imaging system. It does complicate the ability to focus on the midplane of the tube as will be discussed.

The Temperature Calculation from the Interferogram

In order to calculate the temperature from a 2-D interferogram, it is first necessary to determine the fringe number as a function of position (FN = FN(y,z)). One can then invert Eq. (VIII-6) and calculate the refractive index at any point in the phase object. When the geometric path lengths are known and the gradients are orthogonal to the rays, the inversion is straighforward. For radially symmetric phase objects the calculation is more complicated.

Consider the ficticious phase object in Fig. VIII-7, symmetric about the z axis. In this case Eq. (VIII-6) can be written as

$$FN(y) = 2/\lambda \int_y^R \frac{g(r)rdr}{(r^2-y^2)^{1/2}} \qquad \text{(VIII-7)}$$

where

$$g(r) = n(r) - n_0 \qquad \text{(VIII-8)}$$

The inversion of the functional form of Eq. (VIII-7) has been studied extensively in plasma physics for calculating temperature from line of sight emission data. A review and critique of the many techniques is given by Cremers and Birkebak (1966). The method used follows that of Ladenberg et al. (1948)and Bennett et al.(1952) for calculating the density field about supersonic projectiles. This technique was also used by Witte and Weurker (1969) in their work with a diffuse illumination HI.

The numerical inversion technique assumes that the radially symmetric phase object may be broken up into equally spaced annular sections in a plane perpendicular to the axis of symmetry (z axis) as shown in Fig. VIII-7. The refractive index is assumed to be constant throughout each annular section. Equation (VIII-7) can then be rewritten by letting $g_i = g(r)$ for each ring $r_i \le r \le r_{i+1}$, where $r_i = i\Delta r$. For a ray parallel to the x axis at $y = r_i$, Eq. (VIII-7) becomes

$$FN(y_i) = \frac{2}{\lambda} \sum_{K=i}^{I-1} g_K \int_{r_K}^{r_{K+1}} \frac{rdr}{(r^2-r_i^2)^{1/2}} \qquad \text{(VIII-9)}$$

where

$$FN(y)_i = FN(r_i)$$

The integrand can be directly integrated as

$$\int_{r_K}^{r_{K+1}} \frac{rdr}{(r^2-r_i^2)^{1/2}} = [\sqrt{r^2-r_i^2}] \Big|_{r_K}^{r_{K+1}}$$

$$= [(r_{K+1}^2 - r_i^2)^{1/2} - (r_K^2 - r_i^2)^{1/2}]$$

$$= \Delta r\{[(K+1)^2 - i^2]^{1/2} - [K^2 - i^2]^{1/2}\}$$

$$\therefore \quad FN_i\lambda = 2\Delta r \sum_{K=i}^{I-1} g_K\{[(K+1)^2 - i^2]^{1/2} - [K^2 - i^2]^{1/2}\}$$

or

$$FN_i(y) = \frac{2\Delta r}{\lambda} \sum_{K=i}^{I-1} g_K A_{Ki} \qquad \text{(VIII-10)}$$

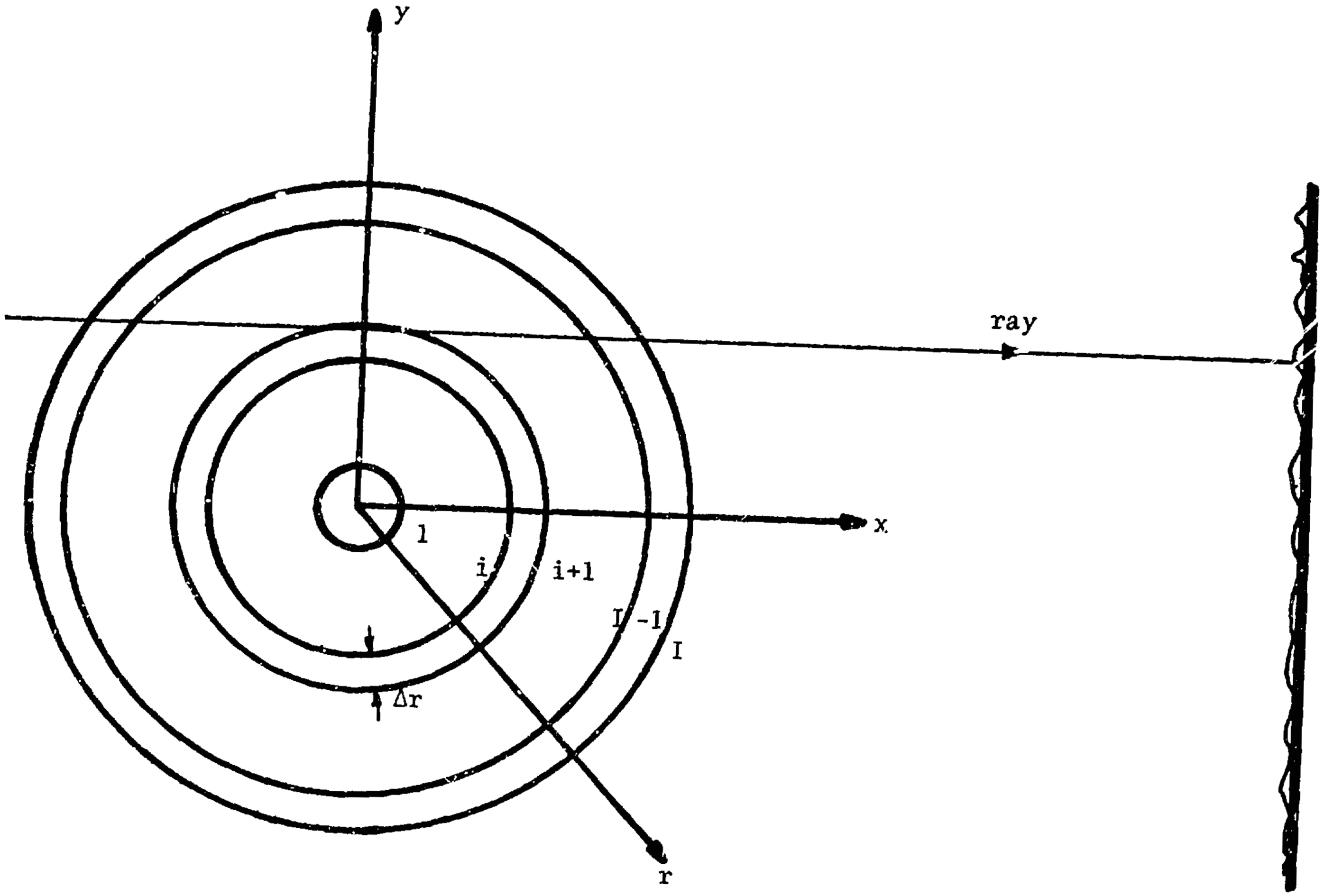

Fig. VIII-7. Annular Rings for Numerical Inversion of Fringe Number.

where

$$A_{K,i} = \{[(K+1)^2 - i^2]^{1/2} - (K^2 - i^2)\}$$

To solve this set of linear equations for $FN_i(y)$, it is easiest to start from the outer ring and sucessively solve for FN_i to the next innermost ring.

These equations may be rewritten so that one may calculate $g(r)$ from a known function $FN(y)$ (see Hauf and Grigell, 1970). The equations for g_i can be written

$$g_i = [(\lambda/2\Delta r)FN_i - \sum_{\ell=i+1}^{I-1} g_\ell A_{\ell i}]/A_{ii}$$

or

$$g_i = [(\lambda/2\Delta r)FN_i - \sum_{\ell=i+1}^{I-1} g_\ell A_{\ell i}]/(2i+1)^{1/2}$$

and

$$A_{\ell i} = \{[(\ell+1)^2 - i^2]^{1/2} - [\ell^2 - i^2]^{1/2}\} \qquad \text{(VIII-11)}$$

Again, the solution starts at the outermost annulus. It should be noted that a singularity exists in Eq. (VIII-9) for the ray passing through $y = 0$ since the denominator of the integrand approaches zero at $y = 0$.

In this study, temperature and not the refractive index is the property of interest. Therefore, the relationship between the two must be developed.

Strictly speaking, η_r changes through a flame due to

1) density changes due to pressure,
2) density changes due to the number of moles,
3) index of refraction changes due to a change in the species present, and
4) density changes due to temperature.

It was demonstrated in Chapter II that the pressure change through a flame is insignificant even in the worst case. It was demonstrated by Weinberg (1963) that changes in ρ due to changes in the number of moles through the flame are also insignificant.

The change in index of refraction due to changes in the type of species present manifests itself in terms of β in Eq. (VIII-2). β is known as the Gladstone-Dale constant and is different for every species. According to Weinberg (1963) and Hauf and Grigull (1970), β remains constant over the temperature range encountered in flames. For a mixture of i species,

$$\beta_{mix} = \sum_{i=1}^{S} Y_i \beta_i$$

where Y is the mass fraction. Weinberg (1963) demonstrated that the change of β between the product and reactant mixtures is negligible. Since it was desirable to measure the temperature through the flame, it was necessary to determine if β_{mix} changes in the preheat and reaction zones of the flame. For this assessment it was necessary to obtain the complete species concentrations through a flame. This is available from theoretical calculations by Hecker (1975) for a 1-D adiabatic flame propagating through a 7% methane-air mixture. This is a more complete version of the data reported by Smoot _et_ _al_. (1976).

The change in the Gladstone-Dale constant (β) at five positions through the flame is listed in Table VIII-1. Only those species that had mole fractions greater than 10^{-2} (major species) were included in these calculations (specifically, CH_4, H_2O, CO_2, CO, O_2 and N_2). The index of refraction of a species is basically a function of the molecular cross section

TABLE VIII-1

CHANGE OF GLADSTONE-DALE CONSTANT THROUGH 7% METHANE-AIR FLAME

(From Hecker (1975))

Y mm	T °K	β mm^3/g
0	300	244
0.76	483	243
1.52	806	245
2.28	1400	240
3.05	1760	241

(even for radical species). Therefore, the refractivity of each of the minor intermediate species is assumed to be of the same order of magnitude as the major species. Since the concentration of the minor species is small ($\chi_i < 10^{-2}$), their contribution to β_{mix} is small enough to be neglected.

This additional information substantiates Weinberg's claim (1963) that the density change through a flame is primarily a function of temperature alone. Therefore, the temperature can be calculated as a function of η_r. From Eqs. (VIII-2 and 8), one can write

$$g_i = \beta(\rho(r) - \rho_o)$$

$$= \beta\rho_o\left(\frac{\rho(r)}{\rho_o} - 1\right) \qquad \text{(VIII-12)}$$

From the equation of state,

$$\frac{\rho}{\rho_o} = \frac{T_o}{T}$$

for a constant pressure and a constant number of moles. Therefore,

$$g = \beta\rho_o(\frac{T_o}{T} - 1)$$

and for a flame where $\rho_o = \rho_u$

$$g_i = \rho_u\beta(\frac{T_o}{T_i} - 1)$$

or

$$g_i = \rho_u\beta\tau_i \qquad \text{(VIII-13)}$$

Combining Eqs. (VIII-11 and 13),

$$\tau_i = \frac{\left(\frac{\lambda}{2\Delta r \rho_u \beta}\right) FN_i - \sum_{\ell=i+1}^{I-1} \tau_\ell A_{\ell i}}{(2i+1)^{1/2}} \qquad \text{(VIII-14)}$$

and

$$A_{\ell i} = \{[(\ell+1)^2 - i^2]^{1/2} - [\ell^2 - i^2]^{1/2}\}$$

Before describing the numerical solution of these equations, the experiment will be described and the resulting interferograms presented.

The Holographic Interferometer

A schematic of the holographic interferometer (HI) used in this study is given in Fig. VIII-8. The Spectra Physics 15 mW HeNe laser used for the LDA system was used for this phase as well. It has a coherence length of approximately 0.12 m. The Maranda 35 mm SLR camera (with its lens removed) described in Chapter V was used as a shutter. The laser beam was positioned at that region of the focal plane shutter which opened first. The beam then intersected a variable density beam splitter made by Jodon Engineering. Part of the light was reflected for the holographic object beam, and part was transmitted for the holographic reference beam. Both the object and reference beams were expanded by a 40x microscope objective and spacially filtered with 25 μm pin holes. The reference beam was a spherical wave when incident on the holographic plate. The object beam was made into a 0.127 m diameter plane wave using a Bausch & Lomb double element condenser with a 0.508 m focal length. The object beam was then passed through a 0.15 x 0.15 m ground glass plate which was 30 mm ahead of the SFLT and 0.18 m ahead of the holographic plate. Both the object and reference beams were overexpanded so that the irradiance 64 mm from the beam centerline was more than 50% of the

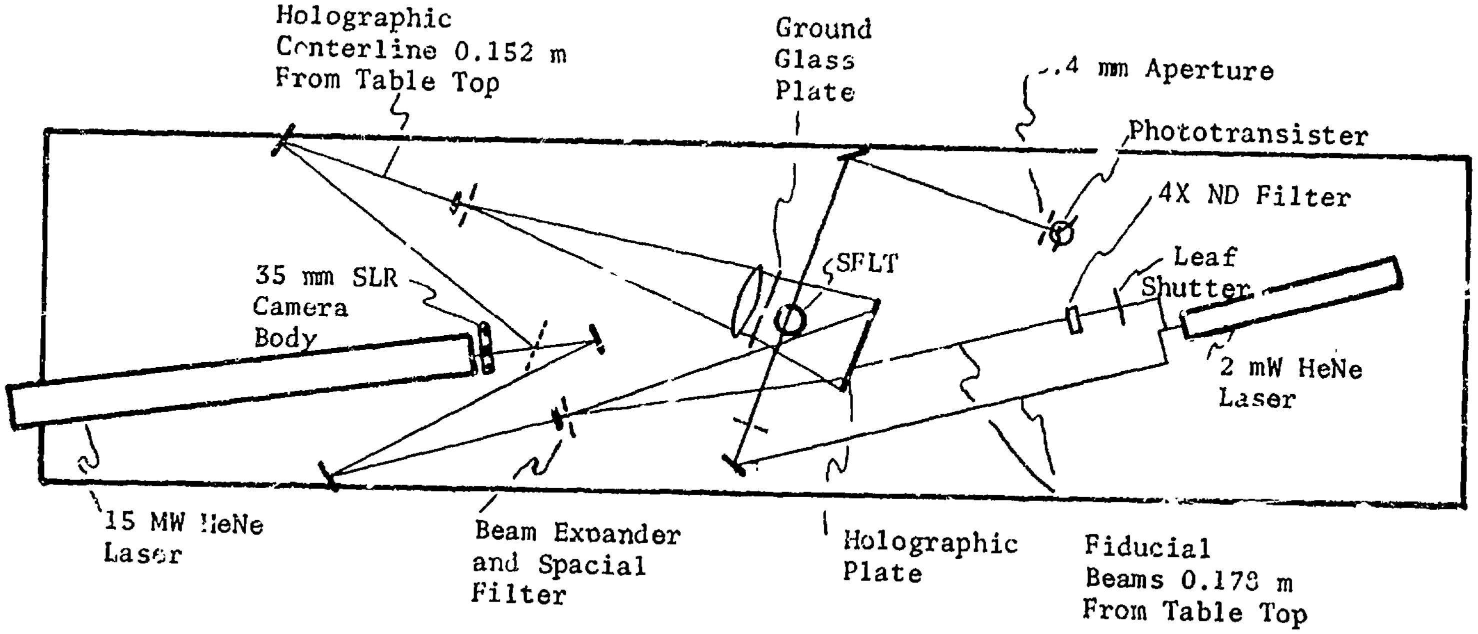

Fig. VIII-8. Schematic of Holographic Interferometer and Reference Systems.

centerline irradiance. A 0.100 m x 0.127 m holographic plate was used with its major axis vertical. The system was adjusted so that there was no more than a 10 mm geometric path length difference between the centerline distances of the holographic object and reference beams. The centerline of the holographic object beam was normal to the holographic plate while the reference beam was offset by 33° ±1°. The path length difference of the holographic reference beam across the holographic plate was 55 mm. The maximum path length difference between the ground glass and the holographic plate was 40 mm. Thus the coherence requirement of the system was less than 0.110 mm which is within the coherence length of the source. The centerline of the optics was 152 mm from the table top (1.85 m from the ignition end of the tube). All of the optical components and the SFLT were mounted on the isolated optical table described in Chapter V. All of the optical hardware used for this study was constructed in the AAE shop unless otherwise noted.

The holographic plate was a Kodak High Speed Holographic Plate Type 131-02. It has a 9 μm thick emulsion on a 1 mm thick glass substrate. It has a maximum resolution of 1250 lines/mm. The plates were developed for 8 min in D-19 at 28°C. Two gm/l of potassium thiocyanate was added to the D-19 as recommended by Jodon Engineering to yeild a 3-4 ergs/cm^2 sensitivity at a film density of 1.0. The holographic plate was mounted in a real time plate holder made by Jodon Engineering. This provided accurate repositioning of the plate for reconstruction. The plate was placed with the emulsion toward the incident light.

In order to determine the proper exposure time, it was first necessary to determine the proper beam split between the object and reference beams. To accomplish this a selinium solar cell (35 x 40 mm) was positioned in the center of the same plane as the holographic plate would ordinarily exist. The output of the cell was put across a resistor in series with an ammeter. The variable density beam splitter was then adjusted until the irradiance of the reference beam and the diffuse light of the object beam were equal. Next, the exposure time was varied until the desired film plate density was found. A Maranda shutter setting of 1/250 (3 ms) was found to give an average film density of about 0.65. This is within the guide lines for a linear emulsion response as described by Landry and Phipps (1975) and Collier et al. (1971).

The beam deflection flame detector (BDFD) used in Chapters V and VII was used to trigger the HI exposure as well. The distance between the centerline of the SFLT and the receiving aperture was maintained so that electronic wave form would be the same as before. The same shutter circuit described in Chapter V was used. Therefore, there was a 32.5 ms time delay between the signal and the beginning of the exposure. A second reference beam was passed through a leaf shutter and on to the back side of the holographic plate. A leaf shutter speed of 1/200 was used to expose the plate. The resulting spot was used as a locating mark. Both reference beams were 0.178 m above the table top. This allowed more of the post-reaction zone to be observed, while the leading edge of the flame was still within the region of the interferogram with good fringe visibility.

Since the holographic plate was exposed to the room lights, the tests had to be conducted in total darkness. The laser was covered by a light-proof cloth, allowing for circulation of cooling air. A black card was placed in front of the holographic plate so that light scattered by the tube from the reference beam would not fog the film. This card was manually removed and replaced to allow exposure of the holographic plate only during the holographic exposures.

The sequence of events used to make a double exposure hologram of the flame is given in Table E-1 of Appendix E. In summary, the tube was cleaned and filled as previously described (only unseeded mixtures were used). The first exposure was made after the tube was filled with the test mixture. The second exposure was triggered by the reference beam as the flame passed.

The interferogram was made after developing the plate by placing it in its original position and reconstructing the hologram. The virtual image was then photographed. The Kodak Graflex camera with a 190 mm f/4.5 lens was used. Prints were made using Polaroid Type 47 high contrast film with an ASA of 3000. The beam splitter was rotated so that all of the laser light was diverted to the reference beam. A shutter speed of 1/10 was needed for exposing the print. For the purpose of data reduction, Polaroid type 46-L low contrast positive transparency film was used. It has an ASA of 400 and required a 1.5 s exposure. In each case, two exposures were made. One was made of the reconstructed hologram creating the interferogram. The camera was focused by optimizing the sharpness of the fringes. The second exposure was made with the hologram removed. A scale was placed next to the SFLT in the image plane and illuminated with the room lights. The image of this scale was used to determine the height of the reference beam and to determine the magnification.

The Results

Holographic interferograms of several lean limit flames were made. In each case, if the flame did not appear to be symmetric, the holographic plate was not developed. Six holograms of flames which appeared symmetric were made. It was discovered that in spite of many attempts a truly symmetric interferogram was never realized. Two photographs of the most symmetric of the 6 interferograms made are shown in Fig. VIII-9. The lower photograph is just magnified. It can be seen that, especially near the leading edge, the flame is asymmetric. The vertical center of the first fringe was calculated to be even with the reference beam at the time the beam deflection started the timed shutter sequence. Therefore, the velocity measurements and the position of the visible image of the flame can be referenced to the vertical center of the first fringe.

One hologram was made of the hot bubble of a flame just after extinction and is shown in Fig. VIII-10. Extinction occurred right at the reference beam. Close inspection of Fig. VIII-10 reveals that the hot bubble is symmetric. This was confirmed by measurements.

In order to calculate the temperature distribution from the interferogram, it was necessary to take the following steps:

1) Measure the fringe number as a function of r at the desired z (vertical) position.
2) Calculate the fringe number at I equally spaced positions.
3) Calculate the temperature in each annulus using Eq. (VIII-14).
4) Repeat 1-3 for each desired z position.

In order to measure the fringe number (FN) as a function of radius (r) it is first necessary to interpret what number is associated with each fringe. Wherever the interferometric object and reference waves are in phase, constructive interference occurs resulting in a bright fringe. Wherever the waves are π radians out of phase destructive interference occurs resulting

Full View

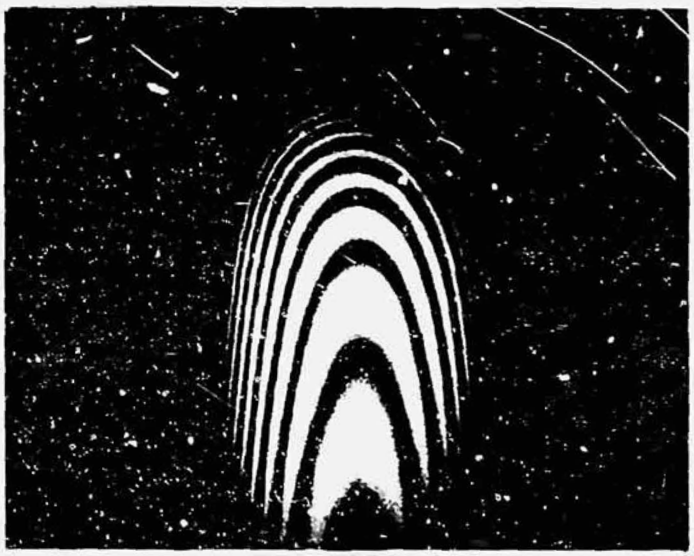

Closeup View

Fig. VIII-9 Interferogram of Upward Propagating Lean Limit Flame.

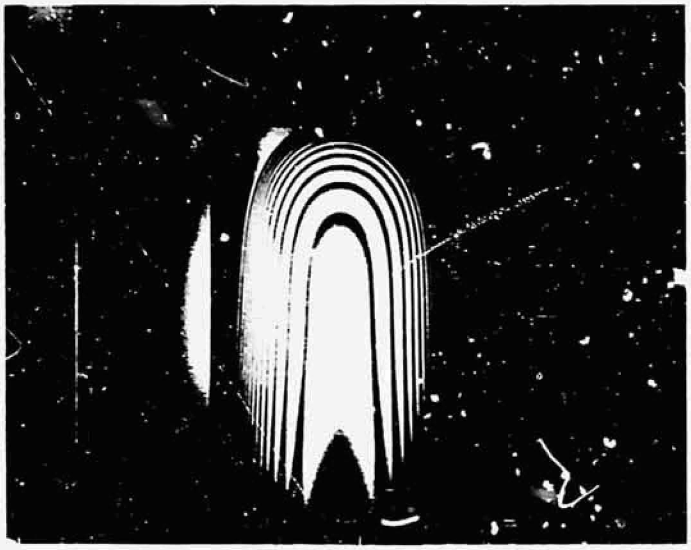

Full View

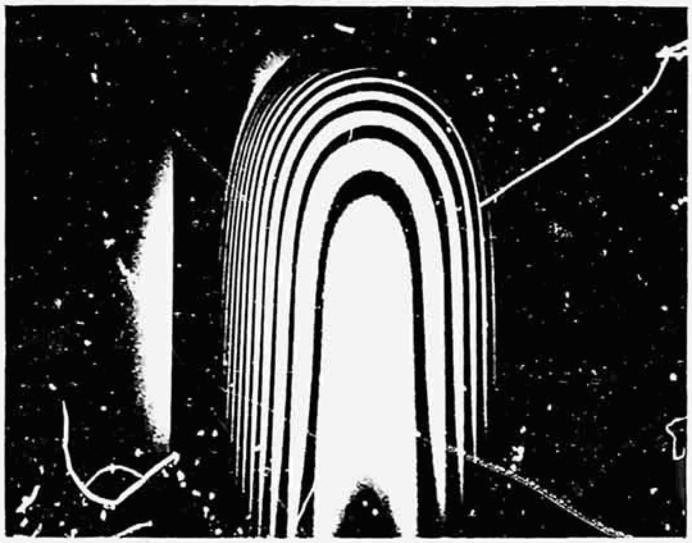

Closeup View

Fig. VIII-10 Interferogram of Hot Bubble After Flame Extinction.

in a dark fringe. A change of one fringe number occurs every 2 π phase shift. Therefore, a dark fringe occurs every (i + 1/2) where i = 0, ±1, ±2... In the flame, as one moves from the outside inward the density decreases. By convention, as one moves from the outside inward in Figs. VIII-9 and 10, each dark fringe encountered represents FN = -1/2, -1 1/2, - 2 1/2 ... in that order. Therefore, FN as a function of r at any z position can be determined simply by measuring the position of each dark fringe. The previously described Bausch & Lomb optical comparator was used for this purpose.

An example of FN vs r in the flame at z = -13.9 is illustrated in Fig. VIII-11. z = -13.9 corresponds to the position of the horizontal plane passing through the vertical center of the thirteenth dark fringe from the top ($FN_{r=0} = -12.5$). z = 0 corresponds to the vertical center of the first dark fringe (FN = -0.5). The data points were found by measuring the average position of the fringes on both sides of the interferogram centerline. For instance, the total distance between the position of the fringe corresponding to FN = -1.5 on both the left and right sides of the centerline was measured and divided by two. This was done to correct for the asymmetry.

It is immediately obvious that the fringes are not equally spaced and that there are few data points near the centerline of the interferogram. Since Eq. (VIII-14) requires FN be known at equally spaced radial positions, an interpolation scheme was required. Interpolation was accomplished using a numerical subroutine known as ICSICU. This is part of a software package created by International Mathematical and Statistical Libraries, Inc. (IMSL).

This subroutine provides interpolation by cubic splines with arbitrary second derivative end boundary conditions. A second subroutine called

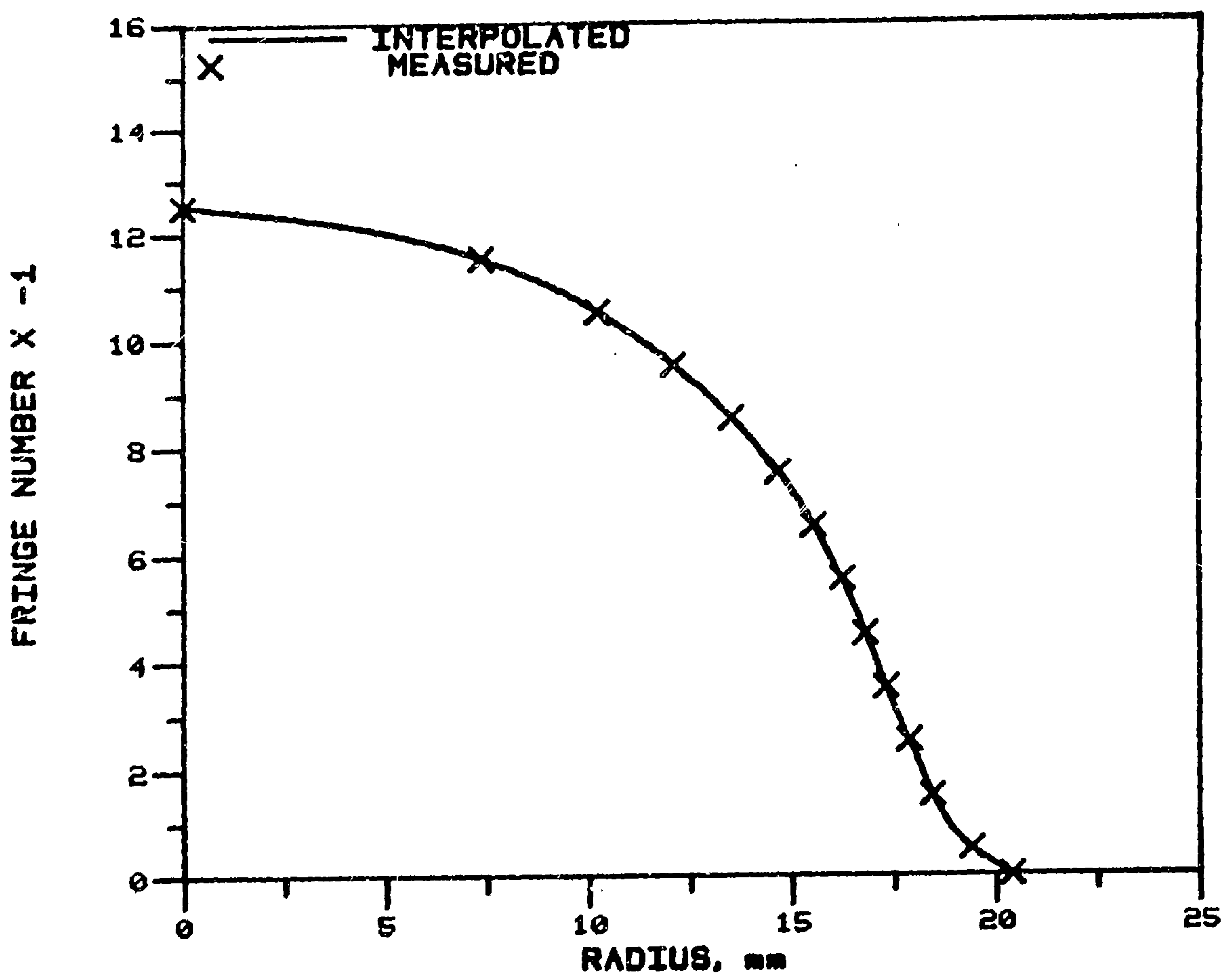

Fig. VIII-11. Fringe Number Distribution at Z = 13.9 in the Lean Flame.

ICSEVU was used to evaluate the splines at the desired radial positions. Descriptions of the library subroutines are given in Appendix D. The fortran program calling these library routines (INTERPOL) is listed in Appendix D. INTERPOL simply reads the measured (FN,R) pairs, fits the data with cubic splines and calculates FN at I equally spaced intervals between r = 0 and r at FN = 0. Since r at FN = 0 could not be measured on the optical comparitor, a "best guess" was made. The solid line in Fig. VIII-12 was constructed from 200 interpolated points. It should be noted that $\frac{d^2FN}{dr^2}$ is arbitrary at the end boundaries while $\frac{dFN}{dr} = 0$ at both end boundaries.

The interpolated values of FN were called by a second program ABELINV2 (see Appendix D). ABELINV2 solved for temperature as a function of r using Eq. (VIII-13). The numerical analysis was done on an IBM-370 at General Motors Research Labs in Warren, Michigan. The required physical parameters were

$\lambda = 632.8$ nm

$\rho_o = 1.1 \times 10^{-6}$ g/mm^3

$\beta = 243$ mm^3/g

$T_u = 300$°K

FN vs r was measured at 16 different vertical positions in the flame and 10 different positions in the post-extinction bubble. In all cases the z position was coincident with the vertical center of a dark fringe at r = 0. (See Tables E-1 and E-2). In this way the value of FN was always known at the centerline. The precision of the measured values is estimated to be ± 0.05 mm. It will be demonstrated that the accuracy is not that good.

The calculated temperature (in the flame) versus radius at z = 13.9 given in Fig. VIII-12. Some of the notable features are:

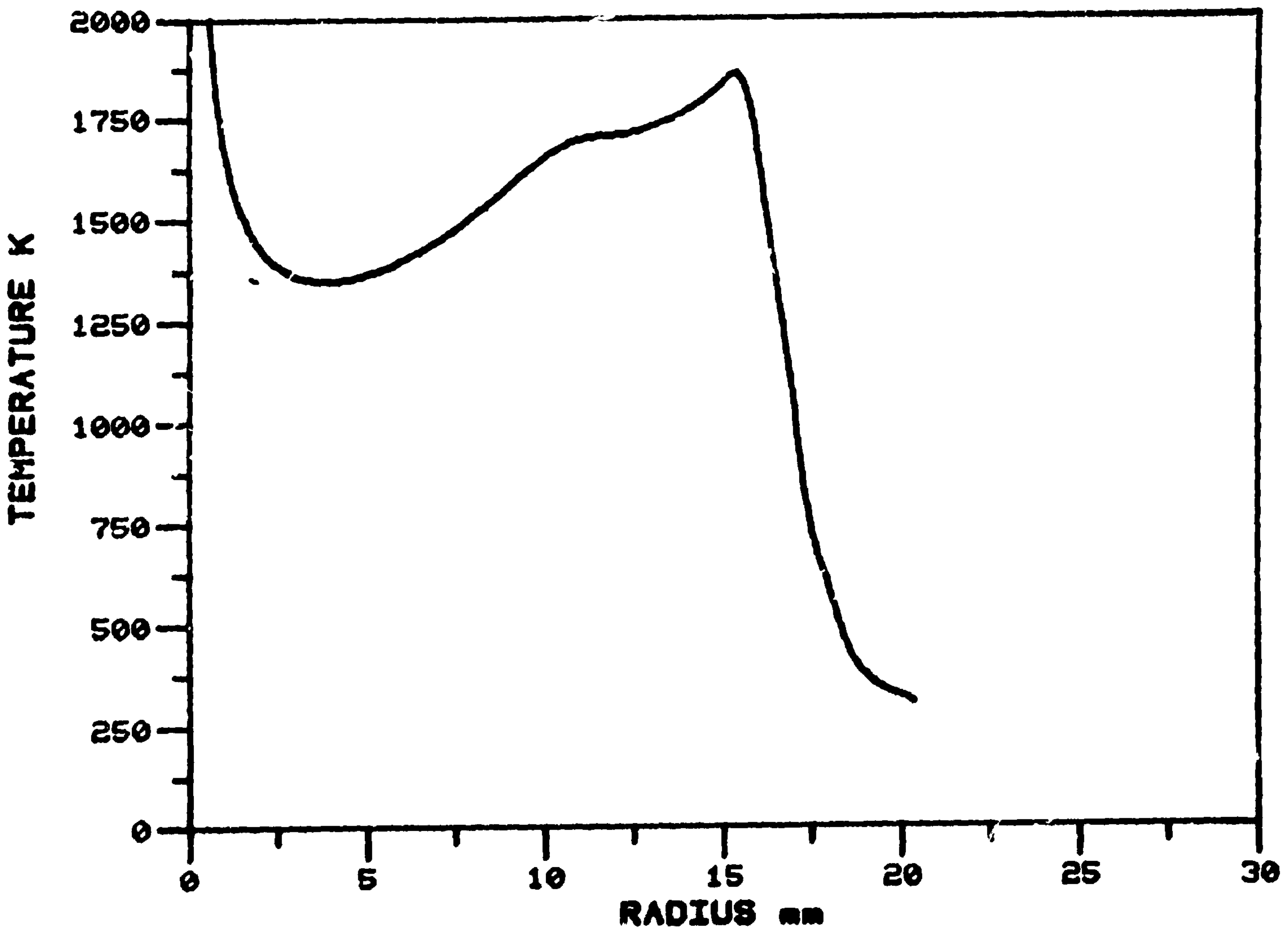

Fig. VIII-12. Temperature Distribution at Z = 13.9 in the Lean Flame.

1) The temperature at $r = 15$ mm is greater than the adiabatic flame temperature (T_{ad}).
2) The temperature drops at $3 \text{ mm} < r < 15$ mm with no mechanism for heat loss in that region.
3) The temperature appears to approach infinity at the centerline.

Before discussing the reason for these errors, it is of interest to determine the accuracy of the calculation procedure. A series of tests were made to

1) determine the proper thickness of the annuli (Δr),
2) determine the error caused by guessing where FN = 0, and
3) determine how sensitive the temperature profile is to errors in FN vs r.

To determine the proper annulus size, the temperature was calculated at $z = 13.9$ using 100, 200, 400 and 1000 annuli over the 20.4 interval. It was found that there was less than 10°K difference between the four profiles at any given radial position. 200 annuli were used for all z positions where r at FN = 0 was greater than 10 mm. 100 annuli were used in all other cases. It should be noted that 200 annuli at $z = 13.9$ yield a $\Delta r = 0.1$ mm. The maximum calculated temperature gradient was about 500°K/mm.

Since it was necessary to guess the radius at which FN = 0, several tests were made to determine how the inaccuracy of this guess affected the temperature profile. The results we plotted in Fig. VIII-13. The best guess was considered to be $r = 20.4$ at FN = 0. $r = 26$ mm is the most extreme case since that is the inside radius of the tube. It was concluded that this method for determining where FN = 0 is adequate.

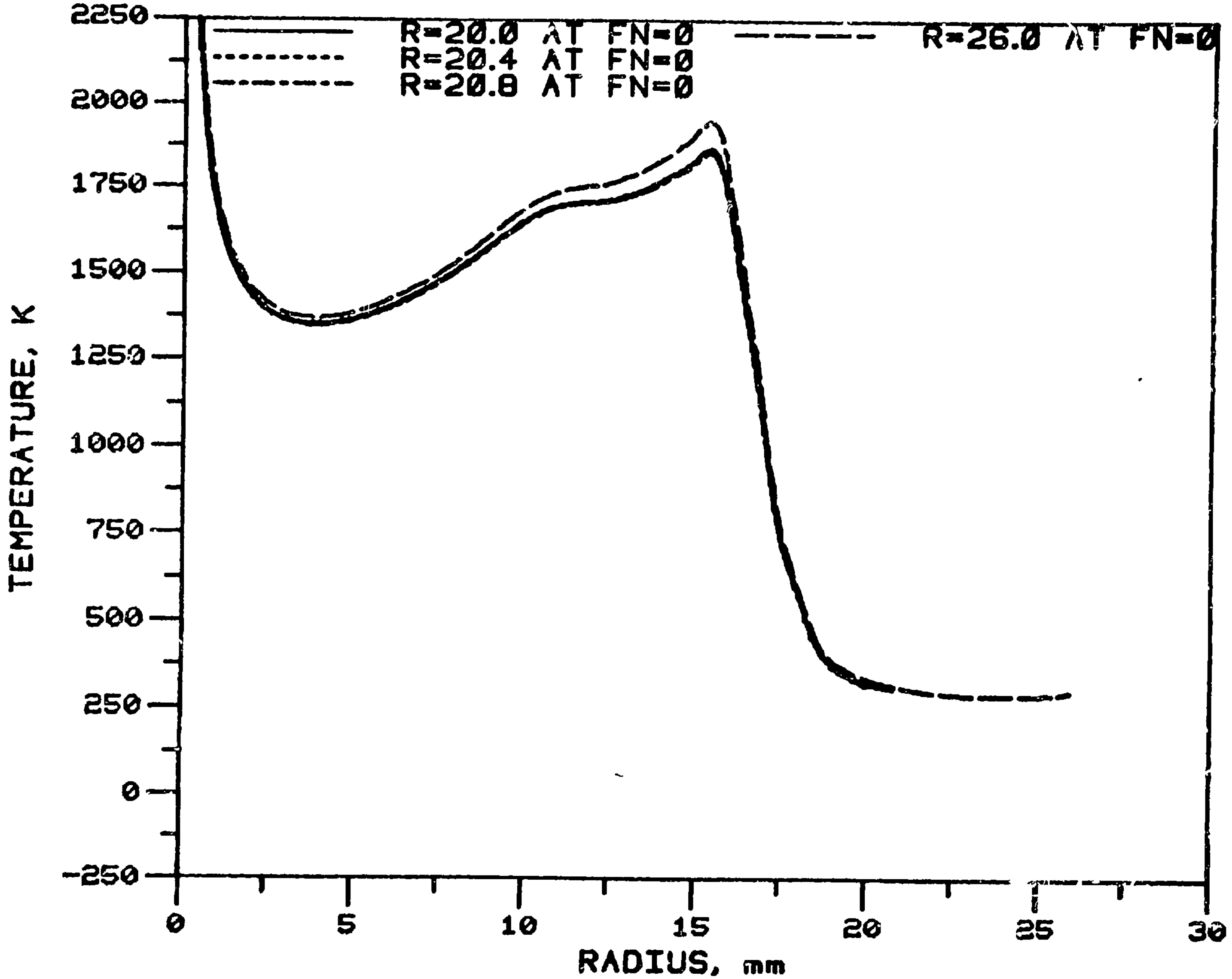

Fig. VIII-13. Temperature Distribution at Z = 13.9 in the Lean Flame.

In order to determine the sensitivity of the temperature profile to inaccuracies in FN vs r, the abscissa of Fig VIII-11 was expanded 5%. Each measured radial position was multiplied by 1.05 and reinterpolated. The recalculated temperature profile is shown in Fig. VIII-14. The peak temperature dropped to about 1500°K (20%) at r ≈ 16 mm.

The sensitivity of the integration technique to the fringe number position was revealed when a bad data point appeared in the fringe number profile of the flame at z = 10.6 mm (see Fig. VIII-15). As shown in Fig. VIII-16), an oscillation occurred in the temperature profile. When this bad point was corrected (Fig. VIII-17), most of the oscillation disappeared as illustrated in Fig. VIII-16. The point of this illustration is that slight ripples in the interpolated FN vs r curve can cause large errors in the calculated temperature profile.

The sensitive nature of the integration scheme was further exemplified by the data taken at z = 18.1. T vs r at z = 18.1 is illustrated in Fig. VIII-18. If one observes FN vs r (Fig. VIII-19) for this profile, small but perceivable ripples can be seen. A different library subroutine known as IQHSCU was used in an attempt to alleviate this problem (see Appendix D). IQHSCU does not impose continuous second derivatives between splines and therefore should lessen the "overshoot" due to the interpolation method. However, the use of IQHSCU had no effect on the oscillation in Fig. VIII-19. Therefore, it was concluded that the oscillations are due to errors in the measurements.

Plots of the temperature profiles at each of the 15 vertical positions in the flame are presented in Figs. E-1 through E-15 of Appendix E. Except for some temperature oscillations, all of the plots have the same general

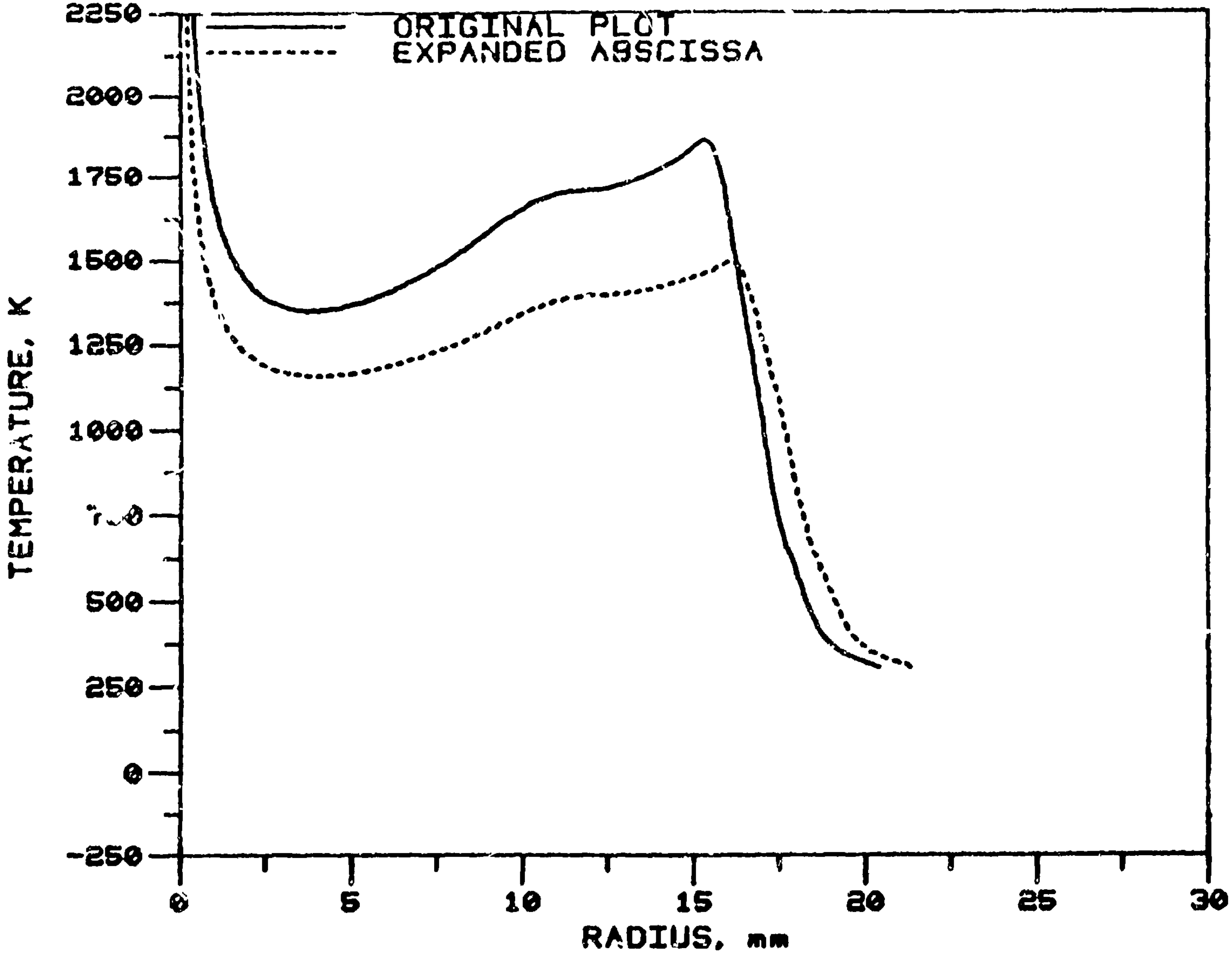

Fig. VIII-14. Temperature Distribution at Z = 13.9 in the Lean Flame.

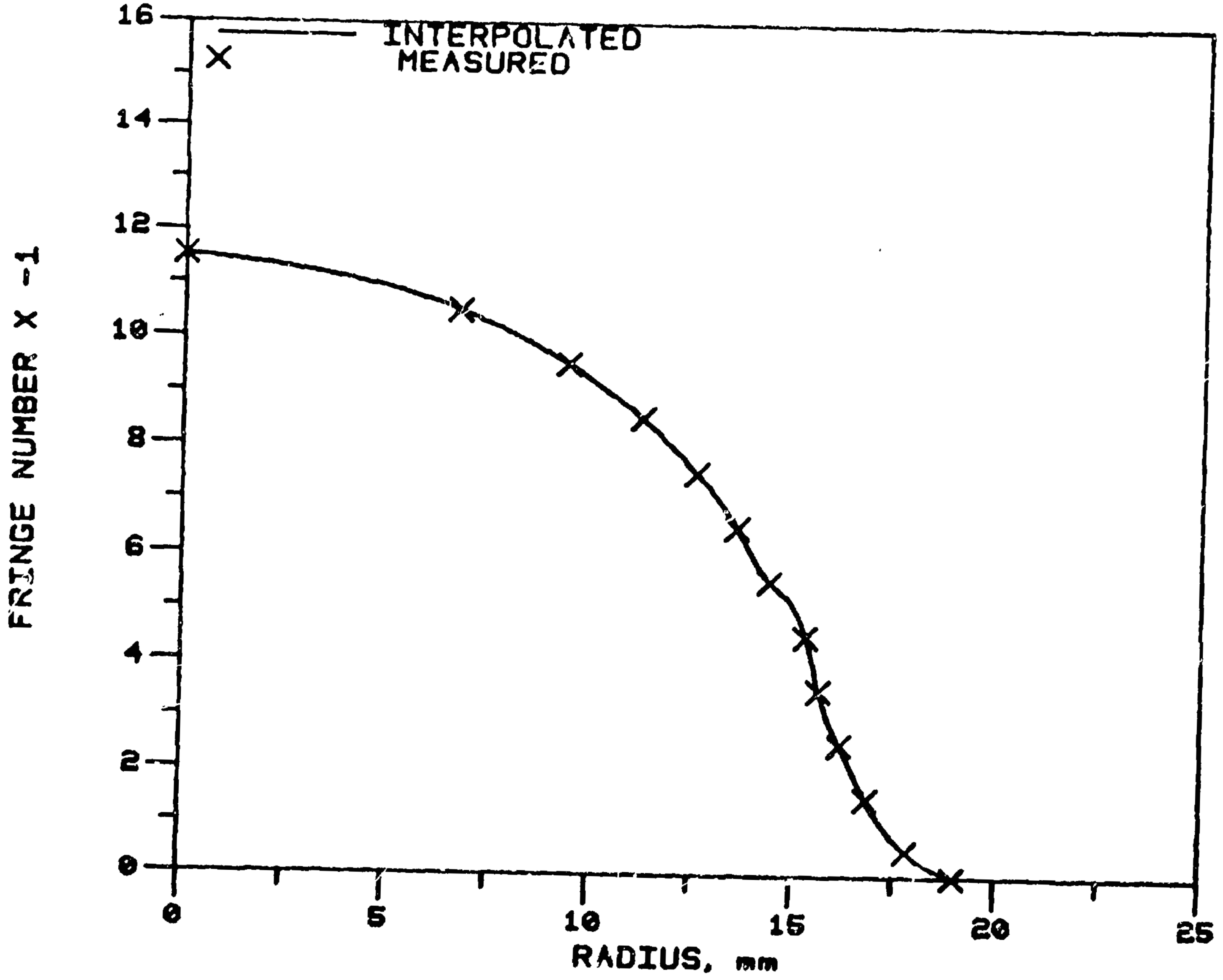

Fig. VIII-15. Incorrect Fringe Number Distribution at Z = 10.6 mm.

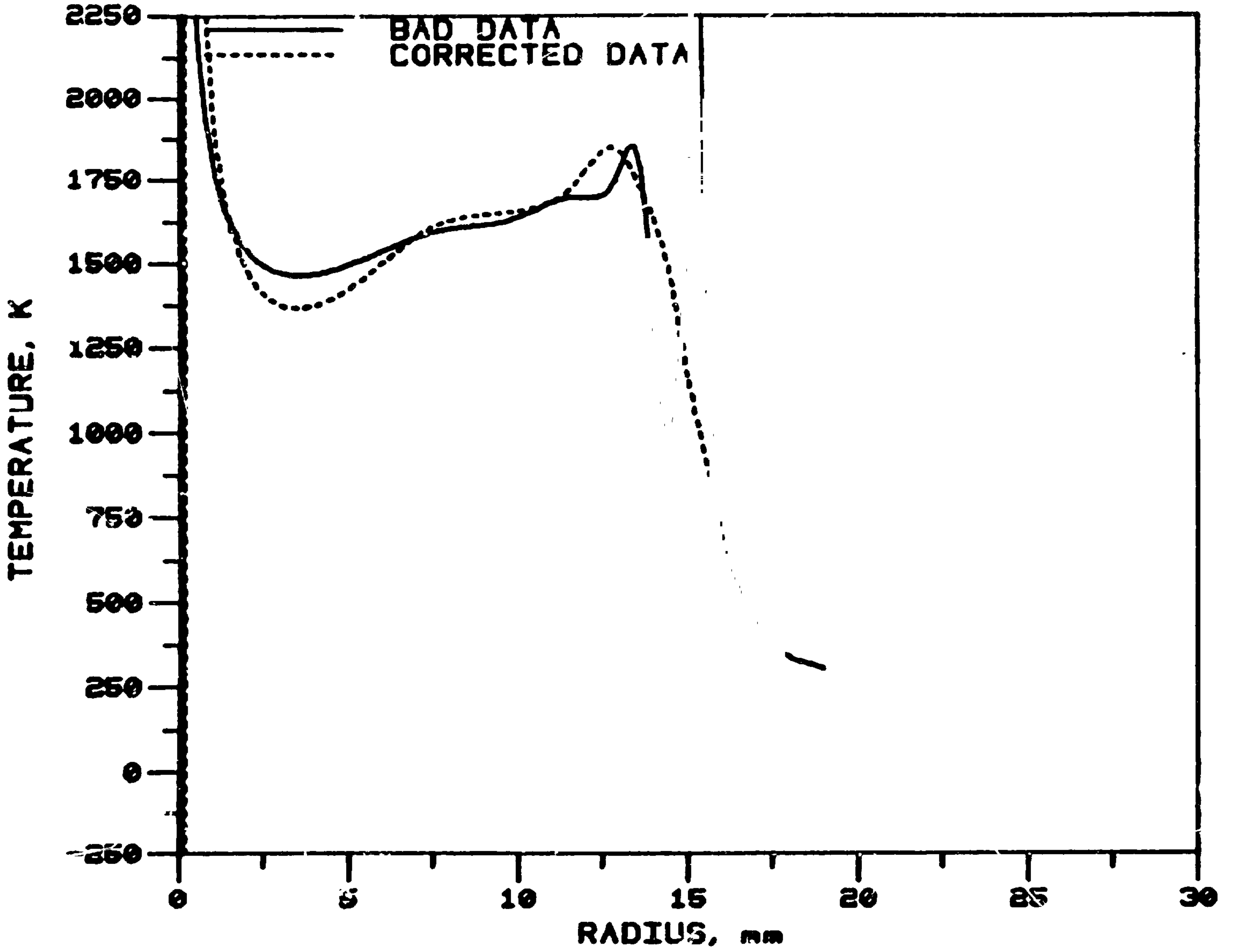

Fig. VIII-16. Temperature Distribution at Z = 10.6 mm for Bad and Corrected Fringe Number Data.

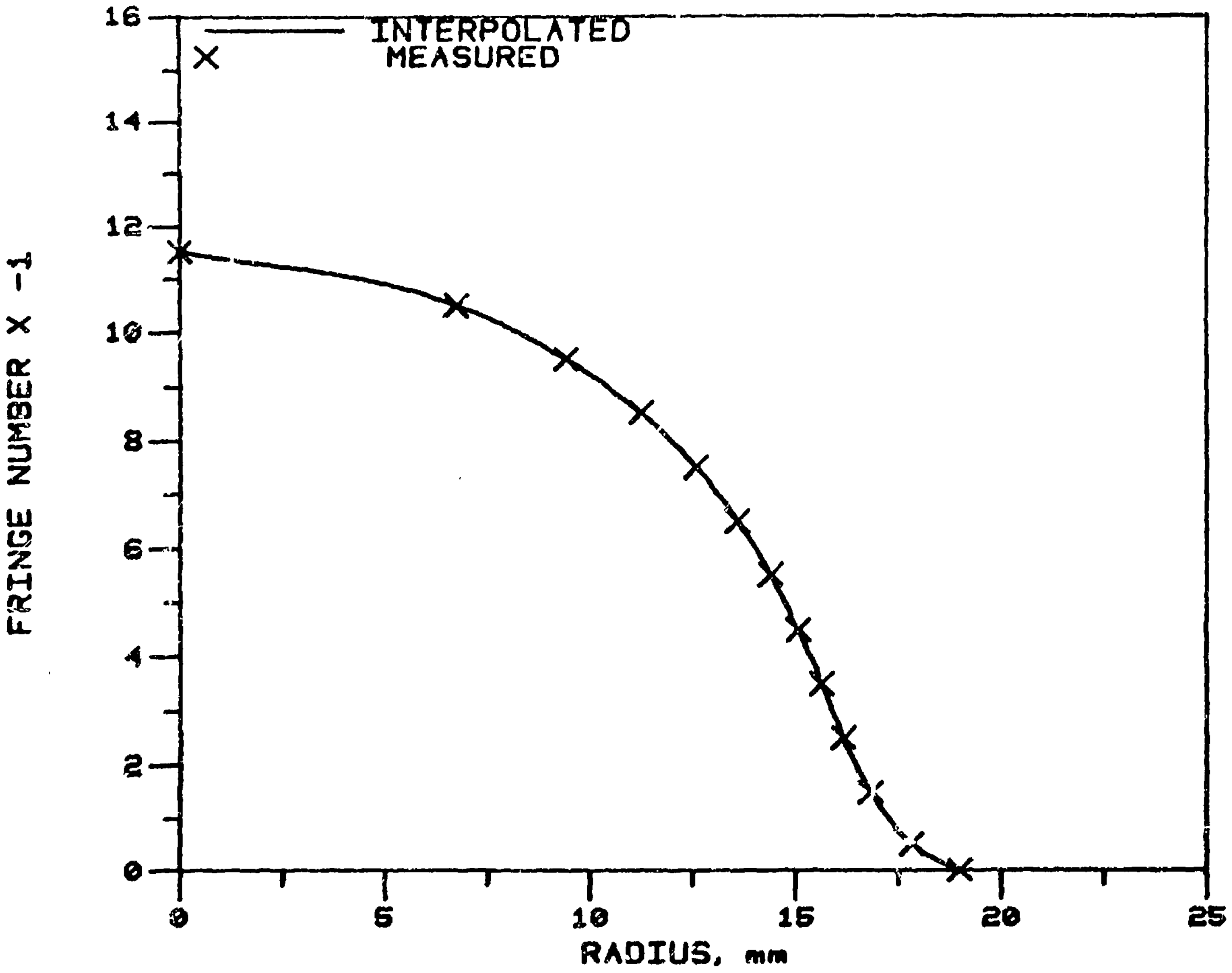

Fig. VIII-17. Corrected Frinte Number Distribution at Z = 10.6 mm.

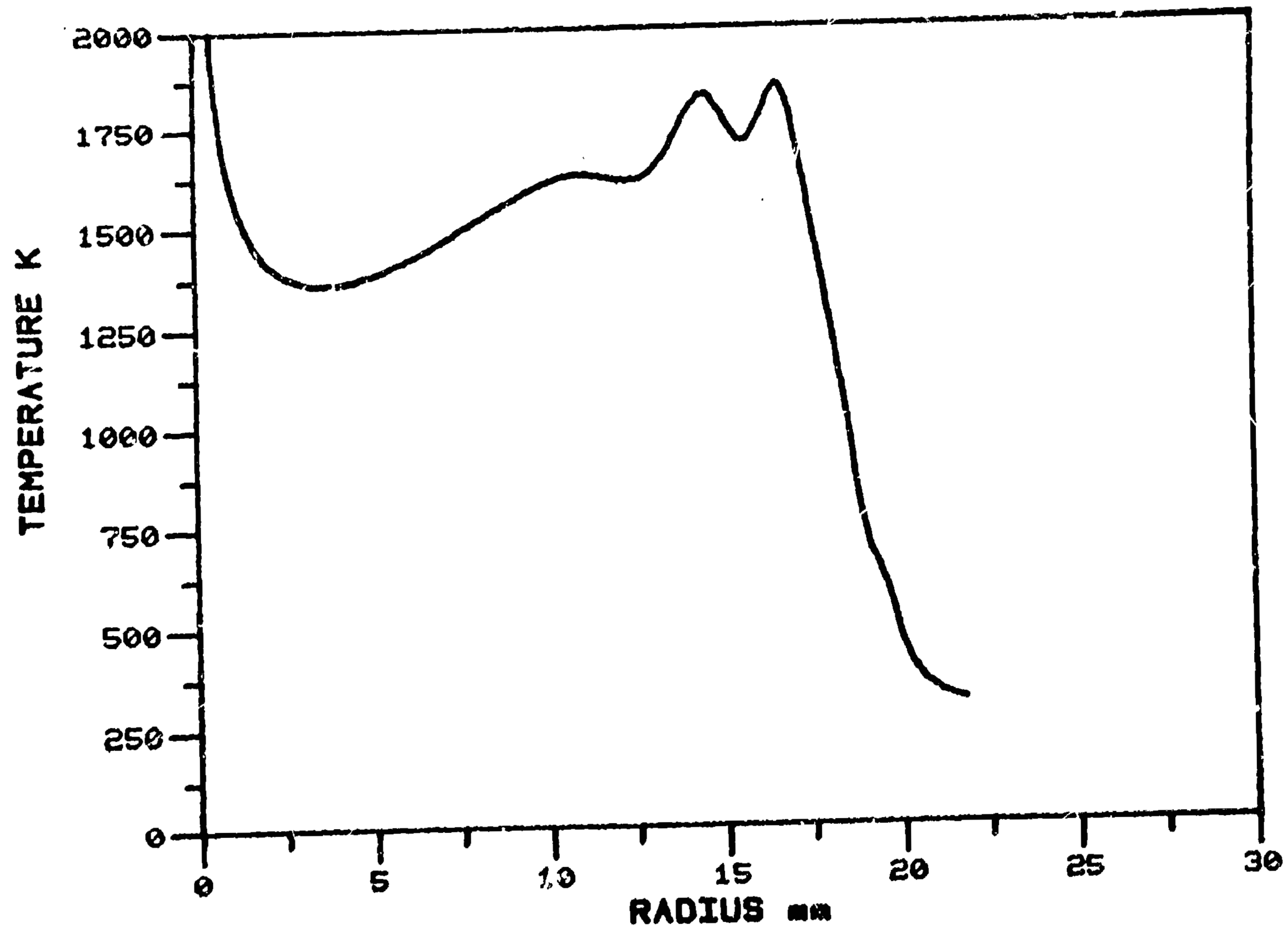

Fig. VIII-18. Temperature Distribution at Z = 18.1 in the Lean Flame.

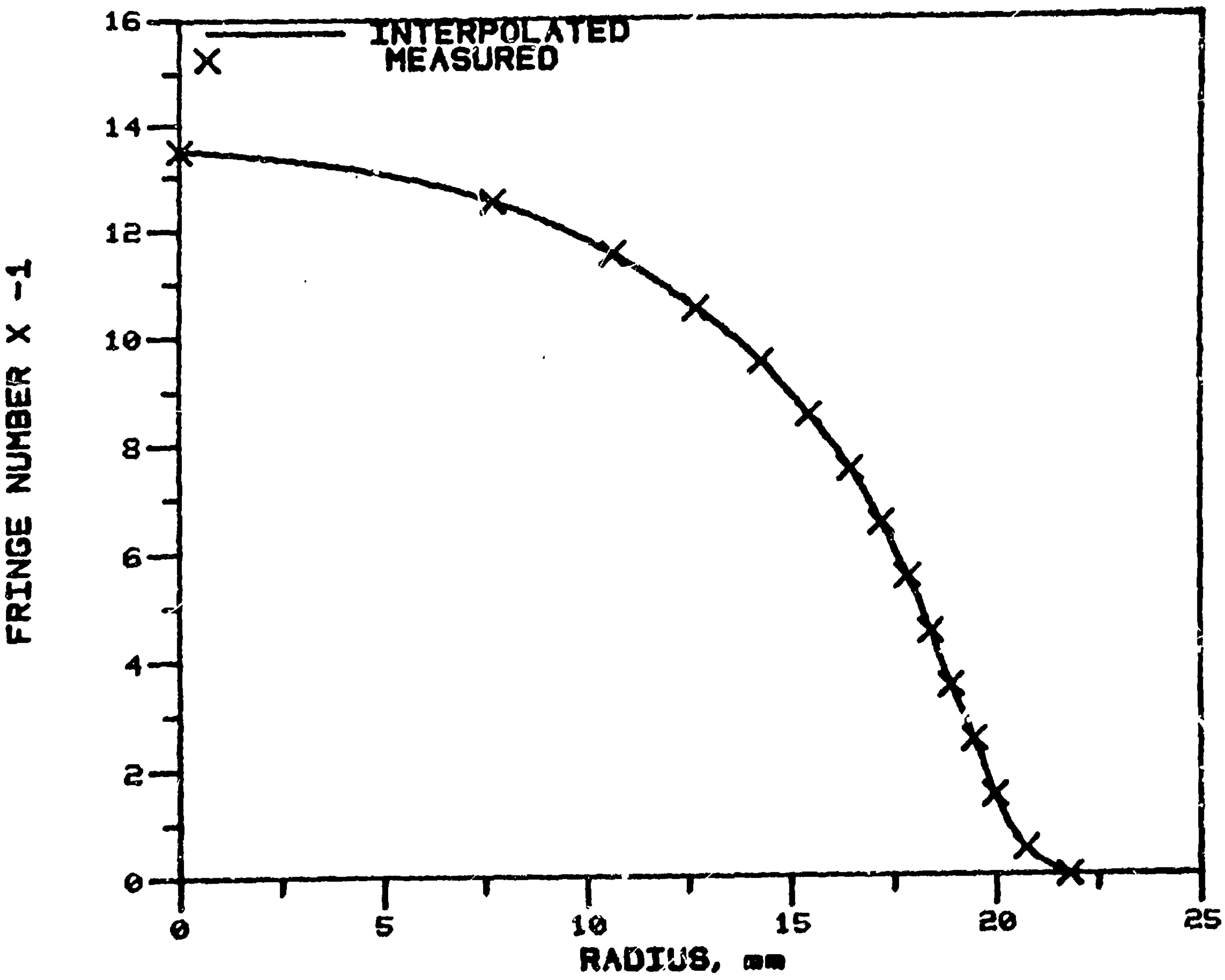

Fig. VIII-19. Fringe Number Distribution at Z = 18.1 in the Lean Flame.

features described for Fig. VIII-12. Namely, $T > T_{ad}$ near the outside of the flame cap, T drops in the midregions and it appears that $T \rightarrow \infty$ near the tube centerline.

The temperature profiles of the post-extinction hot bubble are shown in Figs. E 16 - 27 of Appendix E. These profiles behave somewhat better than the temperature profiles of the flame. The temperature increases near the outside of the bubble and becomes nearly constant in the midregion. In fact, in all cases for $5 < z < 21$ mm, the temperature peaks between 875°K and 925°K. However, as for the flame, T appears to approach infinity near the centerline.

It is assumed that the temperature profiles of both the flame and the post-extinction bubble are in error. It is not feasible for $T > T_{ad}$ in the flame and therefore the absolute values of temperature are wrong. Further, one would expect the temperature to peak near the centerline of the tube and not near the outside edge. Therefore the shape of the profiles are also wrong. It is believed that the apparent erroneous features of the temperature profiles are due to inaccuracy of the measured points and not due to the integration technique. Possible explanations for the inaccuracies are

1) Asymmetry of the flame.
2) Movement of the flame during the exposure.
3) Singularities of the integral at $r = 0$.
4) Inaccuracies of the FN vs r function due to
    a) measurement technique
    b) lack of a sufficient number of data points
    c) refraction by the tube.

The asymmetry of the flame is real and can be observed in Fig. VIII-9. Even at $z = 13.9$ mm, r at FN = 0 for the left and right hand sides of the flame interferogram are 22 mm and 18.8 mm respectively. Therefore, this asymmetry is probably a significant source of error.

Movement of the flame was significant in these tests. The unseeded lean limit flame propagated at 0.235 m/s and the exposures were 3 ms long. Therefore, the flame traveled 0.7 mm during the exposure while the fringe spacing was as small as 0.5 mm. Therefore, the fringes in the interferograms represent the average phase at each location. For an allowable flame motion of 1% of the smallest fringe spacing, an exposure of no more than 20 μs is necessary. A laser source for this short an exposure was not available. This movement is a source of large error near the leading edge in regions where the fringes are perpendicular to the direction of propagation. Away from the leading edge but near the centerline the error would be small since $\frac{dT}{dz}$ would be small.

One might suspect that $T \to \infty$ at $r = 0$ because of the singularity in Eq. (VIII-7). However, this is not the case. In recent work (Reuss, 1979), a program was written to simulate a hemispherical methane flame. The flame was assumed to have a symmetric profile such that

$$T = 1500°\text{K} \quad @ \quad 0 \leq r \leq 15 \text{ mm}$$

$$T = 300 + 600\ \{1+\cos[\frac{\pi}{10}\ (r-15)]\}\ @\ 15 \text{ mm} < r \leq 25 \text{ mm}$$

The interferogram that would result from this flame was calculated in Cartesian coordinates using a finite element method. Therefore the singularity of Eq. (VIII-7) was not a problem. The data from this calculated interferogram was then inverted using INTERPOL and ABELINV2. The inverted temperature profile matched the original ficticious profile to better than 1% at any radial position. The singularity appeared only at the very center anulus (I = 1) where T → 0. It was concluded that this singularity is not the cause of the errors near r = 0.

The use of an optical comparitor for measuring fringe number as a function of space causes inaccuracies for two reasons. There is an inherent error due to the phase modulation of the film density as a function of position. Secondly, there are regions of the interferogram where no data can be taken.

The best way to measure the fringe positions would have been to create a real image of the interferogram in space and then scan the midplane of the real image with a microphotometer. With this instrument, one can measure the actual irradiance of the interferogram as a continuous function of position with 10 µm resolution. The next best technique would have been to record the interferogram on a photographic plate and then scan the plate using a microdensitometer with a 10 µm resolution. In this case the emulsion response is a factor. However, accurate measurement of the original position of the peak irradiance (bright fringe) can be achieved (Witte and Wuerker, 1969). The least desirable method is to measure the position of the dark fringes on a photograph using an optical comparitor. This last method was the only one available and therefore was used for this study.

The problem with measuring the fringe positions with an optical comparitor is that errors inevitably occur. Consider the phase modulated sine wave illustrated in Fig. VIII-20a. A truly linear recording film with an adequate dynamic response would accurately record the shape of that

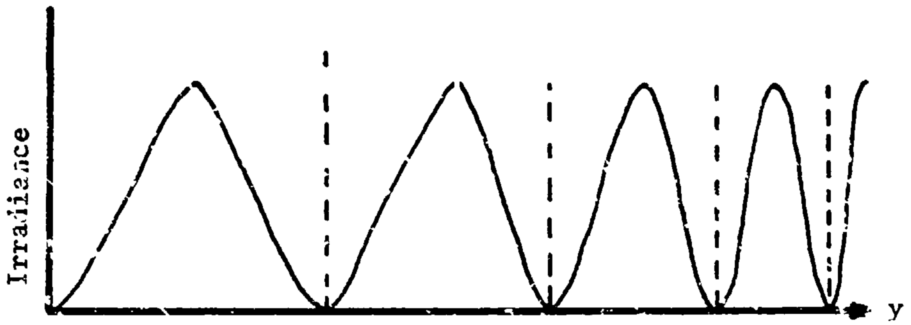

a

Original Irradiance Function

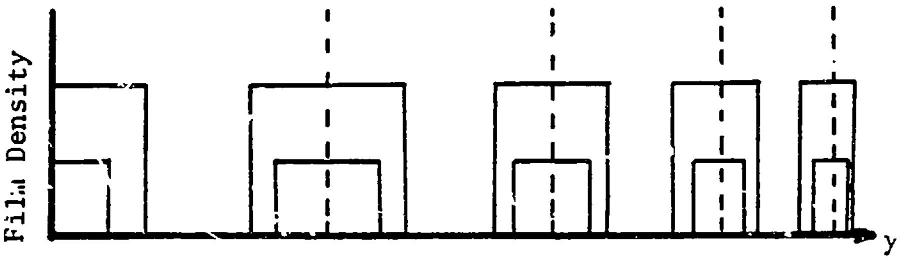

b

Response of Film Emulsion

Fig. VIII-20. Comparitor Measurement Error Due to Phase Modulation.

irradiance. However, if a high contrast film is used, the original irradiance function would be transformed to a square wave function as illustrated in Fig. VIII-20b. As the exposure time increases, the dark fringe would appear thinner. If one assumes that the original minimum of the irradiance function is at the center of the dark fringe, a positional error results due to the phase modulation. It can be seen in Fig. VIII-20b, that as the exposure time is increased, the positional error decreases. One might argue that it would be better to use short exposures and measure the position of the bright fringes. However, in practice the position of the bright fringes was not as easy to determine by eye. Consequently, the dark fringes were measured and the exposure was optimized for this purpose. In the region of high fringe frequency (15 mm < r < 20 mm in Fig. VIII-11) the width of the dark fringe is about half of the fringe spacing and the phase modulation is greatest. Therefore, this source of error is greatest in that region.

The lack of measurable fringes near the centerline of the interferogram was also a source of error attributable to the use of an optical comparitor. Referring back to Figs. VIII-11 and 12, it can be seen that the sharp upturn ($T \to \infty$) occurred between r - 0 and r at FN = 11.5, i.e., between the last two measured fringes. This was found to be true in all of the profiles. One must conclude that the cubic spline in this region did not accurately interpolate the shape of the function in this region. I believe the only way to correct this problem is to get fractional fringe number data in this region using one of the better fringe number measurement techniques.

Inaccuracies in the interferogram may occur due to refraction. Specifically, the position of the fringes at the image plane may be altered due to refraction caused by the flame or by the presence of the SFLT in the imaging system. It was demonstrated by Schultz-Grunow and Wortberg (1961) that refraction of a ray by a flat flame could be neglected by imaging on the midplane of the flame. This was also demonstrated by Vest (1975) for analytic refractive index profiles approximating those found in plasma jets. Therefore, refraction by the flame in this study is considered to be negligible.

The SFLT acts as a cylindrical lens and therefore its presence may alter the fringe number distribution. The tube would act to cause spherical aborations in the imaging optics. This spherical aberration would increase with increasing radius. Therefore, as one observes positions from the centerline of the tube outward, the midplane of the tube was not properly imaged during reconstruction. This simple explanation assumes that imaging of the diffuse illumination interferogram behaves the same as imaging of a diffusely scattering real object. The validity of this assumption is not well understood.

One way to eliminate the tube refraction problems would be to use an initially plane wave instead of diffuse illumination. In this case ray tracing through the tube is simplified and the theory predicting the interferogram is well developed. Therefore, one could calculate the actual path of each ray through the SFLT as a function of its termination position at the plane of the interferogram (see Vest 1975). This would require an imaging lens system with a large physical aperture to assure that all of the refracted rays were collected and imaged.

In summary, the interferometric technique could be modified in three ways to elminate the sources of error which cause the erroneous temperature profiles.

1) Use a shorter exposure from a more powerful laser.

2) Use a microphotometer for measuring the fringes.

3) Use plane wave illumination and ray tracing to correct for refraction.

In this way, only the asymmetry would be a problem. All of the above modifications require equipment which was not available for this study. However, I believe accurate temperature profiles could be measured using holographic interferometry with the proper equipment.

The calculated profiles in Appendix E are assumed to be incorrect and were not transformed to a complete temperature distribution for that reason. A discussion of the expected temperature distribution will be given in Chapter IX.

CHAPTER IX

DISCUSSION AND CONCLUSIONS

The stated goals of this study were:

1) To observe lean limit flame propagation in zero gravity and in earth's gravity.
2) To determine the structure of a lean limit flame propagating through a standard flammability limits tube in earth's gravity.

The stated purpose of the study was to understand:

1) How lean limit flame propagation is affected by gravity.
2) How the lean flammability limit is affected by gravity.
3) Which, if any, of the theories predicting flammability limits accurately model flame extinction.

In this final chapter the results from the four experimental phases of this study will be discussed in order to clarify what understanding has been gained. At the end of the discussion a summary of the achievements and conclusions will be given.

The Effect of Gravity on Lean Limit Flame Structure

The force due to gravity directly affects flame propagation by changing the flow field associated with the flame. The subsequent change in the flame structure is due to the effect the change in the flow field has on heat and mass transport. The momentum of a fluid element passing through a flame is changed by the pressure drop caused by thermal expansion and by the force of gravity (when important). In a one-dimensional flame, thermal expansion is allowed in only one direction. However, in a multi-dimensional flame this restriction cannot be made. The force of gravity acts only in the vertical (z) direction and acts on the fluid associated with the flame rather than on the flame itself. However, if the flame is multi-dimensional, any effect of gravity is multi-dimensional as well.

Consider a horizontal flat flame with horizontal isopycnal planes and density decreasing upward. In this case the force due to gravity (ρg) on a fluid element acts only to change the vertical velocity gradient (dV_z/dz). Therefore, any change in the convective field is in a direction normal to the flame. If the force of gravity is significant, it might alter the flame propagation velocity due to the change in convective energy transport. However, the shape would not change since at any given position in a horizontal plane (x,y), the force on a fluid element due to gravity is the same everywhere. In a multi-dimensional flame, gravity will influence the shape of the flame as well as the overall propagation velocity. This is because any curved flame must contain horizontal density gradients (e.g., $d\rho/dr \neq 0$). As a result of the horizontal gradient the change in the vertical velocity with respect to some horizontal direction (dV_z/dr) will be different in the presence of gravity. Therefore, the change of the convective field due to gravity at each point equidistant from the flame's reaction zone will be different resulting in a change of shape.

As was reported in Chapter II, Ball (1951) predicted that, in the absence of gravity, the preferred shape of a flame in a duct is convex with respect to the unburned gas. The 0-g tests reported in Chapter IV confirm that this is true even for flames in near lean limit mixtures. Therefore, the difference in the shape of upward, downward and 0-g flames is a manifestation of the influence of gravity on the flow field associated with the flame.

The upward propagating flame remained convex with respect to the unburned gas. However, the overall length of the flame cap increased (see Fig. VI-6). In an upward propagating flame, the force due to gravity and the major component of the force due to thermal expansion are acting downward. At any given axial position within the flame cap, the temperature increases with decreasing radius. Therefore, the temperature is maximum (density minimum) at the centerline. Consequently, the gravitational force (ρg) on any given fluid element is a minimum at the centerline for any given axial position within the flame cap. The net result of these forces is that, in the laboratory coordinates, the fluid near the centerline and ahead of the flame first moves upward, becomes stationary near the primary reaction zone in the flame and then moves downward behind the flame. As one moves away from the centerline of the tube a radius is reached when the fluid never moves upward, only downward (see Figs. C1 - C11, Appendix C). It is of greater interest to view the flow field in a coordinate system that is stationary with respect to the flame front. In this coordinate system the temperature, concentration and velocity distributions are assumed to be stationary. Therefore the flame can be modeled as a steady phenomenon. The vertical velocity distribution (V_z) with respect to the flame's coordinates is given in Figs. VII-17 & 18. Some distance ahead of the flame, the fluid and the tube are approaching the flame at approximately 0.235 m/s. The net result of gravity as observed in this coordinate system is that near the centerline, as the flame approaches, the fluid velocity decreases before it reaches the visible flame zone and increases continuously after that. Fristrom and Westenberg (1965) found that the luminous flame zone occurred just at the beginning of the reaction zone in a flat flame. Therefore, the fluid velocity decreases through the preheat zone and then increases through the reaction zone. Due to the refractive index problems described in Chapter VII, an accurate value of the fluid velocity in the region of the visible flame zone could not be determined. However, it can be concluded that the centerline axial velocity profile (as viewed from the flame's coordinates) has a minimum near the position of the visible flame zone. This behavior is not at all like the velocity profiles of a simple 1-D steady flame where the velocity continually increases through the flame. This behavior is also unlike the flow associated with the vertical rise of a fluid bubble in a tube filled with a more dense fluid (e.g., air bubble in a water column). For in the case of bubble rise, the more dense fluid in the column is simply displaced around the bubble. The fluid in the bubble and that in the column remain separate.

The flow field in the region downstream from the visible flame is shown in Fig. VII-18. Inspection of Table C-2 reveals that the fluid velocity near the wall reaches a maximum at about $z = 0.08$ m which is right at the trailing edge of the visible flame cap. The centerline velocity continues to increase until $z = 0.135$. This behavior results in a velocity profile that appears to be flat near the centerline at $z = 0.135$. In the lower regions ($z > 0.15$ m) the fluid near the centerline becomes slower than that near the wall. However, since there are only two data points, this is a rather tenuous conclusion.

It was also possible to calculate the thickness of the preheat zone at the leading edge of the flame cap of the upward propagating lean limit flame.

The beam deflection flame detector provided a reference between the luminous flame zone, the velocity distribution and the interferogram. The fiducial mark occurred at the middle of the first dark fringe (along the centerline of the tube) in the interferogram of the flame. This indicates that the beam deflection occurred early in the preheat zone. However, some heat conduction has occurred upward from that point. The fluid velocity first started to increase about 0.9 s or 20 mm ahead of the fiducial mark. This indicates that the fluid is displaced before it is heated enough for thermal expansion to occur. The luminous flame zone generally occurs at the beginning of the reaction zone. In this study it was measured to be 3.9 mm past the fiducial beam at the centerline of the tube. It can be concluded that at the centerline of the tube, the preheat zone is 4 to 5 mm thick and that the fluid is displaced about 15 mm ahead of the preheat zone. The radius of the tube is 26 mm and the radius of curvature of the flame is about the same. Therefore, the upward propagating lean limit flame is very thick with respect to the radius of curvature.

The effect of gravity on the downward propagating flame is far more complicated than in the case of the upward propagating flame. Near the limit downward propagating flames were relatively flat superimposed with a cellular structure due to preferential diffusion. The cellular structure is not present for downward propagating methane-air flames in smaller diameter tubes or for near lean limit mixtures of hydrocarbons with a higher molecular weight. Therefore, it is believed that the prefered shape of the downward propagating near limit flame is flat. This is reasonable when one considers that a downward propagating flame convex with respect to the unburned mixture would have the highest temperature near the centerline of the tube.

Therefore, when gravity is important, the fluid near the centerline would tend to have a faster upward (downstream) velocity than that in 0-g. However, the flat flame would be expected to have horizontal isotherms with the temperature increasing (ρ decreasing) upward. As previously discussed in this chapter, the shape of this flame is least affected by gravity.

It is also important to note that the cellular structure occurred on downward propagating flames but not on 0-g or upward propagating flames. Previously preferential diffusion has been recognized as the sole cause of cellular flames. However, it must be assumed that gravity is instrumental in causing the cellular structure as well.

The Effect of Gravity on Burning Velocity

In Chapter II, it was stated that each mixture had a single characteristic burning velocity. Conceptually, this is the velocity at which an adiabatic laminar flat flame would propagate through the mixture. For the flames observed in this study, the correct method for calculating the burning velocity is not immediately obvious. In the case of the 0-g and upward propagating flames, the flame is thick with respect to the radius of curvature and it is not immediately clear that the burning velocity is a constant in all regions of the flame surface.

Fristrom (1965) hypothesized that for curved flames the fluid velocity at the primary reaction zone was invariant over the entire surface in spite of variations in the velocity of the approach flow. According to Fristrom, if one were to follow a stream tube through the flame,

$$\frac{M}{\rho_o} = \text{constant}$$

and therefore, at the reaction zone

$$\frac{M}{\rho_o} = \frac{\rho_r V_r}{\rho_o} = V_o \frac{A_o}{A_r} = S_u^* \qquad \text{(IX-1)}$$

The subscript o refers to the far upstream condition and r to the conditions at the reaction zone as defined by the luminous surface. S_u^* is the velocity at a point where $A_o = A_r$. Equation (IX-1) requires that the area of the stream tube remains constant through the reaction zone. In practice, the latter requirement is met when the primary reaction zone is thin with respect to the radius of curvature. Fristrom demonstrated that this is a good assumption using experimental data from a low pressure laminar flat flame. Even though the overall flame thickness was 10 mm, 75% of the heat release occurred in a reaction zone which was about 1 mm thick. Therefore the reaction zone may be thin with respect to the radius of curvature even though the overall flame thickness is not. Fristrom also presented some empirical evidence to verify that S_u^* is constant regardless of the radius of curvature, although it was not conclusive.

Strehlow (1975) solved the Friedman-Burk problem (refer to Chapter II) for 1-D, adiabatic source and sink flames in spherical and cylindrical coordinates. He found that no unique burning velocity could be defined for a curved flame. However, the position of the location in the flame at which the kinetic rate is a maximum was calculated as well as the fluid velocity at that point. The calculations indicated that the fluid velocity at the point of maximum reaction rate is reasonably constant for the different types of flames and at different radii of curvature.

The purpose of the work by Fristrom (1965) and Strehlow (1975) was to demonstrate that, even in curved flames, a properly defined fundamental burning velocity can be defined which is only a function of the initial mixture properties and is constant in all regions of the reaction zone surface. The invariance of S_u^* for the upward propagating flame could have been determined in this study if complete and accurate velocity and temperature profiles had been available.

Due to a lack of the detailed information required for the method of Fristrom, an average burning velocity was calculated by a method used by Coward and Payne (1937). In that work, the fundamental burning velocity was defined as

$$S_u = (V_p - V_g) \frac{A_{tube}}{A_{flame}}$$

where V_g is the velocity of the unburned fluid ahead of the flame with respect to the laboratory coordinates. In the SFLT, $V_g = 0$ and therefore

$$S_u = V_p \frac{A_{tube}}{A_{flame}}$$

This equation assumes that all of the fluid in the tube is consumed by the flame and that S_u is constant over the entire flame surface (A_r = const. in Eq. (IX-1)). If S_u is not constant, this would be an average burning velocity.

One of the important results of this study is the fact that burning velocities, as calculated by the method of Coward and Payne, are different for the three types of flame propagation in equivalent mixtures A tabulation of S_u for 0-g, upward and downward flames propagating through a 5.87% CH_4-Air mixture is given in Table IX-1. The flame area was measured from the

TABLE IX-1

AVERAGE BURNING VELOCITY OF 0-G UPWARD AND DOWNWARD PROPAGATING FLAMES IN A 5.87% CH_4-AIR MIXTURE

	Flame area mm^2	Volumetric flow rate mm^3/s	S_u mm/s
0-G	3.4×10^3	2.2×10^5	64
Upward	5.2×10^3	6.9×10^5	132
Downward	1.9×10^3	1.7×10^5	86

photographs of Fig. VI-6. It was assumed that $A_{flame} = A_{tube}$ for the downward flame so that $S_u = V_p$.

It appears that the differences in burning velocities tabulated in Table IX-1 are real even though they were determined using a rather crude model. Actually, each mixture will have a unique burning velocity only if the flame is one-dimensional and adiabatic. It has been demonstrated both theoretically and experimentally that a nonadiabatic flame will have a burning velocity different from the adiabatic flame. Hardesty and Weinberg (1974) demonstrated that a flame could be made to propagate in mixtures much leaner than the conventional limits (1% CH_4 in air) by imposing energy recirculation from the post reaction gases to the unburned (incoming) gas. They also demonstrated that increasing the amount of energy recirculation will increase the burning rate. The flat flame burner studies described in Chapter III demonstrated the validity of the principle of recirculation as well. The flat flame studies also demonstrated that decreasing the heat loss to the post reaction gases can increase the burning velocity. Therefore, it is reasonable that the upward, downward and 0-g flames propagate with different burning velocities due to different amounts of heat loss.

One can provide a heuristic explanation, based on heat loss, for S_u of the downward propagating flame to be less than S_u of the upward propagating flame. Also, the cellular nature of the downward propagating flame and the fact that it "walks" down the tube causes the actual surface area to be larger than that assumed in the calculation. This explains why the downward flame's calculated burning velocity is greater than that of the 0-g flame.

Flammability Limits and Extinction

The lean flammability limit as measured in the standard flammability limit tube is defined as the leanest mixture composition that will allow a flame to propagate the entire length of the tube. There is an implicit assumption in practice and in theory that flame propagation must be steady (in coordinates that follow the flame) for the mixture to be considered flammable. In order to insure that a steady flame could form in a flammable mixture, fuel enrichment was used at the ignition region (see Chapter V and VI). This was accomplished by using either methane injection near the ignition source, a 0.10 m slug of 5.37% methane-air, or a diffusion flame ignition source. In this way a flame would always form. If the mixture being tested was flammable, the flame would settle to a steady state. In sublimit mixtures a flame did develop near the ignition source. However, instead of relaxing to a steady state the flame remained unsteady until extinction occurred. Had enrichment not been used, an ignition limit would have been found and not a limit of steady state flame propagation. It appears that changes in the flame structure, as a flame propagates to extinction in sublimit mixtures, can give some insight into mechanisms that are controlling during the extinction process and therefore are important in determining the flammability limit. This contention is based on the assumption that those mechanisms that control the extinction process prevent a steady flame from propagating.

When the upward propagating flame extinguished the visible flame collapsed inward as depicted in Fig. V-11. During this transition period and after, the hot gas bubble appeared to remain symmetric and continued to translate upward at the same velocity that the flame had, with no oscillatory or random motion. When an upward flame propagated from a flammable mixture into a sublimit mixture, extinction occurred about 0.6 m past the rich-lean interface. (Here, extinction is defined as that point when the visible emissions disappear.) Some insight into the transition between flame propagation and the post extinction hot bubble can be gained through inspection of the change in the centerline velocity profiles.

Figures VII-20, 21 & 22 are centerline velocity profiles (laboratory coordinates) with extinction occurring at different positions relative to the LDA probe volume. Therefore, at the time of extinction the flame had already passed through the previously described transition. A comparison of Figs. VII-14 and 20 reveal that when extinction occurred 0.5 s (≃ 120 m) past the probe volume, the velocity profiles of the lean limit flame and the near extinction flame were about the same until t = 0.2 s. That is, the fluid first moved upward, came to rest, and began to move downward. However, when extinction occurred, the fluid never attained the downward velocity that occurred in the lean limit flame. Instead, the fluid velocity decreased and apparently went through another flow reversal (see Fig. VII-20 at t = 0.67) and then increased in an upward direction. The interpretation that the flow is upward after extinction is consistent with the flow field one would expect to observe at the centerline of a hot bubble rising through the tube.

When extinction occurred right at the LDA probe volume, the fluid at the centerline never went through a flow reversal (Fig. VII-21). Evidently, the fluid always moved upward. What is surprising is the fact that such a high upward fluid velocity was attained ($V_z \simeq 0.8$ m/s) when the propagation velocity was still about 0.23 m/s. Apparently, there is circulation in the translating post-extinction hot bubble.

When flame extinction occurred at -0.5 s (≃ 120 m) ahead of the LDA probe volume, the velocity profile appeared to become turbulent and interpretation of velocity direction becomes difficult. The velocity first increased, decreased, went through a non-zero minimum and began to increase with an oscillatory fluctuation. One interesting feature is the fact that the minimum occurred about 0.64 s (0.15 m) after extinction. This coincides with the point where Levy (1965) reported that the post-extinction hot bubble began to breakup. It is assumed that the fluid motion in the post-extinction hot bubble has become turbulent at that time.

There are several other noteworthy observations that can be made. For instance, at extinction, the flame has propagated about 0.6 m into the sub-limit mixture. However, the propagation velocity of the post-extinction hot bubbles of Figs. VII-20 & 21 is about the same as that for the lean limit flame. Since the flame was propagating in a sub-limit mixture (5.16%), one would expect the flame to be unsteady and propagating at a lower velocity. It must be concluded that the propagation velocity of these flames is so dominated by gravity that V_p is nearly unaffected by the cooling of the burned gas. One must also question whether a flame propagating in a limit mixture (5.27%) was steady, or if it would have extinguished in a longer tube.

Another important result is the fact that the centerline velocity profile of the sub-limit flame is the same as that of the lean limit flame for at least 0.5 m past the interface. Extinguishment then occurs in the next 0.1 m. This can be inferred from the fact that a flame type profile existed at the LDA probe volume when extinction occurred 0.12 m later. However, the flame to hot bubble transition was completed when extinction occurred right at the LDA probe volume.

After the flame to hot bubble transition occurred, the hot bubble continued to rise at the same velocity at which the flame propagated. The centerline velocity profile remained laminar as well. One might suspect that a nonluminous reaction may exist during this period since V_p remains constant and the flow field remains laminar. However, inspection of the interferogram of the post-extinction hot bubble (Fig. VIII-10) reveals that the fringes are nearly vertical in the lower regions of the bubble. As a result, both the geometric and optical path lengths through the bubble are constant. Therefore, one may conclude that there are small (if any) temperature changes occurring in the vertical direction either near the centerline or at larger radii. One can also observe that the post-extinction hot bubble fringes are further from the wall of the tube than the fringes of the flame. This indicates that the upstream fluid is simply displaced around the hot bubble.

It can be inferred from Fig. VII-22 that only after the post-extinction bubble began to break up did the translation velocity begin to decrease. This is indicated by the longer time between the peaks of the BDFD. It can also be observed that in spite of the fact that the velocity is fluctuating in the post-extinction velocity profile of Fig. VII-22, the output of the BDFD is quite stable. This is unlike the fluctuation that occurred on the BDFD signal from the lean limit downward propagating flame (refer to Fig. V-9a). This indicates that the hot bubble breaks up from the trailing edge of the bubble forward, while the temperature distribution at the leading edge remains with no measurable fluctuations.

In summary, a flame propagating upward through a sub-limit mixture passes through four modes of propagation after ignition:

1) An unsteady limit-like flame becoming weaker but with a nearly constant V_p.
2) A transition from a flame to a hot bubble with laminar circulation and constant V_p.
3) Continued propagation of the hot bubble at the same V_p.
4) Break up of the hot bubble with velocity fluctuation in the circulating flow.

Extinction of downward propagating lean limit flames was quite different from that of the upward propagating flame. In sub-limit mixtures the downward propagating flame never propagated further than 0.10 m with methane injection or diffusion flame ignition (refer to Table VII-3). In some of these cases a convex flame would develop and go out. In other cases a relatively flat flame would form, tip and extinguish. Apparently the sub-limit downward propagating flame never propagated outside of the influence of the enriched ignition region. That is, it would not propagate any significant distance into a sub-limit mixture.

As noted, the downward propagating lean limit flame would tip from side to side as it translated down the tube. In some cases, for flames in mixtures which would normally be considered lean, the limit mixtures would extinguish some distance from the ignition source. When such extinction occurred, the visible flame would tip too far, become nearly vertical and extinguish.

The value of the lean flammability limit for 0-g flame propagation in a methane-air mixture could not be found with absolute certainty due to the short amount of 0-g time available (2.2 s). Instead, flame propagation was observed through progressively leaner test mixtures until extinction was found to occur within the 2.2 seconds of zero gravity. It was found that extinction was observed only in mixtures less than 5.10% (see Table VI-4). Further, extinction occurred 0.10 m or less from the end of the tube. The tests listed in Table VI-3 illustrate that 0.10 m is about the same distance traveled by sub-limit downward propagating flames. It is assumed that flames in these mixtures never propagated outside of the region influenced by the enrichment. It is possible that flames propagating through richer mixtures would have extinguished had more time been available. However, the fact that 0-g flames in mixtures greater than 5.10% appear to have settled to a constant propagation velocity lead to the hypothesis that the 0-g lean limit is about the same as the upward lean limit.

It should be noted that in those tests where extinction occurred, the propagation velocity continually decreased. It can be seen in Table VI-4 that the time and position of extinction were relatively consistent. Because of the low quality of the film, the shape of the flame at extinction could not be documented. However, careful inspection of the original negatives revealed that the flame filled the entire cross section of the tube during the second to the last exposure in which the flame was visible. In the last exposure, the flame appeared to exist only near the center of the tube indicating that the flame extinguished from the outside inward.

Applicability of Theoretical Models

In the past, it has been customary to conceive of a curved flame behaving as 1-D adiabatic flame propagating only normal to itself. It is evident from the material presented that a lean limit flame propagating through a 50 mm diameter tube does not conform to these concepts. Since gravity acts directly on the flow field and it is obvious that gravity is drastically changing the flame structure, one cannot realistically exclude the momentum equation in any model. Since natural convection is multi-dimensional the model must be multi-dimensional as well. That is not to say that 1-D models are completely useless. A 1-D nonadiabatic model would be useful for developing a kinetic model which is adequate for predicting extinction. However, only a multi-dimensional model can adequately predict the heat and mass transport occurring in the flames studied.

The models presented in Chapter III for predicting limits based on convection alone are inadequate. It has been demonstrated that when upward flame extinction occurs a hot bubble continues to rise and that the pre- and post-extinction flow fields are completely different. There is no evidence to indicate that lack of bubble translation or some value of propagation velocity is adequate to predict flammability limits.

It is not obvious that the concept of flame stretch is useful for predicting the flammability limit. According to the concept of a flame propagating as a wave (refer to Chapter II) an element of a flame can propagate only normal to itself. Consequently, an element of a curved flame surface moves along the surface with a velocity $S_{\parallel}$ (refer to Fig. II-1). In the case of the upward propagating and 0-g flames, a flame element originates at the leading most point of the flame cap and then moves outward and downstream along the surface of the flame cap as an expanding cylindrical section of flame. Therefore, every element of the flame cap originates at this leading point. According to Strehlow and Savage (refer to Chapter IV) flame stretch is greatest at the leading point of the flame cap. Therefore, if flame stretch causes failure of the steady flame, the flame would fail first at the leading point of the flame cap. However, there is no evidence indicating that when a mixture could not support steady flame propagation, the flame failed first at the leading edge.

It is not clear whether or not preferential diffusion affects the lean limit of the downward propagating flame. A cellular flame structure does occur in down-near limit downward propagating flames. However, no cellular structure was observed on downward propagating flames in lean limit mixtures. Further, the side to side tipping of the lean limit flame indicates that an instability may dominate the flame at the limit.

It is obvious that S_u becomes small at the flammability limit, however, it is not zero. Since it has been demonstrated that a flame can propagate for some distance into sub-limit mixtures, S_u must have a finite value in those mixtures.

Summary of Achievements and Conclusions

A standard flammability limits tube was constructed and used to study upward and downward flame propagation in limit and near limit methane-air mixtures. A beam deflection flame detector was constructed and used to create an electronic fiducial signal. This signal was used to both measure the flame propagation velocity and act as a reference to interrelate the measured velocity distribution, the structure of the interferogram and the position of the luminous flame as determined by photography.

Flame propagation tests were also conducted at the NASA Lewis Research Center, 2.2 second zero gravity drop tower facility. These tests were made in order to determine the leanest mixture which would support flame propagation in zero gravity and to determine the 0-g propagation velocity. Flames were propagated through mixtures ranging from 4.77% to 6.74% methane in air in that facility.

A laser Doppler anemometer was constructed and used to measure the fluid velocity in an upward propagating lean limit flame. It was discovered that the velocity could not be accurately measured in the immediate vicinity of the reaction zone. It was shown that the output of the laser Doppler anemometer gives false readings in this region due to beam movement or changes in the optical path length caused by changes in the index of refraction of the gas with time.

Diffuse illumination holographic interferograms were made of a lean limit flame and a post-extinction hot bubble. However, accurate temperature distributions could not be calculated. This is because (1) the flame moved during the shortest exposure time available, (2) no means were available to accurately measure the fringe distribution, and (3) the theory used to calculate temperatures from the interferogram may have been inadequate.

The results of the tests conducted in this study revealed that an upward propagating lean limit flame in a 50 mm tube is a complex and relati thick 2-D flame which can not be modeled as a simple 1-D adiabatic thin flame.

The conventionally defined burning velocity of the upward propagating flame was almost twice that of the 0-g flame in a 5.87% mixture. The preheat zone along the centerline of the tube was estimated to be 4 to 5 mm thick. This is considered to be thick enough with respect to the local radius of curvature of the flame such that the flame cannot be considered to be locally 1-D. The axial velocity distribution of the fluid was measured and was found to be quite unlike that of a simple 1-D flame. At the centerline of the tube, the initially quiescent fluid is displaced upward 15 mm ahead of the preheat zone and then passes through a flow reversal. The upward propagating flame would also propagate about 0.5 m into a sub-limit mixture before extinction occurred. The sub-limit flame propagated through four distinct modes of propagation.

The conclusions based on the results of the 0-g tests are tenuous due to the short amount of observation time available in each 0-g experiment. However, flames propagating in a zero gravity environment had nearly the same propagation velocity as a downward propagating flame but a larger surface area. This results in a smaller burning velocity for the 0-g flame. The 0-g flames propagated outside of the influence of the rich ignition region and seemed to have a steady state velocity in mixtures leaner than the downward lean limit. The data indicates that the 0-g flammability limit is near the upward lean limit.

It was previously believed that the downward propagating flame is affected by gravity less than the upward propagating flame. However, the results of this study indicate the opposite is true. The 0-g and upward propagating flames have a shape which is convex with respect to the unburned gas while the downward propagating near limit flames are flat. In the case of methane-air mixtures, the flat flame has a cellular structure which has previously been explained by preferential diffusion. Since the cellular structure did not occur in either the 0-g or upward propagating flames, it must be, at least indirectly, a product of gravity as well. In lean limit mixtures, a steady downward propagating flame does not exist. Instead, a side to side tipping occurs.

REFERENCES

Adrian, R. J. and Fingerson, L. M., Text from a LDA short course sponsored by Thermo Systems, Inc., St. Paul, Minnesota (1976).

Andrews, G. E. and Bradley, D., "Limits of Flammability and Natural Convection for Methane-Air Mixtures", 14th Symposium (International) on Combustion, The Combustion Institute, Pittsburgh, PA (1972a)

Andrews, G. E. and Bradley, D., Combus. and Flame 18, 133 (1972b).

Badami, G. N. and Egerton, Sir Alfred, Proc. Royal Soc. London A-228, 297-322 (1955).

Baker, R. J., Bourke, P. J., and Whitelaw, J. H., J. Inst. Fuel 46, 388 (1973).

Ball, G. A., "A Study of a Two-Dimensional Flame", Harvard University Department of Engineering and Applied Physics (1951).

Bennett, F. D., Carter, W. C., and Bergdolt, V. E., J. Appl. Physics 23 #4 (1952).

Berlad, A. L. and Yang, C. H., Combus. and Flame 4 (1960).

Bone, W. A., Newitt, D. M., and Ginith, C. M., "Gaseous Combustion at High Pressures. Part IX - The Influence of Pressure upon the 'Explosion Limits' of Inflammable Gas-Air, etc., Mixtures", Proc. Royal Soc. A117, 553 (1928).

Born, M. and Wolf, E., Principles of Optics, 5th Ed., Pergamon Press, 1975.

Bregeon, B., Gordon, A. S., and Williams, F. H., Combus. and Flame 33, 33 (1978).

Burgess, M. J. and Wheeler, R. V., Jour. Chem. Soc. 103, 2591 (1914).

Burgoyne, J. H. and Weinberg, F. J., Fuel 33 (4) (1954).

Collier, R. S., Burckhardt, C. B., and Lin, L. H. Optical Holography, Academic Press, 1971.

Coward, H. F. and Hartwell, F. J., J. Chem. Soc., pp. 1996-2004 (1932).

Coward, H. F. and Jones, G. W., "Limits of Flammability of Gases and Vapors" Bureau of Mines Bulletin 503, 1952.

Coward, H. F. and Payman, W., Chem. Reviews 21(3), 359 (1937).

Dixon-Lewis, G. and Isles, G. L., Trans. Faraday Soc. 53, 193 (1957).

Dixon-Lewis, G. and Isles, G. L., "Limits of Inflammability", *7th Symposium (International) on Combustion*, The Combustion Institute (1959).

Durst, F., Melling, A., and Whitelaw, J. H., *Combus. and Flame* *18*, 197-201 (1972).

Durst, F. and Kleine, R., "Velocity Measurements in Turbulent Premixed Flames by Means of Laser Doppler Anemoneters", University of Karlsruhe SFB/EM/3 (1973).

Durst, F., Melling, A., and Whitelaw, J. W., *Principles and Practice of Laser Doppler Anemometry*, Academic Press, 1976.

Egerton, A. C. and Powling, J., *J. Proc. Roy. Soc., London* *A-193*, 172-209 (1948).

Egerton, Sir Alfred and Thabet, S. K., *Proc. Roy. Soc., London* *A-211*, 445-471 (1952).

Ellis, O. C. de ., *Fuel* *7*(1-12) (1928).

Friedman, R. and Burke, E., *J. Chem. Physics* *21*(4), 710 (1953).

Fristrom, R. M., *Physics of Fluids* *8*(2), 273 (1965).

Fristrom, R. M. and Westenberg, A. A., *Structure of Flames*, McGraw-Hill, 1965.

Gaydon, A. G. and Wolfhard, H. G., *Flames: Their Structure, Radiation and Temperature*, Chapman and Hall, 3rd Ed., 1970.

Gaydon, A. G., *The Spectroscopy of Flames*, Wiley, 1974.

Gerstein, M. and Stine, W. B., "Analytical Criteria for Flammability Limmits", 14th Symposium (International) on Combustion (1973).

Günther, R. and Janisch, G., *Combus. and Flame* *19*, 49 (1972).

Hardesty, D. R. and Weinberg, F. J., *Combus. Sci. and Technology* *8*, 201 (1974).

Hauf, W. and Grigull, U., *Advances in Heat Transfer* *6*, 133 (1970).

Hecker, W. C., "A Theoretical Study of the Kinetics, Propagation, and Suppression of Methane-Air Flames", M.S. Thesis, Brigham Young University, 1975.

Heflinger, L. O., Wuerker, K. F., and Brooks, R. E., *J. Appl. Physics* *37*(2), 642 (1966).

Hertzberg, M., "The Theory of Flammability Limits, Natural Convection", Bureau of Mines Report #8127, 1976.

Hirchfelder, J. O. and Curtiss, C. F., J. Chem. Physics 17(11) (1949).

Holman, J. P., Experimental Methods for Engineers, McGraw-Hill, 1966.

Hottel, H. C. and Sarofim, A. F., Radiative Transfer, McGraw-Hill, 1967.

Jarosinski, J. and Strehlow, R. A., "Lean Limit Flammability Study of Methane-Air Mixtures in a Square Flammability Tube", Technical Report, AAE 78-3, Department of Aeronautical and Astronautical Engineering, University of Illinois at Urbana-Champaign (1978a).

Karlovitz, B., Denniston, D. W., Knapschaefer, D. H., and Wells, F. E., "Studies on Turbulent Flames", 4th Symposium (International) on Combustion, The Combustion Instutute, Pittsburgh, PA (1953).

Kydd, P. H. and Foss, W. I., Combus. and Flame 8, 267 (1964).

Odenburg, R. L., Winckler, J., and Van Voorhis, C. C., Physical Rev. 73(11), 1359 (1948).

Landry, M. J. and Phipps, G. S., Appl. Optics 14(9), 2260 (1975).

Levy, A., Proc. Roy. Soc., London A-283, 134 (1965).

Levy, A. and Weinberg, F. J., Combus. and Flame 3, 229 (1959).

Lewis, B. and Von Elbe, G., Combustion, Flames and Explosions, Academic Press, 1951.

Lewis, B. and Von Elbe, G, "Fundamental Principles of Flammability and Ignition", Selected Combustion Problems II AGARD, p. 63 (1956).

Lewis, B. and Von Elbe, G., Combustion, Flames and Explosions of Gases, 2nd Ed., Academic Press, New York, 1961.

Lovachev, L. A., Combus. and Flame 17, 275-278 (1971).

Lovachev, L. A., Babkin, V. S., Bunev, V. A., V'Yun, A. V., Krivulin, V. N., and Baratov, A. W., Combus. and Flame 20, 259 (1973).

Markstein, George H., "Instability Phenomena in Combustion Waves", 4th Symposium (International) on Combustion (1953).

Mayer, E., "A Theory of Flame Propagation Limits due to Heat Loss", Combus. and Flame 1, 438 (1957).

Meagher, G. M., "The Effect of Additives on the Ignition Delay Time for Stoichiometric Propane-Air Mixtures", M.S. Thesis, Department of Aeronautical and Astronautical Engineering, University of Illinois at Urbana-Champaign, 1978.

Melling, A. and Whitelaw, J. H., "Seeding of Gas Flows for Laser Anemometry", DISA Information No. 15, October 1973.

Mehl, L., "An Analysis of the Gaseous Combustion Products in a Coal Dust-Air Flame System", M.S. Thesis, Department of Aeronautical and Astronautical Engineering, University of Illinois at Urbana-Champaign, 1977.

Parker, A., *J. Chem. Soc.* *105*, 1002 (1914).

Payman, W., *J. Chem. Soc.* *115*, 1436 (1919).

Peeters, S. and Mahnan, G.,'Reaction Mechanisms and Rate Constants of Elementary Steps in Methane-Oxygen Flames", 14th Symposium (International) on Combustion, 1973.

Powling, J., *Fuel* *28*, 25 (1949).

Reid, R. C. and Sherwood, T. K., *The Properties of Gases and Liquids*, 2nd Ed., McGraw-Hill, 1966.

Reuss, D. L., To be published. (1980)

Savage, L. D., Personal communication (1978).

Schultz-Grunow and Wortberg, G., *Int. J. Heat Mass Transfer* 2, 56, Pergamon Pergamon Press (1961).

Smoot, L. D., Hecker, W. C., and Williams, G. A., *Combus. and Flame* 26(3) (1976).

Sorenson, S. C., Savage, L. V., and Strehlow, R. A., "Flammability Limits - A New Technique", *Combus. and Flame* 24 (1975).

Spalding, D. B., *Proc. Roy. Soc.* *249*, A957 (1956).

Spalding, D. B., *Combus. and Flame* 1 (1957a).

Spalding, D. B., *Proc. Roy. Soc, London*, *A240*, 83 (1976).

Spalding, D. B., Stephenson, P. L., and Taylor, R. G., *Combus. and Flame* *17*, 55 (1971).

Steffensen, R. S., Agnew, J. T., and Olsen, R. A., "Tables for Adiabatic Gas Temperature and Equilibrium Composition of Six Hydrocarbons", Engineering Bulletin #122, Purdue University, May 1966.

Strehlow, R. A., *Fundamentals of Combustion*, International Textbook Co., 1968.

Strehlow, R. A., "The Effect of Curvature on Flame Structure", Deuxiem Symposium Europeen sur la Combustion, p. 496 (1975).

Strehlow, R. A., Personal communication (1978).

Tanford, C., J. Chem. Physics 13(7)(1947).

Tanford, C. and Pease, N., J. Chem. Physics 15(7)(1942 .

TSI Bulletin #25, An Introduction to the TSI Laser Anemometer, Thermo-Systems, Inc., St. Paul, Minnesota.

Vest, C. M. and Sweeny, D. W., Appl. Optics 9(10), 2321 (1970).

Vest, C. M., Appl. Optics 14, 1601 (1975).

Weinberg, F. J., Optics of Flames, Butterworth, Washington, 1963.

White, A. G., J. Chem. Soc. 125 (1924).

Williams, F. A., Combustion Theory, Addison-Wesley, 1965.

Witte, A. B. and Wuerker, AIAA Paper No. 69-347, AIAA 4th Aerodynamic Testing Conference, Cincinnati, Ohio, April 1969.

Yang, C. H., Combus. and Flame 5, 174 (1961).

Yeh, Y. and Cummis, H., Appl. Phys. Lett. 4, 176-8 (1964).